CL/PACLIM-IATR/92-31

PROCEEDINGS OF THE EIGHTH ANNUAL PACIFIC CLIMATE (PACLIM) WORKSHOP

Asilomar, California – March 10-13, 1991

Edited by
Kelly T. Redmond

Technical Report 31
of the
Interagency Ecological Studies Program
for the
Sacramento-San Joaquin Estuary

March 1992

Copies of this report may be obtained without charge from:

California Department of Water Resources
P.O. Box 942836
Sacramento, CA 94236-0001

PROCEEDINGS OF THE EIGHTH ANNUAL PACIFIC CLIMATE (PACLIM) WORKSHOP

Asilomar, California – March 10-13, 1991

Edited by
Kelly T. Redmond

Technical Report 31
of the
Interagency Ecological Studies Program
for the
Sacramento-San Joaquin Estuary

PACLIM

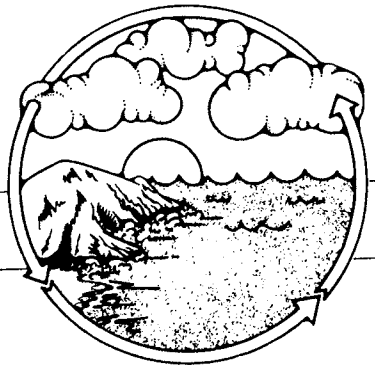

Climate Variability
of the
Eastern North Pacific
and
Western North America

The Seventh Annual Pacific Climate Workshop was sponsored by the

U.S. Geological Survey

National Oceanic and Atmospheric Administration
National Geophysical Data Center

National Oceanic and Atmospheric Administration
Climate Analysis Center

National Park Service
Global Change Program

California Department of Water Resources

Publication of this proceedings has been sponsored by the

Interagency Ecological Studies Program
for the
Sacramento-San Joaquin Estuary

A Cooperative Program of:

California Department of Water Resources
State Water Resources Control Board
U.S. Bureau of Reclamation
U.S. Army Corps of Engineers
California Department of Fish and Game
U.S. Fish and Wildlife Service
U.S. Geological Survey

These proceedings were published by the Interagency Ecological Studies Program for the Sacramento-San Joaquin Estuary (Interagency Program)
in a cooperative effort with the
Western Regional Climate Center, Desert Research Institute, Reno Nevada.
Information generated by the PACLIM workshop provides the
Interagency Program with a climatological perspective that cannot be obtained from its own studies.
Views and conclusions contained in this publication do not necessarily reflect the opinions of the
Interagency Program or its member agencies.

Contents

Authors

Edward Aguado
San Diego State University
Department of Geography
San Diego, CA 92182-0381

Bruce D. Allen
Department of Geology
University of New Mexico
Albuquerque, NM 87131

Roger Y. Anderson
Department of Geology
University of New Mexico
Albuquerque, NM 87131

Brendan M. Buckley
Tree-Ring Laboratory
Lamont-Doherty Geological Observatory
Palisades, New York 10964

Daniel R. Cayan
Climate Research Division
Scripps Institution of Oceanography A-024
University of California San Diego
La Jolla, CA 92903

Jeng-Ming Chen
Department of Meteorology
Naval Postgraduate School
Monterey, CA 93943-5000

Shyh-Chin Chen
Climate Research Division
Scripps Institution of Oceanography A-024
University of California San Diego
La Jolla, CA 92903

Pao-Shin Chu
Department of Meteorology
School of Ocean and Earth Science and
Technology University of Hawaii
Honolulu, Hawaii 96822

Richard G. Craig
Water Resources Research Institute and
Department of Geology
Kent State University
Kent, OH 44242

Rosanne D. D'Arrigo
Tree-Ring Laboratory
Lamont-Doherty Geological Observatory
Palisades, New York 10964

Owen K. Davis
Department of Geosciences
University of Arizona
Tucson, Arizona 85271

Mike Dettinger
U.S. Geological Survey
San Diego, CA 92097

Lisa L. Ely
Department of Geosciences
University of Arizona
Tucson, AZ 85721

Yehouda Enzel
Department of Geosciences
University of Arizona
Tucson, AZ 85721

David C. Garen
U.S. Soil Conservation Service
Portland, OR 97209-3489

G. Glatzmaier
Los Alamos National Laboratory
Los Alamos, NM

Charles R. Goldman
Division of Environmental Studies
University of California
Davis, California 95616

Hermann Gucinski
ManTech Environmental Technology, Inc.
US EPA Environmental Research Laboratory
200 SW 35th St
Corvallis OR 97333

M. S. Halpert
Climate Analysis Center
National Meteorological Center, NWS/NOAA
Washington, D. C. 20233

Patrick A. Harr
Department of Meteorology
Naval Postgraduate School
Monterey, CA 93943-5000

G. Holdsworth
National Hydrology Research Institute, Saskatoon, and
Arctic Institute of North America
Calgary, Canada.

Linda Heusser
Lamont-Doherty Geological Observatory
of Columbia University
Palisades, NY 10964

Neil L. Ingraham
Water Resources Center
Desert Research Institute
2505 Chandler Avenue
Las Vegas, NV 89120

Gordon C. Jacoby
Tree-Ring Laboratory
Lamont-Doherty Geological Observatory
Palisades, New York 10964

Alan D. Jassby
Division of Environmental Studies
University of California
Davis, California 95616

John Jirikowic
Department of Geosciences
University of Arizona
Tucson, Arizona 85271

Robert M. Kalin
Department of Geosciences
University of Arizona
Tucson, Arizona 85271

J. Kao
Los Alamos National Laboratory
Los Alamos, NM

Jeff Kern
ManTech Environmental Technology, Inc.
US EPA Environmental Research Laboratory
200 SW 35th St
Corvallis OR 97333

George King
ManTech Environmental Technology, Inc.
US EPA Environmental Research Laboratory
200 SW 35th St
Corvallis OR 97333

D. Langley
Los Alamos National Laboratory
Los Alamos, NM

Peggy W. Lehman
California Department of Water Resources
3251 S Street
Sacramento, CA 95816

Joseph Morley
Lamont-Doherty Geological Observatory
of Columbia University
Palisades, NY 10964

Tom Murphree
Department of Meteorology
Naval Postgraduate School
Monterey, CA 93943-5000

Andrew J. Nash
Department of Meteorology
School of Ocean and Earth Science and
Technology University of Hawaii
Honolulu, Hawaii 96822

Charles Peterson
ManTech Environmental Technology, Inc.
US EPA Environmental Research Laboratory
200 SW 35th St
Corvallis OR 97333

Fee-Yung Porter
Department of Meteorology
School of Ocean and Earth Science and
Technology University of Hawaii
Honolulu, Hawaii 96822

Derek Pross
Geography Department
Oregon State University
Corvallis OR 97331

Kelly T. Redmond
Western Regional Climate Center
Desert Research Institute
PO Box 60220
Reno, Nevada 89506

Laurence G. Riddle
Climate Research Division
Scripps Institution of Oceanography A-024
University of California San Diego
La Jolla, CA 92903

John O. Roads
Climate Research Division
Scripps Institution of Oceanography A-024
University of California San Diego
La Jolla, CA 92903

C. F. Ropelewski
Climate Analysis Center
National Meteorological Center, NWS/NOAA
Washington, D. C. 20233

Arndt Schimmelmann
Scripps Institution of Oceanography
University of California at San Diego
La Jolla, CA 92093-0215

Nicholas Shackleton
Godwin Laboratory
University of Cambridge
Cambridge England

John F. Stamm
Department of Civil Engineering and
Operations Research
Princeton University
Princeton, New Jersey 08095

Mia J. Tegner
Scripps Institution of Oceanography
University of California at San Diego
La Jolla, CA 92093-0215

David Turner
ManTech Environmental Technology, Inc.
US EPA Environmental Research Laboratory
200 SW 35th St
Corvallis OR 97333

Acknowledgments

I would like to acknowledge the hard work of our technical editor, Vera Tharp of the California Department of Water Resources, in reworking the manuscripts from their various original forms into a common format. This includes insertion of the figures and tables into the body of the text. Her expertise and cheerfulness greatly expedited the process of preparing these proceedings. Any credit for style and presentation should go to Vera.

We have exercised minimal editing of content, confining most changes to those of a technical nature. We thank the authors for their cooperation in providing papers in a timely manner.

We also would like to thank the sponsors who have contributed to the success of this event. They include the U.S. Geological Survey, the National Park Service Global Change Program, the National Geophysical Data Center and the Climate Analysis Center of NOAA, and the California Department of Water Resources.

Kelly Redmond
Editor

Introduction

Kelly T. Redmond

This volume contains a total of 21 papers given in talks or poster sessions at the eighth annual Pacific Climate (PACLIM) meeting at the Asilomar Conference Center in Pacific Grove, California, March 10-13, 1991. Consisting of about a third of the total presentations, this selection gives a representative cross section of the breadth and diversity of topics. With the beautiful and peaceful setting, the relaxed and informal style of the sessions, the diversity of topics, and the quality of presentations, these meetings provide a stimulating atmosphere for cross-disciplinary interaction.

Nearly all the articles deal with climate issues in western North America, and the remainder are concerned with the Pacific Ocean.

The papers are arranged roughly in chronological order according to the age of the subject matter (not the authors!), and from observational studies to theoretical or model-intensive works.

The first paper, by Heusser, Morley, and Schackleton, covers the longest span, a third of the last million years. They use high temporal resolution pollen data to deduce relationships between climate and Japanese vegetation over three full glacial cycles.

In comparison, Allen and Anderson deal with a relative eyeblink, a 5000-year period near the end of the last glacial episode, at Lake Estancia in central New Mexico.

Because the rate of carbon-14 production varies with time, radiocarbon dates show systematic variations from dates known exactly. Davis, Jirikowic, and Kalin discuss calibration of these corrections by use of tree rings.

Tree ring widths have long been used for studies of past climate. In recent years, late-wood density has been shown to add further, and complementary, evidence of past climate changes. Buckley, D'Arrigo, and Jacoby have examined the relationship of both these factors to climate in the Puget Sound area over the instrumental period.

Schimmelmann and Tegner demonstrate that historical accounts may be used to furnish suggestions of past climate behavior. Their paper offers a revealing glimpse into the difficult detective job the historian faces — and the considerable background leg work needed — to fashion a consistent story from fragmentary, and often secondhand, evidence.

The layered record of annual snow accumulation, laboriously and probably breathlessly gathered by Holdsworth in the lofty air high on Mt. Logan, is subjected to spectral analysis. The 9- to 11-year periods commonly reported for small arctic mammals are found in the snow time series. Adding to the host of proxy data being analyzed in climate studies, an index of browse scars on small northern shrubs is formed for a two-century period. A spectral peak at this same period does emerge.

The relationship between chlorophyll production and climatic factors in the Sacramento Delta region is discussed by Lehman. Although it is difficult to untangle the effects of multiple influences, principal components analysis shows that climate is one of the important factors.

The influence of antecedent and concurrent meteorological conditions on the primary productivity of two lakes, one large (Tahoe) and one small (Castle), is reported by Jassby and Goldman. They also used principal components to simplify descriptions of the behavior. The role of external forcing and the path by which the food web is affected ("top-down" or "bottom-up"), a topic of much interest in limnology, is addressed.

Chu, Porter, and Nash contrast two successive winters of markedly different character in Hawaii, and discuss the atmospheric influences associated with each.

The circulation patterns that lead to significant winter floods in the southwestern United States are next presented by Ely, Enzel, and Cayan. There is a clear eastward progression in the center positions of atmospheric anomaly patterns as the affected area changes from the Mojave Desert to the Gila River basin. The analysis indicates also that rather more specific conditions seem to be required for floods south of the Sierra Nevada than in Arizona.

The next paper, by Harr, Chen, and Murphree, discusses the interaction between lower atmospheric wind field regimes and the trajectories of tropical cyclones in the western North Pacific.

Throughout the years, the cooperative network has provided the raw data for hundreds of studies in the United States. Few such studies, however, have made extensive use of the snowfall and snow depth information available therein. Riddle, Cayan, and Aguado give an introduction to some properties of the cooperative snow data in the Sierra and their relationship to traditional snow course observations, another dataset that has received limited attention for climate studies. Their focus is on the effect of circulation pattern variations on precipitation quantity and on snow density.

A companion article by Cayan, Riddle, Garen, and Aguado looks in more detail at the snow course dataset. They show that the several-decade records of snow course observations can provide information that is consistent with and complementary to that from NOAA-derived sources.

As their length of record begins to approach a decade, it would seem that satellite observations could provide other types of time series. In particular, one operational product, the normalized difference vegetation index (NDVI) has been available for several years. Ropelewski and Halpert discuss some of the pitfalls involved in using this AVHRR-derived product for temporal analysis. Among the sources of non-stationarity are sensor degradation, orbital drift, equator crossing times, changes in satellites, and viewing time variations. The effect of all of these is to make NDVI a poor risk for time series analysis at this time.

Although it has been known for some time that changes in observation time among cooperative observers can lead to substantial but artificial "climate changes", Redmond shows that these observations are well-suited for time series analysis as long as a consistent observation time is maintained. This issue is commonly a source of confusion to those not familiar with the network. Also not widely appreciated is the frequency that daily temperature extremes are set at "unusual" or "non-standard" times, the subject of a short discussion closely related to the first topic.

Gucinski, Peterson, Kern, Turner, and King report on progress in determining the carbon budget of the United States. The usual problems involved in determining small differences between large numbers arise — namely, that the uncertainty in the major reservoir and flux values be sufficiently low.

Last is a series of papers oriented toward analysis of model output from numerical simulations.

Stamm and Craig use an interesting and novel approach to interpolate general circulation model results to a 15-km resolution. They then apply the model to the southwestern United States for present and late ice age conditions and present results and validation.

Chen, Cayan, Roads, and Dettinger, running a simplified GCM in background over several months, have generated a 544-year simulation of perpetual winter, among the longest runs ever done. They use the model to infer certain statistics about wet/dry and warm/cool Sierra winter conditions. Because many potential contributors to climate variability are held fixed, the model can furnish information on how much atmospheric dynamics alone can account for such variability.

The latent heat of condensation in tropical cyclones and other areas of extensive precipitation in the tropics provides a significant heat source to the atmosphere. Murphree, Chen, and Harr use a model to show that the imposition of atmospheric heating anomalies in the tropics can lead to extratropical consequences quite far away. The 1988 Midwest drought appears to be a case in point.

Roads, Chen, Kao, Langley, and Glatzmaier provide a short discussion of the properties of the hydrologic cycle of the Los Alamos GCM. Since one purpose of modeling climate is to anticipate possible changes in availability of water resources, the importance of proper simulation of hydrologic processes has been receiving much more attention in recent years.

Using the model mentioned earlier, Craig, Ingraham, and Stamm attempt to compute the change in hydrogen/deuterium ratios from the California coast inland to the Great Basin. The significant but poorly appreciated role of recycled evapotranspiration can be illuminated with studies of stable isotopes.

Variations in Northeast Asian Environments over the Last 350,000 Years Reconstructed from Pollen Records from the Northwest Pacific Ocean

Linda Heusser, Joseph Morley, and Nicholas Shackleton

Abstract: Recent analyses of terrestrial (pollen) and marine microfossils (foraminifera and radiolaria) in cores V28-204 and RC14-99 from the northwest Pacific Ocean extend the continuous, chronostratigraphically-controlled records of the regional vegetation of the Pacific coast of Japan and offshore marine environments through three full glacial cycles. The high-resolution pollen time series show systematic relationships between fluctuations in Japanese vegetation and global ice volume over the last 350 kyr. Intervals of expanded mesothermal vegetation characterized by *Cryptomeria japonica* (Japanese cedar) coincide with periods of significant isotope depletion associated with global warming. Conversely, representation of mesothermal vegetation in eastern Japan is minimal during intervals of isotope enrichment and extensive northern hemisphere glaciation. Comparison with solar insolation at 30°N and with an index of orbital parameters suggests that variation in northeast Asian summer monsoon intensity is related to orbital forcing.

Introduction

Understanding the effects of past and future climate changes on the terrestrial biosphere is severely hampered by the deficiencies of presently available terrestrial paleoclimatic data. Lengthy paleoclimatic records on land, such as the Chinese and central European loess deposits and pollen data from singular sediment cores taken in California, Colombia, Japan, and Europe generally lack continuous, high-resolution chronostratigraphic control and are inadequate for rigorous analysis in either the time or frequency domain (Adam 1988; Hooghiemstra 1989; Fuji 1988; Kukla 1989). Paleoclimatic reconstructions based primarily on deep-sea records provide little direct evidence of the effect of climatic change on the terrestrial biosphere. Only marine pollen data that are directly correlated with global marine chronostratigraphies precisely document the response of terrestrial ecosystems to climatic oscillations over long time spans (Heusser 1986/1987; Hooghiemstra 1988; DuPont and Hooghiemstra 1989).

These pollen data from deep-sea sediment cores clearly show that patterns of temperate forest development and climatic changes in northwest North America, Europe, and Japan over the last 140 kyr parallel global changes in climate reconstructed from marine microfossils (Heusser and Shackleton 1979; Heusser 1989; Morley and Heusser 1989; Rossignol-Strick and Planchais 1989). Particularly striking in the marine pollen records from Japan is the correlation between fluctuations in abundance

In K.T. Redmond, Editor, 1992. Proceedings of the Eighth Annual Pacific Climate (PACLIM) Workshop, March 10-13, 1991: California Department of Water Resources, Interagency Ecological Studies Program Technical Report 31.

of *Cryptomeria japonica* and global ice volume during the last glacial cycle (Heusser 1989). *C. japonica* (Japanese cedar), which is now indigenous to temperate and mixed mesophytic forests of Japan and southern China (Ohwi 1984; Numata 1974; Wang 1961) is frequently used as a paleoclimatic indicator because of the close association between the present natural distribution of *Cryptomeria* and humid maritime monsoon climates in northeast Asia (Tai 1973; Tsukada 1982; Tsukada 1986). Here we extend the record of the relative abundance of *Cryptomeria* to ~340 kyr and use the records of *Cryptomeria* in V28-304 and RC14-99 as a marine pollen index of variation in northeast Asian monsoon climates over the past 350 kyr.

Background

Core RC14-99 (36°58'N, 147°56'E, 5652 m water depth) was taken ~1000 km east of the warm-temperate and temperate forests of Japan, where average January temperature is 4°C and mean August temperature is 22°C (Fukui 1977). The site of V28-304 (28°32'N, 134°08'E, 2942m water depth) is ~500 km south of subtropical Japan, where mean January and August temperatures are 8°C and 26°C, respectively. Annual precipitation on the Pacific coast of Japan, which decreases from 4000 mm in the south to ~1500 mm on the north coast of Honshu, reflects the early summer monsoon rains, as winters on the lee side of the mountains are relatively dry.

Zonal distribution of vegetation, closely related to latitudinal temperature and precipitation variations, is highly influenced by large-scale circulation changes associated with the Asian monsoon. Potential natural montane vegetation of Honshu consists of evergreen and deciduous broad-leafed and evergreen coniferous forests. Characteristic dominants of the warm-temperate forests include evergreen members of the Fagaceae, such as *Quercus* and *Castanopsis*, along with conifers such as *Cryptomeria japonica*, and the secondary species, *Pinus densiflora*. Temperate, deciduous broad-leafed forests are characterized by *Quercus/Fagus* associations in which *Pinus* and *Cryptomeria* are present (Ohwi 1984).

Both cores were sampled at no less than 10-cm intervals. Pollen, radiolaria, and foraminifera, subsets of the same sediment samples, were prepared and analyzed using techniques described previously (Heusser 1979; Morley and Heusser 1989; Heusser 1990). *Cryptomeria* values are based on counts of 300 arboreal and nonarboreal pollen grains representing 35 taxa. Depth of each *Cryptomeria* sample was converted to time using age models constructed from correlation of the oxygen isotope and radiolarian (*Cycladophora davisiana*) records in these two cores with the SPECMAP "stacked" isotope curve and its associated timescale (Imbrie *et al* 1984; Martinson *et al* 1987). The average interval between consecutive samples is ~2-3 kyr.

Results

Well-preserved and relatively abundant (up to 2,000 grains/gm), pollen assemblages from RC14-99 and V28-304 reflect systematic changes in the vegetation of Japan, the principal source of pollen in these cores. Lengthy intervals characterized by boreal elements are punctuated by brief episodes in which warm-temperate components expand (Heusser 1989; Morley and Heusser 1989; Heusser 1990). The 16m-record of the relative frequency of the mesothermal indicator *Cryptomeria* in core RC14-99 shows three sets of high-frequency, high-amplitude oscillations separated by longer intervals of little change (Figure 1). Two bipartite sets of high-amplitude oscillations in *Cryptomeria* occur in the shorter (8m) record from V28-304.

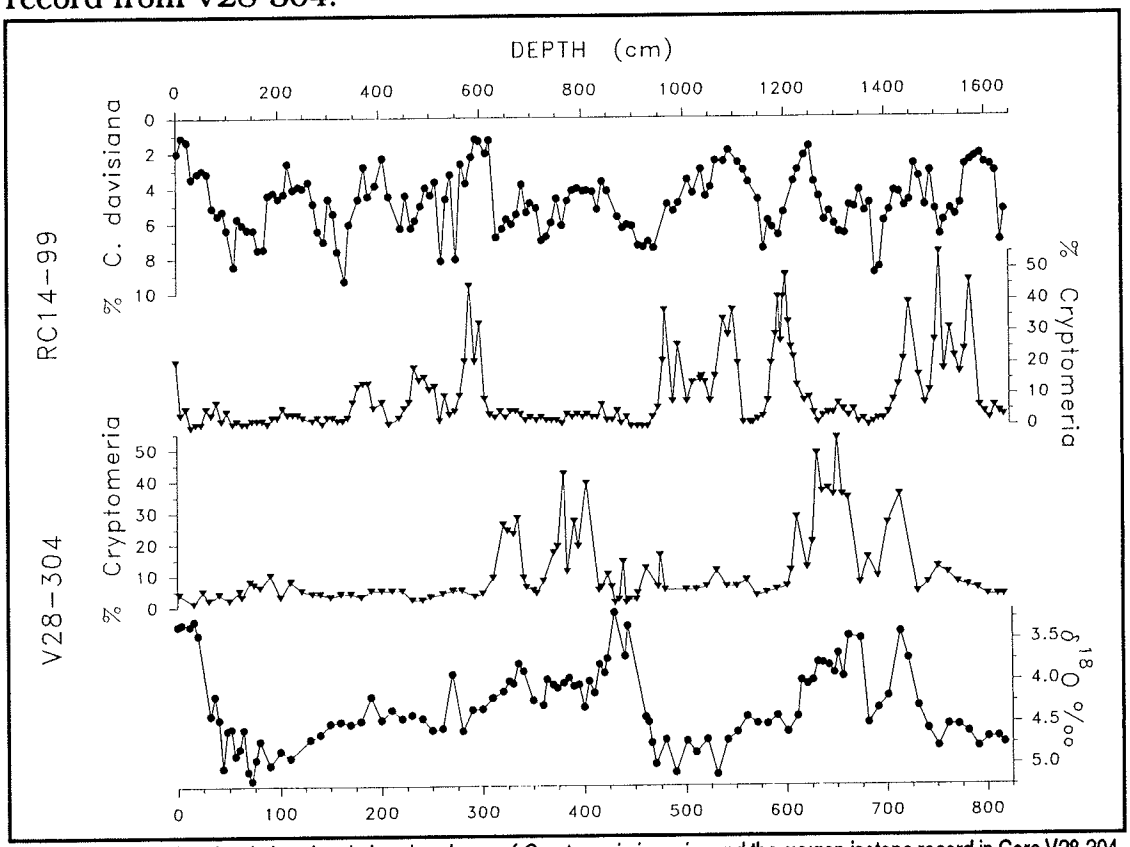

Figure 1. Depth plot of variations in relative abundance of *Cryptomeria japonica* and the oxygen isotope record in Core V28-304 (left) and of variations in abundance of *Cryptomeria* and of the radiolarian *C. davisiana* in Core RC14-99 (right).

When plotted in the time domain (Figure 2), high-amplitude fluctuations of *Cryptomeria* in the two cores appear to be nearly synchronous over the last 250,000 years. Except for a peak in early isotope stage 6 (~181 kyr), all *Cryptomeria* maxima occur within interglacial periods. In RC14-99 and V28-304, a bipartite increase in *Cryptomeria* is separated from a maximum between 230-235 kyr by a brief, deep minimum centered at ~228 kyr. During the last glacial cycle, *Cryptomeria* peaks form a decreasing triad beginning ~122 kyr in the RC14-99 record; in the southern core, V28-304, the basal peak occurs at 105 kyr. A 3-peaked expansion of *Cryptomeria*, centered at ~310 kyr, marks the base of the oldest glacial cycle in the RC14-99 record.

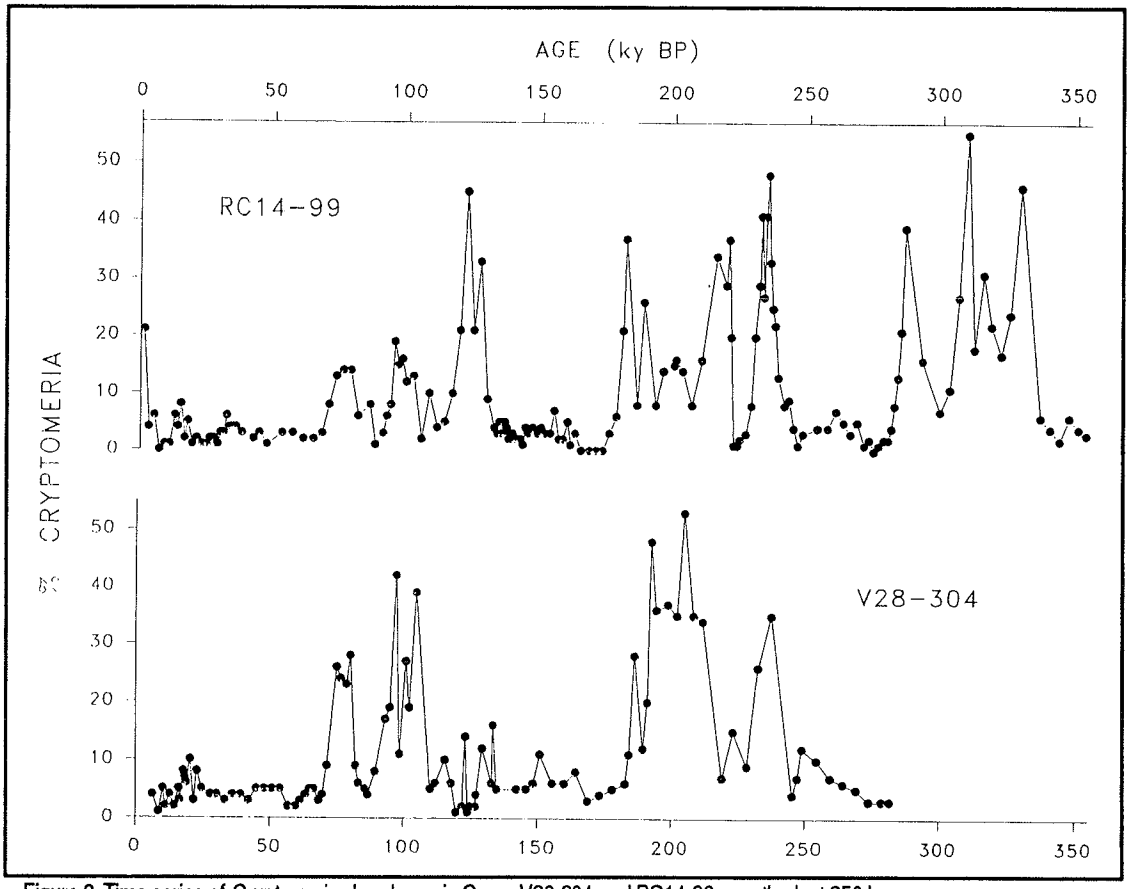

Figure 2. Time series of *Cryptomeria* abundance in Cores V28-304 and RC14-99 over the last 350 kyr.

Discussion

During the past 350 kyr, optimal development of mesothermal *Cryptomeria* forests and inferred climatic optima on the Pacific coast of Japan occur during interglacials (in isotope stages 5, 7, and 9) when northern hemisphere ice sheets, as reconstructed from oxygen isotope analyses, were minimal (Imbrie *et al* 1984; Martinson *et al* 1987). The small but significant differences in the precise timing of some of the *Cryptomeria* optima in the two cores and the absence of a high-amplitude *Cryptomeria* peak at 122 kyr in V28-304 suggests regional differences in the response of temperate and warm-temperate/subtropical environments on the Pacific coast of Japan to climatic changes during the last three glacial cycles.

These results from the direct correlations of northeast Asian and global paleoclimatic variations from deep-sea cores V28-304 and RC14-99 would seem to corroborate previous observations from records of late-Pleistocene terrestrial climatic variations that were indirectly correlated with and/or tuned to deep-sea oxygen isotope chronologies on the assumption that terrestrial climatic variations were synchronous with and of about the same order of magnitude as ice volume fluctuations (Woillard 1978; Prell and Kutzbach 1987; Adam 1988; Fuji 1988; Hooghiemstra 1989; Kukla 1989; Mangerud 1989, 1990). The differences in

magnitude of the vegetational and inferred climatic changes in temperate and sub-tropical Japan suggest that variations in terrestrial paleoenvironments elsewhere may not be the same magnitude as global ice volume fluctuations and that all terrestrial environments do not necessarily exhibit responses of similar magnitude to specific climatic forcing. These differences in magnitude of response — as well as differences in timing of the response relative to global climatic events, such as in ice volume minima — are critical to understanding how the climate system works. Determining the precise timing of responses of various parts of the climate system — including terrestrial components — to Quaternary climatic perturbations is obviously basic in establishing causal relationships and, thus, is critical to evaluating models of past and future climate change.

The *Cryptomeria* records from V28-304 and RC14-99 also suggest terrestrial interglacial environments of the last three glacial cycles are not the same — at least in Japan. Earlier interglacials are not necessarily replicates of the Holocene nor of each other. Although some of these differences in our records from Japan may reflect Holocene anthropogenic influence on the vegetation of Japanese archipelago and/or sediment missing from the core-tops, clear differences exist in the duration and amplitude of *Cryptomeria* development in earlier interglacials of the last 350 kyr (isotope stages 5, 7, and 9). Therefore, our data suggest that, contrary to standard geologic wisdom and practice, the present interglacial is not necessarily a precise analogue for past interglacials — and vice versa.

Comparison of variability in northeast Asian environments over the last ~350 kyr (as represented here by the *Cryptomeria* record from RC14-99) with variations in solar insolation at 30°N and ETP, a composite curve of orbital variations constructed by adding normalized values for eccentricity, obliquity, and precession (Imbrie *et al* 1984) shows a consistent relationship between these proxy climatic indices (Figure 3). With the exception of the peak at 181 kyr, the high-amplitude *Cryptomeria* peaks closely follow maxima in summer insolation and corresponding peaks in ETP. This suggests these changes in the vegetation of Japan are responding to climatic changes related to orbital forcing. Analyses of marine pollen data elsewhere have shown similar relationships between long-term changes in terrestrial environments of Africa and orbital parameters (Prell and VanCampo 1986; DuPont and Hooghiemstra 1989).

Because precipitation, regarded as a prime factor in limiting the present and past distribution of *Cryptomeria*, is concentrated in summer on the Pacific coast of Japan (Fukui 1977), we suggest fluctuations in relative abundance of *Cryptomeria* pollen in RC14-99 and V28-304 serve as a proxy for changes in the position and intensity of the summer (Bai u) monsoon. Therefore, we interpret the relationships between variations in *Cryptomeria*, summer insolation, and orbital parameters (ETP) over the last 350 kyr as suggesting that variability in northeast Asian summer

monsoons, like southeast Asian monsoons (Prell and Kutzbach 1987), is related to orbital forcing.

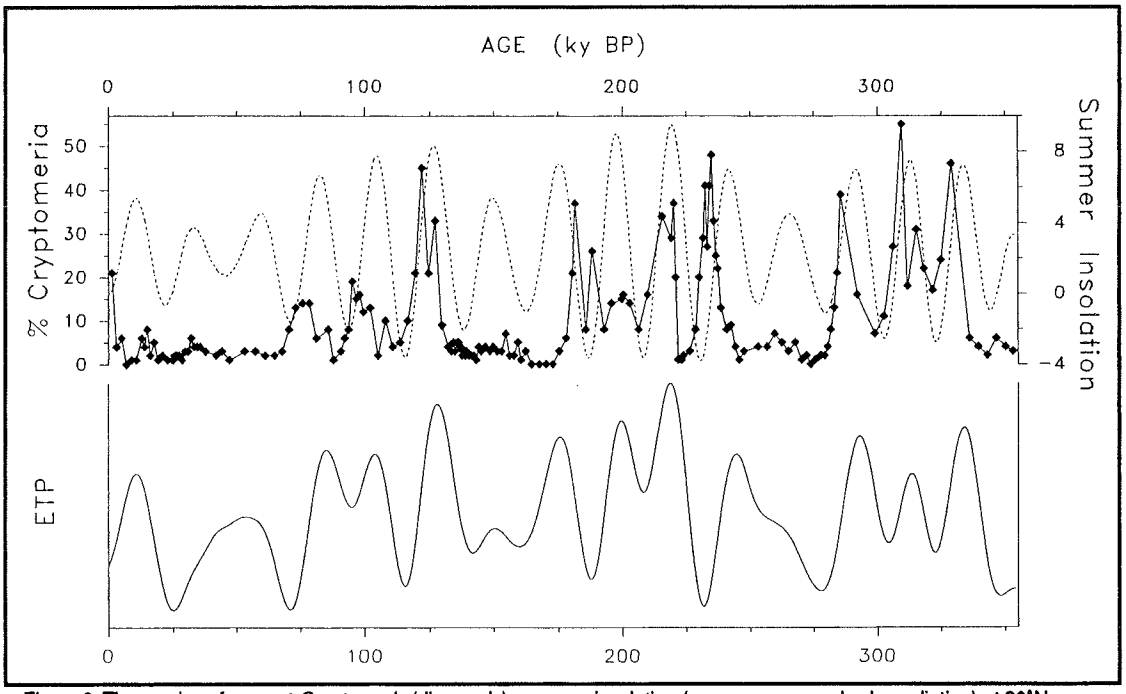

Figure 3. Time series of percent *Cryptomeria* (diamonds), summer insolation (summer averaged solar radiation) at 30°N (expressed as percent difference from present), and ETP (composite curve of eccentricity, obliquity, and precession).

Acknowledgments

This work was supported by National Science Foundation grant ATM 8711397 to L.E.H. and J.J.M. and NERC grants to N.J.S. We are grateful to E. Stock, C. Heusser, and R. Lotti for assistance. Support for the curating facilities of the Lamont-Doherty Geological Observatory Deep-Sea Sample Repository is provided by the National Science Foundation through Grant OCE88-00001 and the Office of Naval Research through Grant N00014-87-K-0204.

Literature Cited

Adam, DP, 1988. Correlations of the Clear Lake, California core CL 73-4 pollen sequence with other long climate records. Pgs. 81-96 in JD Sims (Ed.), *Late Quaternary Climate, Tectonism, and Sedimentation in Clear Lake, Northern California Coast Ranges*. Boulder, CO:Geological Society of America.

DuPont, L, and H Hooghiemstra, 1989. The Saharan-Sahelian boundary during the Brunhes chron. *Acta Botanica Neederland.* 38:405-415.

Fuji, N, 1988. Palaeovegetation and palaeoclimate changes around Lake Biwa, Japan during the last ca. 3 million years. *Quaternary Science Reviews.* 7:21-28.

Fukui, E, 1977. *The Climate of Japan.* 317. New York:Elsevier.

Heusser, L, 1990. Northeast Asian pollen records for the last 150,000 years from deep-sea cores V28-304 and RC14-99 taken off the Pacific coast of Japan. *Review of Palaeobotany and Palynology.* 65:1-8.

_____, 1989. Northeast Asian Climatic Change over the last 140,000 years inferred from pollen in marine cores taken off the Pacific Coast of Japan. Pgs. 665-692 in M Leinen and M Sarnthein (Eds.), *Paleoclimatology and Paleometerology.* Dordrecht:Kluwer.

Heusser, L, and N Shackleton, 1979. Direct marine-continental correlation: 150,000-year oxygen isotope-pollen record from the North Pacific. *Science.* 204:837-839.

Heusser, LE, 1986/1987. Pollen in marine cores: evidence of past climates. *Oceanus.* 29:64-70.

Heusser, LE, and JJ Morley, 1990. Northeast Asian monson climates during the last 350,000 years: correlative evidence from terrestrial and marine microfossils. *Eos.* 71:543.

Hooghiemstra, H, 1989. Quaternary and Upper-Pliocene glaciations and forest development in the tropical Andes: evidence from a long high-resolution pollen record from the sedimentary basin of Bogota, Colombia. *Palaeogeography, Palaeoclimatology, Palaeoecology.* 72:11-26.

_____, 1988. Palynological record from northwest African marine sediments: a general outline of the interpretation of the pollen signal. *Philosophical Transactions of the Royal Society of London B.* 318:431-449.

Imbrie, J, J Hays, D Martinson, A McIntyre, A Mix, J Morley, N Pisias, W Prell, and N Shackleton, 1984. The orbital theory of Pleistocene climate: support from a revised chronology of the marine $\delta^{18}O$ record. Pgs. 269-306 in A Berger, J Imbrie, J Hays, G Kukla and B Saltzman (Eds.), *Milankovitch and Climate.* Dordrecht:Reidel.

Kukla, G, 1989. Long continental records of climate — an introduction. *Palaeogeography, Palaeoclimatology, Palaeoecology.* 72:1-9.

Mangerud, J, 1990. Correlation of the Eemian and the Weichselian with deep-sea oxygen isotope stratigraphy. *Quaternary International.* 3/4:1-4.

_____, 1989. The last interglacial-glacial cycle in Fennoscandia. *Quaternary International.* 3/4:21-29.

Martinson, D, N Pisias, J Hays, J Imbrie, TC Moore Jr, and N Shackleton, 1987. Age dating and the orbital theory of the Ice Ages: development of a high-resolution 0 to 300,00-year chronostratigraphy. *Quaternary Research.* 27:1-29.

Morley, JJ, and LE Heusser, 1989. Late Quaternary atmospheric and oceanographic variations in the western Pacific inferred from pollen and radiolarian analyses. *Quaternary Science Reviews.* 8:263-276.

Numata, M, 1974. *The Flora and Vegetation of Japan.* New York:Elsevier.

Ohwi, J, 1984. *Flora of Japan.* Washington DC:Smithsonian Inst.

Prell, E, and E VanCampo, 1986. Coherent response of Arabian Sea upwelling and pollen transport to late Quaternary monsoonal winds. *Nature.* 323:526-528.

Prell, W, and J Kutzbach, 1987. Monsoon variability over the past 150,000 years. *Journal of Geophysical Research.* 92:8411-8425.

Rossignol-Strick, M, and N Planchais, 1989. Climate patterns revealed by pollen and oxygen isotope records of a Tyrrhenian sea core. *Nature.* 342:413-416.

Tai, A, 1973. A study of the pollen stratigraphy of the Osaka Group, Plio-Pleistocene deposits in the Osaka Basin, Memoirs of the Faculty of Science Kyoto University. *Series of Geology and Minerology.* XXXIX:123-165.

Tsukada, M, 1986. Altitudinal and latitudinal migration of *Cryptomeria japonica* for the past 20,000 years in Japan. *Quaternary Research.* 26:135-152.

_____, 1982. *Cryptomeria japonica*: glacial refugia and late-glacial and postglacial migration. *Ecology.* 63:1091-1105.

Wang, C-W, 1961. *The Forests of China.* Cambridge:Harvard University.

Woillard, G, 1978. Grande Pile Bog: a continuous pollen record for the last 140,000 years. *Quaternary Research.* 9:1-21.

Centennial Oscillation of the Climatic Crescendo During the Last Glacial Maximum: Evidence from Lake Estancia, Central New Mexico

Bruce D. Allen and Roger Y. Anderson

Abstract: Sediments deposited in late Pleistocene Lake Estancia, central New Mexico, contain a paleoclimatic record that includes the last glacial maximum and deglacial episode. Stratigraphic reconstruction of an interval representing the highstand of the lake that occurred during the last glacial maximum reveals ~2000-, ~600-, and ~200-year oscillations in lake level and climate. Shifting position of the polar jetstream in response to expansion and contraction of the North American ice sheet may be partly responsible for the millenial-scale changes in Lake Estancia but probably does not explain the centennial-scale oscillations.

Introduction

Estancia Valley in central New Mexico contains a sequence of lake sediments and shoreline features that reflect the last great expansion of "pluvial" lakes in the western United States. Lake Estancia existed as a perennial lake during the Wisconsin glacial episode, and meter-scale changes in the lacustrine sediments indicate large, millenial-scale fluctuations in lake-level occurred in response to changes in the glacial-age climate. A continuous source of ground water recharge maintained the lake with a surface area greater than ~400 km^2 until about 12,000 years BP, preventing desiccation in the central part of the basin and preventing loss of continuity of the stratigraphic and climatic record.

In addition to preserving information about climatic changes over time intervals comparable to the advance and retreat of the North American ice sheet, the Estancia hydrologic system was responsive to climatic forcing at higher frequencies, including decadal- through millenial-scale changes (Allen and Anderson 1989; Allen 1991). This contribution identifies high-frequency (millennial- to centennial-scale) changes in hydrology and climate during a highstand of Lake Estancia coinciding with the last glacial maximum and early deglacial interval.

Sediments and History of Highstands

The upper part of the lacustrine sequence is exposed in the walls of numerous deflation basins that dot the Estancia valley floor (Figure 1) and includes sediments ranging in age from the time of the last glacial maximum in North America to the desiccation of the lake just prior to the Holocene. Major oscillations in the extent of Lake Estancia during the

In K.T. Redmond, Editor, 1992. Proceedings of the Eighth Annual Pacific Climate (PACLIM) Workshop, March 10-13, 1991: California Department of Water Resources, Interagency Ecological Studies Program Technical Report 31.

latest Pleistocene are recorded in the central part of the basin as alternating intervals of bioturbated and thinly-bedded to laminated sediment. Two major highstands of Lake Estancia are represented in the upper ~5 meters of the basin-center sequence. Radiocarbon dates obtained from organic material deposited in the central part of the basin (Bachhuber 1989; Allen 1991) provide time control for this part of the lacustrine sequence. A "glacial maximum" highstand occurred from about 20,000 years BP until about 15,600 years BP (uncorrected ^{14}C years), resulting in the highest set of well-developed shorelines on the valley floor. Following a relatively brief, sudden drop in lake level, centered at about 15,000 years BP, the perennial lake expanded again at about the same time that lakes in the Great Basin experienced their highest levels in the latest Pleistocene (Benson *et al* 1990).

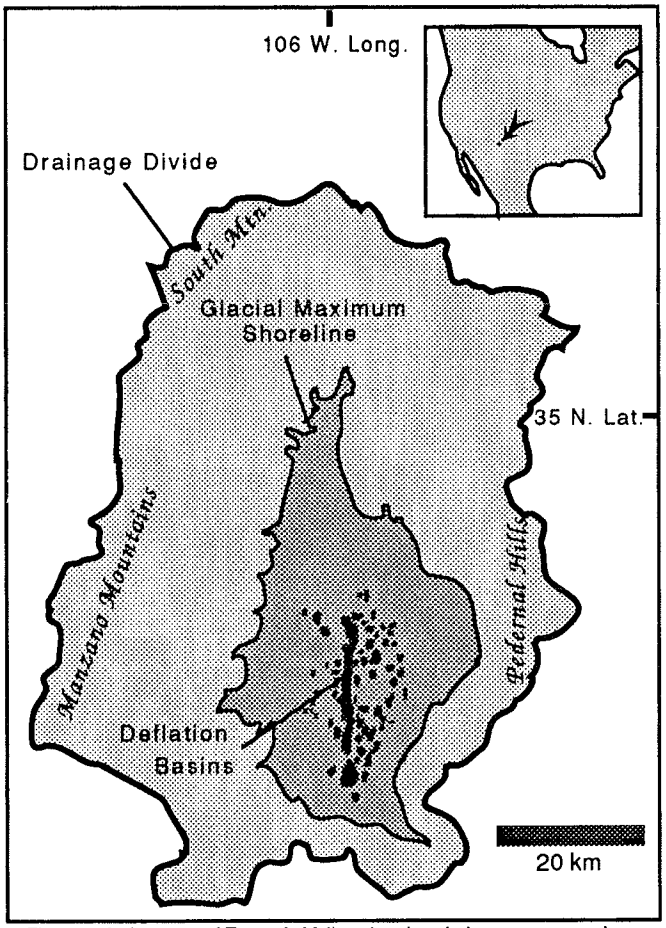

Figure 1. Index map of Estancia Valley showing drainage area, modern deflation basins, and largest extent of Lake Estancia during the glacial maximum highstand.

The sediment deposited in Lake Estancia is a marly clay rich in silt- and sand-sized gypsum. Ostracode valves are extremely abundant in most of the glacial maximum highstand sequence, as are a variety of other biotic components (Bachhuber 1971). Although the sediments deposited during the glacial maximum highstand are bioturbated, the degree of mixing is small and closely spaced samples reveal variability in several components that reflect freshening and expansion and contraction of the lake. Time series for detrital quartz, relative percent gypsum, and relative abundance of various ostracode species illustrate the century-scale oscillations recorded in Estancia sediments.

Detrital Quartz

Relative abundance of detrital quartz was determined from grain counts of the medium sand-sized fraction. A plot of the detrital quartz time series shows three episodes of increased quartz content, each consisting of two peaks in abundance. The average period for major episodes is about 2000

years, with about 200 years elapsing between separate events within the same major episode (Figure 2).

The first two episodes of increased quartz abundance coincide with a marked increase in abundance of the ostracodes *Cytherissa lacustris* and *Candona caudata* (first episode) and *Limnocythere ceriotuberosa* (second episode). Appearance of these ostracode species suggests freshening of the lake relative to intervening periods when *Limnocythere staplini* and *Candona rawsoni*, more saline-tolerent species (Delorme 1989, Figure 2), dominate the ostracode assemblage.

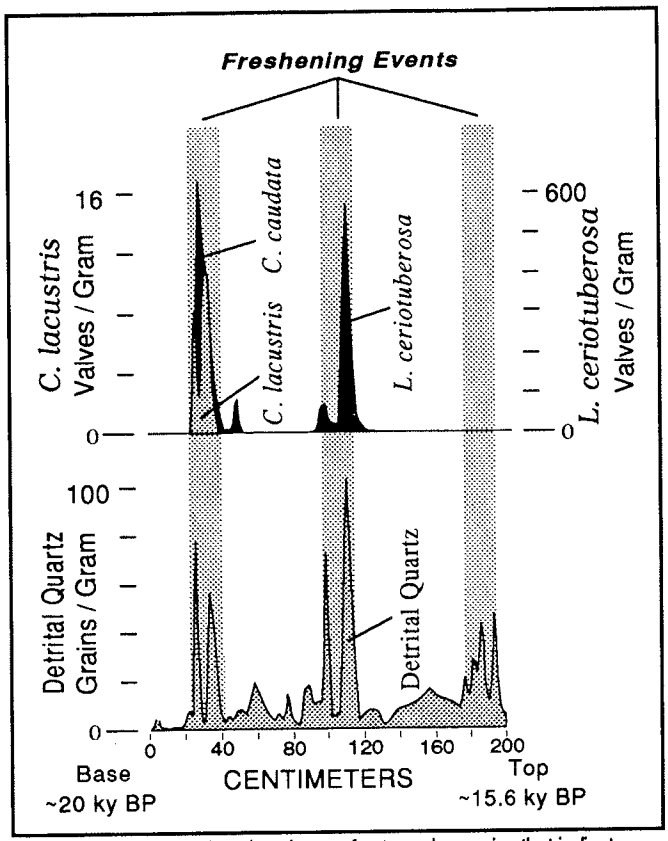

Figure 2. (Top) Relative abundance of ostracode species that indicate events of freshening.
(Bottom) Relative abundance of detrital quartz grains, believed to reflect brief episodes of runoff from the drainage.

Gypsum

Sand- and silt-sized gypsum deposited in Lake Estancia originated as gypsum crystals growing in shallow muds around the margins of the lake (Allen 1991). These crystals were transported to the central part of the lake by currents and winds. This interpretation is supported by comparison of gypsum abundance between laterally equivalent basin-center and near-shore samples. For example, sediments from the *C. lacustris* zone in the central part of the basin contain virtually no gypsum, whereas the sand-sized fractions from the biostratigraphically near-shore equivalent are domi-

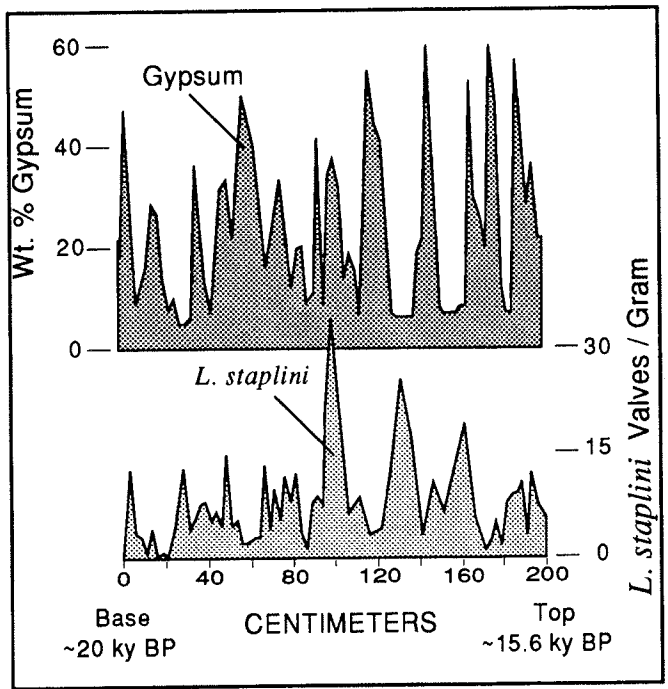

Figure 3. (Top) Relative abundance of detrital gypsum.
(Bottom) Relative abundance of *Limnocythere staplini*.
Note: ~600-year cycles in abundance of gypsum and *L. staplini*.

nated by gypsum. Stratigraphic variations in the percentage of gypsum contained in the glacial maximum highstand sediments are, thus, thought to reflect the proximity of marginal mudflats (gypsum source area) to the depositional site.

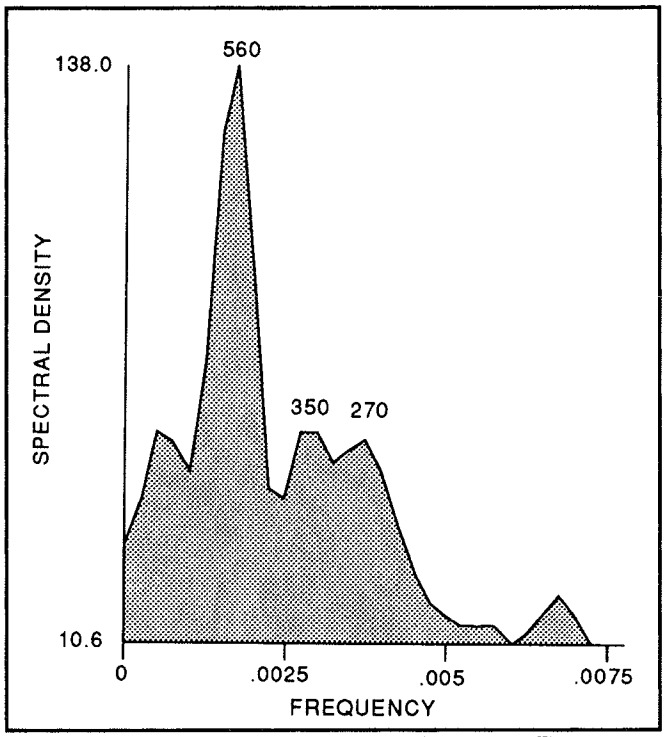

Figure 4. Power spectrum for gypsum time-series shown in Figure 3.

A time series for the weight percent of gypsum in the sediments (Figure 3) reveals repeated pulse-like increases in concentration of detrital gypsum in the central part of the basin. Spectral analysis of the gypsum time series (Figure 4) reveals a strong cycle with a period of ~600 years, with weaker periodicity between ~250 to ~350 years. The ~600 year period is especially noticeable in the younger part of the time series (Figure 3, 100 to 200 cm), and higher frequencies appear in the older half (Figure 3, 0 to 100 cm).

Ostracodes — *Limnocythere staplini*

Cycles of about 600 years, reflected in the abundance of gypsum, can also be recognized in the abundance of the ostracode *L. staplini* (Figure 3). Comparison of *L. staplini* abundance with the percent gypsum time series (Figure 3) shows a nearly inverse relationship between 100 and 190 cm, suggesting that increases in abundance of the ostracode species reflect, in part, lower sedimentation rates between episodes of gypsum influx (dilution effect). Episodes of more favorable water chemistry in the lake also may have contributed to relative increases in abundance of *L. Staplini*, as suggested by its independence from gypsum in the older half of the record.

Discussion

The association between detrital quartz and ostracode abundance (Figure 2) indicates the large pulses in detrital quartz correspond to periods of freshening. We attribute the freshening events that introduced quartz grains into the basin to episodes of surface runoff from the surrounding drainage basin. Major episodes of detrital quartz influx are separated by ~2000 years, suggesting millenial-scale climatic cycles were responsible for maintaining highstands in Lake Estancia during the last glacial

maximum. Our reconstruction shows that, within these larger ~2000-year episodes, freshening occurred in brief pulses separated by ~200 years.

Because flux of detrital gypsum is related to proximity of the sampling locality to the near-shore environment it implies that fluctuations in the gypsum time series record similar oscillations in lake level. Although gypsum content cannot yet be used to quantitatively determine the magnitude of these oscillations, the record reveals ~600-year changes in lake-level in addition to the ~200- and ~2000-year cycles that are reflected in detrital quartz and ostracode abundance. Although changes in abundance of *L. staplini* may reflect either dilution effects or absolute abundance, both responses imply changes in the extent and volume of the lake, but these changes were not accompanied by freshening events of the same magnitude as those responsible for the introduction of detrital quartz.

The timing of major, millenial-scale changes in lake level in Estancia Valley is similar to the record from other paleo-lakes at comparable latitudes (Allen and Anderson 1989) and supports the hypothesis that southerly displacement of the polar jetstream by the North American ice sheet brought increased precipitation and "pluvial" conditions to the western United States (Benson and Thompson 1987). The major high-stand of lakes in the northern Great Basin at ~14,000 years BP (Benson *et al* 1990) is matched by a highstand at Estancia, although not as high as its glacial maximum highstand. The highest stand of Lake Estancia during the glacial maximum suggests the mean position of the jetstream may have been positioned over the Estancia basin during the last glacial maximum and then may have migrated north with the decay of the North American ice sheet.

Although positioning of the polar jetstream over the Estancia basin may be explained by the growth and decay of the ice sheet, it is not clear that the expansion and contraction of Lake Estancia in cycles of ~2000 years is directly related to the ice sheet. It is even less likely that the centennial-scale oscillations are directly related to the growth and decay of the ice sheet, and these cycles suggest there are other controls on the routing of moisture from the Pacific Ocean. Additional high-resolution paleoclimatic reconstructions from climatically sensitive sites will be needed to test the regional extent of the centennial- and millenial-scale changes in the Estancia record.

Acknowledgments

This work was supported by the National Science Foundation through grant EAR-9019134.

References

Allen, BD, 1991. *Effect of climatic change on Estancia Valley, New Mexico: Sedimentation and landscape evolution in a closed-drainage basin.* New Mexico Bureau of Mines and Mineral Resources Bulletin 137. p.166-171.

Allen, BD, and RY Anderson, 1989. Decadal to millennial climate variability in lacustrine deposits from central New Mexico (abs). *EOS.* 70:1129.

Bachhuber, FW, 1989. The occurrence and paleolimnologic significance of cutthroat trout (*Onchorhynchus clarki*) in pluvial lakes of the Estancia Valley, central New Mexico. *Geological Society of America Bulletin.* 101:1543-1551.

_____, 1971, *Paleolimnology of Lake Estancia and the Quaternary history of the Estancia Valley, central New Mexico* (Ph.D. dissertation). Albuquerque:University of New Mexico.

Benson, LV, DR Currey, RI Dorn, KR Lajoie, CG Oviatt, SW Robinson, GI Smith, and S Stine, 1990. Chronology of expansion and contraction of four Great Basin lake systems during the past 35,000 years. *Palaeogeography, Palaeoclimatology, Palaeoecology.* 78:241-286.

Benson, LV, and RS Thompson, 1987. The physical record of lakes in the Great Basin. Pgs. 241-260 in WF Ruddiman and HE Wright Jr (Eds.), *The geology of North American, Vol. K-3, North America and adjacent oceans during the last deglaciation.:* Boulder, CO:Geological Society of America.

Delorme, LD, 1989. Methods in Quaternary Ecology; 7. Freshwater ostracodes. *Geoscience Canada.* 16:85-90.

Radiocarbon Record of Solar Variability and Holocene Climatic Change in Coastal Southern California

Owen K. Davis, John Jirikowic, and Robert M. Kalin

Abstract: The tree-ring calibration of radiocarbon dates may provide a chronology for high-frequency global climatic change. Large (~10 parts per mil) Δ-^{14}C excursions in tree-ring series from North America, Great Britain, and Germany are associated with brief, intense cold periods throughout the Holocene. The coincidence of cold periods and Δ-^{14}C anomalies first was suggested by deVries (1958) for the Little Ice Age. Schmidt and Gruhle (1988) have combined dendrochronologic analysis and radiocarbon dating to demonstrate coincident cool/wet climate and increased ^{14}C production during the Homeric (880-600 BC) and Greek (460-260 BC) minima. Many sites in western North America record cold/wet climate at this time. Pollen analysis and 5 radiocarbon dates for a 687-cm core provide a detailed chronology of environmental change for San Joaquin Marsh at the head of Newport Bay, Orange County, California. Sediment deposition kept pace with sea level rise during the mid-Holocene, but after 4500 years BP, sea water regularly reached the coring site, and salt marsh was the local vegetation. Brief periods of dominance by fresh-water vegetation 3800, 2800, 2300 and after 560 years BP correlate global cooling events and (except the 3800-year BP event) with ^{14}C production anomalies. The coincidence of climate change and ^{14}C anomalies support a causal connection with solar variability, but regardless of the causal mechanism(s) the Δ-^{14}C curves provide a chronology for global, high-frequency climatic change comparable to that of Milankovitch cyclicity for longer time scales.

Basis of Radiocarbon Dating

Since its inception in the 1950s (Libby 1955), radiocarbon dating has been the primary method for dating late Pleistocene and Holocene environmental change. A basic tenet of this technique is that the ratio of $^{14}C/^{12}C$ and, therefore, the production of the ^{14}C has remained nearly constant through time. Unstable ^{14}C isotopes are produced by the $^{14}N(n,p)^{14}C$ reaction in the upper atmosphere, resulting from cosmic ray bombardment. Libby's (1955) preliminary analyses indicated production of ^{14}C was nearly constant. Subsequent studies have shown a pattern of exceptions to constant formation.

Tree-Ring Calibration of Radiocarbon Dates

The most detailed examination of changes in the $^{14}C/^{12}C$ ratio has come from painstaking radiocarbon dating of tree rings (Stuiver and Pearson 1986; Pearson and Stuiver 1986; Pearson *et al* 1986; Linick *et al* 1985; Stuiver *et al* 1986; Kromer *et al* 1986; Linick *et al* 1986). Carefully aged tree-ring samples are ^{14}C dated in 20-year, 10-year, or smaller increments. These meticulous studies, beginning with deVries (1958), show

In K.T. Redmond, Editor, 1992. Proceedings of the Eighth Annual Pacific Climate (PACLIM) Workshop, March 10-13, 1991: California Department of Water Resources, Interagency Ecological Studies Program Technical Report 31.

the $^{14}C/^{12}C$ ratio has varied through time and also show the effects of atomic bomb testing (^{14}C dates too young), the industrial revolution (^{14}C dates too old), and earlier fluctuations in the $^{14}C/^{12}C$ ratio. Prior to the industrial revolution, radiocarbon dates are older than tree-ring ages from 700-2400 years BP (^{14}C years Before Present) and younger than tree-ring ages in samples older than 2400 years BP. The ^{14}C fluctuations are global in extent, and the Δ-^{14}C curves have been reproduced for western North America, Great Britain, and Germany (Stuiver and Kra 1986).

Causes of Radiocarbon Anomalies

Several factors affect the $^{14}C/^{12}C$ ratio, on a variety of time-scales (Damon *et al* 1978). The atmospheric concentration of CO_2 is known to vary from 200 to 300 ppmv during glacial/interglacial climatic cycles (Neftel *et al* 1982; Barnola *et al* 1987; Genthon *et al* 1987) and to vary by 20 ppmv on an annual basis (Keeling *et al* 1989). Both global biomass fluctuations and changes in oceanic circulation have been implicated in atmospheric CO_2 oscillations. Because ^{12}C is by far the more abundant isotope, the $^{14}C/^{12}C$ ratio is less sensitive to CO_2 fluctuations in the atmosphere than to changes in ^{14}C production.

The production of ^{14}C is modulated by effects of Earth's magnetic field and by the solar wind on the rate of cosmic ray bombardment of nitrogen. A strong geomagnetic field deflects cosmic rays and, therefore, reduces the rate of ^{14}C production. Geomagnetic modulation probably is responsible for the long-term (tens of millennia) deviation of ^{14}C dates from tree-ring ages. Stuiver *et al* (1991) suggested it also could be responsible for fluctuations on shorter (millennium) time scales.

A strong solar wind (*ie*, an active sun) also may deflect cosmic rays and decrease ^{14}C production. Solar activity typically is implicated in high-frequency (century to decade) changes in the $^{14}C/^{12}C$ ratio (Stuiver and Braziunas 1988). The timing and magnitude of the Δ-^{14}C fluctuations match the record of cosmogenic ^{10}Be in ice cores at high frequencies (Beer *et al* 1988), so solar forcing is supported.

Periodicity of Radiocarbon Anomalies and Climatic Change

Stuiver and Braziunas (1988) and Hood and Jirikowic (1990) have shown that the high-frequency (century) ^{14}C cycles are similar to one another. Figure 1 shows correlation of Δ-^{14}C values to those of the 2850-2650 BC anomaly (the "Homeric Minimum"; see below). Note that groups of peak correlations (p>95%) recur at 2000-3000 year intervals. The pattern formed by the ^{14}C anomalies is commonly referred to as "Suess wiggles", and the periodicities of these variations is close to that of sunspot cycles: the 200-year cycle (Schove 1955, 1980), the 88-year Gleissberg cycle

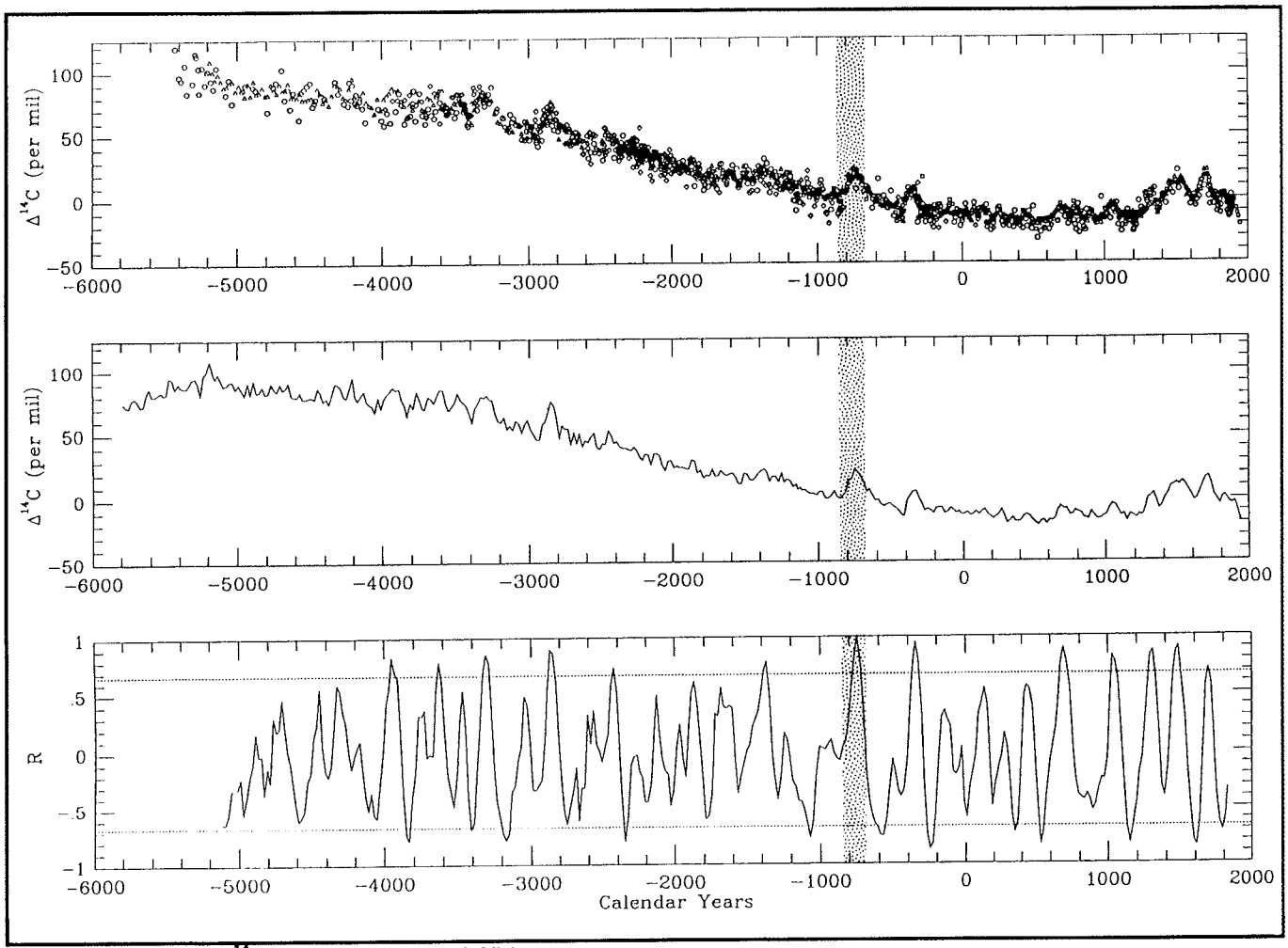

Figure 1. Correlation of Δ-^{14}C anomalies to the Homeric Minimum.
A. Raw Δ-^{14}C determinations. Symbol shapes indicate geographic origin of tree-ring samples: Circle=Suess (1978), Box=Stuiver and Becker (1986), Triangle=Pearson and Stuiver (1986), Solid Box=Linick *et al* (1985).
B. Raw data smoothed by 10-year Gaussian average.
C. Pearson correlation of a moving 200-year window to 200-year interval during the Homeric Minimum (shaded).

Table 1
Periodicities Resulting from Spectral Analysis of the Tree-Ring Calibration of ^{14}C Dates and Spectral Analysis of Ice Cores and Lake Cores

	RADIOCARBON					ICE CORE	LAKE SEDIMENTS	
Sunspot	Sonett	Sonett	Stuiver	Damon	Houtermans	Dansgaard	Halfman	Anderson
Cycle	1990	1990	et al	& Linick	et al	et al	et al	1991
Names	MEM	DFT	1991	1986	1971	1984	1988	
				11,300				
	2241	**2272**	**2014**	**2400**	**2350**	**2000**		
				1200	1300			
	805	909-649	951-720	800				
	504		512		600	540		
	385		444		420			
	232		229				280	
	208	**207**	**208**		**210**	**181**	**195**	**200**
		149	155-147				160	
			130-123	100			98	
Gleissberg	**88**	**88**	**88**	**80**		**78**	**78**	
								50-40
Hale								22
Schwabe			11					

(Gleissberg 1958), the 22-year Hale cycle (Schove 1980), and the 11-year Schwabe cycle (Povince 1983).

The exact lengths of the radiocarbon cycles vary slightly with the mathematical technique used (Sonett 1990), but certain frequencies (*eg*, 2400, 208, and 88 years) are common to nearly all analyses (Table 1). However, time series analysis by Thomson (1990), indicates the 2400-year cycle is categorically different from the shorter cycles (*ie*, the 208-year cycle).

Climate cycles of lengths similar to those of Δ-^{14}C series support the radiocarbon/climate connection. The 2500-year climatic cycle has been detected in many studies of marine and lacustrine sediment and ice cores (DeDeckker *et al* 1991; Shuti and Yujiang 1990; Pestiaux *et al* 1987; Starkel 1987; Dansgaard *et al* 1984; Schnitker 1982; Benoist *et al* 1982; Pisias 1983; Pisias *et al* 1973). Indeed, 2500 years is the fundamental division of the European Environmental sequence (*ie*, Blytt-Syrnander sequence; Iversen 1973). The 208- and 88-year cycles appear in spectral analysis of varved sediment sequences (Halfman *et al* 1988; Anderson 1991) and in the Greenland ice core 18O/16O record (Dansgaard *et al* 1971).

Documenting the Radiocarbon/Climate Connection

The connection between ^{14}C and climate first was postulated by deVries (1958) and was developed by Suess (1965), Damon (1968), Eddy (1977), and Stuiver (1965). Suess (1965) and deVries (1958) noted the correspondence between reduced ^{14}C production, colder global climate, and reduced solar activity during the Maunder (sunspot) Minimum, AD 1645-1715, when several lines of evidence indicate reduced solar activity by about 0.1% (Eddy 1976; Lean 1991), and global temperature was ~1°C less than today (Grove 1988). During the Maunder and other Little Ice Age sunspot minima (Dalton AD 1805-1835, Sporer AD 1400-1510, and Wolf AD 1290-1350), the radiocarbon content of the atmosphere was ~10 parts per mil greater than background values. Earlier ^{14}C production maxima correlate with Holocene glacial advances (Eddy 1977). However, Lamb (1977, Appendix) and Pittock and Shapiro (1982) note the many failures to use sunspot cycles to forecast climate.

A convincing connection between cool/wet climate and increased ^{14}C production 750-200 BC has been made by Schmidt and Gruhle (1988) using climatic reconstructions from and radiocarbon dating of the same tree-ring series.

Holocene cold periods are difficult to associate conclusively with the brief (100-year) ^{14}C production anomalies due to the relative imprecision of dating for sedimentary sequences. However, the correlation of climate change and ^{14}C production must be tested. Regardless of the causal mechanism(s) (solar, climatic, geomagnetic), the Δ-^{14}C curves provide a chronology for global, high-frequency climatic change. That is, 10 parts

per mil Δ-^{14}C excursions are associated with brief, intense cold periods from throughout the Holocene. Complete understanding of the process awaits further theoretical development, but development of explanatory mechanisms must proceed from careful empirical examination of the relationship between ^{14}C fluctuations and climatic change.

Naming ^{14}C Anomalies

Names given to ^{14}C production anomalies are informal and vary among authors, but the names are useful because their ages vary slightly among Δ-^{14}C records and among authors. Although ^{14}C production increases during sunspot minima, the positive anomalies are referred to as "Minima" due to the ^{14}C/sunspot correlation made by Eddy (1977) for the Little Ice Age. Little Ice Age sunspot minima and ^{14}C anomalies are named for solar astronomers, and early Neoglacial ^{14}C production maxima are named for "the general historical period in which the apparent anomaly falls" (Eddy 1977 p. 183).

Eddy simply numbers minima earlier than 1 AD, but Landscheidt (1987) names four of these anomalies: Greek (460-260 BC), Homeric (880-600 BC), Egyptian (1400-1200 BC), and Sumarian (3390-3190 BC) minima. Schmidt and Gruhle (1988) refer to the Homeric and Greek minima together as the Hallstattzeit (705-200 BC) Minimum (= Hallstatt Period or Early Iron Age; Brooks 1949 pp. 337-356). The ^{14}C anomaly 660-770 AD is called the "Medieval Minimum" by Eddy (1977), but Hood and Jirikowic (1990) use the same name for the 940-1140 AD anomaly. The names given to minima in Figure 2 follow Eddy's (1977) precedence; *ie*, Little Ice Age minima are named for astronomers and earlier minima are named for cultural periods and events.

Late Holocene Climate of California

High-resolution chronologies of climate in California generally record cold climate during radiocarbon minima, but certain cold periods lack minima. The analysis of radiolarian assemblages in varved sediments of the Santa Barbara Basin indicate fluctuations of winter (February) sea surface temperature by 12°C with cold periods 3850-3750 (no ^{14}C anomaly), 2830-2550 (Homeric), and 650 (Wolf) years ago (Pisias 1978). In the Campito Mountain tree-ring chronology (LaMarche, 1978), the period 2900-2300 years BP (Homeric) is a cold interval with generally narrow rings. Later, brief periods with very narrow rings occur 1140-1060 (Roman), 560-540 (Sporer), and 340 (Maunder) years BP. Cold climate during the Little Ice Age and Homeric-Greek ^{14}C minima are well represented in the California climate record.

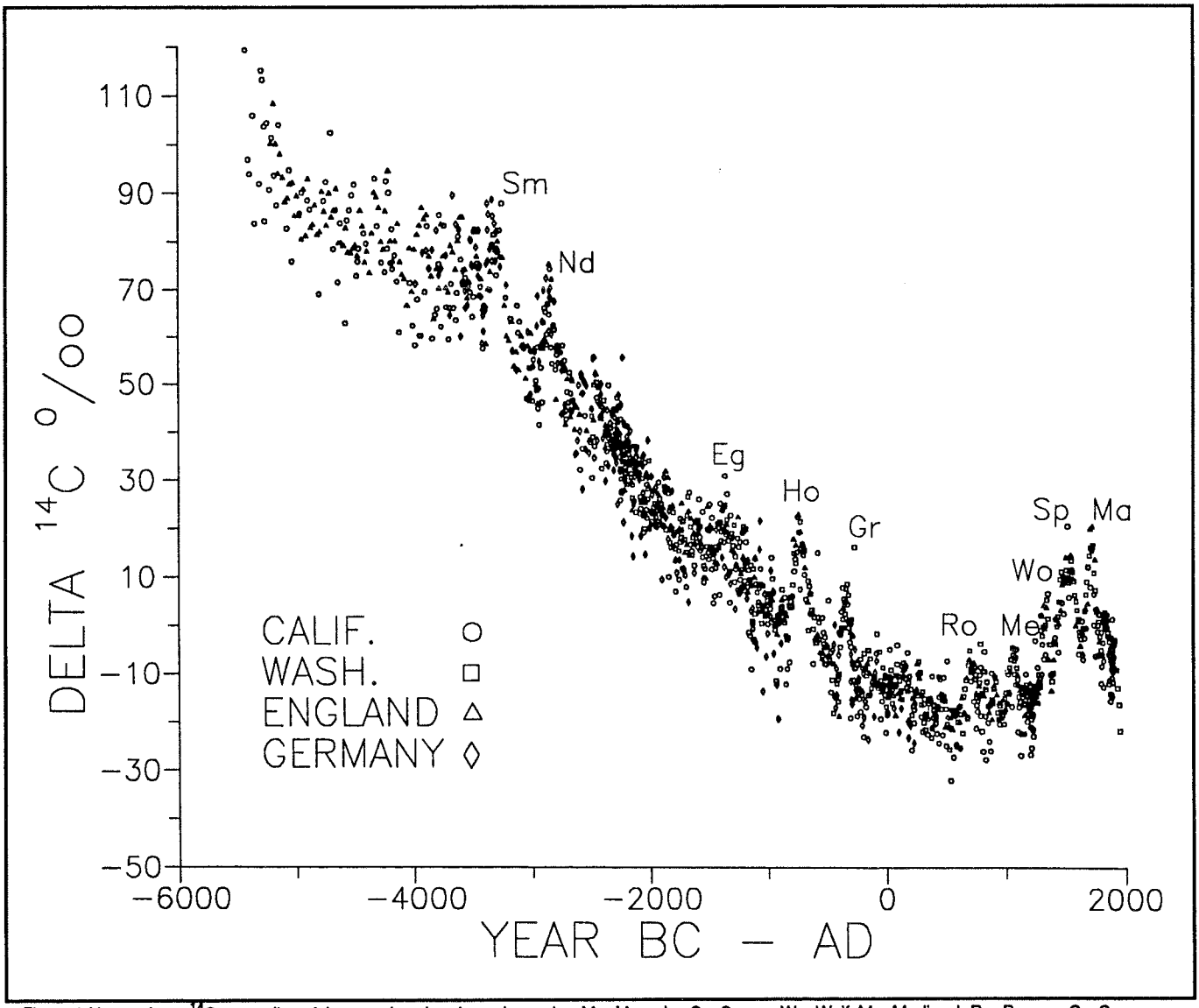

Figure 2.Names for Δ-^{14}C anomalies of the tree-ring-dated wood samples. Ma=Maunder, Sp=Sporer, Wo=Wolf, Me=Medieval, Ro=Roman, Gr=Green, Ko=Homeric, Eg=Egyptian, Nd=Noachan deluge, Sm=Sumarian. Symbol shapes as in Figure 1 but without Linick *et al* (1986) data. Raw determinations rather than smoothed or averaged values are shown to illustrate the coherence of these determinations, made in different global regions.

San Joaquin Marsh

Pollen analysis of a coastal California marsh provides confirmation of climatic change coincident with the radiocarbon production anomalies. San Joaquin Marsh (33°39'30"N, 117°51'30"W, elev. 2-3 m) is a small (82 ha) biotic preserve 7 km from the Pacific Ocean at Newport Bay, Orange County, California (Figure 3). The marsh is underlain by clay with occasional peat layers to ~8.5 m and with sand and clay layers to 12 m (Earth Research Associates 1977). Average annual precipitation at the marsh is 300 mm, with greatest rainfall in January. Mean monthly temperature ranges from 4°C in January to 29°C in September (Gustafson 1984).

Native upland vegetation surrounding the marsh is grassland, with dry bluffs covered by coastal sage scrub. Freshwater vegetation of the marsh is dominated by cattails (*Typha* spp.) and tule (*Scirpus californicus*), with

willows (*Salix* sp.) common on dikes. Saline areas of the marsh and nearby Newport Bay are dominated by members of the Chenopodiaceae, and marsh rosemary (*Limonium californicum*) is common (Stevenson and Emery 1958).

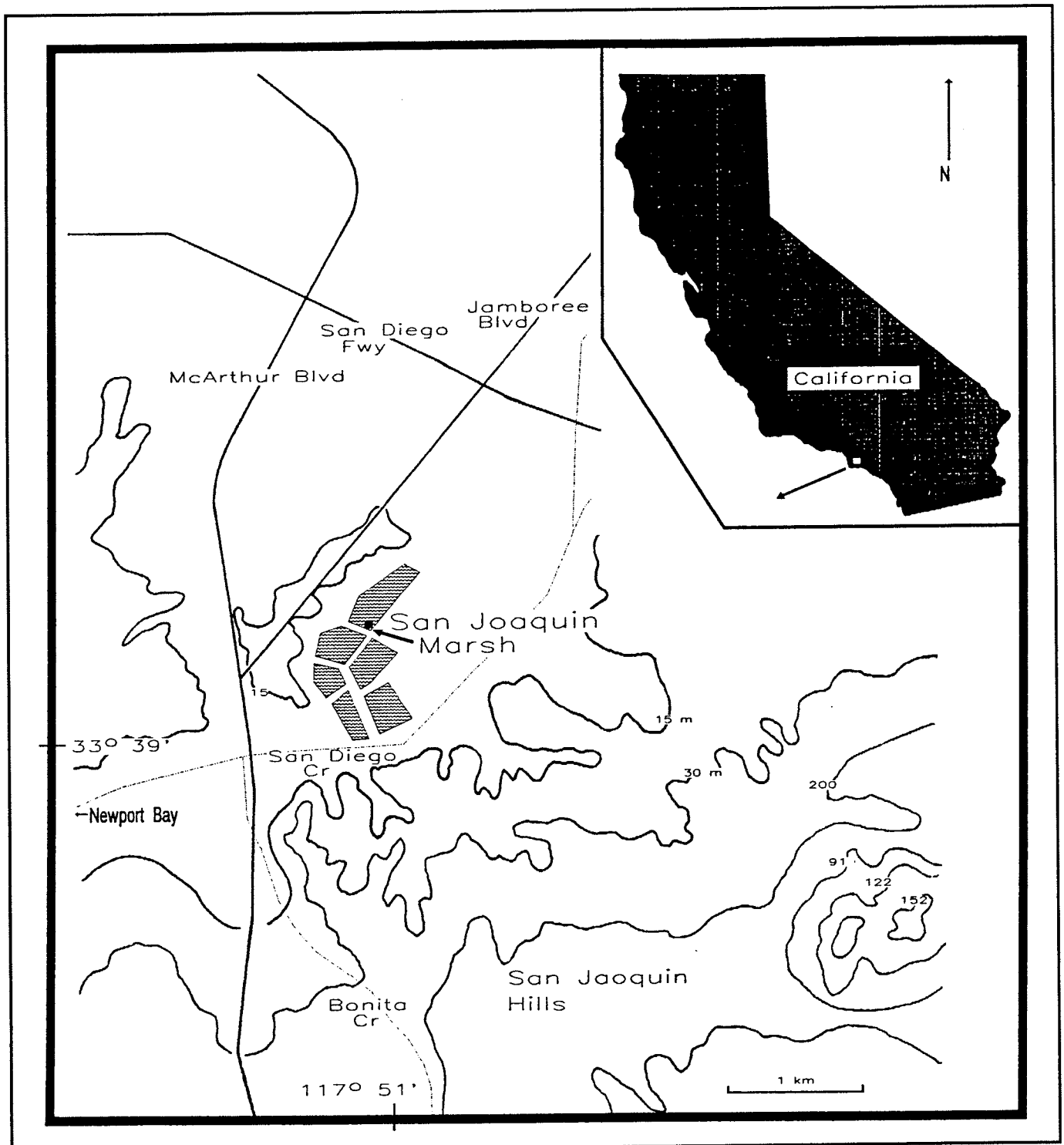

Figure 3.Map of San Joaquin Marsh area. Coring site indicated by black square; wavy pattern for water level controlled by dikes; dashed lines for San Diego and Bonita creeks; solid lines for 15-m contours and roads that influence drainage.

A 687-cm core was taken from San Joaquin Marsh in February 1989. The sediment is silty clay alternating with layers of black silty peat. Chronologic control is based on 5 radiocarbon dates, the first occurrence of the pollen of exotic taxa (AD 1776-1797), and the expansion of aquatic vegetation resulting from construction of the dikes (AD 1950).

Pollen extraction followed standard techniques for aquatic sediment (Faegri and Iversen 1975). Samples below 400 cm were filtered (Nytex(R) 3-10/3, 10-micron opening) because they contained much finely divided organic matter.

Dinoflagellates and the inner tests of foraminifera were recovered in certain samples. These are used as indicators of salt-water incursions without specific identification or additional processing of the sediment to recover calcareous foraminifera remains.

Prehistoric Change of Upland Vegetation

The percentage pollen diagram (Figure 4) is dominated by the "Other Compositae" and Chenopodiaceae-*Amaranthus* curves. Prior to ~3000 years BP, Compositae dominates (40-80%), but from ~3000 to 500 years BP it is supplanted by Chenopodiaceae-*Amaranthus* (40-70%). Chenopodiaceae-*Amaranthus* pollen is produced by xerophytic and halophytic plants in and around the marsh. West (1977) records Chenopodiaceae-*Amaranthus* up to 60% in halophytic vegetation in the Sacramento Delta

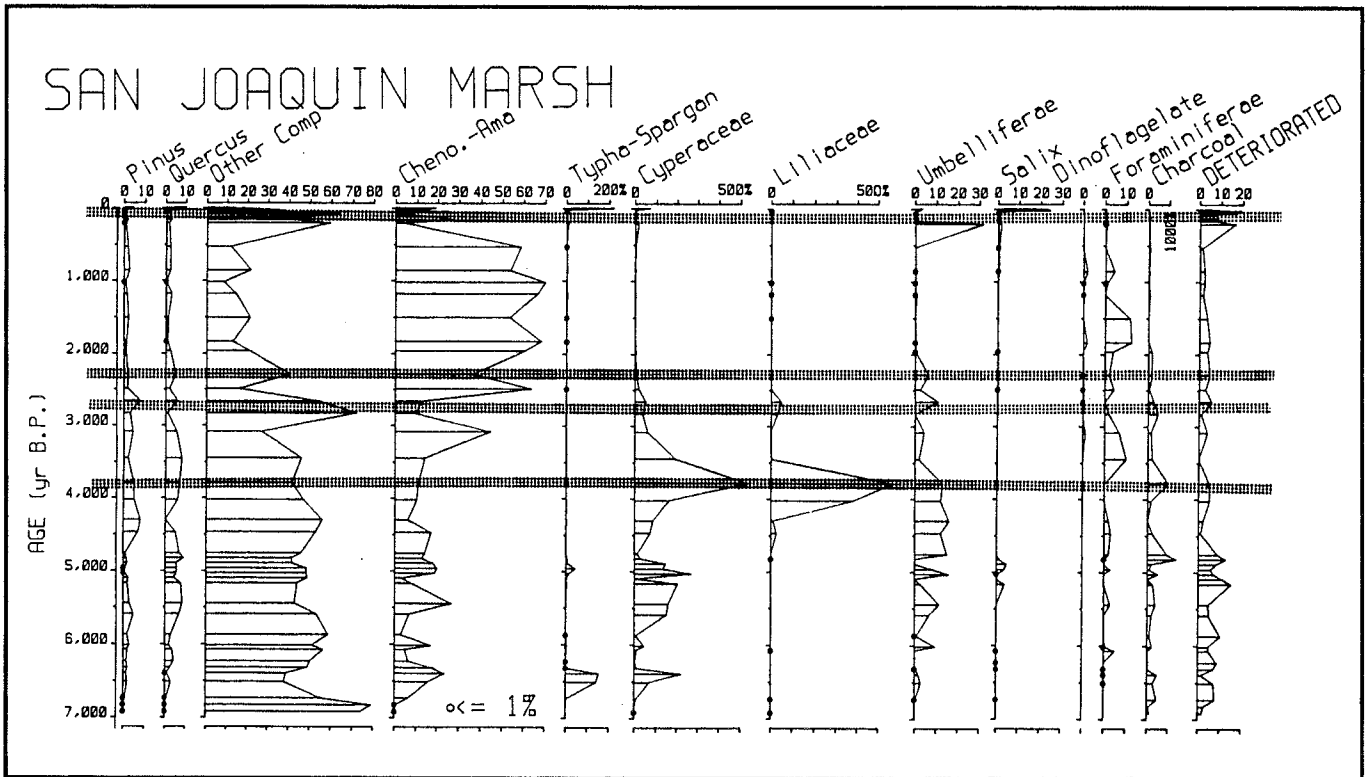

Figure 4. Percentage diagram for the pollen of selected upland and aquatic plants, marine organisms, and charcoal plotted against ^{14}C age. Percentages based on upland pollen sum. Shaded regions represent intervals of cold-wet climate corresponding to Little Ice Age (0-540 cal. BP), Greek (2450-2250 cal. BP), and Homeric (2830-2550 cal. BP) ^{14}C anomalies, and a cold-wet period (4470-3988 cal. BP) not matching a ^{14}C anomaly.

area. "Other Compositae" pollen is produced by many freshwater marsh plants (Gustafson 1984), but it also is abundant (10-40%) in California grassland (Adam 1967; Anderson and Davis 1988). Whether the source is grassland or marsh, a preponderance of Compositae pollen indicates vegetation more mesic than that characterized by Chenopodiaceae-*Amaranthus* dominance.

History of Marsh Vegetation

Prior to 4500 years BP, the pollen of sedges (*Cyperaceae*), lilies (*Liliaceae*), cattails (*Typha-Sparganium*), carrot family (*Umbelliferae*), and willows (*Salix*) documents the freshwater status of the marsh (Figure 4). Later, as sea level neared modern values, halophytic taxa dominated; Chenopodiaceae-*Amaranthus* pollen reaches 68%, and pollen of *Limonium*, a salt marsh plant, is present. Marine/estuarine organisms (dinoflagellates and foraminifera) co-occur with pollen of salt marsh plants, indicating salt water regularly reached the site.

After salt marsh became generally established, freshwater species invaded briefly while salt water was displaced by increased discharge in the watershed. These freshwater events are indicated by increased percentages in pollen of freshwater plants Cyperaceae, Liliaceae, and Umbelliferae (3800 and 2800 years BP), and by decreases of Chenopodiaceae-*Amaranthus*, dinoflagellates, foraminifera, and *Limonium* (2800, 2300, and after 560 years BP) (Figure 4). Abrupt increases of Typha-*Sparganium* and *Salix* show the effects of human management since 1950.

Discussion

The cool/wet periods at about 3800, 2800, 2300, and after 560 years BP, apparent in both the aquatic and upland vegetation (Figure 4), coincide with periods of global cooling, and (except the 3800-year-BP event) with ^{14}C production maximum. The post-560-year-BP period correlates with the Little Ice Age, the Matthes advances in the Sierra Nevada (Scuderi 1984, 1987), cooling in the White Mountains (LaMarche 1978), and reduced sea surface temperatures in the Santa Barbara Basin (Pisias 1978). The match is not exact because Scuderi (1984, 1987) lists four events in the last 500 years, but only two events (Compositae peaks at 140 and 360 years BP) are recorded at San Joaquin Marsh (Table 2).

The freshwater events at 2800 and 2300 years BP match Recess Peak advances (Scuderi 1984), but 1850 and 1100 years BP glacial advances are not recorded at San Joaquin Marsh. The 2800- and 2300-year BP events appear to be very rapid, large-scale climatic fluctuations. Many sites in western North America appear to record cold/wet climate at this time (Table 3). Conifer expansion at low elevation and increased lake levels were widespread in western North America during the Homeric

Minimum. The combined tree-ring calibrated age of this cold/wet climate is 2874-2759 cal BP, closely matching the age (2830-2550) of the ^{14}C anomaly.

Pisias (1978) estimates sea surface cooling in the Santa Barbara Basin by 3°C during the Greek Minimum, but samples dating to the Homeric

Table 2
Age of Neoglacial Climatic Events Recorded at San Joaquin Marsh and Elsewhere in California

San Joaquin Marsh ^{14}C BP, Interpolated (Dendro-corrected BP)	Sierra Nevada Glacial Events Scuderi 1984, 1987 Tree Ring Dates BP	Mono Lake High Stands Stine, 1990 (Dendro-corrected BP)	Delta ^{14}C Anomalies Stuiver & Kra, 1986 Tree Ring Dates BP
40 (290 - 0)	—	Historic High Stand (97 - 35)	Historic Minimum 70 - 40
137 (418 - 0)	Matthes Glaciation 134	—	Dalton Minimum 185 - 155
357 (540 - 0)	Matthes Glaciation 334	Clover Ranch High Stand (375 - 296)	Maunder Minimum 410 - 210
—	Matthes Glaciation 474	Danberg Beach High Stand (550 - 465)	Sporer Minimum 570 - 420
—	—	Rush Delta High Stand (680 - 605)	Wolf Minimum 745 - 620
—	—	Post Office High Stand (926 - 786)	Medieval Minimum 1020 - 880
—	—	—	Roman Minimum 1330 - 1130
2287 (2710 - 2049)	Recess Peak Glaciation 2200	—	Greek Minimum 2450 - 2250
2830 (3318 - 2749)	—	—	Homeric Minimum 2830 - 2550
3787 (4470 - 3988)	—	Dechambeau Ranch High Stand (4025 - 3608)	—

Table 3
Dates of the "Homeric Minimum" Cold/Wet Period in Western North America

Location	Age	Reference
Diamond Pond, OR	2700 ± 50 years BP	Mehringer and Wigand 1986
Rattlesnake Cave, ID	2790 ± 250 years BP	Davis *et al* 1986
Mission Cross Bog, NV	2470 ± 100 years BP	Thompson 1984
Sevier Lake, UT	2560 ± 65 years BP	Oviatt 1988
Montezuma Well, AZ	2885 ± 50 years BP	Shafer 1989
Lake Cahuilla, CA	2630 ± 120, 2600 ± 120 years BP	Waters 1989
Bonfire Shelter, TX	2780 ± 110 years BP	Bryant 1978
CALIBRATED AGE	2874-2759 cal BP - 925-810 cal BC	

Minimum could not be analyzed (a "gray layer" in the core). This cooling is comparable to Little Ice Age cooling in coastal southern California (3°C, Koerper *et al* 1985; 2°C, Pisias 1978).

The magnitude and brief duration of the Homeric, Greek, and Little Ice Age events makes them intriguing examples of rapid climatic change. Their correspondence to radiocarbon anomalies suggests a causal mechanism and permits precise dating of climate change, because the anomalies are dated by tree-rings (VanGeel and Mook 1989). The extent of the ^{14}C/climate association appears to be global. The cooling is recorded throughout western North America (Table 3) and in Europe (Nesje and Kvamme 1991; 2595±85, 2360±80 years BP), Asia (Grove 1988 p. 318; 2980±150, 2920±100 years BP), and the southern hemisphere (Hope and Petersen 1975; 2930±100, 2470±80 years BP).

Regardless of the causal mechanism(s) (solar, climatic, geomagnetic), the Δ-^{14}C curves provide a chronology for global, high-frequency climatic change. Milankovitch cycles have provided a reliable timing mechanism for climate change on long time scales during the Pleistocene (Hays *et al* 1976; Martinson *et al* 1987). The tree-ring chronology of radiocarbon anomalies can provide a similar function for the Holocene. Theoretical studies (Stuiver and Braziunas 1988; Hood and Jirikowic 1990) are needed to understand the causal mechanisms for the ^{14}C/climate association, and precise dating of climatic sequences is needed to confirm the global nature of the association and to identify any Holocene climatic fluctuations produced by other forcing functions.

Acknowledgments

We thank Dr. Philip de Barros, The Chambers Group, and The California Department of Transportation for supporting this project; Bill Bretz, Steward of San Joaquin Marsh, for permission to core the site; Bill Bretz, Henry Koerper, Kevin Moodie, and Jeanne De Lanoise for assistance in coring the marsh; and Henry Koerper, Andy Cohen, and Paul Damon for information and discussion used in preparation of this manuscript. Nicklas Pisias provided temperature data for Santa Barbara Basin, Malcolm Hughes and Lisa Graumlich provided LaMarche's tree-ring data. Supplementary pollen analyses and preparation of the manuscript were supported by NSF grants SES 8719273 and ATM-8619467

References

Adam, DP, 1967. Late Pleistocene and Recent palynology in the central Sierra Nevada, California. In EJ Cushing and HE Wright, Jr., Eds., *Quaternary Paleoecology*, Yale Univ. Press, New Haven, Conn., pp. 275-301.

Anderson, RS, and OK Davis, 1988, Contemporary pollen rain across the central Sierra Nevada, California: The relationship to modern vegetation types. *Arctic and Alpine Res.* 20:448-460.

Anderson, RY, 1991. A Solar/Geomagnetic-^{14}C-climate connection: evidence from mid-Holocene varves in a Minnesota lake. *8th PACLIM Workshop.* Tech. Report 26, Interagency Ecolog. Stud. Progr. Sacramento-San Joaquin Estuary.

Barnola, JM, D Raynaud, TS Korotkevich, and C Loris, 1987. Vostok ice core provides 16,000-year record of atmospheric CO^2. *Nature.* 329:408-413.

Benoist, JP, F Glangeaud, N Martin, JL Lacoume, C Lorius, and A Oulahman, 1982. Study of climatic series by time-frequency analysis. Pgs. 1902-1905 in *Proceedings ICASSP82.* IEEE Press:New York.

Beer, J, U Siegenthaler, G Bonani, RC Finkel, H Oescheger, M Suter, and W Wolfli, 1988. Information on past solar activity and geomagnetism from ^{10}Be in the Camp Century ice core. *Nature.* 331:675-679.

Brooks, CEP, 1949. *Climate Through The Ages.* 1st Ed. Pillans and Wilson:Edinburgh. 439 pp.

Bryant, VM Jr, 1978. Late Quaternary pollen records from the east-central periphery of the Chihuahuan Desert. In RH Wauer and DH Riskind (Eds.) *Symposium on Biological resources of the Chihuahuan Desert Region, United States and Mexico.* USDI Transactions and Proceedings. 3:3-21

Damon, PE, 1968. Radiocarbon and climate (A comment on a paper by H Suess). *Meteorological Monographs.* 8:151-154.

Damon, PE, JC Lerman, and A Long, 1978. Temporal fluctuations of atmospheric 14C: causal factors and implications. *Ann. Rev. Earth Plant. Sci.* 6:457-494.

Damon, PE, and TW Linick, 1986. Geomagnetic-Heliomagnetic modulation of atmospheric radiocarbon production. *Radiocarbon.* 28:266-278.

Dansgaard, W, SJ Johnsen, HB Clausen, and CC Langway Jr, 1971. Climatic record revealed by the Camp Century ice core. Pgs. 37-56 in KK Turekian (ed.) *The Late Cenozoic Glacial Ages.* Yale Univ Press:New Haven.

Dansgaard, W, SJ Johnsen, HB Clausen, D Dahl-Jensen, N Gundestrup, CH Hammer, and H Oescheger, 1984. North Atlantic oscillations revealed by deep Greenland ice cores. *Geophysical Monographs.* 29:288-298.

Davis, OK, JC Sheppard, and S Robertson, 1986. Contrasting climatic histories for the Snake River Plain result from multiple thermal maxima. *Quaternary Research.* 26:321-339.

DeDeckker, P, T Correge, and J Head, 1991. Late Pleistocene record of cyclic eolian activity from tropical Australia suggesting the Younger Dryas is not an unusual climatic event. *Geology.* 19:602-605.

deVries, HL, 1958. Variation in concentration of radiocarbon with time and location on Earth. *Koninkl Nederlandse Akad Wetenschappen, Proc. Ser.B.* 61:94-102.

Earth Research Associates, 1977. *Preliminary soils engineering investigation on the preservation of San Joaquin Freshwater Marsh Project.* Report to the University of California, Irvine, Office of Physical Planning and Construction.

Eddy, JA, 1977. Climate and the changing sun. *Climate Change.* 1:173-190.

_____, 1976. The Maunder Minimum. *Science* 192:1189-1202.

Faegri, K, and J Iversen, 1975. *Textbook of pollen analysis.* Hafner Press, NY. 295 pp.

Genthon, C, *et al,* 1987. Vostok ice core: climatic response to CO^2 and orbital forcing changes over the last climatic cycle. *Nature.* 329:414-418.

Gleissberg, W, 1958. The 80-year sunspot cycle. *British Astron. Assoc. Jour.* 68:148-157.

Grove, JM, 1988. *The Little Ice Age.* Methuen, London.

Gustafson, S, 1984. *San Joaquin freshwater marsh reserve.* University of California Natural Reserve System Brochure.

Halfman, JD, and TC Johnson, 1988. High-resolution record of cyclic climatic change during the past 4 ka from Lake Turkana, Kenya. *Geology.* 16:496-500.

Hays JD, J Imbrie, and NJ Shackleton, 1976. Variations in the Earth's orbit: pacemaker of the Ice Ages. *Science.* 194:1121-1132.

Hood, LL, and JL Jirikowic, 1989. Recurring variations of probable solar origin. *Geophysical Research Letters* 17:85-88.

Hope, GS, and JA Peterson, 1975. Glaciation and vegetation in the high New Guinea Mountains. In RP Suggate and MM Cresswell, Eds., *Quaternary Studies,* Royal Society New Zealand, pp. 155-162.

Houtermans, JC, 1971. *Geophysical interpretations of bristlecone pine radiocarbon measurements using a method of Fourier analysis for unequally spaced data.* PhD dissertation. University of Bern:Switzerland.

Iversen, J, 1973. The development of Denmark's nature since the last glacial. *Danmarks Geologiske Undersogelse.* 5(7C).

Keeling, CD, SC Piper, and M Heimann, 1989. A three-dimensional model of atmospheric CO_2 transport based on observed winds. 4. Mean annual gradients and interannual variations. *AGU Geoph. Mon.* 55.

Kromer, B, M Rhein, M Bruns, H Schoch-Fischer, KO Munnich, M Stuiver, and B Becker, 1986. Radiocarbon calibration data for the 6th to 8th millennia BC. *Radiocarbon.* 28(2B):954-960.

LaMarche, VC Jr, 1978. Tree-ring evidence of past climatic variability. *Nature.* 276:334-338.

Lamb, HH, 1977. *Climate history and the future.* Princeton University Press.

Landscheidt, T, 1987, Long-Range forecasts of solar cycles and climate change. Pgs. 421-445 in MR Rampino, JE Sanders, WS Newman, and LK Konigsson (eds.) *Climate History, Periodicity, and Predictability.* Van Nostrand Reinhold:New York.

Lean, J, 1991. An esitmate of the sun's photon output during the Maunder Minimum. *Abstract SH41A-3 Spring AGU Meeting.* p.224.

Libby, WF, 1955. *Radiocarbon dating.* Univ. Chicago Press.

Linick, TW, A Long, PE Damon, and CW Ferguson, 1986. High-precision radiocarabon dating of bristlecone pine from 6554 to 5350 BC. *Radiocarbon.* 28(2B):943-953.

Linick, TW, HE Suess, and B Becker, 1985. La Jolla measurements of radiocarbon in south German oak tree-ring chronologies. *Radiocarbon.* 27:20-32.

Martinson, DG, NG Pisias, JD Hays, J Imbrie, TC Moore Jr, and MG Shackleton, 1987. Age dating and orbital theory of the ice ages: development of a high-resolution 0-300,000-year chronostratigraphy. *Quaternary Research.* 27:1-29.

Mehringer, PJ Jr, and PE Wigand, 1986. Western Juniper in the Holocene, In RL Everett (ed.) *Westwide Pinyon-Juniper Conference.* U.S. Forest Service Gen. Tech. Report INT-215.

Neftel, A, H Oeschger, J Schwander, B Stauffer, and R Zumbrunn, 1982. Ice core sample measurements give atmospheric CO_2 content during the past 40,000 years. *Nature.* 295:220-223.

Nesje, A, and M Kvamme, 1991. Holocene glacier and climate variations in western Norway: Evidence for early Holocene glacier demise and multiple Neoglacial events. *Geology.* 19:610-612.

Oviatt, CG, 1988. Late Pleistocene and Holocene lake fluctuations in the Sevier Lake Basin, Utah, USA. *Journal Paleolimnology.* 1:9-21.

Pearson, GW, JR Pilcher, MGL Baillie, DM Corbett, and F Qua, 1986. High-precision ^{14}C measurement of Irish oaks to show the natural ^{14}C variations from AD 1840-5210 BC. *Radiocarbon.* 28(2B):911-934.

Pearson, GW, and M Stuiver, 1986. High-precision calibration of the radiocarbon time scale, 500-2500 BC. *Radiocarbon.* 28(2B):839-862.

Pestiaux, P, JC Duplessy, and A Berger, 1987. Paleoclimatic variability at frequencies ranging from 10^{-4} cycle per year to 10^{-3} cycle per year — Evidence for nonlinear behavior of the climate system. Pgs. 285-299 in MR Rampino, JE Sanders, WS Newman, and LK Konigsson (eds.) *Climate History, Periodicity, and Predictability.* Van Nostrand Reinhold:New York.

Pisias, NG, 1983. Geologic time series from deep-sea sediments: Time scales and distortion by bioturbation. *Marine Geology.* 51:99-113.

_____, 1978. Paleoceanography of the Santa Barbara Basin during the last 8000 years. *Quaternary Research.* 10:366-385.

Pisias, NG, JP Dauphin, and C Sancetta, 1973. Spectral analysis of late Pleistocene-Holocene sediments. *Quaternary Research.* 3:3-9.

Pittock, AB, and Shapiro, 1982. Assessment of evidence of the effect of solar variations on weather and climate. In *Solar Variability, Weather, and Climate*: National Academy Press.

Povince, P, 1983. Short-term variations in radiocarbon concentration with the 11-year solar cycle. *Radiocarbon.* 25:259-266.

Schmidt, B, and W Gruhle, 1988. Klima, Radiokohlenstoffgehalt und Dendrochronologie. *Naturwissenschafliche Rundschau.* 41(5):177-182. (Translation by T Jull).

Schnitker, D, 1982. Climatic variability and deep ocean circulation, Evidence for the North Atlantic. *Palaeo. Palaeo. Palaeo.* 40:213-234.

Schove, DJ, 1980. The 200-, 22-, and 11-year cycles and long series of climatic data, mainly since A.D. 200. Pgs. 807-100 in *Sun and Climate.* Centre National d'Etudes Spatales.

_____, 1955. The sunspot cycle, 649 B.C. to A.D. 2000. *Jour. Geophys. Research.* 60:127-146.

Scuderi, LA, 1987. Glacier variations in the Sierra Nevada, California, as related to a 1200-year tree-ring chronology. *Quaternary Research.* 27:220-231.

_____, 1984. *A dendroclimatic and geomorphic investigation of late-Holocene glaciation, southern Sierra Nevada, California.* PhD dissertation. Univ. California:Los Angeles, 247 pp.

Shafer, DS, 1989. *The timing of late Quaternary monsoon precipitation maxima in the southwest United States.* PhD dissertation. University of Arizona:Tucson. 234 pp.

Shuti, H, and Y Yujiang, 1990. Paleoclimatic variation of the Balikun Lake Region of Xinjiang during the past 35,000 years. *Acta Geographica Sinica.* 45:350-362. (Translation by D Kumai).

Sonett, CP, 1990. Atmospheric 14C variations: a Bayesian prospect. Pgs. 143-159 in PF Fougere (ed.) *Maximum Entropy and Bayesian Methods.* Kluwer Academic Publ.:Netherlands.

Starkel, L, 1987. Long-term and short-term rhythmicity in terrestrial landforms and deposits. In MR Rampino, JE Sanders, WS Newman, and LK Konigsson, Eds., *Climate: History, Periodicity, and Predictability,* Van Nostrand Reinhold Company, NY. pp. 323-332.

Stevenson, RE, and KO Emery, 1958. *Marshlands at Newport Bay, California.* University Southern Calif. Occasional Paper 20.

Stine, S, 1990. Late Holocene fluctuations of Mono Lake, eastern Calfiornia. *Palaeo. Palaeo. Palaeo.* 78:333-381.

Stuiver, M, 1965. Carbon-14 content of 18th and 19th Century Wood: Variations Correlated with Sunspot Activity. *Science.* 149:533-537.

Stuiver M, and B Becker, 1986. High-precision decadal calibration of the radiocarbon time scale AD 1950-2500 BC. *Radiocarbon.* 28(2B):863-910.

Stuiver, M, and TF Braziunas, 1988. The solar component of the atmospheric ^{14}C record, Pgs. 245-266 in FR Stephenson and AW Wolfendale (eds.) *Secular Solar and Geomagnetic Variations in the Last 10,000 Years.* Kluwer Academic Publishers:Dorchredt.

Stuiver, M, TF Braziunas, B Becker, and B Kromer, 1991. Climatic, solar, oceanic, and geomagnetic influences on late-Glacial and Holocene atmospheric 14C/12C change. *Quaternary Research* 35:1-24.

Stuiver, M, and RS Kra, 1986. Proceedings of the twelfth international radiocarbon conference - Trondheim, Norway. *Radiocarbon.* 28(2B).

Stuiver M, B Kromer, B Becker, and CW Ferguson, 1986. Radiocarbon age calibration back to 13,300 years BP and the ^{14}C age matching of the German oak and US bristlecone pine chronologies. *Radiocarbon.* 28(2B):969-979.

Stuiver, M, and GW Pearson, 1986. High-precision calibration of the radiocarbon time scale, AD 1950-500 B.C. *Radiocarbon.* 28(2B):805-838.

Suess, HE, 1978. La Jolla measurements of radiocarbon in tree-ring dated wood. *Radiocarbon.* 20:1-18.

_____, 1965. Secular variations of the cosmic-ray-produced carbon 14 in the atmosphere and their interpretations. *J. Geophys. Res.* 70:5937-5952.

Thomson, DJ, 1990. Time series analysis of Holocene climate data. *Phil. Trans. Roy. Soc. Lond. Ser.A.* 330:601-616.

Thompson, RS, 1984. *Late Pleistocene and Holocene environments in the Great Basin.* PhD dissertation. University Arizona, Tucson, 209 pp.

Van Geel, B, and WG Mook, 1989. High-resolution 14C dating of organic deposits using natural atmospheric 14C variations. *Radiocarbon* 31:151-155.

Waters, MR, 1989. Late Quaternary lacustrine history and paleoclimatic significance of pluvial Lake Cochise, southeastern Arizona. *Quaternary Research* 32:1-12.

West, GJ, 1977. *Late Holocene vegetation history of the Sacramento-San Joaquin Delta, California.* Report to Calif. Department of Parks and Recreation, Interagency Agreement B-50173.

Tree-Ring Records as Indicators of Air-Sea Interaction in the Northeast Pacific Sector

Brendan M. Buckley, Rosanne D. D'Arrigo, and Gordon C. Jacoby

Abstract: Climate conditions in land areas of the Pacific Northwest are strongly influenced by atmosphere/ocean variability, including fluctuations in the Aleutian Low, Pacific-North American (PNA) atmospheric circulation modes, and the El Niño-Southern Oscillation (ENSO). It thus seems likely that climatically sensitive tree-ring data from these coastal land areas would likewise reflect such climatic parameters. In this paper, tree-ring width and maximum latewood density chronologies from northwestern Washington State and near Vancouver Island, British Columbia, are compared to surface air temperature and precipitation from nearby coastal and near-coastal land stations and to monthly sea surface temperature (SST) and sea level pressure (SLP) data from the northeast Pacific sector. Results show much promise for eventual reconstruction of these parameters, potentially extending available instrumental records for the northeastern Pacific by several hundred years or more.

Introduction

Atmosphere-ocean interactions play an extremely important role in the climatic variability over western North America. Linkages have been demonstrated between northeast Pacific SLP and SST and other indicators of atmosphere/ocean interaction (such as the Aleutian Low Index and PNA) and climate over land (Walsh and Richman 1981; Namias *et al* 1988; Trenberth 1990; Leathers *et al* 1991). The role of the northeastern Pacific sector in large-scale climatic dynamics, including teleconnections with ENSO events, has also been well documented (Andrade and Sellers 1988; Cayan 1980; Emery and Hamilton 1985; Namias *et al* 1988; Niebauer 1988; Ropelewski and Halpert 1986).

In this paper we explore relationships between tree-ring width and maximum latewood density chronologies from the Pacific Northwest and climatic data from coastal/near-coastal land stations, as well as SST and SLP records from the northeastern Pacific sector. Previous researchers have used tree rings to model and reconstruct air/ocean parameters, including sea surface temperatures (Douglas 1980; Lough 1986), sea level pressure (Blasing and Fritts 1975) and ENSO events (Lough and Fritts 1985, 1989; Michaelson *et al* 1987). In their reconstructions, Lough and Fritts (1985, 1989) employed a grid of 65 chronologies representing a variety of species over a wide geographic area of western North America. We use an approach more similar to those of Douglas (1980) and Michaelson *et al* (1987), in which a small subset of tree-ring chronologies, found to be the most sensitive to specific variables of interest, were

In K.T. Redmond, Editor, 1992. Proceedings of the Eighth Annual Pacific Climate (PACLIM) Workshop, March 10-13, 1991: California Department of Water Resources, Interagency Ecological Studies Program Technical Report 31.

retained for final analysis. Our study represents one of the first attempts to relate North American maximum latewood density data (in addition to ring widths) to features of atmosphere/ocean circulation such as SLP and SST.

Climate and Tree-Ring Data

Four sets of climatically sensitive, maritime tree-ring chronologies of both ring width and maximum latewood density from sites in northwestern Washington State and southwestern British Columbia were selected for this study (Figure 1). Three tree species are represented: *Pseudotsuga menziesii* (Douglas fir), *Abies amabilis* (Pacific silver fir), and *Tsuga mertensiana* (mountain hemlock). The raw data were processed in Switzerland and supplied to us by Dr. Fritz Schweingruber of the Swiss Federal Institute of Forestry Research. Final chronologies (Figure 2) were developed from the raw data at the Tree-Ring Laboratory at Lamont-Doherty Geological Observatory, using standard dendrochronological techniques (Fritts 1976; Cook and Kairiukstis 1990). The common period of the eight chronologies is 1750 to 1983.

The tree-ring data were first compared to monthly temperature and precipitation instrumental records from nearby individual land climate stations, obtained from the Historical Climate Network. After screening all available nearby stations, four were averaged into a regional series: Blaine, Bellingham, Clearbrook, and Port Angeles — all in northwestern Washington (Figure 1). A monthly SST dataset for the northeastern Pacific, at 5x5 degree grid resolution and extending from 1947 to 1990, was supplied to us by Dr. D. Cayan of Scripps Institute of Oceanography. Monthly sea level pressure data, also at 5x5 degree grid resolution (available from 1899 to 1980), was obtained from Dr. K. Trenberth of the National Center for Atmospheric Research.

Response of Tree Growth to Land Climate

The climatic response of the density and ring-width series was evaluated using simple correlation and linear regression analyses. Correlations were determined between the ring width and maximum latewood density chronologies and the regionally averaged monthly temperature and total precipitation data for a 17-month dendroclimatic year (beginning in June of the year prior to growth and extending to October of the growth year) for the common period from 1903 to 1983 (Figure 3).

The maximum latewood density chronologies show a much more consistent response to land climate, across both site and species, than does ring width. For all four density series, there is a strikingly clear, positive correlation between tree growth and growing season (April through August) temperatures and a corresponding negative correlation with late growing season (June through August) precipitation. Although the ring

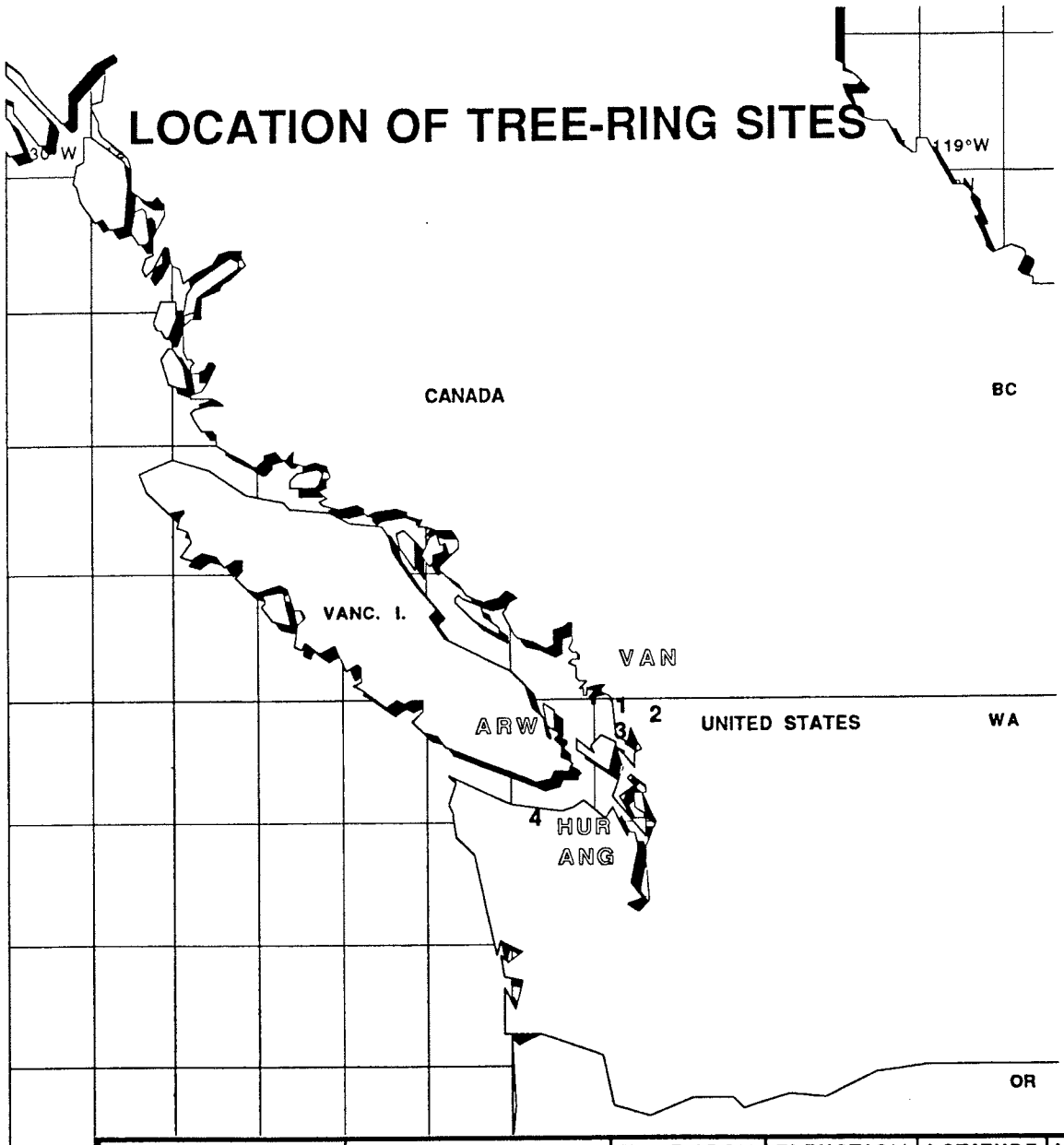

TREE RING SITES	TREE RING SPECIES	TIME SPAN	ELEVATION	LATITUDE	LONGITUDE
ARROWSMITH MTN	Tsuga Mertensiana	1629-1983	1020 M	49 09 N	125 14 W
ARW					
HURRICANE RIDGE	Abies Amabilis	1698-1983	1560 M	47 57 N	123 28 W
HUR					
MOUNT ANGELES	Pseudotsuga Men.	1750-1983	1360 M	47 58 N	123 26 W
ANG					
VANCOUVER	Tsuga Mertensiana	1413-1983	1110 M	49 20 N	123 20 W
VAN					

Figure 1. Map showing tree-ring sites in Washington state and British Columbia. Locations of climate stations are marked by numbers: 1=Blaine, 2=Clearbrook, 3=Bellingham, and 4=Port Angeles.

width/climate relationships agree qualitatively with those of latewood density, the ring width data also show a tendency for a response to growing season climate of the prior year (a negative response to temperature and a positive response to precipitation). In addition, variability in response is greater between species and between sites for ring width (see Figure 3). Thus the ring width and density data provide different types of climatic information, and both contribute to our understanding of the tree growth response to climate at these sites.

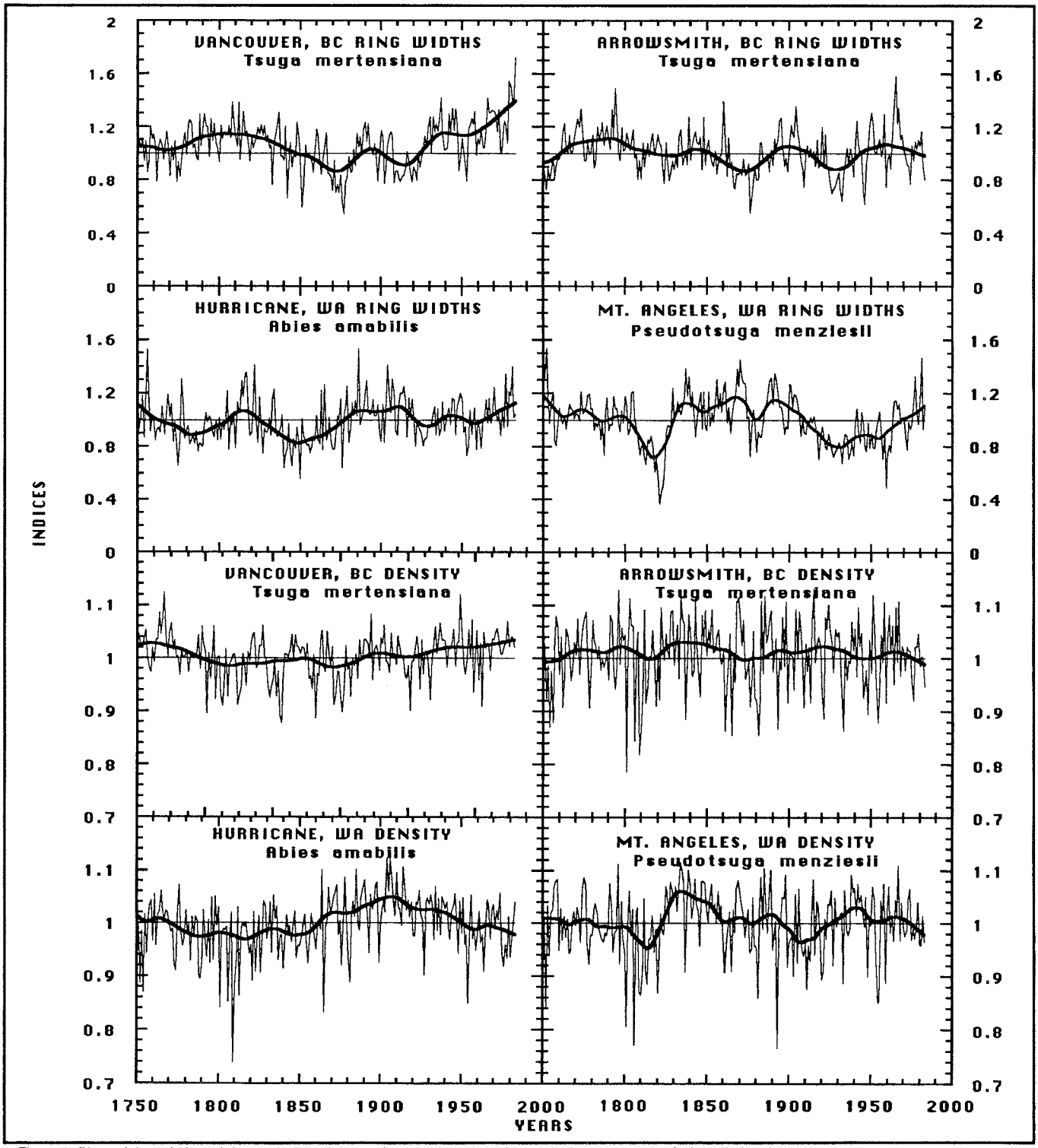

Figure 2. Plots of ring width and density indices from each of the four sites. Shown is the common period of all sites from 1750 to 1983.

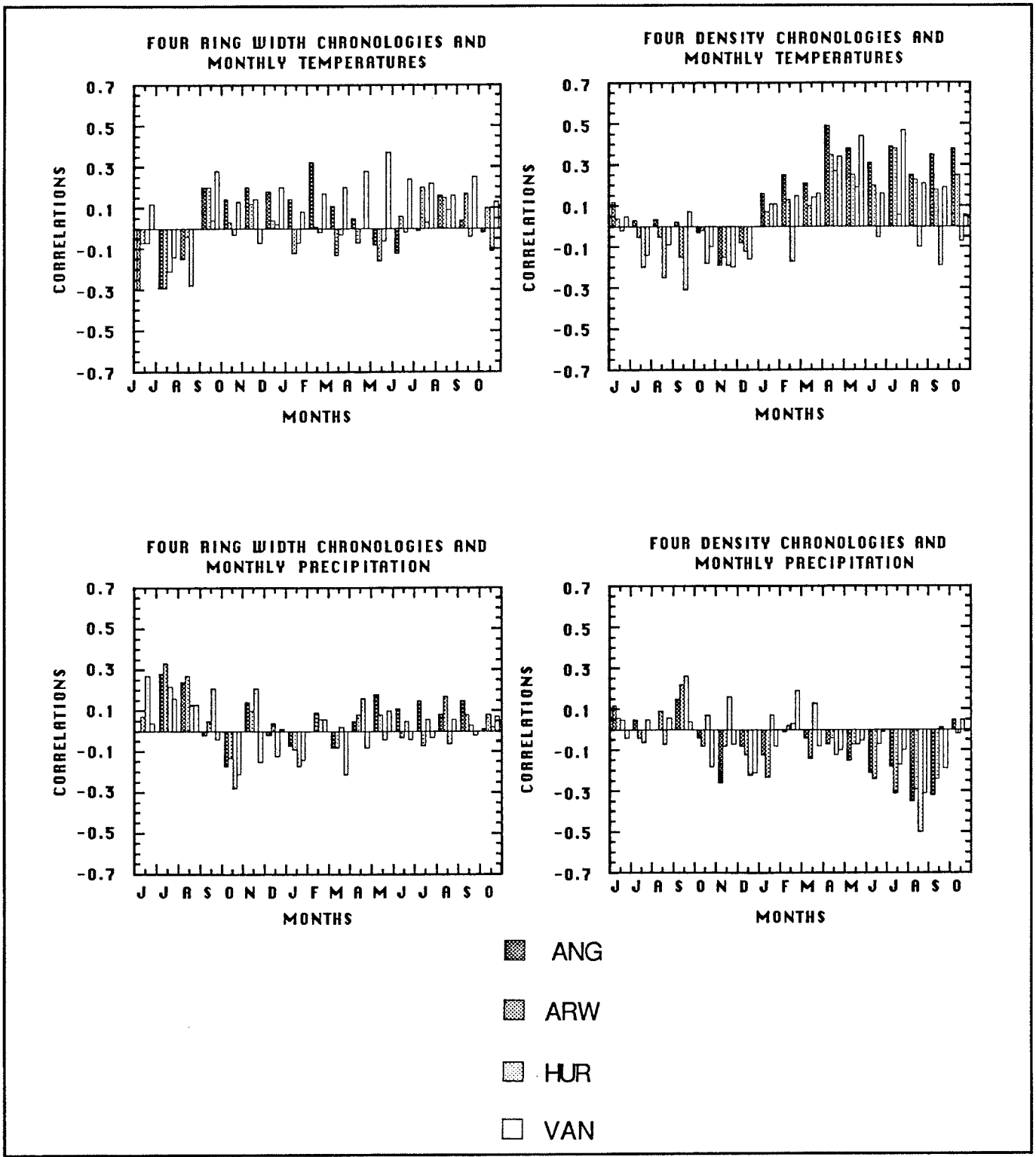

Figure 3. Bar graphs of correlations between tree growth and climate for ring width and maximum latewood density. Note the more uniform cross-species response of the density series for both temperature and precipitation and the greater prior season response for ring width. The most significant values are the positive correlation of density with spring temperature and the negative correlation of density with summer precipitation.

Land/Ocean Climate Linkages in the Northeast Pacific Sector

Previous research has determined that relationships exist between climate over the Pacific Ocean and western North America (Walsh and Richman 1981; Douglas *et al* 1982; Andrade and Sellers 1988; Emery and Hamilton 1985; Namias *et al* 1988). We analyzed the relationship between land instrumental records and northeast Pacific SST and SLP for a series of grid points ranging from 35 to 55 degrees North and 125 to 150 degrees West. The regionally-averaged land temperatures were compared with SSTs for four seasons: fall (OND), winter (JFM), spring (AMJ), and summer (JAS). The strongest correlations (positive) were found in spring and summer (Figure 4). A striking geographic pattern was found, with those SST gridpoints nearest to shore having the strongest correlations with land climate. The somewhat weaker correlations in summer might be explained by the increasing role of radiative heating and cooling of the continent during the region's dry season and also of the late-seasonal changes in circulation over the Pacific with the migration of the sun's declination, the westward displacement of the Aleutian Low, and the northward displacement of the Subtropical High.

Tree Growth and Sea Surface Temperatures

The four sets of chronologies (ring width and density data for each site) were compared to SST data for the same gridpoints as those previously compared to land temperatures (Figure 5). Overall the strongest correlations were found with summer SST. Maximum latewood density demonstrated a significant, positive correlation with summer SST, with the highest correlation at the gridpoint 45N/135W. The strength of the correlations decrease rapidly from this gridpoint in all directions, as shown in Figure 5. The ring-width chronologies show a moderately strong correlation with a zone away from shore centered on 45N, 140W, while the near-shore gridpoints show a weak, negative correlation. While the most significant gridpoint was five degrees farther west than that for density, the ring-width correlations were still strongly positive for 45N/135W. It was, therefore, determined that the strongest relationship overall is between summer SSTs for 45N/135W, and combined maximum latewood density and ring width data.

Summer SST at gridpoint 45N/135W was estimated using two density chronologies and one ring-width chronology (which showed the strongest correlations) as predictors in linear regression analysis for the common period from 1947 to 1983 (Figure 6). Agreement is good between the recorded and estimated SSTs, with 42% variance explained (adjusted for degrees of freedom). However, the relationship appears to break down in the late 1960s and into the 1970s.

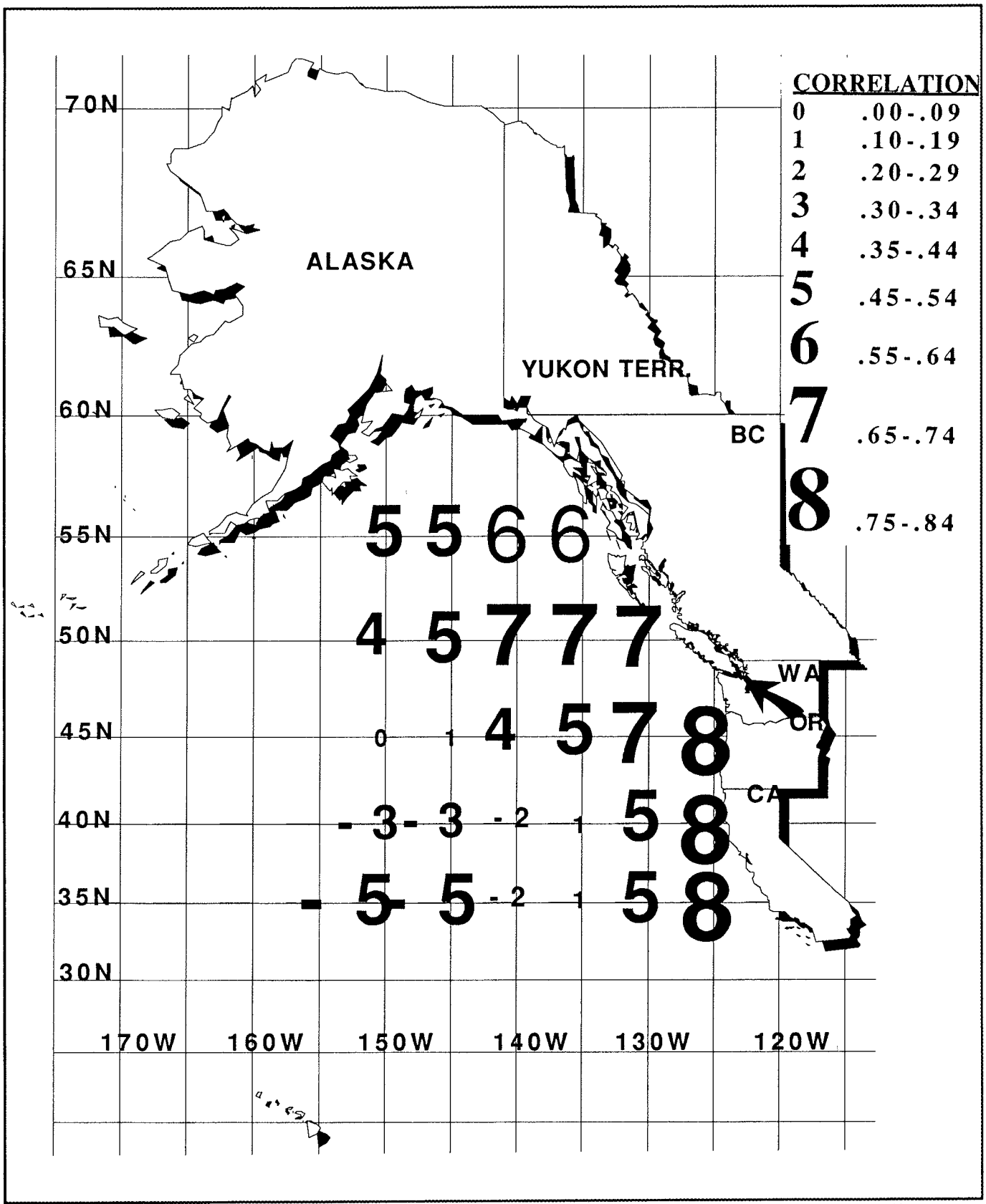

Figure 4. Map showing areal correlation between regional spring temperature (AMJ) for the selected climate stations (indicated by the arrow) with sea surface temperatures for the same period. Note the very strong correlations with SST along the coast and northwestward into the Gulf of Alaska.

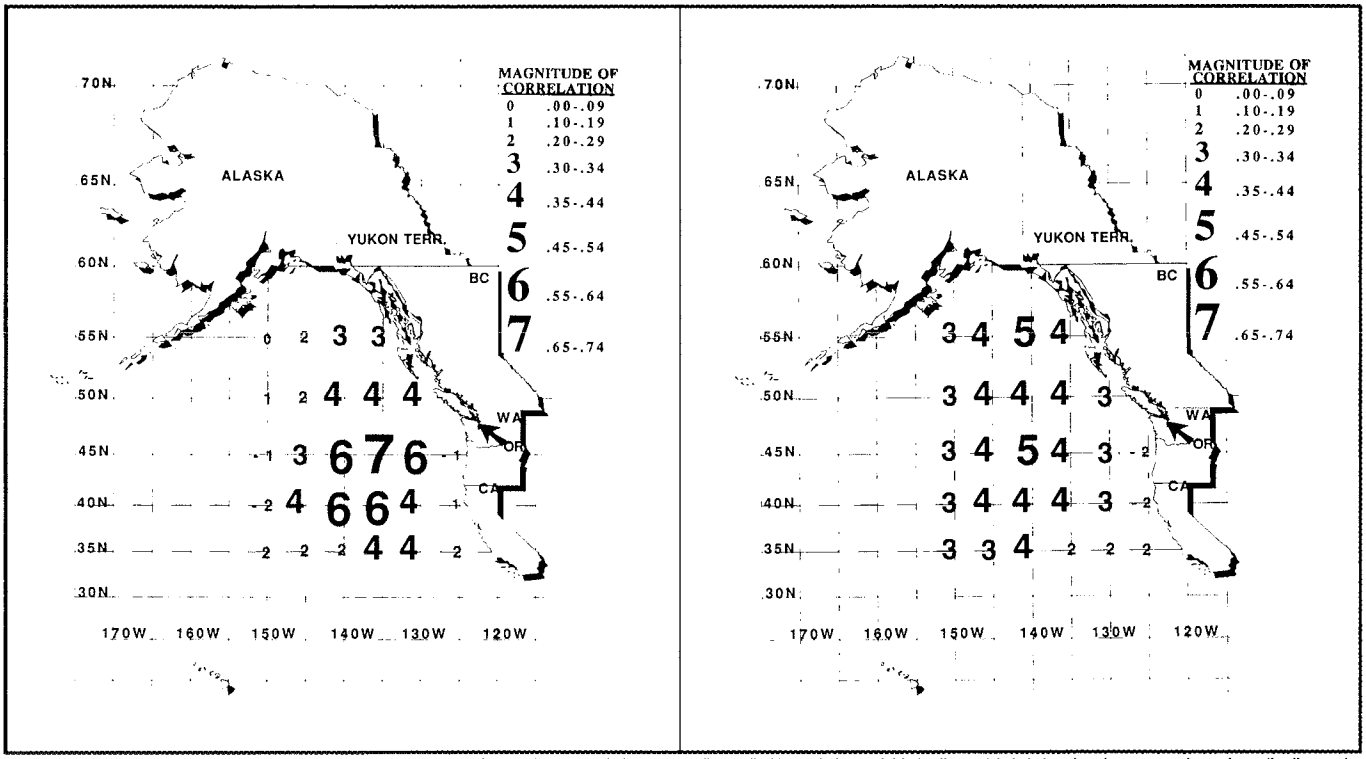

Figure 5. Map showing areal correlation between maximum latewood density indices (left) and ring width indices (right) for the four tree-ring sites (indicated by the arrow) and summer (JAS) sea surface temperature. The strongest correlation (positive) is with the grid point 45N, 135W and maximum latewood density, with a very compact zone of significant correlation around that point. Correlations for ring width basically agree with those for density, although with less significant correlations and over a broader region.

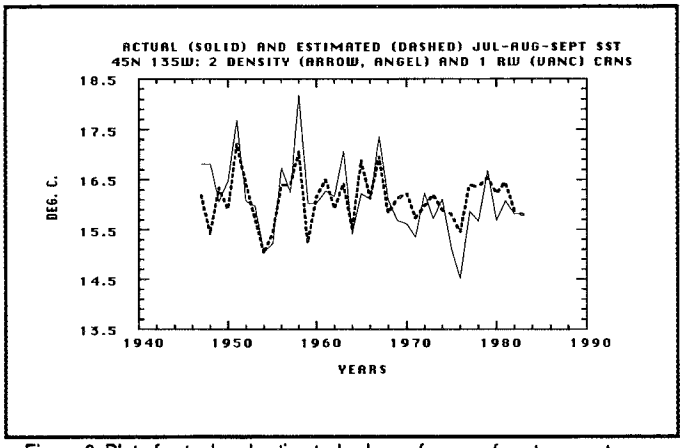

Figure 6. Plot of actual and estimated values of sea surface temperatures for the grid point 45N, 135W, using two density chronologies and one ring width chronology. The amount of variance explained (adjusted for degrees of freedom) is 42 percent.

Tree Growth and Sea Level Pressure

A dominant feature of northeast Pacific circulation is the Aleutian Low (Namias *et al* 1988; Emery and Hamilton 1985). The Aleutian Low Index (ALI) is a representation of the strength of the low, measuring the pressure gradient between two points: 40N/120W and 50N/170W, where the latter is subtracted from the former. A higher value of ALI indicates a stronger gradient and, therefore, a deeper Aleutian Low. Lower values indicate weak development of the low.

Our study region is affected by this system in the following simplified way. In years of a strong Aleutian Low, the near-shore ocean climate is influenced by the northward flow of warm, subtropical water; in years of a weak development in the Aleutian Low, the near-shore ocean climate is influenced by cooler waters, as the northward flow of warm, subtropical water is inhibited. We compared our averaged land temperatures against SLP at 50N/170W and confirmed that the winter strength of the Aleutian Low has a significant, negative correlation with land temperatures all through the year and is consistent with the findings of Namias *et al* (1988). As the winter Low gets stronger (lower), average temperatures at the sites will be higher all year long. It was also shown that the strength of the Low in spring was significantly and negatively correlated with land temperatures for that same period.

We compared our four density chronologies to SLP data representing the three elements of the ALI for 1900-1980. Figure 7 shows the correlations of the density chronologies with 40N/120W (top graph), 50N/170W (middle graph), and the ALI (bottom graph). While there is some indication of a relationship between maximum latewood density and winter

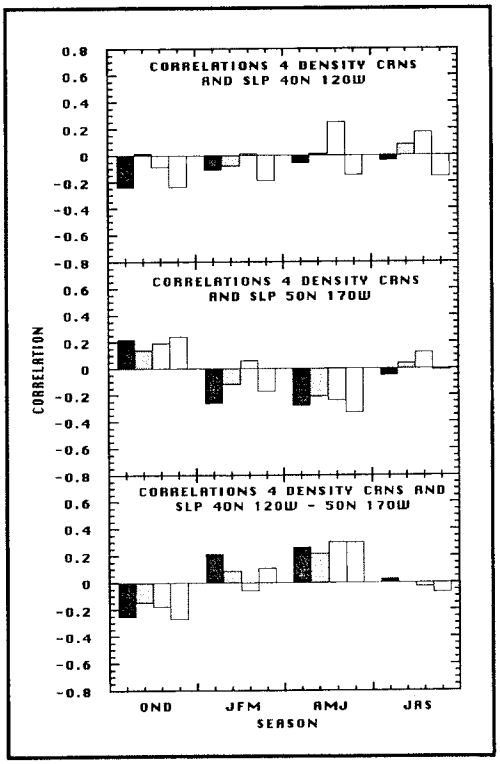

Figure 7. Correlations of the four density chronologies with three parameters of the Aleutian Low Index for four seasons (1900-1980). The top graph compares density with sea level pressure at 40N, 120W; the middle graph at 50N, 170W; and the bottom graph compares density with the Aleutian Low Index itself (the difference between the two points shown above). Note the strong correlation with the spring (AMJ) in the middle and bottom graphs (negative correlation for 50N, 170W, and positive correlation with the Aleutian Low Index). This indicates that maximum latewood density in trees in the study region increases in years of a strengthened springtime Aleutian Low.

intensity of the Aleutian Low, the real influence is from the spring period, which was demonstrated to be an important link between the Aleutian Low and temperature on land. This spring period is strongly affected by the persistence of the winter Aleutian Low (Namias *et al* 1988) and may, therefore, be considered to reflect the strength of the winter development of the Low. This would seem to indicate that maximum latewood density is increased in those years where the spring ALI is greater as the result of the persistence of a strengthened winter Aleutian Low.

Summary

In this paper we have explored some of the linkages between tree-ring data from coastal and near-coastal sites in the Pacific Northwest and several variables related to air/ocean interaction and atmospheric circulation in this region. The land temperature data showed significant positive correlations with SSTs (at 5x5 grid resolution) during the growing season and, in particular, for the spring months (April, May, and June). Monthly SLP data for gridpoints known to be representative of the strength of the Aleutian Low were also demonstrated to influence land temperatures at the stations selected for study: with an increase in the strength of the Aleutian Low during winter, there is an increase in temperature for the rest of the year. Both ring-width and maximum latewood density indices were linked to SST and SLP, with the strongest correlations for the spring months.

Our results indicate that density data is equally or even more sensitive to climate in this region than are ring widths. To date there have been relatively few studies that have modeled or reconstructed Pacific sea surface temperatures using tree-ring data, and these have been almost exclusively through the use of ring-width data (Douglas 1980). From this preliminary study we conclude that reconstructions of northeast Pacific SST and SLP are possible for several centuries or more using maximum latewood density and ring-width chronologies from the Pacific Northwest. There is also the potential for eventual integration of these tree-ring data with other types of proxy records, including varves (Leclerc and Schrader 1987; Baumgartner *et al* 1989). Future research will involve developing a tree-ring database with added geographical coverage to improve prospects for long-term, high-resolution reconstruction of climate in this area.

References

Andrade, ER Jr, and WD Sellers, 1988. El Niño and its Effect on Precipitation in Arizona and Western New Mexico. *Journal of Climatology.* 8:403-410.

Baumgartner, TR, J Michaelson, LG Thompson, GT Shen, A Soutar, and RE Casey, 1989. The recording of interannual climatic change by high-resolution natural systems: tree-rings, coral bands, glacial ice layers, and marine varves. *Geographical Mon.* 55:1-14.

Blasing, TJ, and HC Fritts, 1975. Past climate of Alaska and northwestern Canada as reconstructed from tree-rings.Pgs. 48-58 in G Weller and AA Bowling (eds), *Climate of the Arctic.* 24th Alaska Science Conf., Geophys. Instit., Univ. of Alaska at Fairbanks.

Cayan, DR, 1980. Large-Scale Relationships Between Sea Surface Temperature and Surface Air Temperature. *Monthly Weather Review.* 108:1293-1301.

Cook, ER, and LA Kairiukstis, 1990. *Methods of Dendrochronology.* Kluwer Acad. Publ.:Dordrecht.

Douglas, AV, 1980. Geophysical Estimates of Sea Surface Temperatures Off Western North America Since 1671. *CALCOFI Rep.* 21:102-112.

Douglas, AV, DR Cayan, and J Namias, 1982. Large-Scale Changes in North Pacific and North American Weather Patterns in Recent Decades. *Monthly Weather Review.* 110:1851-1862.

Emery, WJ, and K Hamilton, 1985. Atmospheric Forcing of Interannual Variability in the Northeast Pacific Ocean: Connections With El Niño. *Journal of Geophysical Research.* 90:857-868.

Fritts, HC, 1976. *Tree-Rings and Climate.* Academic Press:New York.

Juillet-Leclerc, A, and H Schrader, 1987. Variations of Upwelling Intensity Recorded in Varved Sediment from the Gulf of California During the Past 3,000 Years. *Nature.* 329:146-149.

Leathers, DJ, B Yarnal, and MA Palecki, 1991. The Pacific/North American Teleconnection Pattern and United States Climate; Part I: Regional Temperature and Precipitation Associations. *Journal of Climate.* 4:517-528.

Lough, JM, 1986. *Reconstructed Sea Surface Temperatures of the Eastern North Pacific: Comparisons with Other Dendroclimatic Reconstructions.* Laboratory of Tree-Ring Research Technical Note No. 44. Tucson, AZ.

Lough, JM and HC Fritts, 1989. Historical aspects of El Niño-Southern Oscillation - information from tree-rings. In PW Glynn (ed.), *Ecological Consequences of the 1982-83 El Niño.* Elsevier (in press).

_____, 1985. The Southern Oscillation and tree-rings: 1600-1961. *J. Clim. Appl. Met.* 24:952-66.

Michaelsen, J, L Haston, and FW Davis, 1987. 400 Years of Central California Precipitation Variability Reconstructed From Tree-Rings. *Water Resources Bulletin.* 23(5):809-818.

Namias, J, Y Xiaojun, and DR Cayan, 1988. Persistence of North Pacific Sea Surface Temperature and Atmospheric Flow Patterns. *Journal of Climate.* 1:682-703.

Neibauer, HJ, 1988. Effects of El Niño-Southern Oscillation and North Pacific Weather Patterns on Interannual Variability in the Southern Bering Sea. *Journal of Geophysical Research.* 93:5051-5068.

Ropelewski, CF, and MS Halpert, 1986. North American Precipitation and Temperature Patterns Associated with the El Niño/Southern Oscillation (ENSO). *Monthly Weather Review.* 114:2352-2362.

Trenberth, KE, 1990. Recent Observed Interdecadal Climate Changes. *Symposium on Global Change Systems.* Feb. 5, 1990, Anaheim, CA:American Meteorological Society.

Walsh, JE, and MB Richman, 1981. Seasonality in the Associations between Surface Temperatures over the United States and the North Pacific Ocean. *Monthly Weather Review.* 109:767-783.

Historical Evidence of Abrupt Coastal Climatic Change in Southern California, 1790-1880

Arndt Schimmelmann and Mia J. Tegner

Abstract: Historical sources of the late-18th and 19th centuries were searched for information on coastal weather conditions in Southern California. Relatively calm winters until 1828 were followed by unusually stormy winters from about 1829 to 1839. Later periods were again predominantly calm, with notable exceptions related to the ENSO events of 1845 and 1878. Following decreases through the stormy 1830s, sizes of kelp forests appear to have rebounded in the 1840s. ENSO occurrences and eruption of the volcano Cosiguina in 1835 are likely causes for changing wind patterns. Our results link the unique AD 1840 *Macoma leptonoidea* pelecypod shell layer in laminated Santa Barbara Basin sediment ("*Macoma* event") to abruptly changing oceanographic and weather patterns.

Introduction

The end of the "Little Ice Age" during the 19th century brought dramatic climatic events on time scales of years to decades to the Northern Hemisphere (Grove 1988; Mock 1991 and references therein), and presumably also to Southern California (Rowntree 1985). Coastal weather of California in the 19th century was rarely recorded instrumentally, and tree-ring data are of limited significance for reconstruction of storm-dominated coastal weather. We searched historical literature of the late 18th and 19th centuries to gain a climatic perspective on the Santa Barbara Basin record of laminated sediment of the 1830s, where an unusual pelecypod shell layer (*Macoma leptonoidea*) testifies for abnormal oceanographic conditions from AD 1835 to 1839/40 (Schimmelmann *et al* in press). This "*Macoma* event" is the brief flourishing of a macrofaunal community in the deep center of the Santa Barbara Basin, from which large organisms are normally excluded by the lack of oxygen.

Chronology of Climatic Information 1790s though 1870s

Southern California's "winter storm season" from October to May was of predominant importance for ships, merchants, and travellers. "Southeasters" were especially perilous to sailing vessels when they were caught by surprise at anchor close to shore. Ships sometimes "slipped their anchor" or chain, meaning they left their anchor behind (tied to a marker buoy, for later recovery) in a speedy attempt to "make the offing" to the open sea.

In K.T. Redmond, Editor, 1992. Proceedings of the Eighth Annual Pacific Climate (PACLIM) Workshop, March 10-13, 1991: California Department of Water Resources, Interagency Ecological Studies Program Technical Report 31.

Southeasters as well as El Niño/Southern Oscillation (ENSO) events are capable of extensive destruction of kelp forests, especially in the Santa Barbara Basin where coastal geography shields most kelp forests from the predominant northerly storms (Tegner and Dayton 1987). Forests of giant kelp, *Macrocystis pyrifera*, may require several years to recover, making the size of forests in the Santa Barbara Basin a useful indicator for preceding storms. The intensity of surf is a proxy for the strength of prevailing winds, especially if the location is shielded from certain directions, as at Santa Barbara. Until the construction of piers in the late 19th century, surf at Santa Barbara was a noteworthy obstacle for trading vessels, which had to use rowboats to shuttle between coast and ship.

Fog during summer in the Santa Barbara Basin is favored by cold upwelling water, in contrast to ENSO conditions. Historical ENSO events reported from Peru (Quinn *et al* 1987) would have arrived off Southern California with a lag of about one year. Storms off Baja California and north of Cape Mendocino follow different seasonal patterns; consequently they were not used in this compilation.

The following chronology contains hiatuses with few data; *eg*, 1794-1816. We caution that we extrapolated our interpretation of climate over such hiatuses based on compatible bracketing observations.

1790s through 1828: Relatively Calm Winters

The mild weather and the character of natural environments in the Santa Barbara Basin and off San Diego in November and December 1793 are reported by Captain George Vancouver (Wilbur 1953) and by his accompanying botanist, Archibald Menzies (1924). During his presence off Southern California, Vancouver anchored relatively close to shore and never prepared to slip nor actually slipped his anchor at the appearance of a storm. At Santa Barbara in November, "the weather was serene and pleasant" (Menzies p.322) and they "always got on shore from the boats pretty easy" (Menzies p.327) under "perfectly smooth and tranquil" conditions (Wilbur, p.147). "Weeds [kelp] were seen growing about the roadstead [Santa Barbara Channel] in many places" (Wilbur, p.161) and were also reported from Point Loma, extending "two miles into the ocean" (Wilbur p.183). Large kelp forests off Santa Barbara and Point Conception had been mapped 9 years earlier by Juan Pantoja (Figure 1; Ruhge 1987 p.3-5). Vancouver emphasizes that, in contrast to conditions farther north, "the south-easterly storms are scarcely ever known to the southward of Cape Mendocino" (Wilbur p.258).

Two months after a strong earthquake in 1806, a severe gale nearly destroyed buildings damaged by the trembler at the Santa Barbara Mission (Hawley 1987 p.60).

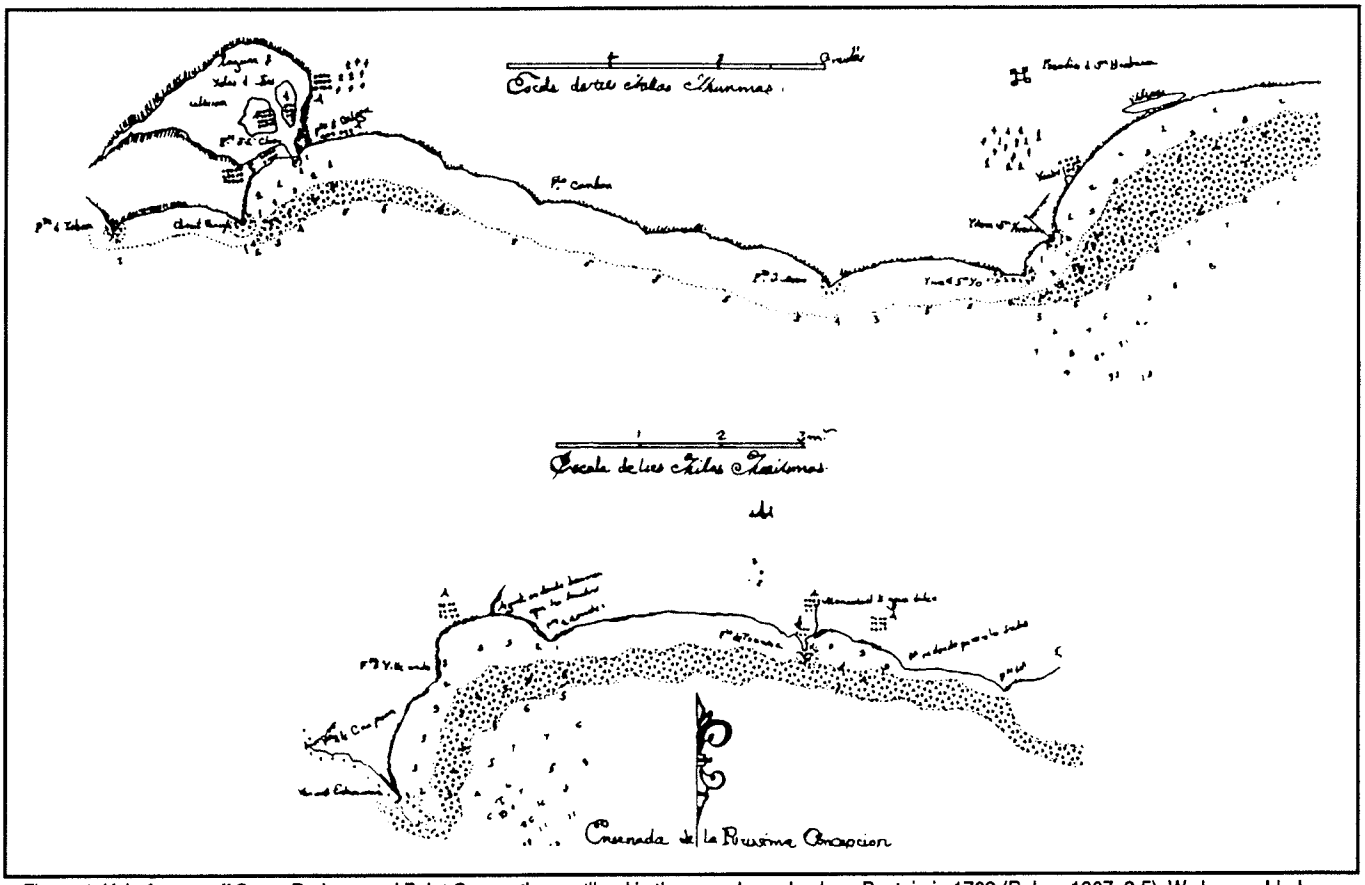

Figure 1. Kelp forests off Santa Barbara and Point Conception, outlined in the map drawn by Juan Pantoja in 1782 (Ruhge 1987, 3-5). We have added stippling to enhance the delineation of the kelp canopy.

Ogden's (1941 p.77) description of one trader's voyage, "riding in with a storm, the *Traveller* put in at Santa Barbara on January 8, 1817" may indicate a storm in 1817 was not truly dangerous.

From July 1817 through January 1819, Peter Corney (1965) sailed from Cape Mendocino to Cape St. Lucas. His detailed report mentions no adverse weather off Southern California, much in contrast to his earlier reports from the Columbia River region.

In September 1822, kelp forests off Santa Barbara were dense enough to entangle the schooner *Eagle* (Ruhge 1987 pp. 5-5, 13-12, 13-13).

"In February, 1824, ... all were sent immediately [from San Francisco] to San Pablo Bay, in order not to miss the calm days" (Ogden 1941 p.97).

Captain Frederick William Beechey visited the California coast at San Francisco and Monterey in November/December 1826 and again in November/December 1827 during his transit to San Blas (Gough 1973). Only one possible southeaster is reported for both observation periods, on the way from San Francisco to Monterey.

Captain William H. Cunningham's (1985) ship log of the *Courier* gives detailed weather observations off Southern California for 1826 to 1828. He reports no southeasters, no difficulty in landing at Santa Barbara, and no slipping the anchor. Foggy months in summer 1826 and July 1827 contrast with rare fog in the Santa Barbara Basin from April to September 1828, possibly due to the onset of a very strong El Niño in 1828 (Quinn *et al* 1987).

The naturalist Auguste Bernard Duhaut-Cilly travelled the California Coast for about a year in 1827/28, visiting Santa Barbara on several occasions (Carter 1929). He reports abundant kelp forests at Santa Barbara (p.161) and Point Loma (p.118), but no heavy surf at Santa Barbara and only three southeasters for that winter (p.321). This compares with at least a dozen storms in the winter of 1835/36 reported by Richard Henry Dana (1936). However, we learn indirectly that it was dangerous to anchor close to shore in winter: "As it was summer [June 1828], and sea winds were not to be feared, we anchored in six fathoms, inside the algae [off Santa Barbara], three cable's lengths from the beach" (p.328).

1829-1839: A Decade of Severe Southeasterly Winter Storms

Winter conditions were deteriorating. "Abounding" kelp forests at Santa Barbara were still present in 1829/30 (Robinson 1969 p.41), and some kelp remained in 1833 (p.154) and 1836 (Ruhge 1987 p.3-8), but "from the month of October [1829], till the beginning of May, vessels anchor at least a lime outside of these bearings, and ships are necessarily prepared for slipping their cables, and getting under way, should the wind, as is often the case, chop in suddenly from the S.E." (pp.37-38). Storms in December 1829 and January 1830, possibly related to a strong ENSO event in 1828 (reported off Peru, Quinn *et al* 1987), wrecked the brig *Danube* at San Pedro (White 1956 pp.28-30). Alfred Robinson (1969) also reports southeasters for 1832 and 1833 (pp.132, 144).

In his book *Two Years Before the Mast*, Richard Henry Dana (1936) describes his visits to Southern California from January 1835 until May 1836 and again in summer 1859. His detailed description of events and environments of 1835 and 1836, including Santa Barbara, never mentions any kelp in the Santa Barbara area, but he reports kelp covering rocks at low tide near San Pedro (p.98) and ships "lying at anchor inside of the kelp" off San Pedro on 11 September 1835 (p.195). Dana explains that they had "...to anchor at the distance of three miles from the shore [off Santa Barbara], in eleven fathoms water, and bent a slip-rope and buoys to our [anchor] cables" to be able to slip their anchor, get under sail, and leave the coast quickly in the unpredictable advent of a southeaster. As a deck hand, Dana frequently had to row boats laden with cow hides and tallow from shore to ship. Kelp forests would have been a noteworthy obstacle for loaded row-boats. The lack of mention of kelp in 1835 and 1836 off Santa Barbara, together with the fact Dana was aware

of kelp forests near San Pedro, is interpreted as evidence that kelp had not been present in significant quantities off Santa Barbara. Also, Dana describes the surf on Santa Barbara's beach as usually so high as to make it extremely difficult, even for trained seamen, to pass row boats through (pp.59-60).

Faxon Dean Atherton, who visited Santa Barbara between 1836 and 1839, reports in June 1836 that "the harbour of Sta Barbara is nothing but a roadstead open to the S.E. and subject to frequent heavy blows from that quarter at which time vessels have to get under way and stand out in the canal, frequently for 15 or 20 days. In the summer vessels anchor inside of the kelp which extends across the harbour about 500 yards from the shore, but in the winter season they anchor outside of it, so far as to be able to fetch clear of the Point should a S.E. come on. This was formerly the place where most if not all vessels traveling on the coast cured their hides, but owing to the difficulty and delay experienced in loading by the S.E., they have most of them moved their houses to San Diego...." (Ruhge 1987 p.3-8). The kelp forests mentioned by Atherton are apparently limited in extent and density in comparison with dense kelp forests at Santa Barbara in 1875 ("At Santa Barbara [the steamer *Hassler*] relieved the ship *Arkwright* by passing the *Hassler* out to lead through the kelp..." (US Coast and Geodetic Survey 1875 p.53).

In April 1835, George Nidever "started from Santa Cruz to Santa Barbara when a very strong South Easter sprang up and it was with difficulty that we made land at Goleta several miles above Sta. Barbara. During the same storm ... a merchant vessel, went ashore..." (Ellison 1937 p.46; timing of event corrected according to Ogden 1941 p.209).

Another shipwreck occurred in April 1838, 6 miles west of Santa Barbara (Ruhge 1987 p.5-9).

The frigate *Venus* of the French navy, under Captain Abel du Petit-Thouars, stayed at Monterey from October 18 through November 14, 1837, and on November 9 they experienced a violent southeaster (Du Petit-Thouars 1956 pp. 71, 75). The weather from November to March is characterized as "the bad season", during which "the S.E. wind is accompanied by the worst weather" (p.75).

1839/1840 through 1844/45: A Calm Interlude

Alfred Robinson (1969) reports no southeasters for 1840 to 1842, after he had returned to Southern California following a few years of absence. Sir James Douglas experienced no storm off Monterey in December 1840 and January 1841 (Douglas 1929). For May 1841, Eugène Duflot de Mofras describes "large masses of seaweed" at Santa Barbara (Ruhge 1987 2-54, 4-34). In April 1843, the US sloop-of-war *Dale* anchored 4 or 5 miles off Santa Barbara and put small boats ashore. Philo White describes "... a long pull; and there is so much kelp in the water for half

a mile off shore, that we had some difficulty in working the Boat through it; and the surf breaks so heavily on the beach, that we availed ourselves on a surf-boat to land in, which enabled us to get ashore with dry feet" (White 1965 p.72). One possible southeaster is mentioned by William Heath Davis (1967 p.75) at San Francisco during winter 1841/42. No storm reports were found for 1843 to 1846.

1846-1847/48: ENSO-Related Winter Storms

Renewed reports of stormy winters fall into the wake of the strong Peruvian ENSO event of 1845 (Quinn *et al* 1987). A record low temperature was observed in Ventura in 1847, when ice froze 0.75 inch thick (Mason 1961 p.458). The memory of southeasters in the 1830s was still alive, possibly refreshed by R. H. Dana's then-popular book *Two Years Before the Mast*. James Lynch, who landed at Santa Barbara on April 8, 1847, describes the situation with strikingly similar words to what Dana had used a decade earlier: "What is called the harbor of Santa Barbara is only an open roadstead, and a vessel has to anchor far from shore, or, at least, that is what had to be done when we were there, and if a southeaster began to blow, a vessel had to slip her cable and put out to sea. In my time, two ships [*Franchesca* and *Elizabeth*] were wrecked in trying to round Point Santa Barbara, the sou'easter coming too quickly for them. So the *Moscow* had to anchor far from the beach .... The surf was angry..." (Ruhge 1987 pp.15-4, 15-5). Interestingly, Lynch does not mention any kelp, probably for the same reason described earlier for R. H. Dana's report.

1849 through early 1870s: Predominantly Calm Winters

Six weeks of fog in the Santa Barbara Basin in summer 1850 indicate upwelling conditions had resumed (US Coast and Geodetic Survey 1889 p.55). There are only a few reports of non-ENSO-related storms from 1849 to 1890. Mason (1961 p.92) mentions one southeaster in the Santa Barbara Basin in 1852, possibly responsible for wrecking the brig *Pilgrim* at Santa Barbara in that year (Ruhge 1987 p.5-13). The following excerpt from a Santa Barbara newspaper, *Gazette* (13 January 1856), testifies to the rarity of severe storms: "Early on Tuesday the wind began to blow from the southeast, and continued to increase in violence during the day... The surf rolled in with great fury, and the mad force of the waves dashed into fragments the hulls of two large vessels, the *Hallowell* and *Pilgrim*, which, for several years, have been comparatively undisturbed by the tide" (Ruhge 1987 p.5-13; Mason 1961 p.100).

In 1859, when R. H. Dana returned to Santa Barbara, he confirmed that "...the climate has altered; that the south-easters are no longer the bane of the coast they once were, and that vessels now anchor inside the kelp [forests] at Santa Barbara and San Pedro all the year round." (Dana 1936 p.419). An 1853 map of the U.S. Coast Survey (Ruhge 1987 4-35) shows extensive kelp forests off Santa Barbara (Figure 2).

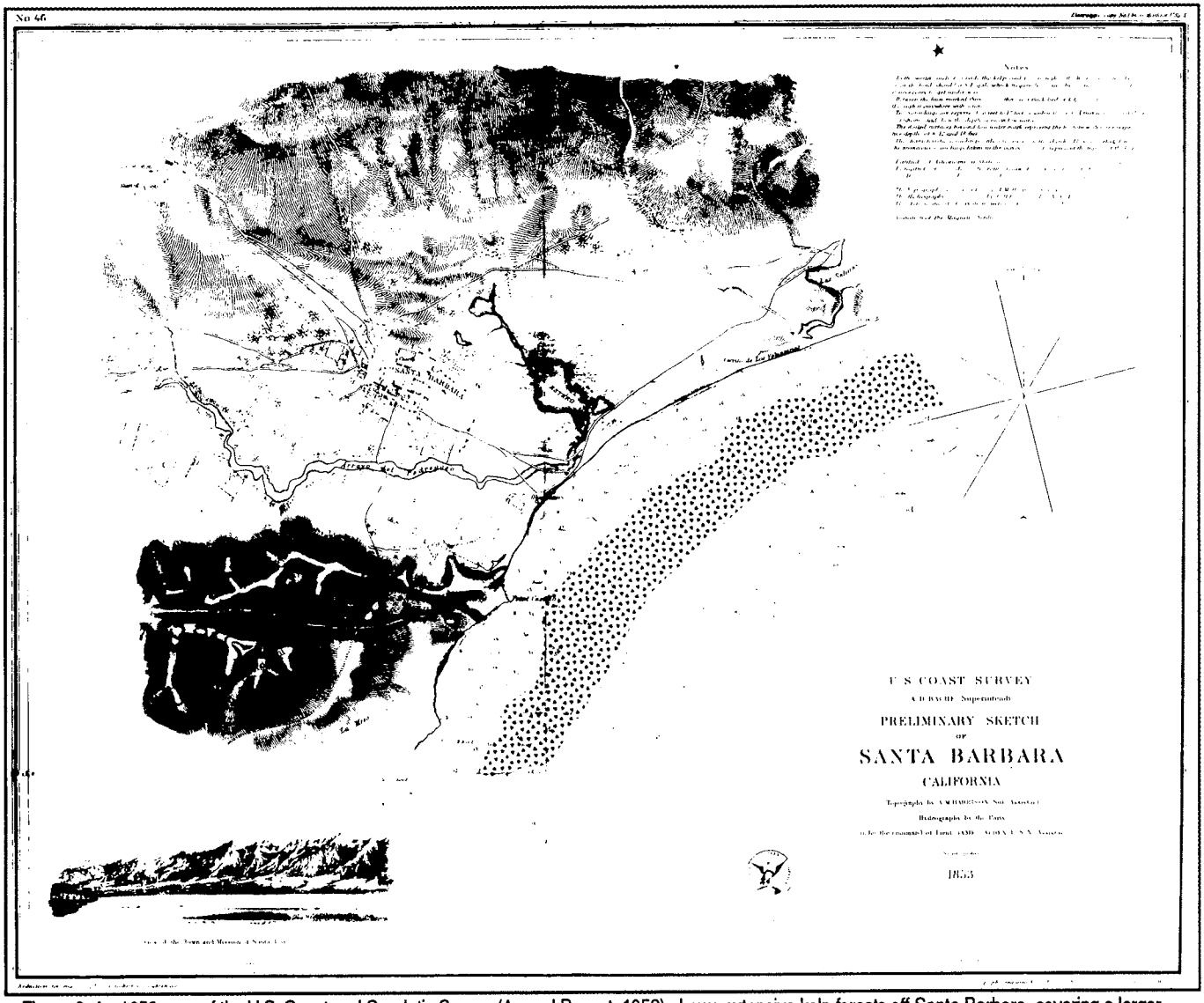

Figure 2. An 1853 map of the U.S. Coast and Geodetic Survey (Annual Report, 1853) shows extensive kelp forests off Santa Barbara, covering a larger area than in Figure 1. We have added stipling to enhance the delineation of the kelp canopy.

Fourteen years later, beginning in February 1873, severe winter storms at Santa Barbara were documented once again (Mason 1961 p.467), where in 1874/75 great storms broke wharfs (Mason 1961 p.223). Mason reports a "rain-storm" for November 1875 "accompanied with high winds, levelling trees and compelling vessels in the harbor to slip their anchor and go to sea". Several ships were lost during that winter (p.468).

ENSO-Related Storms of 1877/78

Drought conditions of 1876/77 (Mason 1961 pp.215, 370, 469) ended abruptly with the onset of the very strong ENSO event of 1877/78 (Quinn *et al* 1987). A variety of resulting weather extremes in the Santa Barbara area was observed (Mason 1961) involving loss of ships and wharfs (pp. 223, 370, 469), temperature extremes (pp. 458, 469, 470), floods (pp. 256, 270, 469), a cyclone and a tornado (pp. 225, 226, 470). We have no evidence of severe storms for the remaining years of the 19th century.

Discussion and Conclusions

The onset of stormy winters around 1829/30 is probably linked to ENSO conditions at that time (reported for 1828 off Peru; Quinn *et al* 1987), generating southeasterly storms by offshore low pressure fields. Severe ENSO events are associated with warm, nutrient-depleted surface waters and ineffectual upwelling off Southern California. Productivity and organic fallout are thus sharply reduced, permitting more oxygen to reach the benthic environment in the Santa Barbara Basin.

Stormy winters after 1834 are possibly related to the sudden climate changes from overall warm to cold conditions in many regions of the Northern Hemisphere immediately after 1835 (Lamb 1972, 1982), the year of the volcanic eruption of Cosiguina (Nicaragua). This eruption in January 1835 caused a dust veil index that is the highest on record between 1602 and 1900 (Lough and Fritts 1987; Catchpole and Hanuta 1989). The following late summer ice event was the most severe on record in Hudson Bay between 1751 and 1870 (Catchpole and Hanuta 1989), presumably as a consequence of dust-produced cooling (*cf*, Bradley 1988).

The decrease in abundance of kelp forests in the Santa Barbara Basin in the 1830s coincides with the higher frequency of kelp-destructing severe southeasterly storms reported for that time. Kelp forests appear to have recovered in the 1840s, and by the 1850s they were mapped as large (Figure 2).

Pelecypods (*Macoma leptonoidea*) colonized the benthic environment in the central Santa Barbara Basin around 1836, when R. H. Dana experienced extreme winter storms. Necessary oxygen for the macrobenthic community may have been provided by unusual water circulation driven by storms or by changed currents at that time. Shortly after, around 1839/40, with the onset of calm winters, the demise of *Macoma leptonoidea* in the Santa Barbara Basin was caused by resumption of low oxygen conditions in bottom waters (Schimmelmann *et al* in press).

Our compilation of historical climatic information provides further evidence that the extreme weather conditions of the 1830s in the Santa Barbara Basin, which link with the "*Macoma* event" recorded in the sediment, were not just a local anomaly, but the result of profound disturbances in weather patterns over the eastern North Pacific and the North American continent.

Acknowledgments

This work was supported by National Oceanic and Atmospheric Administration grant NA16RC00083-01 to Mia J. Tegner and by National Science Foundation grant ATM87-23024 to W. H. Berger. We are indebted to C. Arnold and M. Redmon for assistance in the collection of data.

References

Bradley, RS, 1988. The explosive volcanic eruption signal in Northern Hemisphere continental temperature records. *Climatic Change.* 12:221-243.

Carter, CF, 1929. DuHaut-Cilly's account of California in the years 1827-1828. *Quarterly of the California Historical Society.* 8:130-166, 214-250, and 306-336.

Catchpole, AJW, and I Hanuta, 1989. Severe summer ice in Hudson Strait and Hudson Bay following major volcanic eruptions, 1751 to 1889 A.D. *Climatic Change.* 14:61-79.

Corney, P, 1965. *Early voyages in the North Pacific 1813-1818 by Peter Corney.* Ye Galleon Press:Fairfield, Washington. 238p.

Cunningham, WH, 1985. Log of the *Courier* 1826-1827-1828. *Early California Travels Series XLIV.* Glen Dawson:Los Angeles. 75p.

Dana, RH, 1936. *Two years before the mast.* Random House:New York. 443p.

Davis, WH, 1967. *Seventy-five years in California.* John Howell:San Francisco. 345p.

Douglas, Sir J, 1929. A voyage from the Columbia to California in 1840. *California Historical Society Quarterly.* 8:97-115.

Du Petit-Thouars, A, 1956. Voyage of the *Venus*: Sojourn in California. *Early California Travels Series XXXV.* Glen Dawson:Los Angeles. 114p.

Ellison, WH (Ed.), 1937. *The life and adventures of George Nidever* [1802-1883]. University of California Press:Berkeley. 128p.

Gough, BM (Ed.), 1973. *To the Pacific and Arctic with Beechey. The journal of Lieutenant George Peard of H.M.S. "Bossom", 1825-1828.* Cambridge University Press:Glasgow. 272p.

Grove, JM, 1988. *The Little Ice Age.* Routledge:London. 498p.

Hawley, WA, 1987. *Early days of Santa Barbara by Walter A. Hawley.* Third edition, enlarged and edited by JC Woodward. Santa Barbara Heritage:Santa Barbara, California.

Lamb, HH, 1982. *Climate, history and the modern world.* Methuen:London. 387p.

_____, 1972. *Climate: present, past and future: v.1, fundamentals and climate now.* Methuen:London. 613p.

Lough, JM, and HC Fritts, 1987. An assessment of the possible effects of volcanic eruptions on North American climate using tree-ring data, 1602 to 1900 A.D. *Climatic Change.* 10:219-239.

Mason, JD (Ed.), 1961. *Reproduction of Thompson and West's history of Santa Barbara & Ventura Counties.* Howell-North:Berkeley, California. 477p.

Menzies, A, 1924. Archibald Menzies' journal of the Vancouver expedition. *California Historical Society Quarterly.* 2:265-340.

Mock, CJ, 1991. Historical evidence of a cold, dry summer during 1849 in the northeastern Great Basin and adjacent Rocky Mountains. *Climatic Change.* 18:37-66.

Ogden, A, 1941. *The California Sea Otter Trade, 1784-1848.* University of California Press:Berkeley. 251p.

Quinn, WH, VT Neal, and SE Antunez de Mayolo, 1987. El Niño occurrences over the past four and a half centuries. *Journal of Geophysical Research.* 92(C13):14,449-14,461.

Robinson, A, 1969. *Life in California.* Da Capo Press:New York. 341p.

Rowntree, LB, 1985. A crop-based rainfall chronology for pre-instrumental record Southern Califiornia. *Climatic Change.* 7:327-341.

Ruhge, JM, 1987. *Gunpowder and Canvas.* Quantum Imaging Associates:Goleta, California.

Schimmelmann, A, CB Lange, WH Berger, A Simon, SK Burke, and RB Dunbar. Extreme climatic conditions recorded in Santa Barbara Basin laminated sediments: the 1835-1840 *Macoma* event. *Marine Geology.* (in press).

Tegner, MJ, and PK Dayton, 1987. El Niño effects on Southern California kelp forest communities. *Advances in Ecological Research.* 17:243-279.

US Coast and Geodetic Survey, 1889. *Coast Pilot.* 4th ed. Government Printing Office:Washington, 721p.

_____, 1875. *Annual Report.* Government Printing Office:Washington.

_____, 1853, *Annual Report,* Government Printing Office:Washington.

White, MC, 1956. California, all the way back to 1828. *Early California Travels Series XXXII.* Westernlore Press:Los Angeles. 96p.

White, P, 1965. *Philo White's Narrative of a Cruize in the Pacific to South America and California in the U.S. Sloop-of-war "Dale" 1841-1843.* CL Camp (ed.), FA Rosenstock Old West Publishing Company:Denver. 84p.

Wilbur, ME (Ed.), 1953. *Vancouwer in California.* Glen Dawson:Los Angeles. 274p.

Evidence from the Pacific Northwest for Solar Modulation of Climate and of Northern Ecosystems

Gerald Holdsworth

Abstract: The 250-year net annual snow accumulation, or *mass balance*, time series derived from the Mt. Logan (Yukon) ice core has been spectrally analyzed and is found to contain a nominal 11-year waveform. The stable isotope time series contains a significant amount of power between 9 and 13 years, although this record is evidently not a straightforward proxy for air temperatures. The signal in the mass balance time series exhibits a close relationship with the sunspot cycle waveform and is, therefore, assumed to be related to it. Waveforms showing a high correlation with the solar cycle are found in other climate data in the region: for example, in north Pacific sea surface temperatures and station temperatures for parts of Alaska where an approximately decadal period waveform can be seen in the raw data without sophisticated processing. Temperature-sensitive trees at the northern tree limit in the Yukon show 11-year peaks in power spectra. Similarly, a 9- to 11-year waveform can be seen in many small mammal population time series, although, as expected, peaks are lagged with respect to the solar cycle. A power spectrum of the snowshoe hare fur return data shows a clear peak at 11.2 years, but this seems to be unique among the small mammals, which tend to have cycles close to 10 years. Taken collectively, the data point to a link between solar variability, atmospheric variability, climate, and selected ecological dynamics in the Pacific Northwest, but other data, not presented, indicate these relationships may hold elsewhere. So far, the evidence is empirical; complete details of the physical mechanisms involved have yet to be synthesized in a satisfactory way.

Introduction

Spectral analyses of the climatically based Mt. Logan ice core time series (mass balance and stable isotopes), representing annual data spanning 250 years (Holdsworth *et al* 1989; Holdsworth *et al* 1991) show there is significant power at about 11 years. To see if this could be related to the sunspot cycle, the waveform in the 0.11-0.077 cycles/year frequency band (9- to 13-year period) was generated from maximum entropy analysis of the net annual snow accumulation time series (RG Currie, personal communication). The power spectrum of this series possesses a sharp peak at 10.9 years. This waveform shows a definite relationship with the sunspot waveform, although it is far from straightforward to interpret this relationship physically. Because the climate at the Mt. Logan site is essentially maritime, these signals are evidently originating in Gulf of Alaska storm systems. Minimal processing of oceanographic temperature data (Royer 1989) and of coastal Alaskan station air temperatures shows the presence of an approximately decadal signal that is closely coherent with the sunspot cycle (or 10.7-cm wavelength flux). The behavior of the Aleutian Low and of storms originating in this region may be influenced by solar variability (Herman and Goldberg 1985).

In K.T. Redmond, Editor, 1992. Proceedings of the Eighth Annual Pacific Climate (PACLIM) Workshop, March 10-13, 1991: California Department of Water Resources, Interagency Ecological Studies Program Technical Report 31.

Species of spruce (*Picea*) growing along the northern (boreal) tree limit in the Yukon Territory are sensitive to temperature (Jacoby and Cook 1981). Power spectra of some of these series show weak power at about 11 years (D'Arrigo and Jacoby 1991). The climatic regime here is Arctic (Bryson and Hare 1976) and, in terms of precipitation, the region is quite different from the St. Elias Mountains in which Mt. Logan is located. However, long-term temperature trends and variations are expected to be similar in the two regions judging from the more recent instrumental records. Temperature variations may be an important climatic factor that propagate the solar signal into floral and faunal domains. Precipitation (affecting soil moisture) would appear to be an important factor, but the data show no strong coherency on a continental scale.

It has long been known that an approximately decadal cycle exists in the population time series of many small mammals living in the boreal forest region of Canada. In particular, the snowshoe hare (*Lepus americanus*) exhibits very large oscillations in population levels since records began in 1790. Finerty (1980) shows there is a pronounced peak in the power spectrum at 11.2 years. This is so close to the nominal sunspot cycle that further investigation is justified. Investigations involving generation of a tree-ring-based proxy hare population record show that, during certain periods, the hare cycle is closely related to the solar cycle and to the corresponding cycle in the ice core time series, although this does not prove the hare cycle is related to cycles in precipitation.

There are two main mysteries: How is the solar signal propagated into Earth's atmospheric domain with an apparently large amplification factor and, assuming a climate-generated biospheric response is possible, how does the signal acquire additional gain within apparently only one small mammal species?

Solar Variability-Climate Link

There is a steadily growing literature in the field of solar variability-climate relationships. The few criticisms of study results are justified, but they have hardly succeeded in undermining the mounting evidence that points to a solar-weather link. Significantly, the evidence is of an interdisciplinary nature. The latest breakthrough has been the discovery that if climatic variables are partitioned according to the phase of the Quasi-Biennial Oscillation (QBO), correlations of those variables with the solar 10.7-cm flux (closely related to the sunspot numbers) are greatly enhanced (Labitzke 1987). The method has been extended from the stratosphere to the troposphere with equal success (vanLoon and Labitzke 1988). The limitation of this technique is that it is presently restricted to data post-dating 1952.

The QBO phase-partitioning technique was applied to the ice core annual mass balance data, which were converted to synthetic monthly values using the seasonal distribution of precipitation at Yakutat, Alaska. While

direct correlation with the solar flux was not high, a visual correlation (both positive and negative) was evident, especially when Yakutat precipitation was simultaneously compared to it.

Alaskan coastal station temperatures have also been used to see if the solar relationship holds. The one station so far processed (Seward) indicates a clear positive correlation. The sea surface temperature (SST) data for the Gulf of Alaska (Royer 1989) show a fair correspondence with the solar data over 2 cycles, even without QBO phase partitioning.

The strongest criticisms against claims of correlations of terrestrial or atmospheric datasets with the solar data are that many of the records are too short to be statistically meaningful, or that phase drift occurs, or that after a few cycles the correlation disappears. In addition, a physically robust theory for linking solar activity to terrestrial systems has not yet been advanced. These objections are now addressed. Recently it has been found that certain (pressure related) output from numerical atmospheric global circulation models (GCMs), when subjected to spectral analysis, exhibit strong power at decadal periods (James and James 1989). This has been extended to the air/ice/ocean system for the Northern Hemisphere, which may experience a type of resonance in which feedback processes in the system are important (Ikeda 1990). It follows that "beating" between the atmospheric waveform forced at the solar frequency and another close (approximately decadal) natural atmospheric frequency could occur. This system can be used to explain the phase shifts, the amplitude modulation in some of the signals, and the periodic disruption in the correlations (Holdsworth 1990). Some progress has been made in the search for the solar/atmosphere linkage (Tinsley 1988) but, whereas qualitative mechanisms have been suggested, so far no complete quantitative model has been advanced to explain the necessary amplification of the signal.

If it is agreed that a case has been established for a solar variability-climate link, it is logical to anticipate that the solar signal might be further propagated into the biosphere. The solar signal has been found in vegetation time series (*eg*, Currie 1988, 1991); D'Arrigo and Jacoby 1991), although the mechanism of the signal transfer has not been modeled.

Because the population dynamics of small mammals involves a vegetation component (*ie*, through the food supply), it is logical to suppose a (lagged) solar generated signal in vegetation yields might be involved in modulating mammal population levels. The other component in a dynamics model is the predator. For the snowshoe hare, there are several predators, both avian and mammalian, each with their own cycles, which are related to, but in general do not coincide with the hare cycle. Rather than discussing possible mechanisms (*eg*, Sinclair *et al* 1988), only the empirical evidence relating to the hare cycle is discussed here. The material is taken from an unpublished paper by Sinclair *et al.*

Snowshoe Hare Cycle

Until recently, the only data that could be used as proxy for hare population levels have been obtained from fur records kept by Hudson's Bay Company (1790-1825 and 1844-1904) and from trapper questionnaires (1905-1935) (MacLulich 1937). Only qualitative estimates of peaks in the cycle have been made since then. The discovery that a proxy hare population record exists in stress marks in the growth rings of white spruce in the Yukon has provided an opportunity to study the relationship the hare cycle has to the solar cycle and to climatic cycles since 1751.

The basis of the proxy record reconstruction is as follows. Yukon hares normally browse on fast-growing birch and willow shrubs, but when these are in short supply due to a rising population of hares, the apical shoot of small white spruce is eaten. Beyond a height of 1.5 meters (corresponding to an average age of 50 years) the tops of the trees become inaccessible to the hares. The stress on the tree produced by the loss of the apical shoot is registered as a dark mark or band on the ring of that year, but it may also cover subsequent annual rings. These dark bands are similar to climatically induced stress marks.

A direct connection was first made between hare density (numbers/km^2), the number of apical shoots cut, and the number of dark marks on a statistically significant number of trees in a control plot. Next, 368 trees, cut to install a fence around the control plot, were examined for evidence of dark marks. A tree mark ratio was obtained by dividing the number of tree marks counted for a given year by the number of trees showing the marks for that year (determined by ring counts). A time series was thus established from 1751 to 1983. This time series suffers from cut-off at low hare numbers, but it represents the only continuous proxy series for hare population levels in Canada for 233 years. It was subjected to statistical analyses.

Both auto-correlation and standard spectral analyses indicate the presence of a 10- to 11-year cycle. When overlapping data blocks of 20 to 40 years are cross-correlated with the corresponding sunspot number data blocks, it is found that the phase shift remains relatively constant only for certain intervals. These intervals correspond closely to the intervals in which the sunspot maxima reach greatest amplitude (1730-1790; 1830-1870; 1940-1983). During the intervening times, the phase shift tends to drift (Figure 1).

These results imply there is a limited solar modulation of the hare cycle during times of maximum solar activity. During times of weak solar activity, the hare cycle continues either as a free, internal, biological oscillation (Trostel *et al* 1987) or as a result of continued atmospheric forcing due to an apparent "natural" oscillation of about a decade in the ocean/ice/troposphere system (Ikeda 1990).

Available evidence indicates that, with some phase shift anomalies, the hare cycle is, within 1-2 years, closely in phase across Canada. This implies a continent-wide forcing function. If this is a climatic factor, then temperature would seem the most likely candidate. Long-term (1860-1988) records of sea ice extent off the coast of Newfoundland (Hill and Jones 1990) indicate a close synchrony with the 11.7-cm solar flux. The main climatic variable here is assumed to be temperature. Hence, there is evidence of in-phase temperature variations from the west and the east coasts of Canada. This evidence is, thus, consistent with a continent-wide climatic forcing function hypothesis.

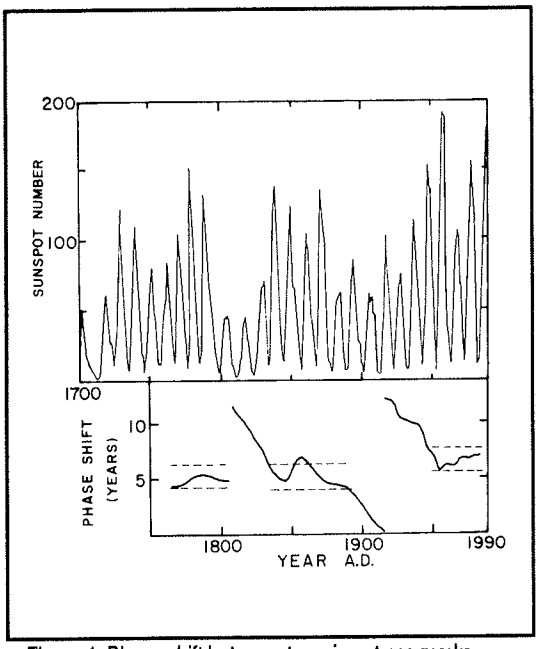

Figure 1. Phase shift between tree-ring stress marks (proxy for hare population levels) and sunspot numbers compared with amplitude of sunspot variations, showing close phase-lock only during times of maximum sunspot number groups.

There is weak amplitude modulation in the tree-ring dark mark time series, but it is not in phase with the amplitude modulation seen in the sunspot time series. This implies the solar influence is not dominant but is just sufficient to act as a trigger that can influence the frequency of the hare cycle, which is already in motion.

Summary

Solar related signals are apparently embedded in oceanographic and atmospheric instrumental data as well as in "proxy" dendro-climatic and ice core-climatic time series and, discontinuously, in snowshoe hare population dynamics. Although the solar-weather link has not yet been fully elucidated and the mode of propagation of the solar signal into the biological realm not uniquely modeled, statistical evidence continues to argue for further study of the subject in a search for the mechanisms involved.

References

Bryson, RA, and FK Hare, 1976. Climates of North America. In H Landsberg (ed.) *World Survey of Climatology*. v.11, Elsevier:Amsterdam.

Currie, RG, 1991. Determinstic signals in tree rings from the corn belt region. Submitted to *Annales Geophysicae*.

_____, 1988. Climatically induced cyclic variations in United States crop production: implications in economic and social science. Pgs. 181-241 in G Erickson and CR Smith (eds.) *Maximum entropy and Bayesian methods in Science and Engineering*. v.2D. Reidel:Dordrecht.

D'Arrigo, RD, and GC Jacoby Jr, 1991. Dendroclimatic evidence from northern North America. In RS Bradley and PD Jones (eds.) *Climate since A.D. 1500.* Harper Collins Acedemic:London (in press).

Finerty, JP, 1980. *The population ecology of cycles in small mammals.* Yale University Press:New Haven and London.

Herman, JR, and RA Goldberg, 1985. *Sun, weather and climate.* Dover:New York.

Hill, BT, and SJ Jones, 1990. Newfoundland ice extent and the solar cycle from 1860-1988. *Journal of Geophysical Research.* 95:5385-5394.

Holdsworth, G, 1990. Sunspot cycles and climate. *Nature.* 346:705-706.

Holdsworth, G, HR Krouse, and M Nosal, 1991. Ice core climate signals from A.D. 1700-1987, Mt. Logan, Yukon. In RS Bradley and PD Jones (eds.) *Climate since A.D. 1500.* Harper Collins Academic:London (in press).

Holdsworth, G, HR Krouse, M Nosal, MJ Spencer, and PA Mayewski, 1989. Analysis of a 290-year net accumulation time series from Mt. Logan, Yukon. Pgs. 71-79 in *Snow cover and glacier variations.* IAHS Publ. 183.

Ikeda, M, 1990. Decadal oscillations of the air-ice-ocean system in the northern hemisphere. *Atmosphere-ocean.* 28:106-139.

Jacoby, GC, and ER Cook, 1981. Past temperature variations inferred from a 400 year tree ring chronology from Yukon Territory, Canada. *Arctic and Alpine Research.* 13:409-4.

James, IN, and PM James, 1989. Ultra-low frequency variability in a simple atmospheric circulation model. *Nature.* 342:53-55.

Labitzke, K, 1987. Sunspots, the QBO, and the stratospheric temperature in the north polar region. *Geophysical Research Letters.* 14:535-537.

MacLulich, DA, 1937. *Fluctuations in the numbers of the varying hare (Lepus americanus).* University of Toronto Press:Toronto.

Royer, TC, 1989. Upper ocean temperature variability in the northeast Pacific Ocean: Is it an indicator of global warming? *Journal of Geophysical Research.* 94:18,175-18,183.

Sinclair, ARE, JM Gosline, G Holdsworth, CJ Krebs, V Nams, S Boutin, JNM Smith, R Boonstra, and M Dale, (unpublished). Can the solar cycle and climate synchronize the snowshoe hare cycle in Canada? Evidence from tree rings and ice cores. *American Naturalist* (in review).

Sinclair, ARE, CJ Krebs, JNM Smith, and S Boutin, 1988. Population biology of snowshoe hares. III. Nutrition, plant secondary compounds and food limitation. *Journal of Animal Ecology.* 57:787-806.

Tinsley, B, 1988. The solar cycle and the QBO influences on the latitude of storm tracks in the north Atlantic. *Geophysical Research Letters.* 15:409-412.

Trostel, K, ARE Sinclair, CJ Walters, and CJ Krebs, 1987. Can predation cause the 10-year hare cycle? *Oceologia.* 74:185-192.

vanLoon, H, and K Labitzke, 1988. Association between the 11-year solar cycle, the QBO, and the atmosphere. Part II: Surface and 700 mb in the northern hemisphere in winter. *Journal of Climate.* 1:905-920.

Influence of Climate on Environmental Factors Associated with Long-Term Changes in Chlorophyll Production for the Sacramento-San Joaquin Delta and Suisun Bay, California

Peggy W. Lehman

Abstract: Long-term changes in chlorophyll production were predicted from environmental variables for the Sacramento and San Joaquin rivers and Suisun Bay using Box-Jenkins transfer function models. Data used for the analyses were collected semimonthly or monthly between 1971 and 1987. Transfer function models developed to describe changes in chlorophyll production over time as a function of environmental variables were characterized by lagged responses and described between 39 and 51 percent of the data variation. Significant correlations between environmental variables and the California climate index (CA SLP) were used to develop a conceptual model of the link between regional climate and estuarine production.

Introduction

Phytoplankton production within Suisun Bay, part of the upper reach of San Francisco Bay, and the Sacramento-San Joaquin River Delta, upstream, declined between 1969 and 1982. Average chlorophyll *a* concentration decreased among regions of the Delta by 58-31% for the spring/summer and 41-15% for the fall (Interagency Ecological Study Program 1990). The decline in average chlorophyll *a* concentration after 1976 was accompanied by decreased cell densities and a shift in species composition (Lehman and Smith 1991). Presently it is unknown why these long-term changes in phytoplankton production occurred and how these changes will affect estuarine production in the future.

Previous studies have determined significant environmental variables that affect phytoplankton production, but none of these factors has been proven the cause of observed long-term changes in phytoplankton production. Significant environmental factors include water transparency (DiToro *et al* 1971; Arthur and Ball 1979; Cloern and Cheng 1981; Peterson and Festa 1984) and residence time (Conomos 1979; Peterson 1979; Peterson *et al* 1989) and may depend on development of an entrapment zone near Suisun Bay (Arthur and Ball 1979; Cloern *et al* 1983). In recent years, attention has focused on the biological factor, benthic herbivory (Nichols 1985).

The purpose of this study is to use 17 years of measured water quality data and the time series modeling approach of Box-Jenkins transfer function models (Box and Jenkins 1976) to examine associations

In K.T. Redmond, Editor, 1992. Proceedings of the Eighth Annual Pacific Climate (PACLIM) Workshop, March 10-13, 1991: California Department of Water Resources, Interagency Ecological Studies Program Technical Report 31.

between long-term interannual changes in monthly phytoplankton chlorophyll *a* production and environmental factors in Suisun Bay and the Delta. The study will address three questions:

- Are there are environmental factors associated with long-term changes in chlorophyll concentration?
- Could any of these environmental factors be influenced by climate?
- How does this information help us understand processes that influence estuarine production?

Materials and Methods

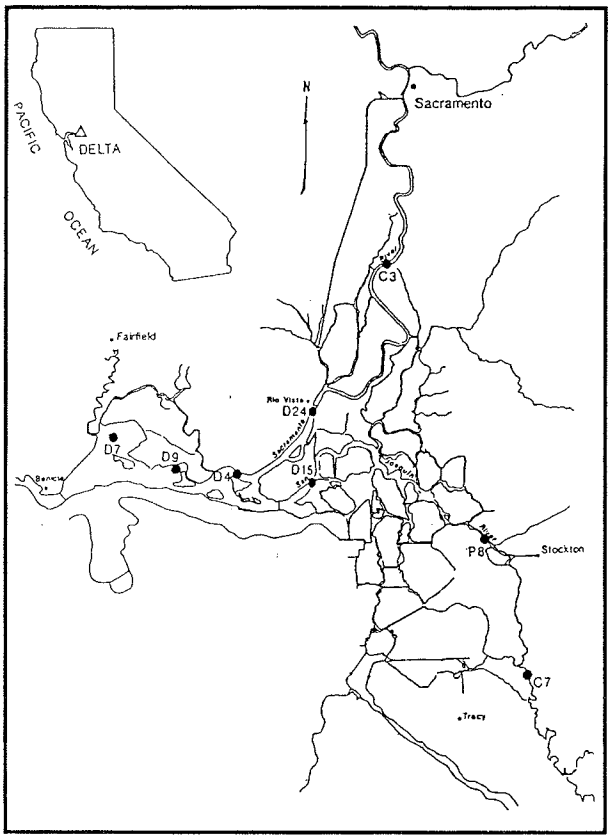

Figure 1. Sampling sites in the Sacramento-San Joaquin Delta and Suisun Bay.

Physical, chemical, and biological data were collected by the California Department of Water Resources, California Department of Fish and Game, and US Bureau of Reclamation between 1971 and 1987 on a semimonthly or monthly basis (California Department of Water Resources and US Bureau of Reclamation 1976; California Department of Water Resources 1975-1987). Three sites in each river and two sites in Suisun Bay were used for the analysis (Figure 1). The following biological and environmental variables were included in the analysis: chlorophyll concentration, zooplankton biomass, Sacramento and San Joaquin river flow, Delta export flow, Secchi disk depth, suspended solids, turbidity, pH, specific conductance, nitrate, phosphate and silicate concentration, air and water temperature, and wind velocity.

Statistical Analyses

Before analyses, data for each river and Suisun Bay were averaged by month and standardized to an anomaly value. Standardization required two steps. First, the monthly data were centered to remove seasonal variation. Second, non-homogeneity of the variance was removed by dividing by the standard deviation.

Principal component analysis was used to summarize groups of functionally related environmental variables that were highly intercorrelated. Highly intercorrelated variables can introduce computational and interpretational problems within transfer function models.

Chlorophyll and environmental anomaly time series were modeled using Box-Jenkins transfer function models (Box and Jenkins 1976). A transfer function modeling approach was chosen for this study because it removes the trend and autocorrelation in time series data that confound simple correlation analysis and includes lag responses inherent in biological processes.

Results

Environmental Variables

Of the 14 environmental variables examined, only those significantly cross-correlated with chlorophyll anomalies in the first 5 lags were retained for further analysis. Among these selected environmental variables, those that were highly correlated ($r>0.60$), were summarized (Table 1) using the following three principal component axes:

- PAXIS, which describes streamflow (+) and specific conductance (-).
- LAXIS, which describes Secchi disk depth (-), turbidity (+) and suspended solids (+).
- TAXIS, which describes air and water temperature (+).

Nutrients were not included in the analysis even though they were significantly cross-correlated with chlorophyll anomalies because the negative direction of the cross-correlations suggested the phytoplankton were regulating their immediate chemical environment —not the reverse.

Transfer function models described between 39 and 51 percent of the variance in chlorophyll anomalies for the Sacramento and San Joaquin rivers and Suisun Bay (Table 2). For the rivers, a negative association of chlorophyll anomalies with PAXIS at lag 1 suggested higher chlorophyll concentrations were associated with lower flows and higher specific conductance during the previous month. Chlorophyll anomalies were also negatively associated with turbidity (LAXIS) during the same or previous month for the Sacramento River and Suisun Bay. In contrast, turbidity was positively associated with chlorophyll anomalies during the previous month (lag 1) for the San Joaquin and two months before (lag 2) for Suisun Bay. Chlorophyll anomalies were positively associated with air and/or water temperature (TAXIS) for the San Joaquin River but negatively associated with water temperature for Suisun Bay four months before. For all models, predicted chlorophyll anomalies matched the long-term pattern of monthly chlorophyll anomalies quite well (Figures 2 through 4).

Table 1
Correlations between Environmental Anomalies and Principal Component Axes Used to Summerize Groups of Correlated Environmental Variables

	PAXIS					
	SACRAMENTO RIVER		SAN JOAQUIN RIVER		SUISUN BAY	
	axis 1	axis 2	axis 1	axis 2	axis 1	axis 2
specific conductance	-0.77	0.61	-0.81	0.55	-	-
San Joaquin River flow	0.82	0.50	0.91	0.06	-	-
Sacramento River flow	0.92	0.06	0.84	0.47	-	-
PROPORTION	71%	21%	73%	18%		
EIGENVALUE	2.1	0.6	2.2	0.5		

	LAXIS					
	SACRAMENTO RIVER		SAN JOAQUIN RIVER		SUISUN BAY	
	axis 1	axis 2	axis 1	axis 2	axis 1	axis 2
turbidity	0.94	0.11	0.88	-0.34	0.95	0.31
suspended solids	0.91	0.34	0.80	0.60	-	-
Secchi disc depth	-0.87	0.48	-0.90	0.20	-0.95	0.31
PROPORTION	83%	12%	74%	17%	90%	10%
EIGENVALUE	2.5	0.4	2.2	0.5	1.8	0.2

	TAXIS					
	SACRAMENTO RIVER		SAN JOAQUIN RIVER		SUISUN BAY	
	axis 1	axis 2	axis 1	axis 2	axis 1	axis 2
water temperature	-	-	0.88	-0.46	-	-
air temperature	-	-	0.88	0.46	-	-
PROPORTION	78%	22%				
EIGENVALUE	1.6	0.4				

Table 2
Transfer Function Models Developed to Predict Chlorophyll Anomalies ($aCHL_t$) for the Sacramento and San Joaquin Rivers and Suisun Bay, 1971-1987 *(n=202)*
Notation: $B^n(Y_t)=Y_{t-n}$, where Y=aCHL; e_t=Independent normally distributed random error.

SACRAMENTO RIVER

$$aCHL_t = -0.30PAXIS_{t-1} + 0.13LAXIS_{t-1} + (1-0.50B)^{-1}(1-0.16B^{3})^{-1}(1-0.15B^{10})^{-1}e_t$$

$R^2_{adj.} = 0.39$

SAN JOAQUIN RIVER

$$aCHL_t = -0.40PAXIS_{t-1} - 0.16LAXIS_t + 0.15TAXIS_t + (1-0.51B)^{-1}(1-0.16B^{5})^{-1}(1-0.16B^{6})^{-1}e_t$$

$R^2_{adj.} = 0.51$

SUISUN BAY

$$aCHL_t = (0.24_t + 0.18_{(t-2)})LAXIS - 0.12WATER\ TEMPERATURE_{t-4} + (1-0.57B)^{-1}(1+0.16B^{5})^{-1}e_t$$

$R^2_{adj.} = 0.46$

California SLP Index

To determine if there was a link between estuarine environmental conditions and regional climate, cross-correlations were calculated between a California climate index (CA SLP) and the environmental variables used in the transfer function models for each region. The CA SLP was negatively cross-correlated with the streamflow axis, PAXIS, for both the Sacramento and San Joaquin rivers at lag 1 (Table 3). For LAXIS, the cross-correlation with the CA SLP index was negative for the rivers and positive for Suisun Bay. The CA SLP index was not significantly cross-correlated with TAXIS or water temperature.

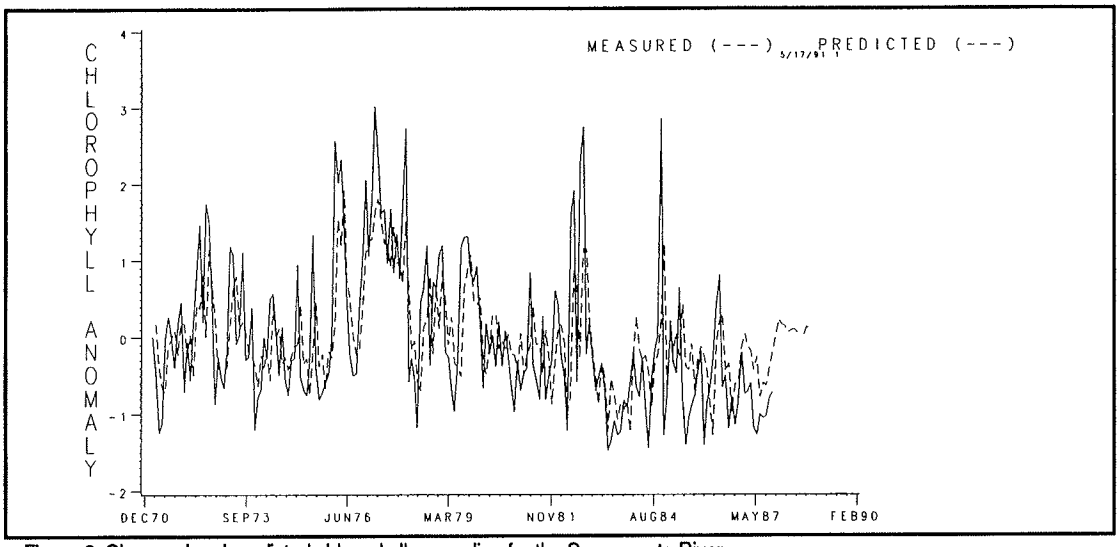

Figure 2. Observed and predicted chlorophyll anomalies for the Sacramento River.

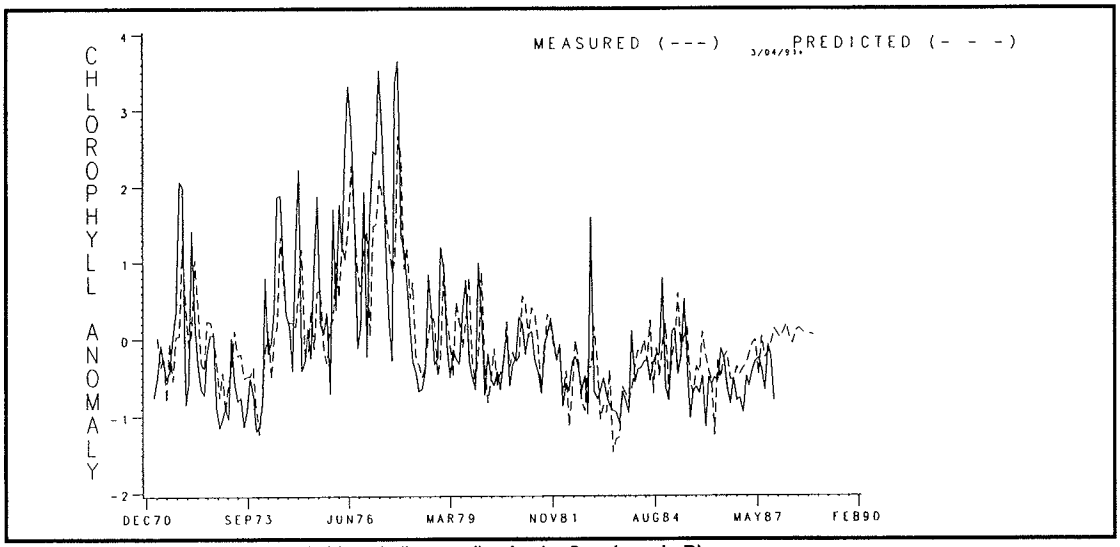

Figure 3. Observed and predicted chlorophyll anomalies for the San Joaquin River.

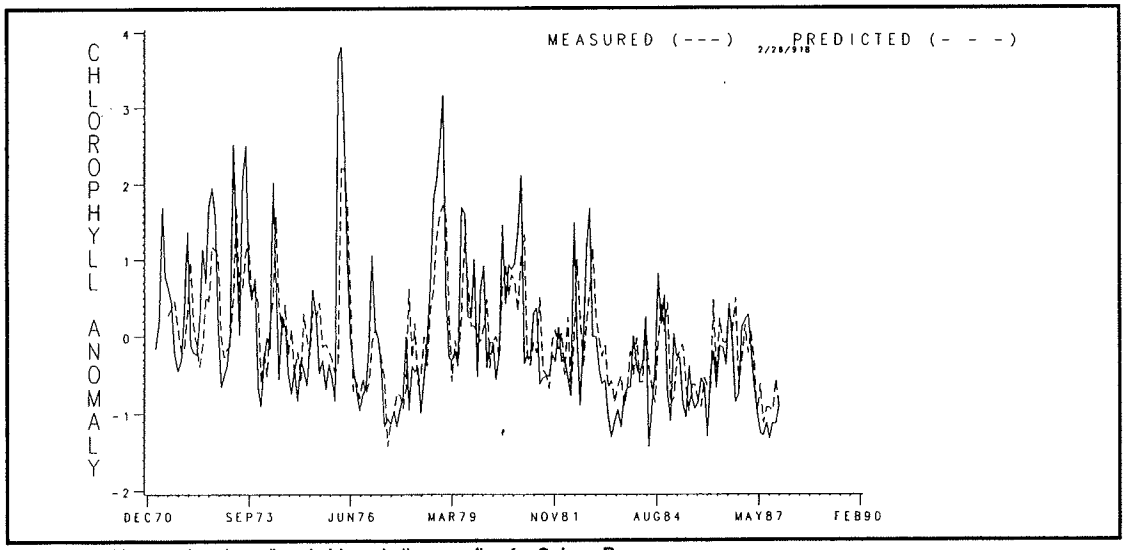

Figure 4. Observed and predicted chlorophyll anomalies for Suisun Bay.

Table 3
Cross-Correlations between Significant PCA Axes and the CA SLP Climate Index for the Sacramento and San Joaquin Rivers and Suisun Bay
(n=193)

	SACRAMENTO RIVER			SAN JOAQUIN RIVER			SUISUN BAY		
	lag	corr	sig	lag	corr	sig	lag	corr	sig
PAXIS	1	-0.31	<0.01	1	-0.30	<0.01		—	
LAXIS	1	-0.32	<0.01	1	-0.20	<0.01	1	0.20	<0.01
TAXIS			—			NS			—
Water Temperature			—			—			NS

NS = Not Significant

Zooplankton Biomass

The possible influence of long-term changes in chlorophyll concentration on the estuarine food web was examined by correlations between chlorophyll *a* concentration and zooplankton biomass. For both rivers, significant correlations were calculated between chlorophyll concentration and copepod and cladocera biomass (Table 4). For Suisun Bay, chlorophyll concentration was significantly correlated with copepod biomass.

Table 4
Correlations between Average Monthly Chlorophyll Concentration and Copepod or Cladocera Biomass for the Sacramento and San Joaquin Rivers and Suisun Bay, 1971-1987

	Copepod			Cladocera		
	r	sig	n	r	sig	n
Sacramento River	0.39	<0.01	153	0.28	<0.01	151
San Joaquin River	0.26	<0.01	154	0.35	<0.01	154
Suisun Bay	0.56	<0.01	160	0.16	NS	90

NS = Not Significant

Discussion

Transfer function models indicated an association between long-term high frequency changes in chlorophyll anomalies and environmental variables relating to streamflow, water clarity, and air and water temperature. For the rivers, lower streamflow during the previous month probably increased residence time and facilitated accumulation of biomass (Conomos 1979; Peterson 1979; Peterson *et al* 1989). Streamflow was not associated with chlorophyll concentrations in the shallow bay sites, where internal processes are probably more influential than flow (Cloern *et al* 1983, 1985; Cloern and Cheng 1981; Nichols 1985). In keeping with the theory that the estuary is light-limited (DiToro 1971; Ball and Arthur 1979; Cloern and Cheng 1981; Peterson and Festa 1984), turbidity was negatively associated with chlorophyll anomalies for the Sacramento River and Suisun Bay. The positive association between chlorophyll anomalies and turbidity in the San Joaquin River suggests other processes besides light limitation are occurring and may include self-shading,

agricultural loading, water management practices, or resuspension of benthic phytoplankton. Air and water temperature were either positively associated with chlorophyll anomalies as for the San Joaquin River or reflected a possible ocean influence for Suisun Bay where increased production may be related to cooler water temperatures associated with upwelling along the coast (Cloern *et al* 1983; Cloern and Cheng 1981).

Significant cross-correlations between the environmental axes associated with chlorophyll production and CA SLP, suggest climate may influence estuarine production. The CA SLP index describes sea level pressure at 130°W and 40°N and is associated with average seasonal precipitation, streamflow, snowpack, and snowmelt for central California. The cross-correlation between December through August Sacramento River flow and the winter CA SLP index is -0.6 (Cayan and Peterson 1989). For this study, a significant cross-correlation was calculated between the CA SLP index and monthly changes in streamflow and turbidity. Stable weather conditions associated with high sea level pressure decrease precipitation and produce low streamflow. With decreasing streamflow, soil erosion and mixing are reduced and turbidity decreases (Krone 1979). For Suisun Bay, cross-correlations suggest a somewhat different mechanism. Turbidity increased with high sea level pressure or stable conditions. Stable conditions would be accompanied by decreased 2-layered flow and increased mixing during tidal incursion, which would decrease the influence of a clearer freshwater lens.

The pattern of associations among the biological and environmental variables suggests a conceptual model of how regional climatic conditions are linked with estuarine production (Figure 5). The process would begin by a shift in regional sea level pressure. One month later, local precipitation would affect streamflow and associated water quality variables. During the following month or two, water quality would affect chlorophyll production and eventually the rest of the food web. A longer term teleconnection may affect phytoplankton production in Suisun Bay, based on the lag 4 cross-correlation between chlorophyll anomaly and water temperature.

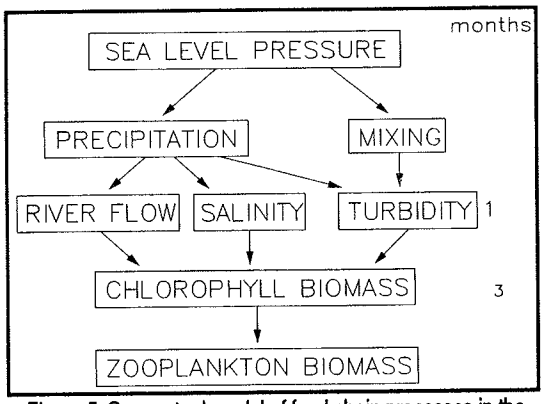

Figure 5. Conceptual model of food chain processes in the Sacramento-San Joaquin Delta and Suisun Bay.

Literature Cited

Arthur, JF, and MD Ball, 1979. Factors influencing the entrapment of suspended material in the San Francisco Estuary. Pgs. 143-174 in TJ Conomos (ed.) *San Francisco Bay: The Urbanized Estuary*. Pacific Division of the American Association for the Advancement of Science:San Francisco.

Box, GEP, and GM Jenkins, 1976. *Time Series Analysis: Forecasting and Control.* Revised Edition. Holden-Day:Oakland, CA. 575 pp.

California Department of Water Resources, 1975-1987. *Sacramento-San Joaquin Delta water quality surveillance program. Vol I.*

California Department of Water Resources and US Bureau of Reclamation, 1976. *Delta-Suisun Bay ecological studies.* A water quality data report of the coordinated monitoring program. Methods and data for 1974. 299p.

Cayan, DR, and DH Peterson, 1989. The influence of North Pacific atmospheric circulation on streamflow in the west. Pgs. 375-397 in DH Peterson (ed.) Aspects of Climate Variability in the Pacific and Western Americas. *A.G.U. Monograph 55.*

Cloern, JE, AE Alpine, BE Cole, RLJ Wong, JF Arthur, and MD Ball, 1983. River discharge controls phytoplankton dynamics in the northern San Francisco Bay. Estuary. *Estuarine Coastal and Shelf Science.* 16:415-429.

Cloern, JE, and RT Cheng, 1981. Simulation model of *Skeletonema costatum* population dynamics in northern San Francisco Bay, California. *Estuarine Coastal and Shelf Science.* 12:83-100.

Cloern, JE, BE Cole, RLJ Wong, and AE Alpine, 1985. Temporal dynamics of estuarine phytoplankton: A case study of San Francisco Bay. *Hydrobiology.* 129:153-176.

Conomos, TJ, 1979. Properties and circulation of San Francisco Bay waters. Pgs. 47-84 in TJ Conomos (ed.) *San Francisco Bay: The Urbanized Estuary.* Pacific Division of the American Association for the Advancement of Science:San Francisco.

DiToro, DM, DJ O'Connor, and RV Thomann, 1971. A dynamic model of the phytoplankton population in the Sacramento-San Joaquin Delta. Pgs. 131-180 in *Non-equilibrium Systems in Natural Water Chemistry.* Advances in Chemistry Series 196. American Chemical Society:Washington, DC.

Interagency Ecological Study Program. 1990. *Evaluation of biological factors that may have contributed to the drought and post-drought decline in chlorophyll a concentrations.* June 1984 Technical Summary of Findings of the Phytoplankton Task Force Biological Committee. Technical Report 22. California Department of Water Resources:Sacramento. 45 pp.

Krone, RB, 1979. Sedimentation in the San Francisco Bay system. Pgs. 85-96 in TJ Conomos (ed.) *San Francisco Bay: The Urbanized Estuary.* Pacific Division of the American Association for the Advancement of Science:San Francisco.

Lehman, PW, and RW Smith, 1991. Environmental factors associated with phytoplankton succession for the Sacramento-San Joaquin Delta and Suisun Bay Estuary, California. *Estuarine Coastal and Shelf Science.* 32(2):105-128.

Nichols, FH, 1985. Increased benthic grazing: an alternative explanation for low phytoplankton biomass in northern San Francisco Bay during the 1976-1977 drought. *Estuarine Coastal and Shelf Science.* 21(3):379-388.

Peterson, DH, 1979. Sources and sinks of biologically reactive oxygen, carbon, nitrogen, and silica in northern San Francisco Bay. Pgs. 175-193 in TJ Conomos (ed.) *San Francisco Bay: The Urbanized Estuary.* Pacific Division of the American Association for the Advancement of Science:San Francisco.

Peterson, DH, and JF Festa, 1984. Numerical simulation of phytoplankton productivity in partially mixed estuaries. *Estuarine Coastal and Shelf Science.* 19:563-589.

Peterson, DH, DR Cayan, JF Festa, FH Nichols, RA Walters, JV Slack, SE Hager, and LE Schemel, 1989. Climate variability in an estuary: effects of riverflow on San Francisco Bay. Pgs. 419-442 in DH Peterson (ed.) *Aspects of climate variability in the Pacific and western Americas.* AGU Monograph 55. Washington, DC.

Meteorological Signals in Primary Productivity at Two Mountain Lakes

Alan D. Jassby and Charles R. Goldman

Abstract: Fluctuations in primary productivity at two subalpine lakes reveal both meteorological and biological influences. At Castle Lake, California, large-scale climate events such as the El Niño/Southern Oscillation affect total annual production and, combined with human fishing activity, modify the seasonal pattern of productivity. At Lake Tahoe, California-Nevada, local spring weather conditions modulate annual production and its seasonality by determining the depth of mixing and resulting internal nutrient load. Climatic conditions also contribute to deviations from the long-term trend in productivity by increasing the incidence of forest fires and through anomalous external nutrient loads during precipitation extremes. A 3-year cycle in productivity of as yet unknown origin has also been detected at Lake Tahoe.

Introduction

Food webs in lakes, as in most ecosystems, exhibit considerable variability on just about any time scale. The reasons can be classified in several ways. A traditional approach in ecology has been to divide them into two groups: density-dependent versus density-independent mechanisms. "Density-dependent" refers to variability that arises from intrinsic dynamics of the ecosystem. "Density-independent" refers to variability set in motion by external forces, often, but certainly not always, meteorological.

Recent interest in limnology has focused on a different grouping of these mechanisms. Is variability controlled by forces acting at the base of the food web? Or do these forces first operate on higher organisms, with the effects cascading down the food web through predation. Known as the "top-down/bottom-up" issue (Mills and Forney 1988), this problem is actually not a well-posed one because of feedback loops in food webs. One can legitimately ask, however, where in the food web *external* forces first impinge: at the bottom, the top, or perhaps in several places?

We present here some time series for two northern California lakes in the context of these issues. Our emphasis is on interannual variability, both in annual averages and in the mean seasonal pattern. The longest series available for these two lakes are measurements of photosynthesis with the carbon-14 method. The series are sufficiently long to identify contributions of the El Niño/Southern Oscillation (ENSO) to overall variability. First, we review some work published recently on Castle Lake and then present results from a similar analysis for Lake Tahoe. The statistical evidence is emphasized here, but there is much supporting evidence from experiments and field observations as well. The references can be

In K.T. Redmond, Editor, 1992. Proceedings of the Eighth Annual Pacific Climate (PACLIM) Workshop, March 10-13, 1991: California Department of Water Resources, Interagency Ecological Studies Program Technical Report 31.

consulted for additional information (Goldman *et al* 1989, 1990; Goldman and Jassby 1990; Jassby and Powell 1990; Jassby *et al* 1990).

Castle Lake

Castle Lake is a small (0.20 km^2) subalpine lake in the Klamath Mountains near Mt. Shasta (41°13'N, 122°22'S). It lies in a cirque basin at an altitude of 1657 meters. Because the lake is covered by ice for much of the year, it is sampled routinely only in summer. So the "annual" primary productivity (Figure 1) is actually the average of data for only four months, June through September. Occasional year-round studies indicate, however, that most of the production takes place in this June-September interval.

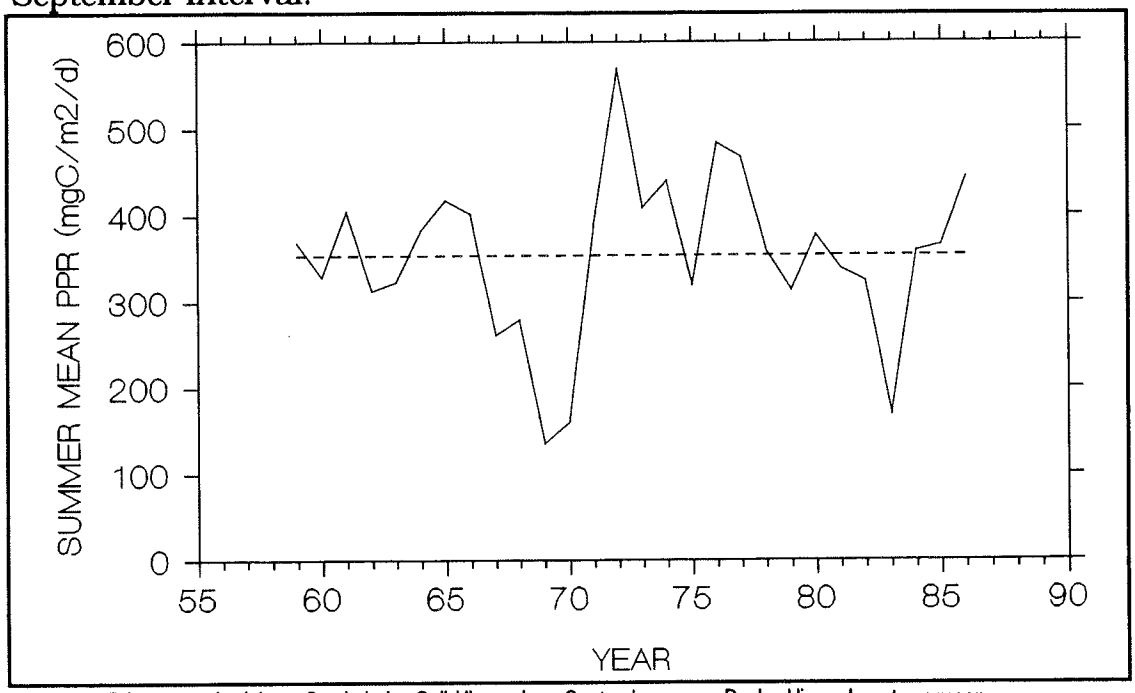

Figure 1. Primary productivity at Castle Lake. Solid line = June-September mean; Dashed line = long-term mean.

Primary productivity has no clear long-term trend, but interannual variability is high. Many of the most extreme years happen to be years in which ENSO events took place (Goldman *et al* 1989). Sometimes ENSO years are unusually high, sometimes unusually low, but their spread is significantly greater than for other years (Siegel-Tukey test, $p<0.01$). The exact role of ENSO events can be better understood by examining the seasonal pattern.

The average seasonal pattern of productivity at Castle Lake exhibits two local maxima (Figure 2a). The early summer deep-water maximum is caused by diatoms and dinoflagellates. Crustacean grazers are low in numbers at this time and fish, primarily rainbow trout, feed mostly on emerging insects. The late summer mixed-layer maximum, in contrast, is dominated by blue-greens. Mesozooplankton grazers, particularly *Daphnia rosea*, become abundant and the rainbow trout now feed heavily

on *Daphnia*. The averaged contour plot disguises the tremendous amount of year-to-year variability (Figure 2b). Most of the variability in productivity is associated with the two blooms.

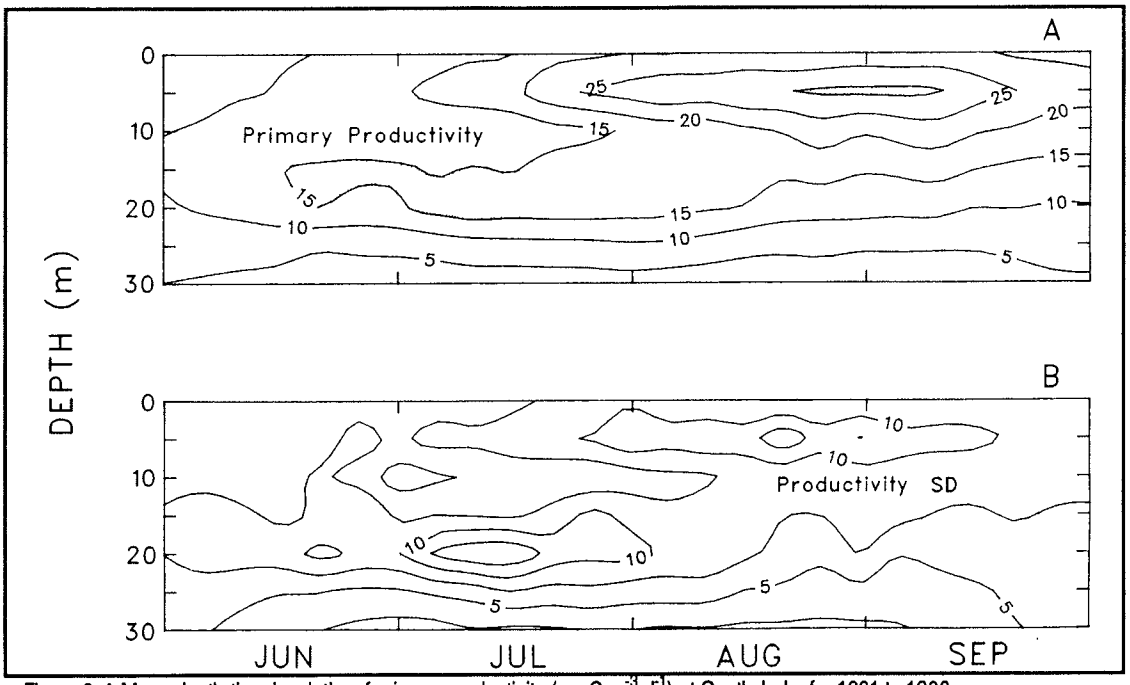

Figure 2. A Mean depth-time isopleths of primary productivity (mg C m^{-3} d^{-1}) at Castle Lake for 1961 to 1986. B Same as A but isopleths of primary productivity standard deviation.

For any given year, we can bin the data for separate regions of the depth/time plane. For this analysis, we divided the plane into 5-meter deep by 1-month long bins, a total of 24 bins. So the depth/time contour plot for a given year can be thought of as a single realization of a 24-dimensional variable. The sequence of contour plots is then equivalent to a multivariate time series. This time series can be analyzed with principal component analysis (PCA), much like the data for a spatial array of surface stations, permitting us to decompose the overall variability (Figure 2b) into its constituent modes (Jassby and Powell 1990). Two significant modes were found, one corresponding to the early bloom, the second corresponding to the later one (Jassby *et al* 1990). The modes were well-behaved statistically according to a variety of criteria, so we have confidence in these patterns.

The amplitude time series for each mode was quite revealing. The first mode was negatively associated with ice breakup time, which simply sets the length of the growing season (Table 1). The ice breakup time is linked, in turn, to the amount of winter snowfall. The snow/ice pack is often deep (2 meters) and no solar radiation can penetrate. Most heat for melting is derived from the underlying water, so increased snowfall delays ice breakup. The accumulating snow also represents negative latent heat that must be balanced by heat income. *Total* precipitation preceding the spring bloom, including snow *and* rain, was also negatively associated with the first mode. An analysis of partial correlations showed this association was independent of ice breakup time (Goldman *et al* 1989).

Table 1
Notable Associations[1] for the Amplitudes of Primary Productivity Modes at Castle Lake
(The modes, PC-1 and PC-2, were determined by principal component analysis followed by a varimax rotation.)

Variable	Years	PC-1	PC-2
Ice Breakup Time	17	-0.77*	0.03
Precipitation	24	-0.58*	-0.33
Daphnia Biomass (September)			
All Years	18	0.06	-0.45**
All Years Except 1983	17	-0.11	-0.56*
Rainbow Trout	11	0.04	0.68*
Percent of Total Variance		30	31

1 Spearman rank correlations
* $p<0.05$
** $p=0.07$

About a third of the lake is rapidly flushed out following ice thaw, and total precipitation probably exerts its effects through flushing of the algal community. Consequently, both the presence of an ice cover and a hydraulic residence time of order 1 year enable climate to modulate the size of the spring bloom, accounting for the anomalous values seen during ENSO events when precipitation at Castle Lake is often extreme.

The second mode, corresponding to the late summer bloom, was *negatively* associated with late summer populations of the main grazer in the lake, the cladoceran *Daphnia rosea* (Table 1). The association is significant at the 0.05 level if we exclude 1983, when the ice did not thaw until July and zooplankton populations were extraordinarily low. This mode was also *positively* associated with rainbow trout, the main predator of *Daphnia*. Using a variety of other experiments and observations, we were able to conclude that this second mode originated in variability of the trout populations and cascaded down to phytoplankton through the food web via *Daphnia* (Jassby *et al* 1990). The trout are stocked every year and heavily fished, and at least part of the fluctuation in trout populations arises from variable fishing intensity. The second mode does not seem to have a strong link to climate, but because the rainbow trout population forms essentially a put-and-take fishery, natural recruitment plays a minor role at Castle Lake. In lakes with unmanaged fish communities, one might well expect a climatic influence on this mode as well.

Lake Tahoe

Lake Tahoe presents a completely different picture. This large lake (501 km^2) straddles the border between California and Nevada (39°N, 120°W), lying in a graben at an altitude of 1898 meters. Productivity at Tahoe has been increasing since sampling began in the late 1960s. This long-term increase, which is due to nutrient loading from the atmosphere and watershed, is accompanied by much short-term variability (Figure 3). Tahoe does not have an ice cover. It also has an extremely long hydraulic residence time of about 700 years. So the particular features that permit

climatic variability to impinge on Castle Lake are absent. Other mechanisms, of course, can mediate a climatic impact, but the year-to-year variability is much less at Tahoe than at Castle, and ENSO events do not leave as consistent a mark on the record.

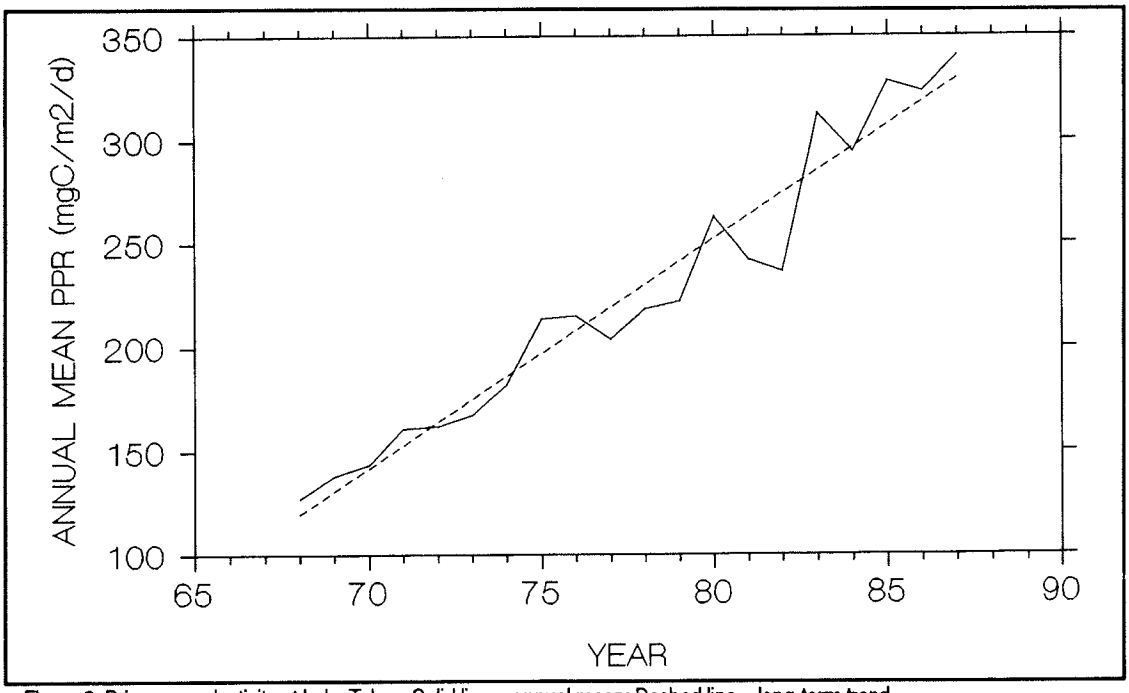

Figure 3. Primary productivity at Lake Tahoe. Solid line = annual mean; Dashed line = long-term trend.

We do know that in at least one case, a large forest fire affected the seasonal pattern and, perhaps, the annual mean of primary productivity at Tahoe (Goldman *et al* 1990). July 1985 was the time of a major fire in Las Padres National Forest that had a dramatic effect on the Lake Tahoe basin. The entire basin was shrouded in smoke, and the sun appeared as a dull orange sphere. Measurements showed, however, that productivity increased dramatically in mid-July, despite the lower light levels (Figure 4a). We did some bioassays using atmospheric fallout collected at this time. It was indeed stimulating to productivity in a manner similar to that obtained with nutrient additions. We believe the dry fallout was a source of limiting nutrients, but were unable to establish exactly which ones. Although phosphorus was probably the main limiting macronutrient in 1985, Tahoe bioassays have a history of responding to chelating agents such as EDTA, implicating a role for trace metals (Goldman 1981). In any case, the 1985 fire resulted in the biggest July anomaly on record (Figure 4b). Insofar as fire intensity and frequency can be attributed to climate conditions (Swetnam and Betancourt 1990), this represents yet another way in which climate underlies interannual variability. Note that other large fires in the region have *not* had any detectable effect on the lake. Fuel source, temperature of burning, and distance from the Tahoe watershed all probably affect the composition of smoke entering the basin and its potential for stimulating primary productivity.

PCA techniques similar to those used for Castle Lake can be applied to the Tahoe productivity data. However, there are not enough years of data

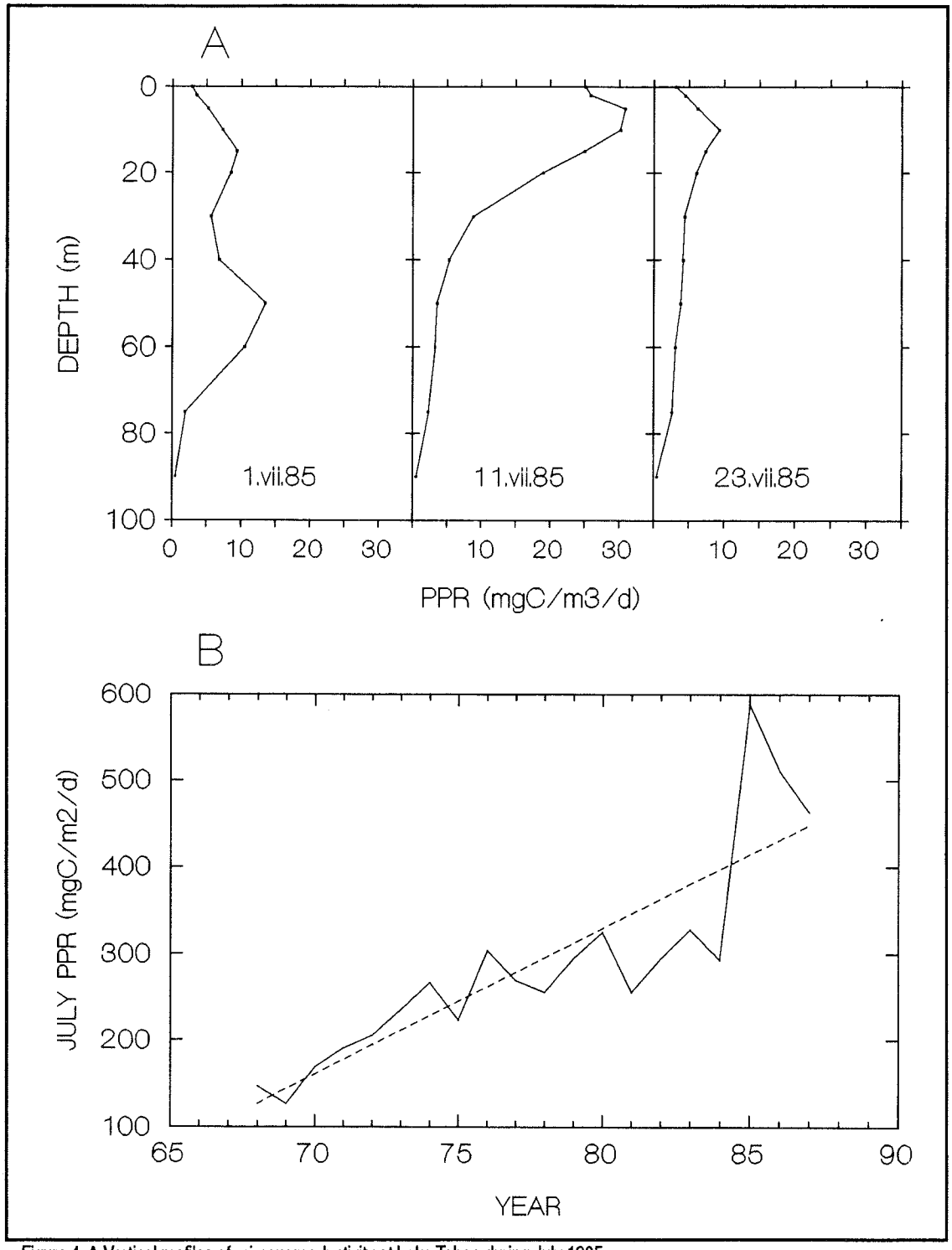

Figure 4. A Vertical profiles of primary productivity at Lake Tahoe during July 1985.
B Primary productivity at Lake Tahoe. Solid line = July mean; Dashed line = long-term trend.

to get adequate resolution in both the time and depth dimension. We looked instead at data aggregated by month for the entire water column. Because the July 1985 fire was unique, we removed its influence by replacing the productivity value for that month with the long-term July mean. The series was then divided by the trend to remove the trend and stabilize the variance. Again, two significant modes were found.

The first mode peaked in May, and its amplitude time series was associated with the depth of maximum spring mixing, usually occurring in March. Tahoe is very deep (500 meters) and the ratio of its maximum depth to its average fetch is quite small, so the lake is predisposed to incomplete spring mixing. The variable spring mixing upwells different quantities of nutrients into the photic zone from one year to the next, contributing to year-to-year fluctuations of productivity in late spring (Goldman and Jassby 1990). The relationship can be detected in the annually-averaged data (Figure 5) and not just for a particular mode isolated by the eigenvector analysis. Although certain years are exceptional, mixing depth is correlated with deviations from the long-term linear trend in productivity (p=0.046). The depth of mixing was shown to reflect the intensity of storms during isothermal conditions in March. So although there may be fewer ways for *climate* events to express themselves (because of the lack of ice cover and long residence time), local *weather* events at certain times of the year can be critical. This mixing mechanism does have a connection with climate in that the probability of a severe storm during isothermal conditions increases during anomalously wet years. The connection, however, is a loose one. During the wet winter of 1986, for example, the lake mixed down to only 200 meters.

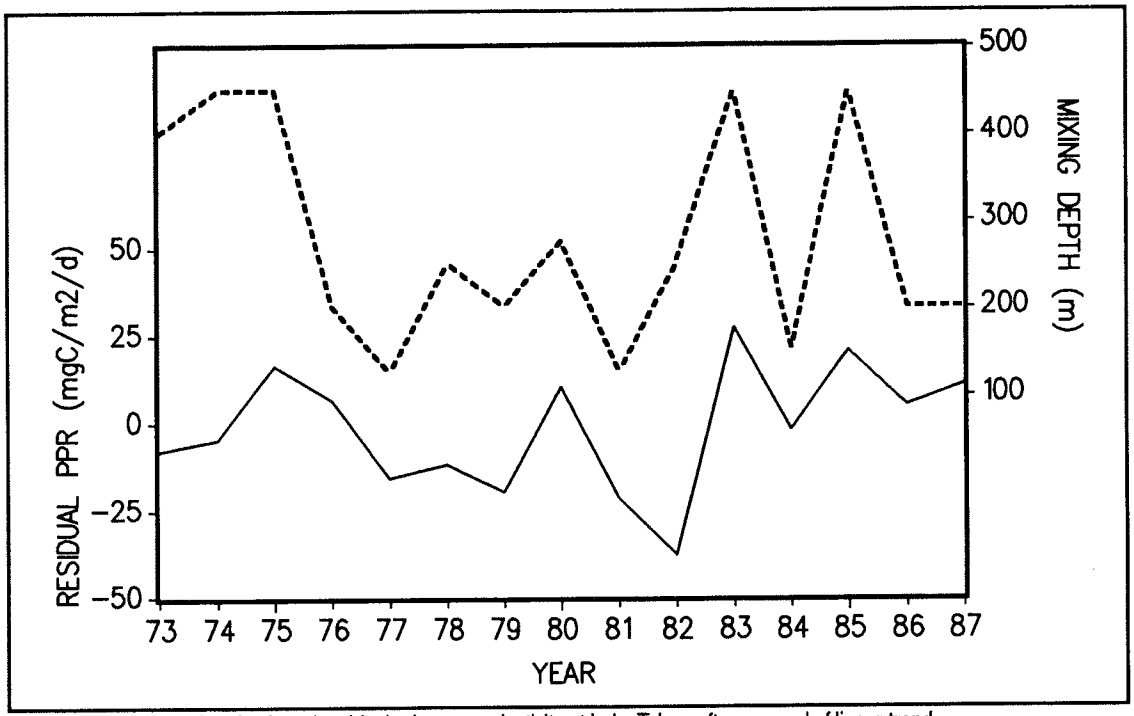

Figure 5. Spring mixing depth and residual primary productivity at Lake Tahoe after removal of linear trend.

Anomalous climatic events may also have a more direct effect through external loading. Fluctuations in primary productivity at Tahoe reflect anomalies in the amount of nutrients introduced into the photic zone each year, whether they are derived from internal or external loading. Anomalies in the internal load dominate, so that depth of mixing is the critical controlling mechanism. During years of precipitation extremes, however, anomalies in the external loading may contribute to productivity fluctuations. In 1983, for example, a combination of deep mixing *and*

unusually high precipitation was probably responsible for the most positive residual in productivity on record (Figure 5). For the record as a whole, annual precipitation has a weakly significant partial correlation with the productivity residuals after accounting for depth of mixing (p=0.081), but adds little explanatory power compared to mixing depth alone.

The final mode remains a mystery. It does, however, have some curious features. With a few exceptions, the amplitude time series for this mode seems to have a 3-year cycle. This 3-year cycle can be pulled out directly from the data, even without first accounting for the 1985 fire and the depth of mixing, by computing the spectrum (Figure 6). The biggest peak of course corresponds to the annual cycle. The 3-year cycle also is obvious. The 1.5-year cycle is probably a harmonic of the 3-year cycle. The reason for this 3-year cycle is not yet known. It can be shown theoretically that animal populations tend to oscillate with a period equal to their generation time (Carpenter 1988). Consequently, a 3-year cycle in phytoplankton might be attributable to cascading effects from a population at higher trophic levels. At Tahoe, however, field measurements and experiments suggest the higher trophic levels are simply too sparse to have a grazing impact. In fact, the trophic cascade should be important only in lakes of higher productivity, like Castle Lake (Elser and Goldman 1991).

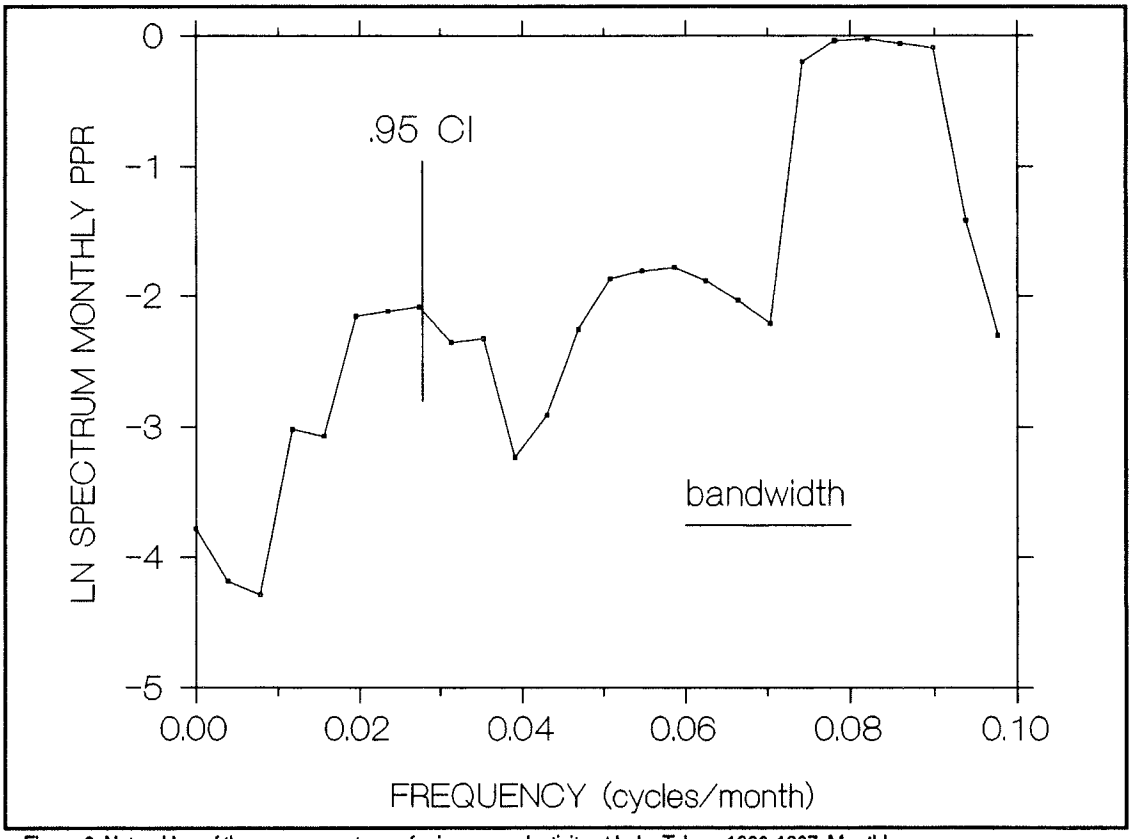

Figure 6. Natural log of the power spectrum of primary productivity at Lake Tahoe, 1968-1987. Monthly means were log-transformed to stabilize the variance, and the long-term trend was removed. The .95 confidence interval (CI) and bandwidth are indicated. The line indicating the confidence interval is positioned at a frequency of 0.0278 cycles month^{-1} (corresponding to a 3-year period).

We are investigating alternative possibilities. One is the effect of nutrient removal from the upper layers by zooplankton, particularly *Mysis relicta*, that feed near the surface during the night and migrate to depths during the day where most of the excretion takes place. This is known to be a significant transport mechanism in certain oceanic situations (Longhurst and Harrison 1988). Zooplankton, therefore, may transmit variability from higher trophic levels through nutrient transport rather than through grazing. Other mechanisms can be proposed as well, however, and no definitive statements are possible at this time.

Concluding Remarks

To sum up, we do not appear to be at the point where grand generalizations about interannual variability in productivity are possible. We can, however, start to draw up a kind of taxonomy of causal mechanisms. Consider just Castle Lake and Lake Tahoe. External forces include the influence of climate on growing season and on flushing losses. Climate also can influence external nutrient loading through atmospheric deposition during fires and through precipitation volume. Local weather events can influence internal nutrient loading through the depth of spring mixing. External forces also can act top-down through the food web, such as variable fishing intensity cascading down through different trophic levels. And — as suggested by the spectral analysis at Tahoe — intrinsic cycles may be present as well. Seven significant causal pathways have been identified in just two lakes. If we can generalize at all, it is that the causes of interannual variability are surprisingly diverse.

Acknowledgments

We thank Bob Richards and Scott Hackley for their contributions to the long-term data acquisition program at Lake Tahoe and Patty Arneson for her help with the data management and figures. This work was supported by the National Science Foundation (grant BSR 89-18448 to CRG) and the Lake Tahoe Interagency Monitoring Program.

References

Carpenter, SR, 1988. Transmission of variance through lake food webs. Pgs. 119-135 in SR Carpenter (ed.) *Complex interactions in lake communities.* Springer-Verlag:New York.

Elser, JJ, and CR Goldman, 1991. Zooplankton effects on phytoplankton in lakes of contrasting trophic status. *Limnology and Oceanography.* 36:4-90.

Goldman, CR, 1981. Lake Tahoe: two decades of change in a nitrogen deficient oligotrophic lake. *Verhandlungen Internationale Vereinigung Limnologie.* 21:45-70.

Goldman, CR, and A Jassby, 1990. Spring mixing depth as a determinant of annual primary production in lakes. Pgs. 125-132 in MM Tilzer and C Serruya (eds.) *Large lakes: ecological structure and function.* Springer-Verlag:New York.

Goldman, CR, AD Jassby, and E deAmezaga, 1990. Forest fires, atmospheric deposition and primary productivity at Lake Tahoe, California-Nevada. *Verhandlungen Internationale Vereinigung Limnologie.* 24:499-503.

Goldman, CR, A Jassby, and T Powell, 1989. Interannual fluctuations in primary production: meteorological forcing at two subalpine lakes. *Limnology and Oceanography.* 34:308-321.

Jassby, AD, and TM Powell, 1990. Detecting changes in ecological time series. *Ecology.* 71:2044-2052.

Jassby, AD, TM Powell, and CR Goldman, 1990. Interannual fluctuations in primary production: direct physical effects and the trophic cascade at Castle Lake, California. *Limnology and Oceanography.* 35:1021-1038.

Longhurst, AR, and WG Harrison, 1988. Vertical nitrogen flux from the oceanic photic zone by diel migrant zooplankton and nekton. *Deep-Sea Research.* 35:881-889.

Mills, EL, and JL Forney, 1988. Trophic dynamics and development of freshwater pelagic food webs. Pgs. 11-30 in SR Carpenter (ed.) *Complex interactions in lake communities.* Springer-Verlag:New York.

Swetnam, TW, and JL Betancourt, 1990. El Niño-Southern Oscillation (ENSO) phenomena and forest fires in the southwestern United States. Pgs. 129-134 in JL Betancourt and AM MacKay (eds.) *Proceedings of the Sixth Annual Pacific Climate (PACLIM) Workshop.* March 5-8, 1989. Interagency Ecological Studies Program Technical Report 23.

Case Studies of Two Contrasting Rainfall Episodes in Hawaii

Pao-Shin Chu, Fee-Yung Porter, and Andrew J. Nash

Introduction

Hawaii experienced large interannual rainfall variability in the early 1980s; a severe and persistent drought prevailed in 1981 (Haraguchi and Giambulluca 1981) and excessive rainfall occurred in 1982. Drought in Hawaii is a perennial problem and has a direct impact on water supply, soil moisture, crops, and livestock. State and municipal water agencies, as well as many in the private sector, are in need of drought information for better water planning and management. On the other hand, unusually long rainy spells are also of immense concern to a host of weather-dependent endeavors such as construction and tourism, which provide the major income to Hawaii. These facts exemplify the need to better understand the physical causes of insufficient and excessive rainfall episodes.

Deficient rainfall and streamflow in Hawaii tend to follow the occurrence of the El Niño/Southern Oscillation (ENSO) phenomenon (Horel and Wallace 1981; Ropelewski and Halpert 1987; Chu 1989; Cayan and Peterson 1989). However, Hawaiian droughts have occurred in the absence of an apparent ENSO phenomenon, such as the drought in late 1980 and a large portion of 1981. The onset, duration, and strength of drought varied on each island. While this drought was relatively short and weak on Oahu, it was the longest and severest for the island of Hawaii according to a 56-year record (Figure 1; Giambulluca *et al* 1990). The drought there began in October 1980 and lasted until November 1981.

The physical processes responsible for the wet episodes have been studied even less than those for the drought. The rainfall index for winter 1982 was 1.33% above the long-term mean. In light of this large interannual rainfall variability between dry 1981 and wet 1982, the present study utilizes a large dataset to investigate the circulation mechanisms of rainfall anomalies.

Data and Rainfall Time series

Monthly rainfall totals from 27 stations selected in the earlier studies by Meisner (1976) and Chu (1989) are used. Figure 1 shows distribution of

In K.T. Redmond, Editor, 1992. Proceedings of the Eighth Annual Pacific Climate (PACLIM) Workshop, March 10-13, 1991: California Department of Water Resources, Interagency Ecological Studies Program Technical Report 31.

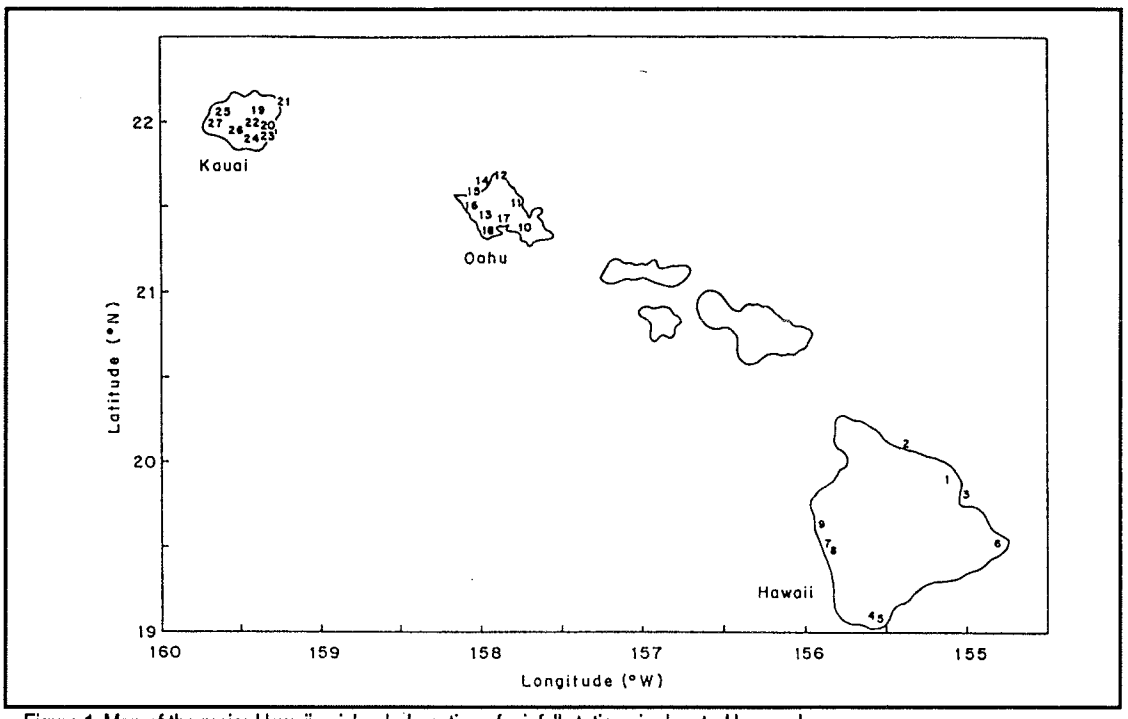

Figure 1. Map of the major Hawaiian islands. Location of rainfall stations is denoted by numbers.

the stations in the major Hawaiian Islands. A normalization technique is first applied to each individual station, and a regional index is then calculated as the arithmetic average of all station indices.

Ship observations over the North Pacific during 1951 to 1987 are available from the Comprehensive Ocean-Atmosphere Data Set (COADS) and interim COADS, made by the Environmental Research Laboratory of NOAA. Daily upper-air data from the European Center for Medium Range Weather Forecasts for 1979 to1987 are archived at the University of Hawaii. The variables available to us include wind and geopotential height at a 2.5° latitude-longitude resolution at two levels (*ie*, 850 and 200 hPa).

Figure 2 shows the time series of the regional monthly rainfall index from November through April of 1980/1981 and 1981/1982. These six months were chosen because they comprise the rainy season for most stations on the islands. Rainfall was deficient for six consecutive months from November 1980 to April 1981 and above normal for six consecutive months from November 1981 to April 1982, indicating a large interannual rainfall variability in Hawaii from 1980/1981 to 1981/1982.

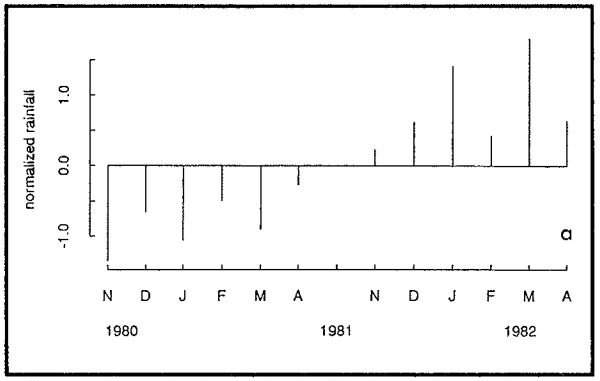

Figure 2. Normalized monthly rainfall index for Hawaii, November 1980 to April 1981 and November 1981 to April 1982.

Surface Circulation Patterns

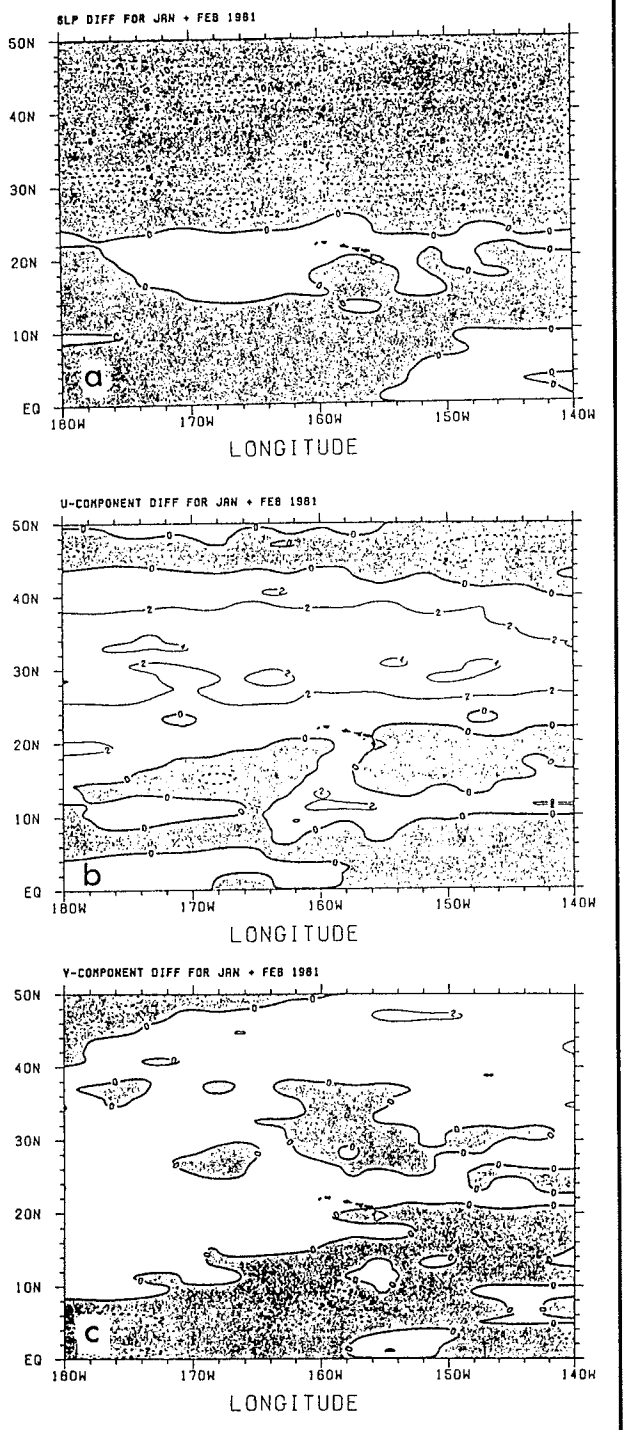

Figure 3. Departure maps for January/February 1981.
A Sea level pressure. Contour interval is 2 hPa. Regions with negative departures are shaded.
B Zonal wind component.
C Meridional wind component. Contour interval is 2 m s^{-1}. Regions with negative departures are shaded.

Departure maps of key meteorological variables during the dry and wet episodes in Hawaii are analyzed. For simplicity, maps are presented only of SLP (sea level pressure), u (zonal component of the wind), and v (meridional component of the wind) at the peak season of dry and wet episodes. Departure is understood as the difference of individual monthly value from the median, which is determined from ship records for 1951 to 1987. To stabilize results of the analysis, bimonthly maps during the extreme episodes are presented (eg, November/December, *etc*).

In January/February 1981, the entire extratropical belt of the eastern North Pacific was marked by the negative SLP anomalies, signaling the wintertime transient disturbances across the ocean from East Asia (Figure 3a). The pressure departures were as large as 10 hPa in an area poleward of 46°N between the dateline and 160°W. A narrow band of positive but small SLP departures was found in the subtropics. The map of zonal wind in January/February 1981 (Figure 3b) depicts positive zonal wind anomalies (stronger westerlies) to the north of Hawaii and negative zonal wind anomalies (easterly anomalies) to the south of Hawaii. The easterly trade winds in Hawaii were much reduced. Haraguchi (1981) also noted this feature.

Since the major rainfall patterns during winter, in decreasing order of importance, are the trade wind pattern, southwest wind pattern, and mid-latitude frontal rainfall pattern (Lyons 1982), a substantial reduction of trades implies a dry winter. The map of meridional wind departures, Figure 3c, also reveals northerly anomalies to the east and southerly anomalies to the west of the islands. A synthesis of these wind patterns suggests an anomalously strong anticyclonic circulation in the vicinity of the islands.

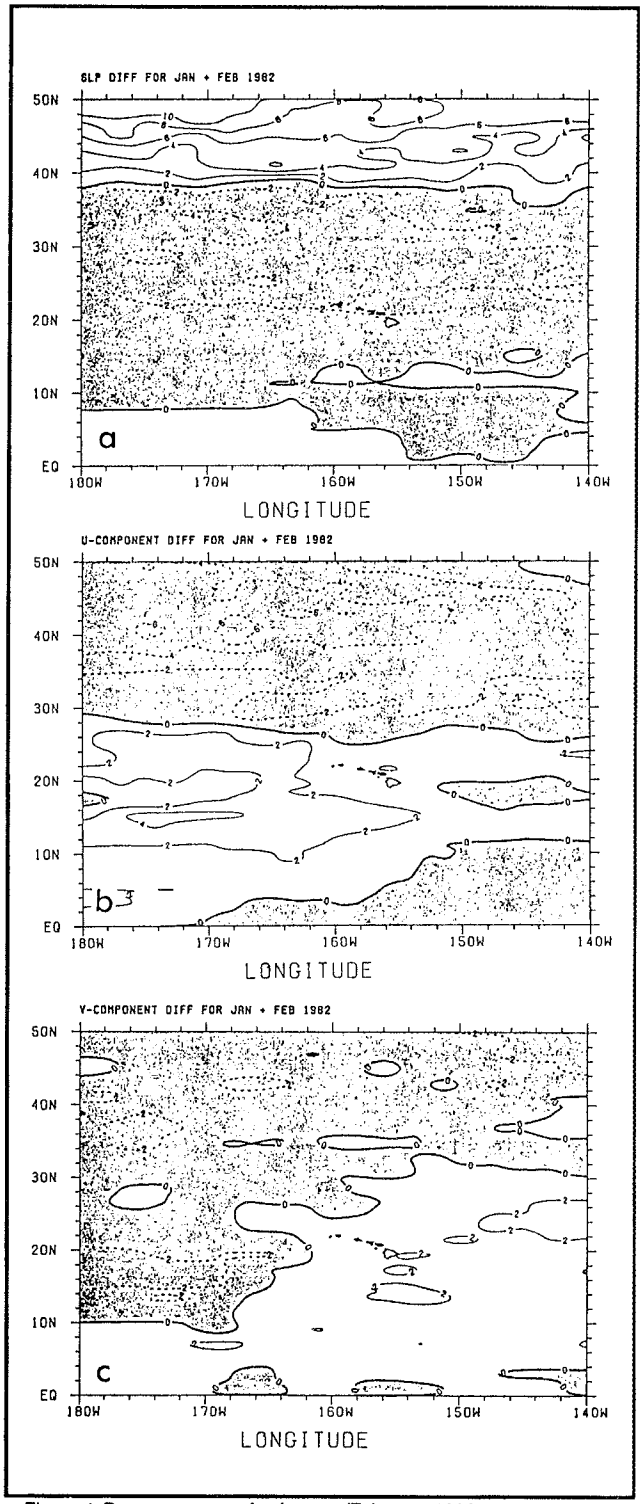

Figure 4. Departure maps for January/February 1982.
A Sea level pressure. Contour interval is 2 hPa. Regions with negative departures are shaded.
B Zonal wind component.
C Meridional wind component. Contour interval is 2 m s^{-1}. Regions with negative departures are shaded.

Figure 4a shows SLP departures for January/February 1982. The entire area poleward of 38°N was marked by positive departures, with departure values being as large as 10 hPa in the higher latitudes of the central North Pacific. This suggests a filling of the central North Pacific low. Cayan and Peterson (1989) also noted that wet winter in Hawaii is related to a weak central North Pacific low. Also notable in Figure 4a are negative SLP anomalies in a large area equatorward of 38°N; thus, in a broad sense, the meridional pressure gradient in the eastern North Pacific is weaker. Another interesting feature is a pocket of large, negative anomalies (less than 4 hPa) to the northwest of Hawaii. By examining the daily Pacific synoptic charts archived at the University of Hawaii, we noted that cyclonic systems stalled to the northwest of the islands in January and February 1982. These types of subtropical cyclones, termed "Kona storms" by local weather forecasters, occasionally bring flooding to the islands (Ramage 1962).

The map of zonal wind anomalies in January/February 1982 (Figure 4b) shows the mid-latitude eastern North Pacific was marked by strong easterly anomalies and the subtropics were marked by westerly anomalies; likewise, southerly anomalies were found to the east and northerly anomalies to the west of the islands (Figure 4c). Thus, an anomalously cyclonic circulation prevailed in the vicinity of the islands, and this pattern was opposite to that of dry 1981.

Upper-Air Circulation Patterns

The distribution of geopotential height at 850 hPa over the North Pacific and Asia during January/February 1981 is shown in Figure 5a. A vigorous Aleutian low developed, with a strong, meridional height gradient between the Aleutian low and the subtropical ridge over Hawaii. Hawaii was in the center of an elongating subtropical anticyclone that extended westward across the entire Pacific. In the center of this system, air subsided and warmed adiabatically, producing a strong subsidence and lowering humidity.

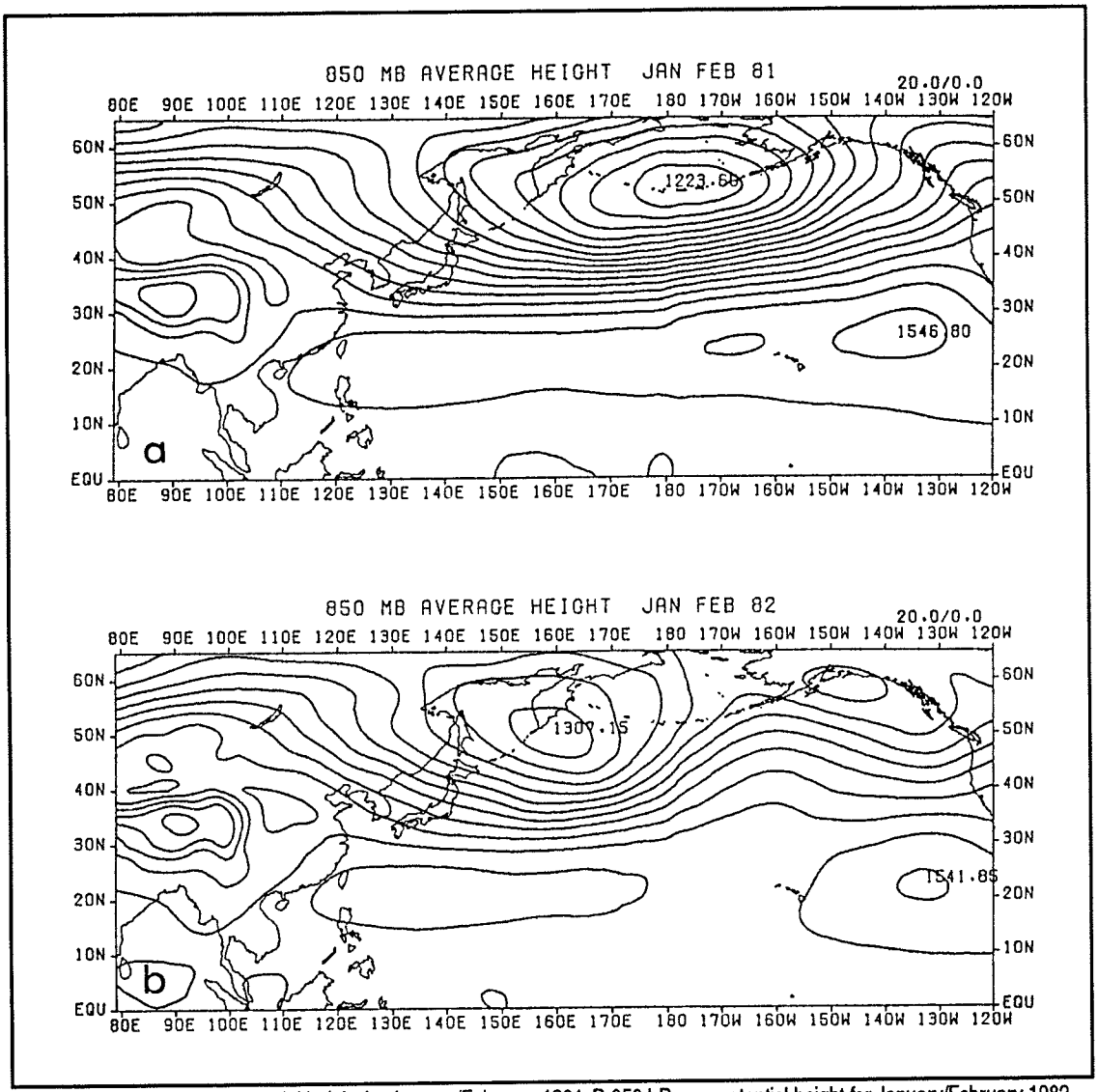

Figure 5. A 850 hPa geopotential height for January/February 1981. B 850 hPa geopotential height for January/February 1982. Contour interval is 20 gpm.

For wet 1982, the lower tropospheric chart reveals a wavy structure over extratropical Asia and the North Pacific (Figure 5b). Hawaii was marked by moist southwesterly flows because the islands were situated on the western flank of the eastern subtropical high.

In January/February 1981 (Figure 6a), the jet stream became strong and extended farther eastward; the maximum wind speed in the core of the jet increased to 85 m/s^{-1}. Hawaii was near the south of the exit region of the jet, in an area of upper level convergence that would favor lower tropospheric divergence, acting to enhance the subtropical ridge at 850 hPa (Figure 5a). The difference in divergence between 200 hPa and 850 hPa, D_{200}-D_{850}, during the extreme episodes is presented (Figure 6b). This difference in divergence may be considered a crude measure of the vertical motion at mid-troposphere. In January/February 1981, a small area of negative divergence differential was found near the islands. This pattern would infer sinking motion, thereby decreasing humidities and inhibiting cloud formation.

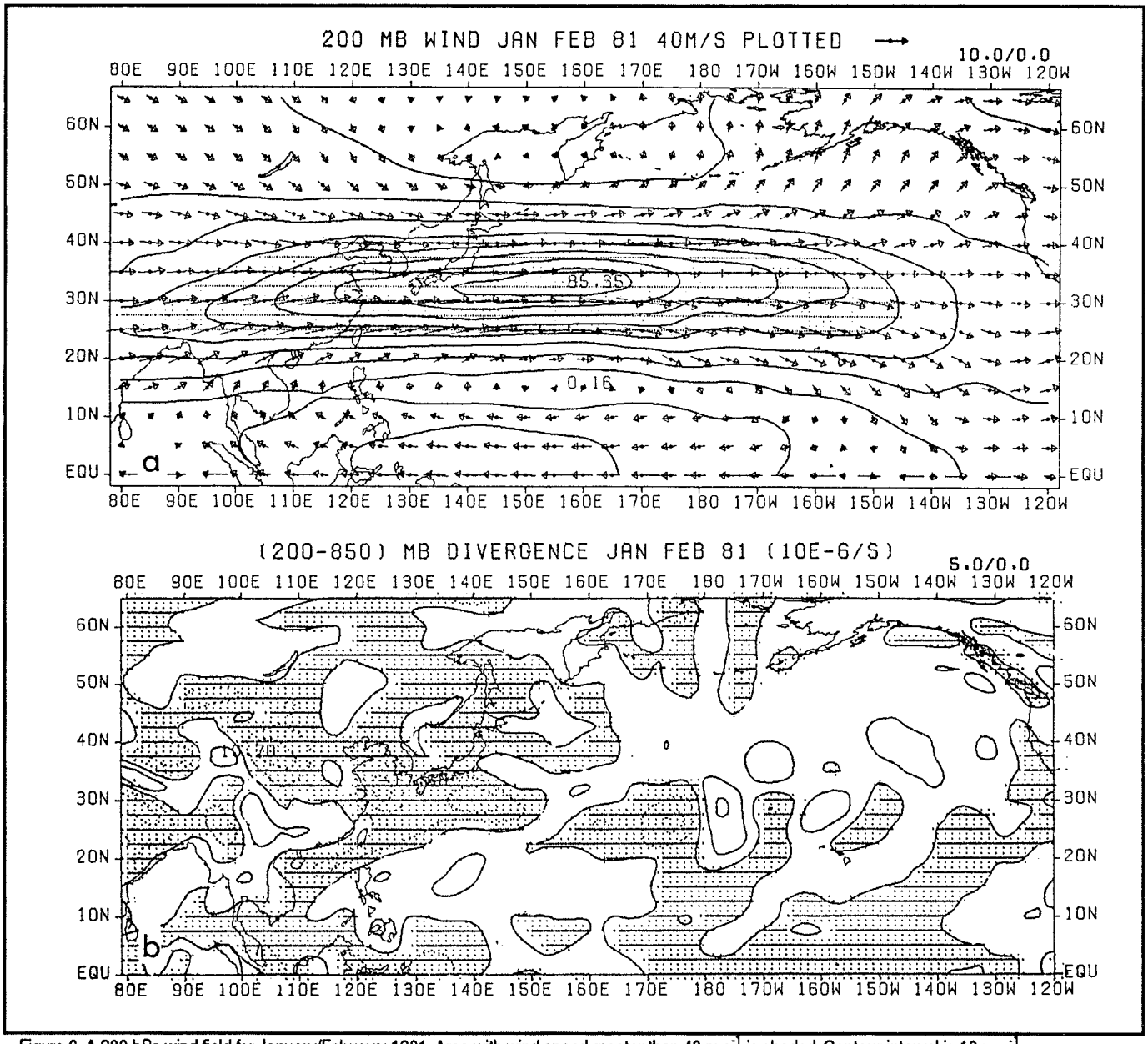

Figure 6. A 200 hPa wind field for January/February 1981. Area with wind speed greater than 40 $m\ s^{-1}$ is shaded. Contour interval is 10 $m\ s^{-1}$. B Divergence difference between 200 hPa and 850 hPa for January/February 1981. Unit: $10^{-6}\ s^{-1}$. Areas with negative values are shaded.

A dramatic change took place in January/February 1982 (Figure 7a), during which the jet stream remained mainly to the west of the dateline. The distance the jet stream from Hawaii and the lack of a well-organized upper-level convergence to the north of Hawaii seem to be important signals for wet winter 1982. The kinematic field at the height of the wet episode shows that a large area of rising motion developed over Hawaii (Figure 7b).

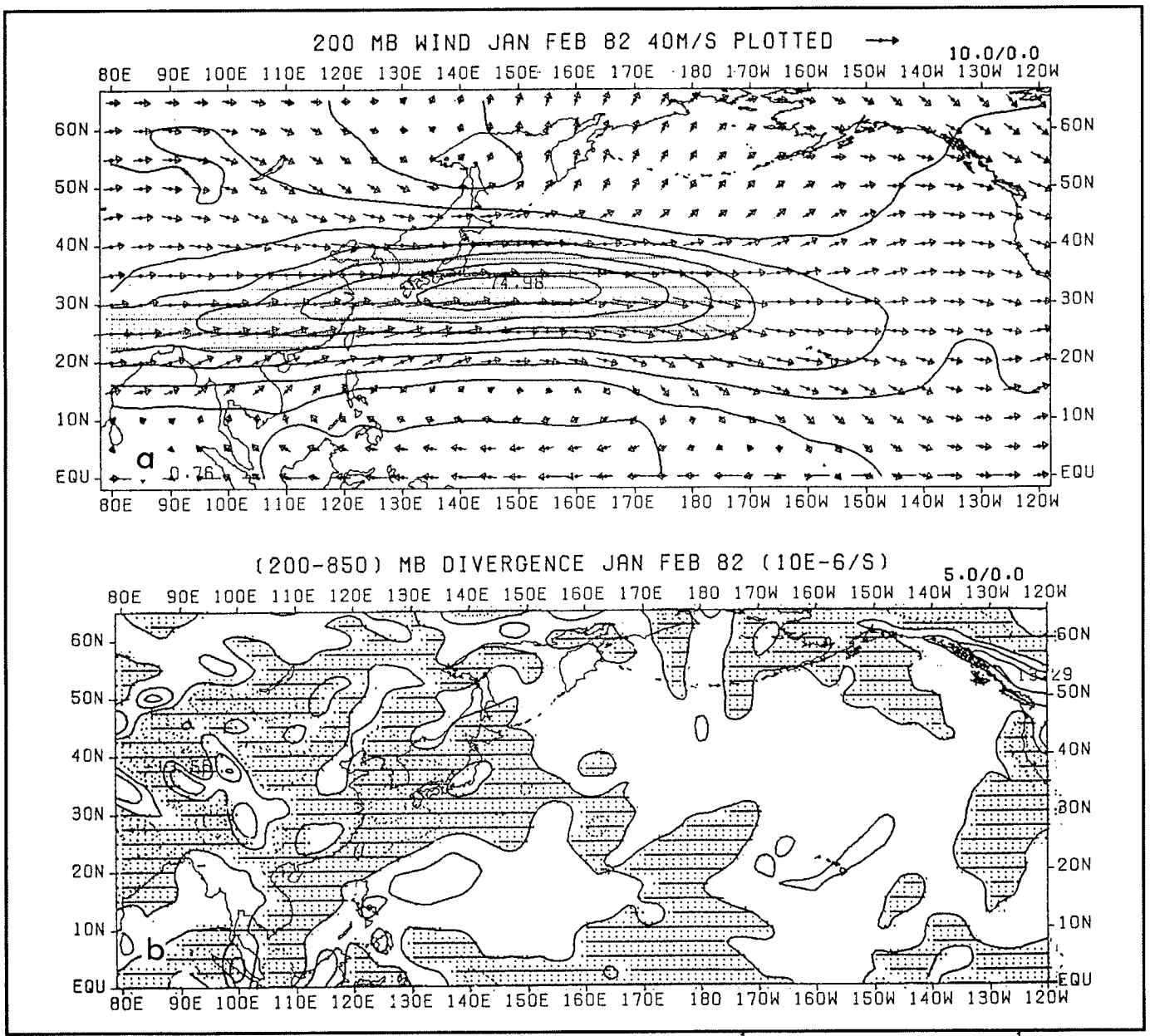

Figure 7. A 200 hPa wind field for January/February 1982. Area with wind speed greater than 40 m s^{-1} is shaded. Contour interval is 10 m s^{-1}.
B Divergence difference between 200 hPa and 850 hPa for January/February 1982. Unit: 10^{-6} s^{-1}. Areas with negative values are shaded.

Summary

This case study, utilizing surface and upper-air data, has attempted to shed light on the mechanisms that exerted control on two contrasting rainfall episodes in Hawaii. The broad surface circulation associated with dry 1981 is characterized by a deeper low pressure system and stronger westerlies in the extratropical eastern North Pacific, as well as stronger easterly trades to the south of Hawaii. The anomalously anticyclonic circulation, together with reduced trades, was characteristic of the dry winter of 1981. Concomitantly, Hawaii was dominated by an extensive subtropical high pressure ridge in the lower troposphere. At 200 hPa, the westerly jet stream over the central and eastern North Pacific was enhanced, and Hawaii was to the south of the jet exit region; as a result, upper level convergence and sinking motion at mid-troposphere were observed in the vicinity of Hawaii. These, together with the aforementioned circulation features at lower troposphere, reinforced the drying processes.

For the abundant rainfall in 1982, a weaker central North Pacific low and an anomalously strong cyclonic circulation prevailed over the region between mid-latitudes and subtropics. The latter circulation feature was associated with Kona storms and/or troughs in the easterlies. Hawaii was marked by moist flow from equatorial regions at 850 hPa, as a shallow trough lay to the immediate west. Aloft, the jet stream over the eastern North Pacific was reduced, and an area of ascending motion at mid-troposphere might exist over the islands. The circulation features corresponding to the peak phase of dry and wet episodes are illustrated schematically in Figure 8.

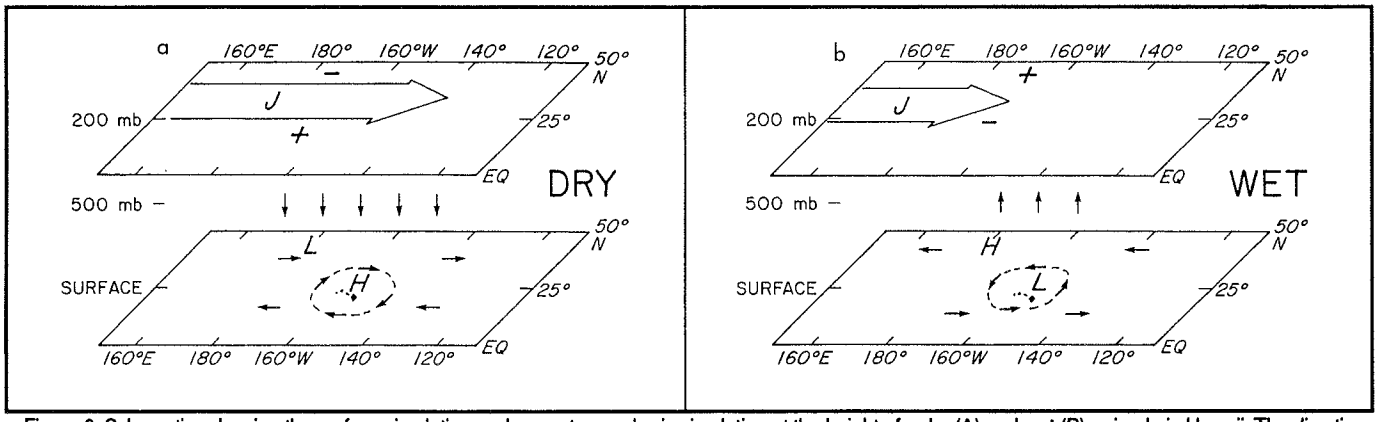

Figure 8. Schematics showing the surface circulation and upper tropospheric circulation at the height of a dry (A) and wet (B) episode in Hawaii. The direction of vertical motion at 500 hPa is also indicated. At 200 hPa, the position of the subtropical jetstream is denoted by "J". The plus and minus signs refer to height anomalies. Near surface, the arrows indicate the anomalous winds. "H" denotes anomalous anticyclone and "L" denotes cyclone.

Acknowledgments

This research has been supported by the Department of Land and Natural Resources, State of Hawaii, and the Board of Water Supply for the City and County of Honolulu.

References

Cayan, DR, and DH Peterson, 1989. The influence of North Pacific atmospheric circulation on streamflow in the west. Pgs. 375-397 in DH Peterson (Ed.), Aspects of Climatic Variability in the Pacific and the Western Americas, *Geophysical Monograph 55*. American Geophysical Union.

Chu, P-S, 1989. Hawaiian drought and the Southern Oscillation. *International Journal of Climatology*. 9:619-631.

Giambulluca, TW, MA Nullet, MA Ridgley, JET Moncur, and S Price, 1990. *Drought in Hawaii*. Department of Land and Natural Resources, State of Hawaii.

Haraguchi, P, 1981. *Drought of December 1980-February 1981, Island of Hawaii*. Division of Water and Land Development, Department of Land and Natural Resources, State of Hawaii. Circular C85, 38pp.

Haraguchi, P, and T Giambulluca, 1981. *Drought report, south Kohala-Hamakua, Island of Hawaii, March-November 1981*. Division of Water and Land Development, Department of Land and Natural Resources, State of Hawaii. Circular C89, 58pp.

Horel, JD, and JM Wallace, 1981. Planetary scale atmospheric phenomena associated with the Southern Oscillation. *Monthly Weather Review*. 109:813-829.

Lyons, SW, 1982. Empirical orthogonal function analysis of Hawaiian rainfall. *Journal of Applied Meteorology*. 21:1713- 1717.

Meisner, BN, 1976. *A study of Hawaiian and Line Islands rainfall*. Department of Meteorology, University of Hawaii. UHMET-76-04. 83pp.

Ramage, CS, 1962. The subtropical cyclone. *Journal of Geophysical Research*. 67:1401-1411.

Ropelewski, CF, and MS Halpert, 1987. Global and regional scale precipitation patterns associated with the El Niño Southern Oscillation. *Monthly Weather Review*. 115:1606-1626.

Anomalous Atmospheric Circulation and Large Winter Floods in Six Subregions of the Southwestern United States

Lisa L. Ely, Yehouda Enzel, and Daniel R. Cayan

Abstract: We examined atmospheric circulation conditions conducive to occurrence of winter floods that exceed the 10-year peak discharge on rivers in six hydroclimatic subregions in Arizona, southern Utah, Nevada, and California. Composite maps of anomalies in daily 700-mb heights indicate floods in all of the subregions are associated with a low pressure anomaly off the California coast and a high pressure anomaly over the Aleutians or Gulf of Alaska. Monthly sea level pressure anomalies associated with large floods since 1899 are less intense, but mirror the daily 700-mb patterns. Shifts in locations of the low- and high-pressure anomalies over the North Pacific appear to control which subregions experience floods. High-elevation topographic features exert a major control over the specific atmospheric circulation conditions that generate large floods in each hydroclimatic region. This relationship between flooding and broad-scale atmospheric patterns in the modern record will aid in paleoclimatic interpretations of paleoflood records over the last few thousand years.

Introduction

In the southwestern United States, large floods are caused by anomalous meteorological conditions that transport large quantities of moisture into the normally arid and semiarid environment (Hansen and Schwarz 1981). The types of storms and atmospheric circulation patterns associated with floods vary with geographic location and season (Hirschboeck 1985). Storms that cause floods in the Southwest fall into three general categories: winter North Pacific frontal storms, late-summer and fall tropical cyclones from the eastern North Pacific, and local summer convective thunderstorms (Webb and Betancourt 1990).

We characterized the anomalous atmospheric circulation conditions associated with winter floods with exceedance probabilities ≤ 0.10 on rivers in each of six subregions in Arizona, Utah, and southern California to identify general circulation features that cause floods in the Southwest and to determine whether shifts in these features control which subregions experience flooding.

The six subregions (Figure 1) were delineated primarily by geographic location and topography. Regional variations in the dominant flood-generating storm types also consistently follow these divisions. The substantial differences in seasonal distribution of precipitation over distances of a few hundred kilometers (*eg*, Figures 2 and 3) are probably controlled by large-scale topographic features and proximity to air mass sources.

In K.T. Redmond, Editor, 1992. Proceedings of the Eighth Annual Pacific Climate (PACLIM) Workshop, March 10-13, 1991: California Department of Water Resources, Interagency Ecological Studies Program Technical Report 31.

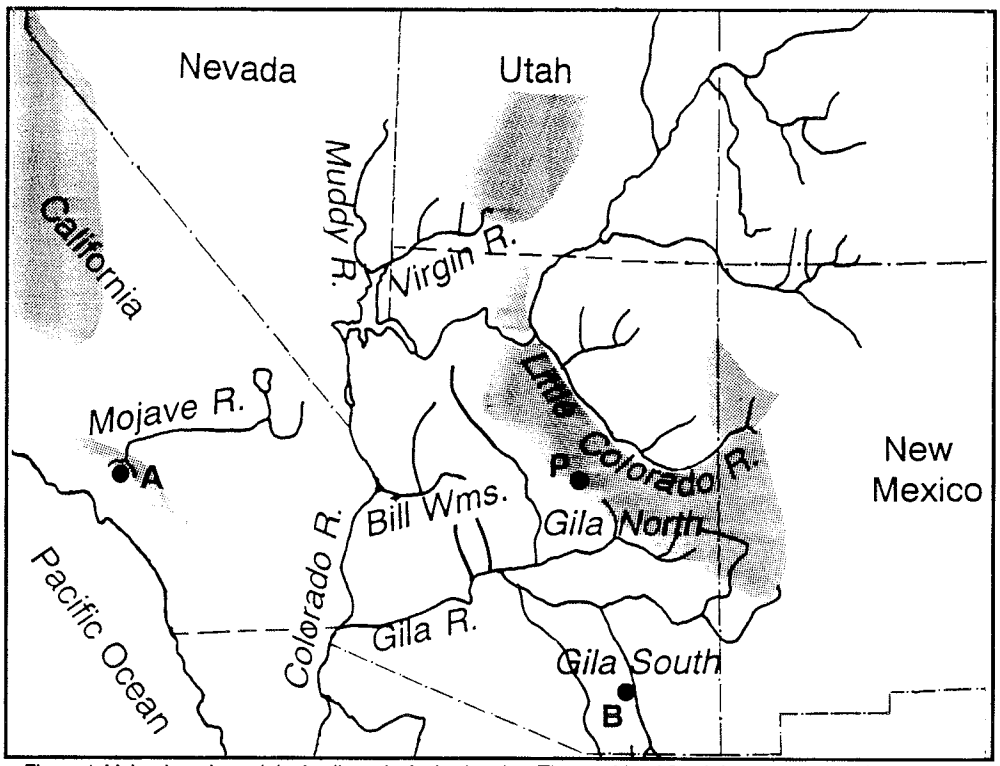

Figure 1. Major rivers in each hydroclimatological subregion. The combined flood dates on 1 to 5 principal rivers in each region were used for the analysis. Major topographic features above 2000m elevation are shaded. Dots indicate precipitation stations used in Figure 3: A=Arrowhead Lake, P=Payson, B=Benson.

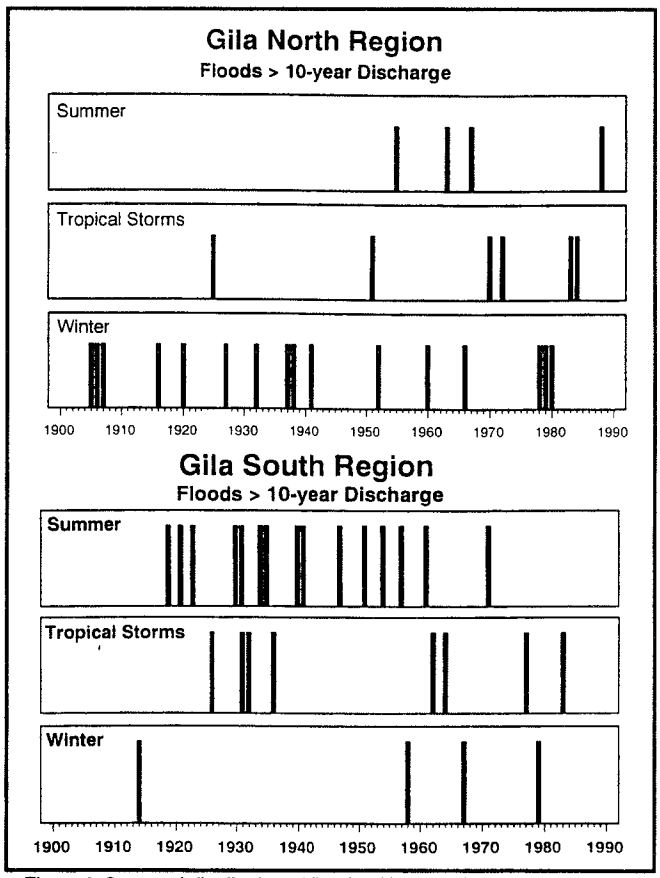

Figure 2. Seasonal distribution of floods with exceedance probabilities ≤0.10 in the Gila North and Gila South subregions. Differences between these adjacent regions are caused partly by orographic effects.

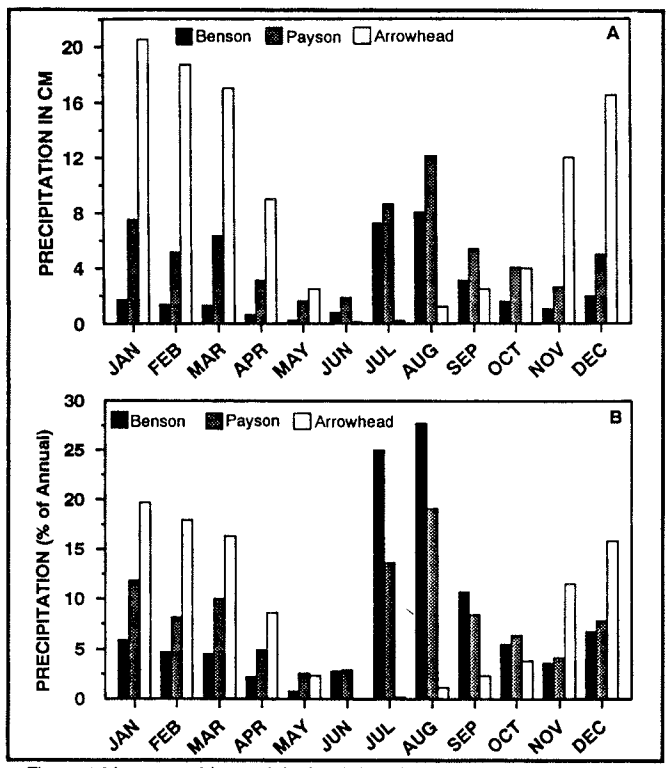

Figure 3.Mean monthly precipitation (A) and mean monthly precipitation as a percent of mean annual precipitation (B) at representative stations from Gila South (Benson), Gila North (Payson), and the headwaters of the Mojave River basin (Arrowhead Lake). Although there is a peak in summer precipitation in Gila South and Gila North, winter precipitation is greater in Gila North and Mojave stations than in Gila South. Precipitation seasonality differences are accentuated when only the extreme events are considered (see Figure 2).

The Mogollon Rim escarpment sweeps diagonally across northeastern Arizona (Figure 1), intercepting moist winter Pacific air masses from the southwest and increasing winter precipitation and floods in the Gila North and Bill Williams regions. The influence of this topographic barrier on winter precipitation, particularly the extremes, decreases toward the Gila South region (Figures 2 and 3). Floods in Gila South are mainly caused by summer thunderstorms and tropical cyclones (Webb and Betancourt 1990). Winter Pacific frontal storms are the sole source of large floods on the Mojave River, where the coastal mountains also exert a strong orographic control on precipitation from the west (Enzel *et al* 1989) (Figure 3). Floods in the Virgin/Muddy and Little Colorado regions are caused by mixtures of summer, winter, and tropical storms.

For our initial analysis, we focused only on winter floods (November-March), which affect all of the subregions to some degree. Winter storms have caused many of the most extreme floods, even in those subregions in which they are not the most common source of floods. These storms generally result from relatively strong, persistent, large-scale atmospheric patterns over the North Pacific (Weaver 1962; Pyke 1972).

Determining the atmospheric circulation patterns associated with large floods in the modern record creates a link between individual events and climate that is necessary for paleoclimatic interpretations of long-term paleoflood data. Flood deposits (Kochel and Baker 1988) and flood-scarred or damaged trees (McCord 1990) have preserved evidence of large floods over periods of hundreds to thousands of years on several rivers within these six subregions (Ely in prep). These records form one of the only sources of paleoclimatic information about the temporal and spatial distribution of individual extreme events. The specific circulation features that currently generate floods in each subregion can be applied through a probabilistic approach to paleofloods that occurred over the last few thousand years on rivers in the same subregion (Hirschboeck 1988).

Procedure

Floods with exceedance probabilities ≤ 0.10 (Anderson and White 1979) were chosen for analysis from gaged discharge records on the largest rivers in each subregion. The Mojave, Bill Williams, and Little Colorado regions each consist of discharge records from a single river, the Virgin/Muddy region has two rivers, and Gila North and Gila South have five rivers each. Dates of floods for all rivers within a subregion were combined (Table 1). In all cases the lag time between the maximum precipitation in the subregion and the peak flood discharge is one day or less, confirming that the floods are responding directly to specific storms.

Composite anomaly maps of the 700-mb height patterns associated with the floods in each subregion were constructed using gridded daily 700-mb height values over the North Pacific and western North America on a

Table 1
Dates of Winter Storms that Produced Floods with Exceedance Probabilities <0.10

South Gila	North Gila	Bill Williams	Little Colorado	Virgin/ Muddy	Mojave	Regional Floods[1]
12/23/14	01/10/05	01/19/16	11/05/05	03/25/06	12/31/09	11/05
11/01/57	11/27/05	02/16/27	02/10/32	02/—/07	01/18/16	01/16
12/20/67	12/03/06	02/07/37	02/09/37	12/31/09	12/21/21	02/37
12/18/78	01/19/16	03/04/38[2]	03/05/38	01/21/22	03/02/38	03/38
	11/27/19	03/14/41	03/15/41[2]	03/03/38	01/25/69	03/78
	02/22/20	12/06/66	01/20/52	10/29/47	03/03/78	12/78
	02/17/27	02/09/76	12/23/78	11/06/60[2]	02/17/80	02/80
	02/10/32	03/01/78		12/06/66	03/02/83	
	02/07/37	12/18/78		01/25/69		
	03/04/38	02/19/80				
	03/14/41	03/03/83				
	12/31/51					
	01/18/52					
	12/26/59					
	12/23/65					
	03/01/78					
	11/24/78					
	12/18/78					
	02/19/80					

1 Floods that affected at least four rivers in at least two subregions.
2 Peak discharge was slightly less than the 10-year flood.

5° latitude-longitude grid beginning in 1947 (Figure 4). The 700-mb height values for each day in which a flood occurred were subtracted from the long-term (1947-1972) mean 700-mb height of that specific month to determine the 700-mb height anomaly. The composite anomaly maps represent the mean anomaly for all flood dates from 1947 to 1988 in each subregion. To survey a longer record of floods, a second set of monthly composite anomaly maps were constructed in the same manner using gridded mean sea level pressure (SLP) values beginning in 1899 (Trenberth and Paolino 1980) (Figure 5). In this analysis, the mean monthly SLP values for the month in which a flood occurred were used rather than daily values.

Atmospheric Circulation Anomalies

Extreme events are infrequent, and analyses involving such small sample populations rarely produce statistically significant results. However, all of the composite anomaly maps show a consistent general atmospheric circulation pattern associated with floods in this area of the Southwest (Figure 4). Floods in each subregion are associated with a low-pressure anomaly off the coast of California and a high-pressure anomaly over the Aleutian Islands or the Gulf of Alaska. This southern location of the low-pressure anomaly results in enhanced southerly to southwesterly cyclonic flow (Cayan and Peterson 1989) that brings moisture into the interior Southwest.

When viewed together, the composite anomaly maps suggest there are systematic differences between the atmospheric circulation patterns

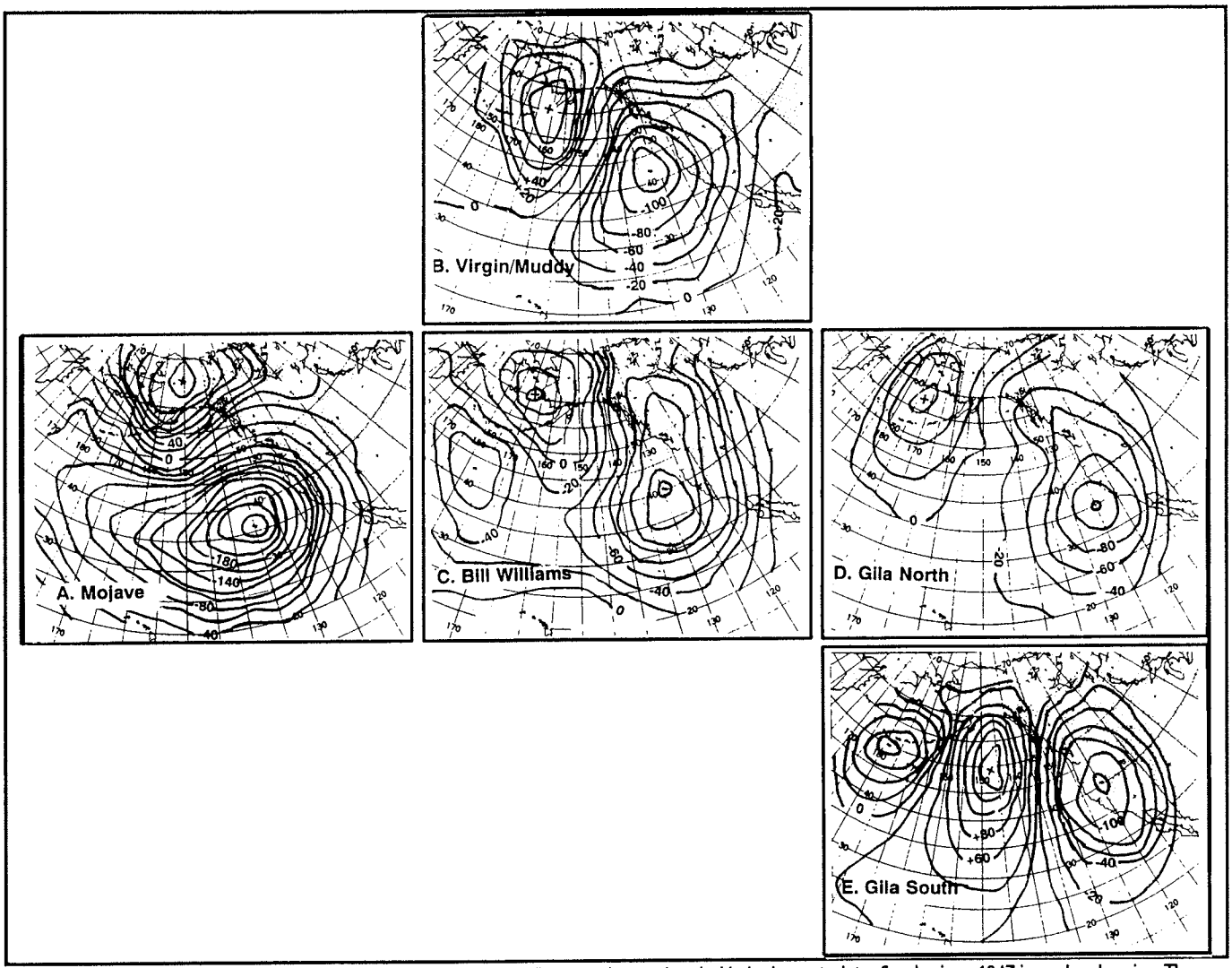

Figure 4. Composite anomaly maps of daily 700 mb height values (in meters) associated with the largest winter floods since 1947 in each subregion. The maps are arranged in their relative geographic positions. The Little Colorado subregion was excluded because there have been only two floods since 1947. Some storms are included in more than one subregion, but many caused floods in only one region (Table 1). Therefore, the maps do not merely reflect the migration of single storms across the study area. Note the changes in extent of the high-pressure anomaly and the shoft in the center of the low-pressure anomaly associated with floods in the westernmost subregion (the Mojave), the central subregions, and finally the Gila South region, which is the farthest south and east. Winter floods in these successive subregions are associated with circulation patterns that tend toward increasingly southerly flow from the Pacific Ocean.

associated with floods in each subregion. Although the same broad-scale pattern produces precipitation in all parts of the study area, regional shifts in circulation may control which basin experiences extreme floods. The location and extent of the low-pressure anomaly and its associated flow appear to be especially important. The Mojave and Gila South patterns are the end members of the series, with the patterns for the other subregions falling between these two extremes. For the Mojave River floods, the center of the low-pressure anomaly is relatively far offshore and extends across the entire Pacific (Figure 4A). The high-pressure anomaly is relatively small and centered far north over Alaska.

Of all the basins considered here, the Mojave is closest to the coast and is impacted by storms or moisture that come onto the continent from the west and southwest and move directly into the southern California mountains (Enzel *et al* 1989). The Virgin/Muddy and Bill Williams flood

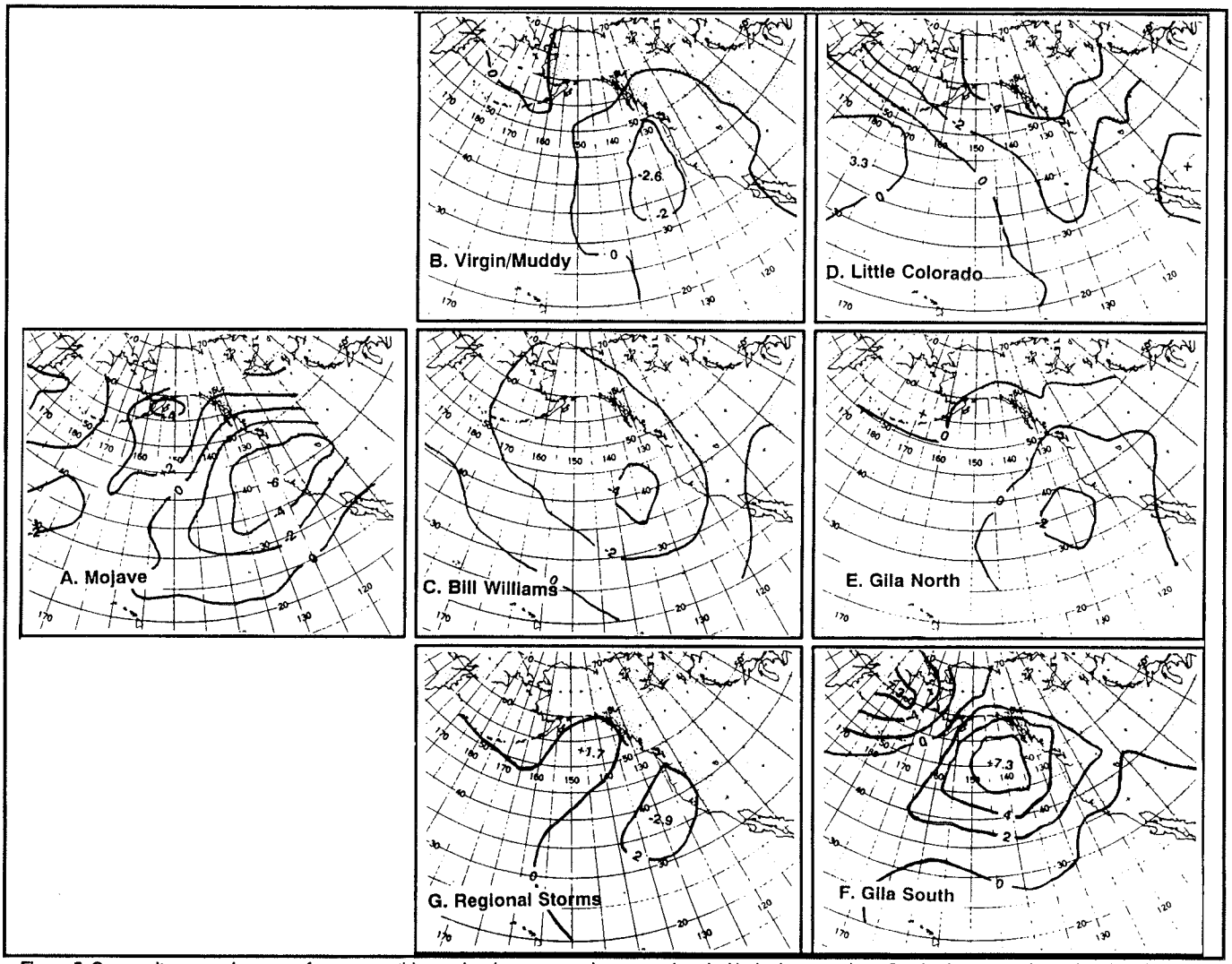

Figure 5. Composite anomaly maps of mean monthly sea-level pressure values associated with the largest winter floods since 1899 in each subregion (Table 1). Although they are weaker, the monthly patterns mirror the daily 700-mb composite anomalies (Figure 4), affirming the magnitude and persistence of the anomalous atmospheric circulation conditions associated with the largest floods. The regional flood map (G) is composed of those storms that caused floods on at least four rivers in at least two subregions (Table 1). The anomaly pattern associated with these exceptional storms is not notably different from the individual subregion patterns, with the exception of Gila South.

composite patterns are fairly similar to the Mojave pattern, with negative anomaly centers stationed offshore, inducing enhanced westerly/southwesterly flow (Figure 4B,C). For floods in the Gila South region, the Gulf of Alaska high-pressure anomaly extends very far south and pushes the center of the low-pressure anomaly onshore over the California/Nevada border (Figure 4E). This high-amplitude pattern causes more southerly flow, bringing moisture into southern Arizona from the south-southwest. The Gila North flood composite pattern (Figure 4D) is a hybrid of those for the Mojave and Gila South; it has less extensive westerly/southwesterly flow than the Mojave, and the low is not as far onshore as for Gila South.

The composite 700-mb height anomalies associated with the Mojave River floods are much stronger than for the other subregions, indicating the floods result from a very specific circulation pattern (Enzel *et al* 1989). The weaker composite anomaly patterns associated with the other subre-

gions result from greater variation in the individual atmospheric circulation patterns that produce intense storms in these interior areas. Storms are directed onto the continent and into the interior subregions over a relatively broad range of latitudes, from Baja California through central California. Because the Mojave subregion is so close to the coast, and perhaps because of the strong orographic control of the coastal mountains, storms that directly impact this basin can only enter the continent over a very restricted latitudinal range.

There are obvious advantages to using the 700-mb height values; the circulation patterns show up much more clearly with the upper air data than with the SLP values because the flow aloft is not complicated by surface influences. However, the 700-mb dataset only begins in 1947, which greatly restricts the sample size of extreme events. A period of frequent large floods in the Southwest in the first four decades of the century can be included when the monthly SLP data since 1899 are used. (Daily SLP maps prior to 1947 have not been digitized.)

Although they are much weaker, the composite mean monthly SLP anomalies for each subregion mirror the patterns in the daily 700-mb composite anomaly maps (Figure 5). This relationship indicates the atmospheric circulation patterns associated with the extreme flood-generating storms are persistent or strong enough to influence the average SLP values over an entire month. The relative magnitude of anomalies associated with the Mojave River floods compared with those of the other subregions are even more pronounced with the monthly SLP values than with the daily 700-mb height values.

The general position of the low-pressure anomaly associated with the extreme events is similar to the position of a low-pressure anomaly in winter SLP that correlates with anomalously high cumulative December-August streamflow in two southwestern drainages analyzed by Cayan and Peterson (1989): the Salt River (Gila North subregion) and Arroyo Seco near Pasadena, California. In these and other rivers throughout the arid and semi-arid Southwest, most of the total annual streamflow in high-flow years is contributed by a few distinct large flood events, partially explaining the similarity in these two anomaly patterns.

Conclusions

Seasonality in occurrence of large floods is distinctly different in different subregions of the Southwest. In winter, storms that cause the largest floods in the southwestern United States are repeatedly associated with distinct anomalies in 700-mb heights and sea level pressure over the Northern Pacific, consisting of a low-pressure anomaly off the California coast and a high-pressure anomaly over the Aleutian Islands or Gulf of Alaska. Floods in subregions separated by only a few hundred kilometers are often associated with distinct differences in the position and extent of these circulation features. Orographic influences on the movement of

air masses through the region are a major factor in determining these differences. Relationships between floods and atmospheric circulation place regional hydrologic processes on the continent into a broader atmospheric and climatic context and can lend the necessary insight for paleoclimatic interpretations of spatial and temporal patterns in long-term paleoflood data.

Acknowledgments

We thank R.H. Webb for helpful discussion and assistance. This research was partially supported by the Engineering Directorate, Natural and Manmade Hazards Mitigation Program, National Science Foundation, Grant BCS-8901430. This publication is Contribution No. 9 of the Arizona Laboratory for Paleohydrological and Hydroclimatological Analysis (ALPHA), University of Arizona.

References

Anderson, TW, and ND White, 1979. *Statistical summaries of Arizona streamflow data.* US Geological Survey Water-Resources Investigations 79-5.

Cayan, DR, and DH Peterson, 1989. The influence of North Pacific atmospheric circulation on streamflow in the West. Pgs. 375-397 in DH Peterson (ed.) *Aspects of Climate Variability in the Pacific and the Western Americas.* American Geophysical Union Geophysical Monograph 55.

Ely, LL, in prep. *Spatial and temporal patterns in extreme floods in the southwestern U.S. in relation to late Holocene climatic variations.* PhD dissertation. University of Arizona:Tucson.

Enzel, Y, DR Cayan, RY Anderson, and SG Wells, 1989. Atmospheric circulation during Holocene lake stands in the Mojave Desert: evidence of regional climate change. *Nature.* 341:44-48.

Hansen, EM, and FK Schwarz, 1981. *Meteorology of important rainstorms in the Colorado River and Great Basin drainages.* Hydrometeorological Report 50, US Dept. of Commerce, National Oceanic and Atmospheric Administration:Washington, DC

Hirschboeck, KK, 1988. Flood hydroclimatology,Pgs. 27-49 in VR Baker, RC Kochel, and PC Patton (eds.) *Flood Geomorphology.* John Wiley and Sons:New York.

Kochel, RC, and VR Baker, 1988. Paleoflood analysis using slackwater deposits Pgs. 357-376 in VR Baker, RC Kochel, and PC Patton (eds.) *Flood Geomorphology.* John Wiley and Sons:New York.

McCord, VAS, 1990. *Augmenting flood frequency estimations using flood-scarred trees.* PhD dissertation. University of Arizona:Tucson.

Pyke, CB, 1972. *Some meteorological aspects of the seasonal distribution of precipitation in the western United States and Baja California.* University of California Water Resources Center Contribution 139. Los Angeles.

Trenberth, KE, and DA Paolino, 1980. The northern hemisphere sea-level pressure data set trends, errors, and discontinuities. *Monthly Weather Review.* 108:855-872.

Weaver, RL, 1962. *Meteorology of hydrologically critical storms in California.* Hydrometeorological Report 37, US Weather Bureau, Washington, DC. 207 pp.

Webb, RH, and JL Betancourt, 1990. *Climatic variability and flood frequency of the Santa Cruz River, Pima County, Arizona.* US Geological Survey Open-File Report 90-553. 69 pp.

The Relationship of Western Pacific Monsoon and Tropical Cyclone Activity to North Pacific and North American Climate Anomalies

Patrick A. Harr, Jeng-Ming Chen, and Tom Murphree

Introduction

Several seasonal extremes occurred throughout the North Pacific region during the spring and summer of 1988. During April, May, and June, North America experienced widespread drought (Ropelewski 1988). During the summer, the Asian monsoon was very active, and Japan experienced a prolonged "Baiu" season. Also, Japan experienced a very cool and wet August.

The North American drought conditions have generally been attributed to a positive Pacific-North American (PNA) circulation pattern (Wallace and Gutzler 1981) characterized by negative height anomalies over the northeast Pacific, positive height anomalies over North America, and negative height anomalies over the western Atlantic. Trenberth *et al* (1988) suggested this circulation pattern was caused by a northward shift in the intertropical convergence zone over the eastern and central tropical Pacific.

During June, July, and August, when drought conditions eased over North America, the height anomaly pattern over the Pacific region changed from a positive PNA pattern to a wavelike pattern that stretched from the subtropical western Pacific to North America (Ropelewski 1988). The placement of centers of positive and negative height anomalies was such that large negative height anomalies were centered over Japan and slightly negative anomalies were centered over central North America. Nitta (1987) described similar patterns, but with opposite phase, as atmospheric Rossby waves generated by enhanced convection over the Philippine Sea.

Although a positive sea surface temperature anomaly of about 0.5°-1.0°C was present in the Philippine Sea during August (Nitta 1990), outgoing long-wave radiation (OLR) anomalies were positive (NOAA 1988), which indicates less convection than normal. However, large negative OLR anomalies that represent enhanced convection were found between 20°N-35°N and 125°E-170°E (NOAA 1988). These positive OLR anomalies were associated with a northward shift in the western Pacific monsoon trough and tropical cyclone activity (Figure 1). The anomalous concentration of eight tropical cyclones resulted in a large anomalous heat

In K.T. Redmond, Editor, 1992. Proceedings of the Eighth Annual Pacific Climate (PACLIM) Workshop, March 10-13, 1991: California Department of Water Resources, Interagency Ecological Studies Program Technical Report 31.

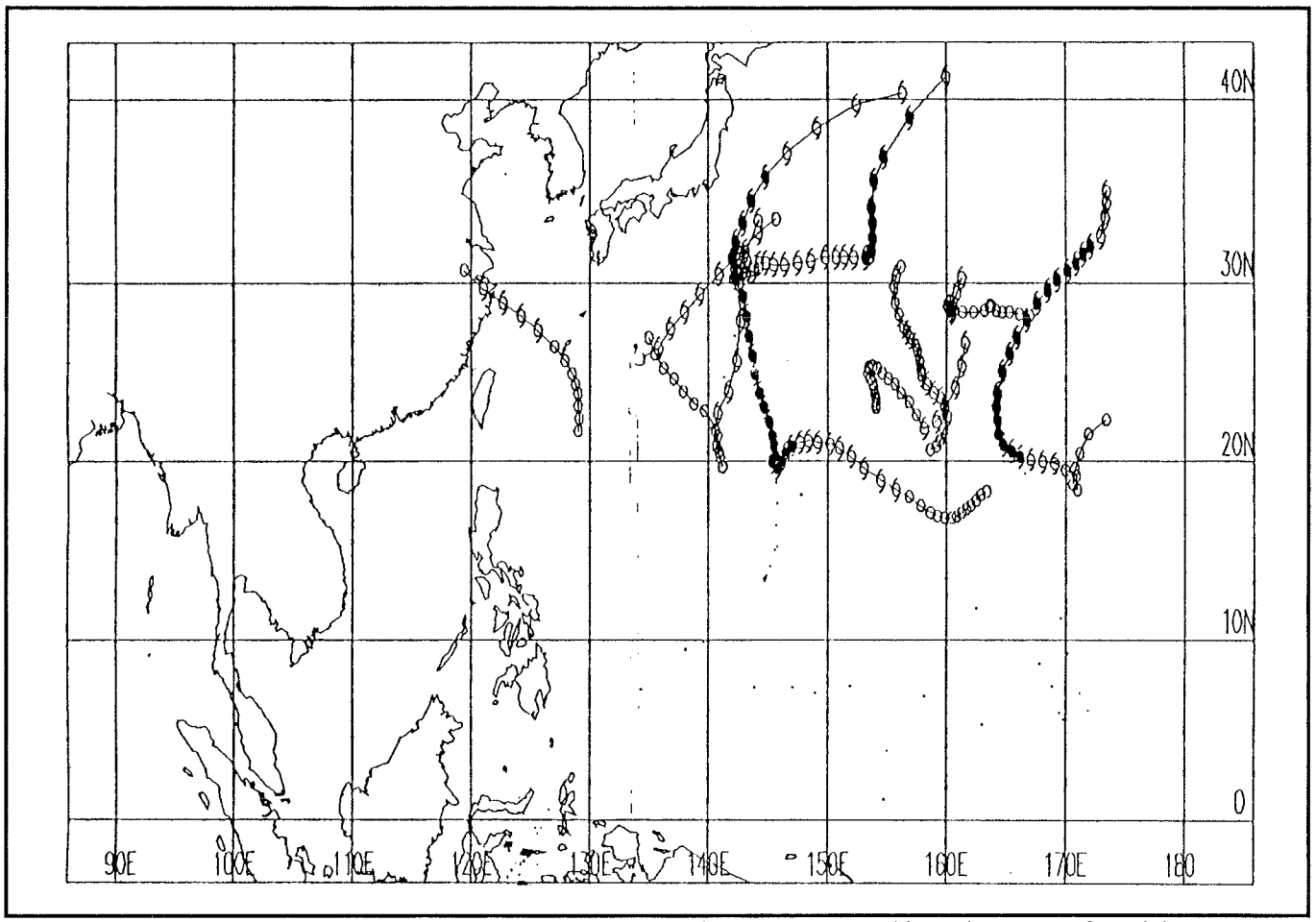

Figure 1. Positions each 6 h of western North Pacific tropical cyclones that occurred between August 1 and September 15, 1990. Open circles represent tropical depression intensity. Open hurricane symbols represent tropical storm intensity. Closed hurricane symbols represent typhoon intensity.

source over the subtropical western Pacific. Murphree (1991) examined the extratropical atmospheric response to various locations of anomalous tropical heat sources.

This present study investigates the influence of western Pacific tropical cyclone activity as possible centers of anomalous tropical heating on the large-scale circulation over the Pacific region. The characterization of tropical cyclone activity via an index based on anomalous 700 mb zonal wind is described first. Patterns of anomalous large-scale extratropical circulation anomalies based on composites of similar periods of tropical cyclone activity are then presented, followed by general conclusions.

Tropical Cyclone Activity

Tropical cyclones over the western North Pacific occur during all months, with the peak season occurring during July to October. The tropical cyclones may be characterized according to their track type (Figure 2). Tropical cyclones following straight tracks generally move to the west or northwest. Recurving tropical cyclones begin as straight-moving storms, but then pass through north. Periods of inactivity that last at least ten days have also been observed during the peak tropical cyclone season.

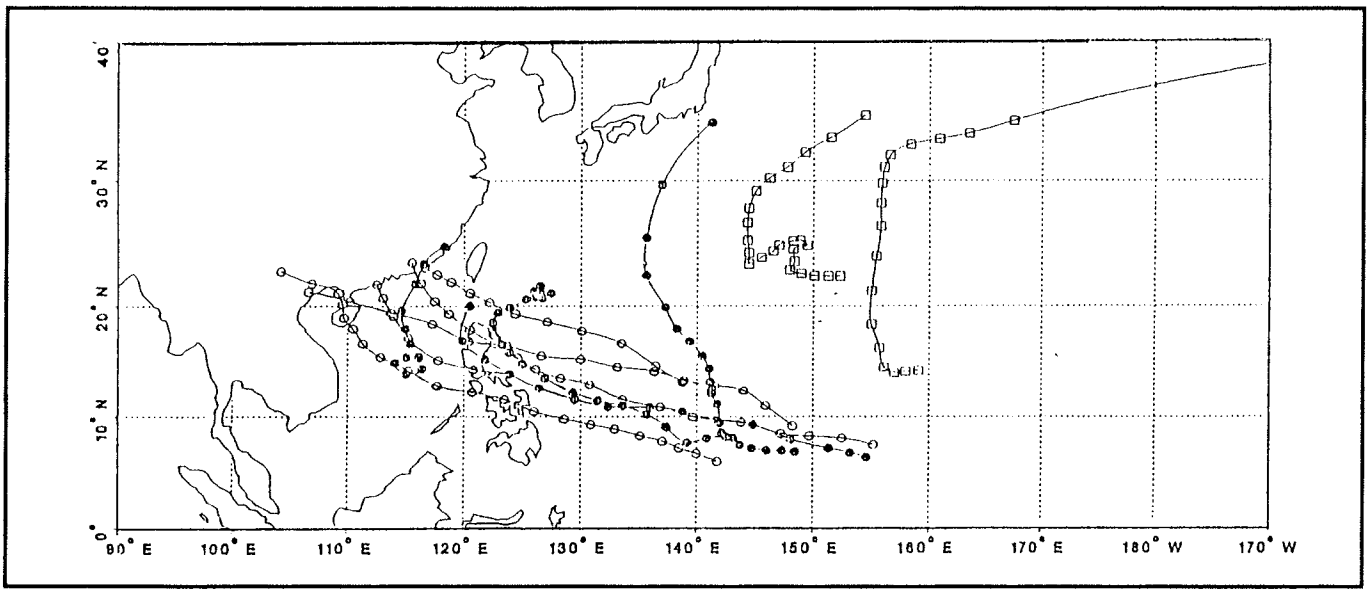

Figure 2. Representative western North Pacific tropical cyclone tracks. Open circles represent straight-moving tracks. Closed circles represent recurving-south tracks. Open boxes represent recurving-north tracks.

Based on an extensive tropical cyclone climatology, Harr and Elsberry (1991) suggested tropical cyclones that form north of 20°N or east of 150°E and north of 10°N have a climatological preference to follow a recurving track. These are labelled recurve-north in Figure 2. Recurving tropical cyclones that form in regions where there is no climatological preference between a straight or recurving track are labelled recurve-south.

Harr and Elsberry (1991) identified physically and statistically significant May-October large-scale anomalous 700-mb circulation patterns over the western North Pacific that are linked to prolonged periods of straight-moving, recurving-south and recurving-north tropical cyclones. They also identified anomalous large-scale circulations associated with inactive periods. Physically, these patterns identify anomalous lower-tropospheric winds associated with changes in monsoon trough and subtropical ridge positions and intensities.

The anomalous circulation patterns are summarized by an index composed of the 700-mb anomalous zonal wind summed between 100°E-140°E in 5-degree-latitude bands from the equator to 30°N (Figure 3). This index is used to categorize anomaly charts based on 12-h objectively analyzed wind fields into one of the four circulation types. The temporal variability of the western North Pacific anomalous tropical circulation can then be examined using time series of the resulting index categorizations.

North Pacific Circulation Anomalies

The tropical circulation index is used to identify regimes of similar tropical cyclone activity (track types) or inactivity between May and October from 1979 to 1988. A regime is identified when the circulation

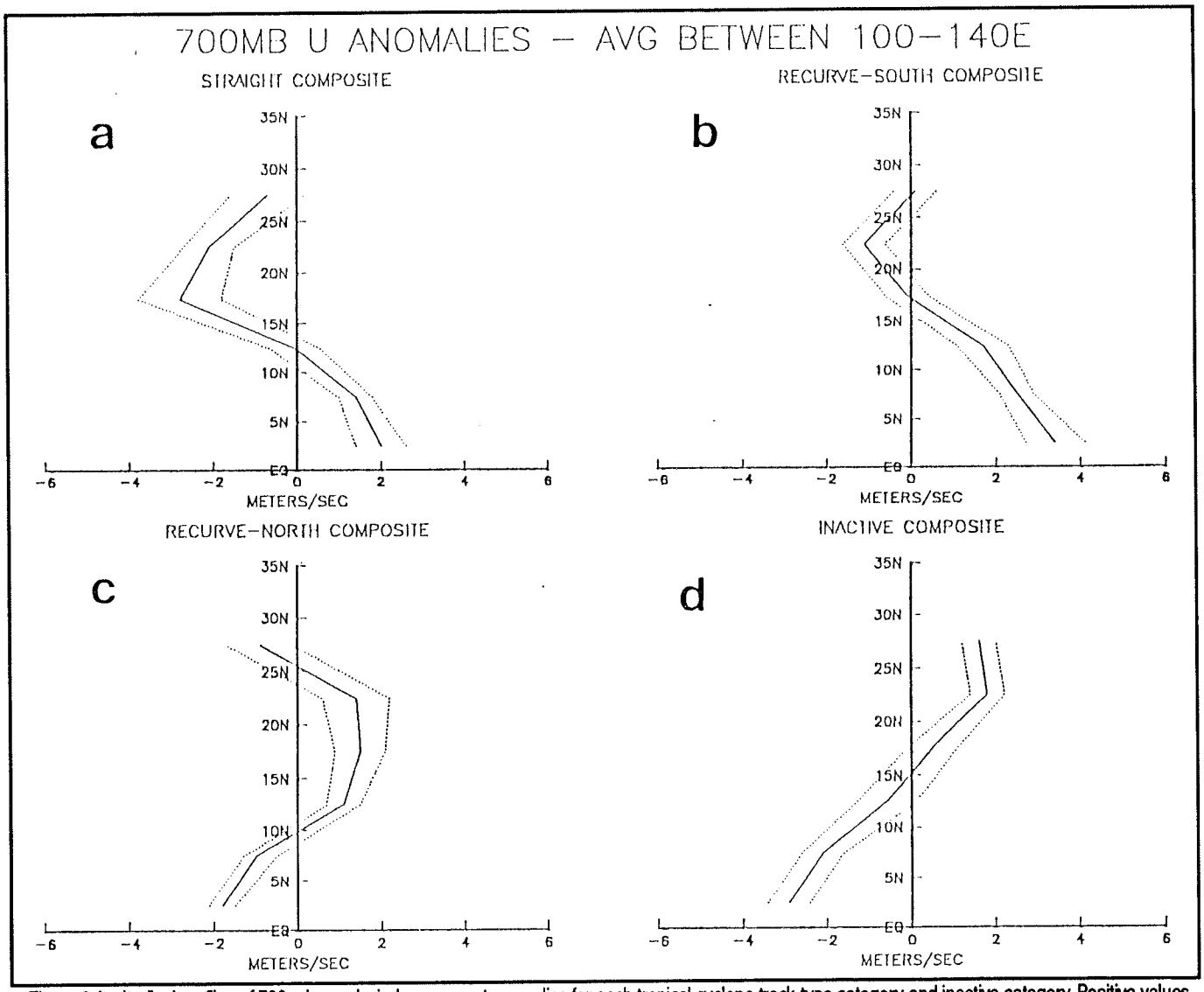

Figure 3. Latitudinal profiles of 700 mb zonal wind component anomalies for each tropical cyclone track-type category and inactive category. Positive values indicate westerly anomalies, and negative values indicate easterly anomalies. The dotted lines represent plus/minus one standard deviation.

index does not change for 7 consecutive days. Time periods meeting this criterion are combined to form 700-mb composite extratropical circulation patterns associated with tropical cyclone activity or inactivity.

In Harr and Elsberry (1991), inactive periods are defined as periods with no tropical cyclones. Their analysis indicated that during these periods, the monsoon trough is displaced far to the north of its climatological position in the Philippine Sea. The inactive and recurving-north regimes identified by easterly anomalies between the equator and 10°N (Figure 3) are combined into one group, which represents conditions with tropical cyclone activity when the monsoon trough is displaced north of the Philippine Sea. During this regime, the 700-mb height anomalies across the North Pacific consist of alternating cyclonic and anticyclonic anomalous circulations (Figure 4). A large anticyclonic anomaly over the Philippine Sea is associated with the northward displacement of the monsoon trough and tropical cyclone activity. There are cyclonic anomalies over

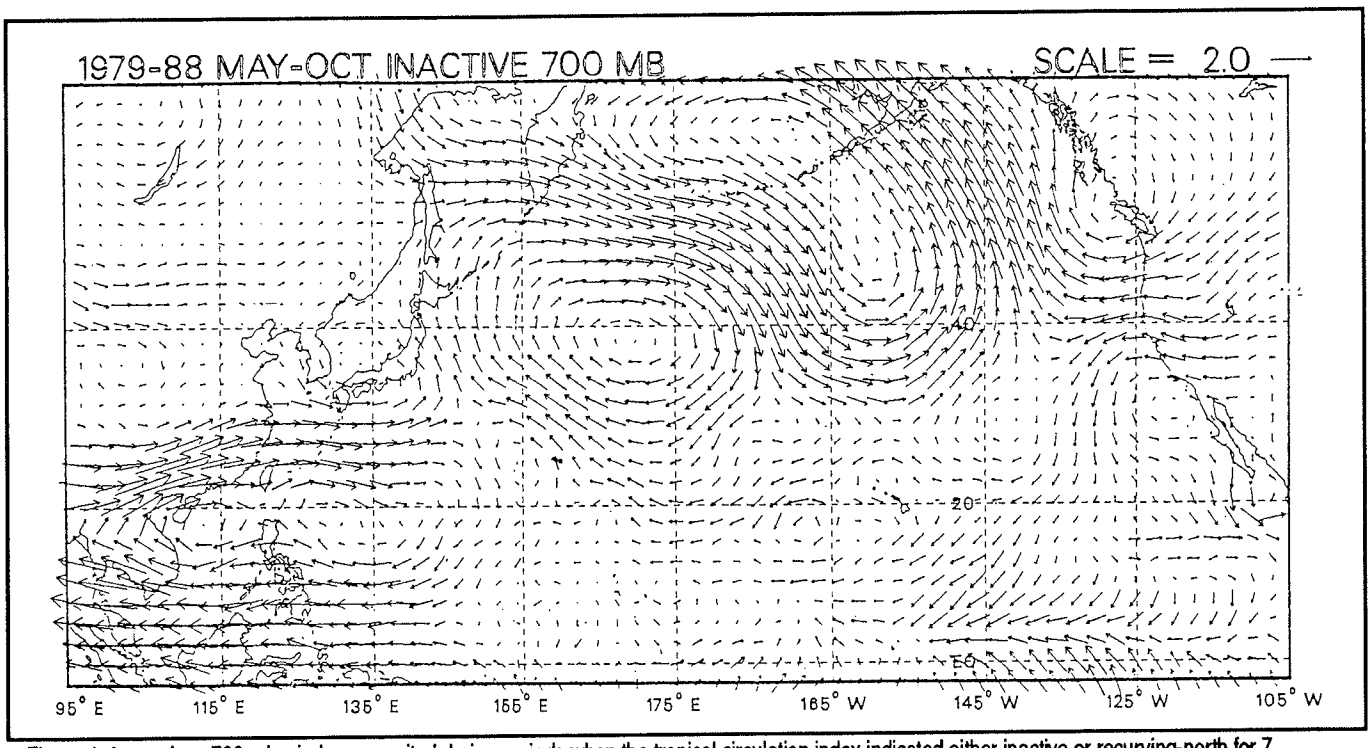

Figure 4. Anomalous 700-mb winds composited during periods when the tropical circulation index indicated either inactive or recurving-north for 7 consecutive days. In this composite, 714 fields were used. Units are meters per second.

Japan and anticyclonic anomalies over northwestern North America. This anomaly pattern is similar to the anomalous circulation during August 1988, when the tropical cyclone activity was shifted northward (Figure 1).

The recurving-south regime is associated with an active monsoon trough throughout the South China Sea and northern Philippine Sea (Harr and Elsberry 1991). During this regime, alternating cyclonic and anticyclonic anomalous circulations also stretch across the North Pacific (Figure 5). However, these circulations are nearly opposite in phase to those associated with the recurving-north and inactive regimes (Figure 4). The recurving-south circulation pattern contains large westerly anomalies throughout the tropical western Pacific, which suggests the monsoon trough is very active throughout the Philippine Sea. Cyclonic anomaly centers oriented southwest-northeast between 20°N-30°N and 120°E-155°E enhanced tropical cyclone activity over that region. Farther downstream, a large cyclonic circulation anomaly exists over the Gulf of Alaska.

During the straight-moving regime, the western Pacific monsoon trough is active, and tropical cyclones move toward the west or northwest under the influence of a strong subtropical ridge that exists over the East China Sea (Harr and Elsberry 1991). The wavelike features in the extratropical anomalous circulation pattern are weaker and do not seem to be associated with the tropical circulations during the straight-moving regime (Figure 6). It is hypothesized that the subtropical ridge, which prevents both the monsoon trough and tropical cyclones from moving into the subtropics, prevents the anomalous heating associated with these

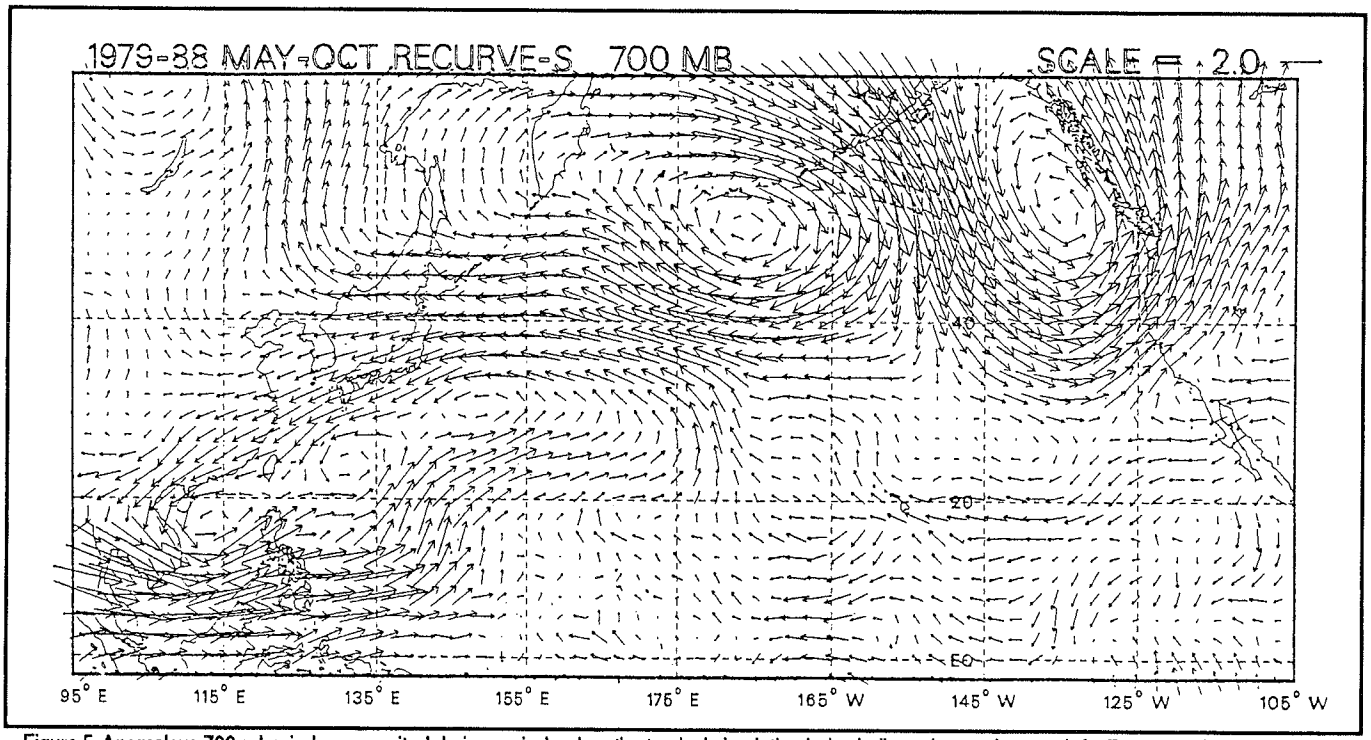

Figure 5. Anomalous 700-mb winds composited during periods when the tropical circulation index indicated recurving-south for 7 consecutive days. In this composite, 341 fields were used. Units are meters per second.

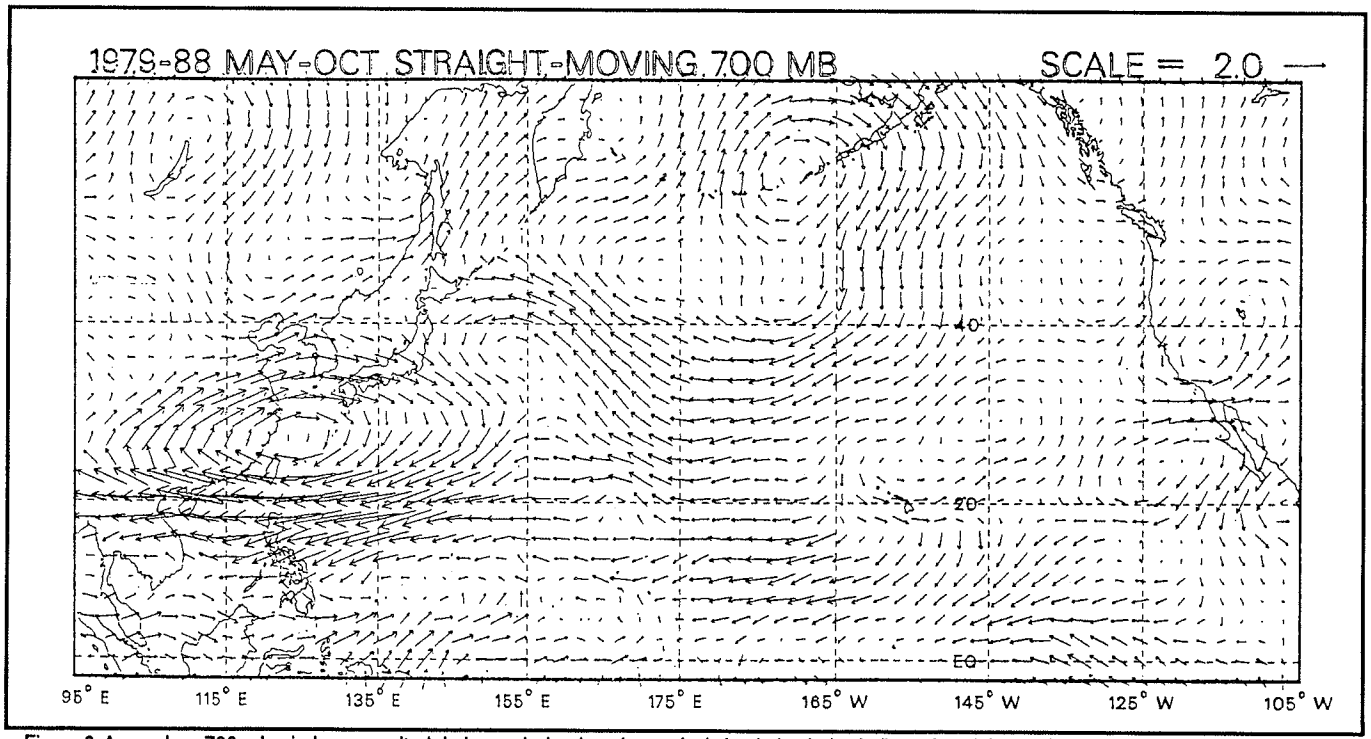

Figure 6. Anomalous 700-mb winds composited during periods when the tropical circulation index indicated straight-moving for 7 consecutive days. In this composite, 335 fields were used. Units are meters per second.

features from reaching a region that can influence the extratropics. This effect was investigated further by defining a new composite that omits recurving-south time periods when tropical cyclones moved north of 20°N (Figure 7). The anomalous westerlies over the South China Sea and Philippine Sea are larger than in the recurving-south composite because

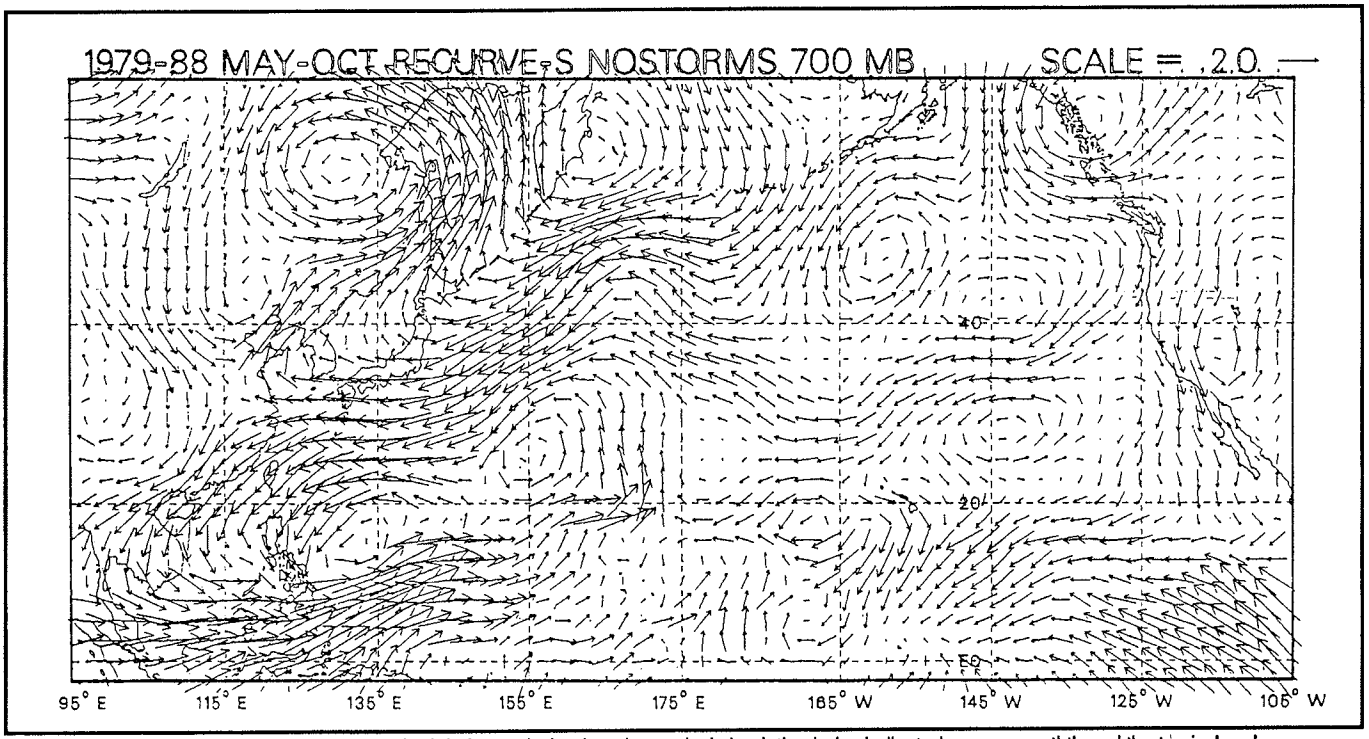

Figure 7. Anomalous 700-mb winds composited during periods when the tropical circulation index indicated recurve-southth and the tropical cyclones were south of 20°N. In this composite, 105 fields were used. Units are meters per second.

this composite highlights periods when tropical cyclones are moving over the Philippine Sea before they recurve into subtropical latitudes. Over the extratropical regions, there no wave-train anomaly features as in Figure 5. When the effect of the tropical cyclones is limited to south of 20°N, no coherent anomaly patterns extend across the North Pacific.

These composite analyses have been subjected to statistical significance tests defined by Livezey and Chen (1983). The large-scale circulation anomalies over the central and eastern North Pacific that are part of the inactive and recurve-south patterns are statistically significant. No significant anomalies are found north of 20°N in either the straight-moving or abbreviated recurve-south composites.

Discussion

Extratropical wavelike anomalous circulations across the North Pacific Basin have been identified with anomalous western North Pacific tropical circulation regimes. The tropical circulation regimes were identified with reference to western North Pacific monsoon and tropical cyclone activity. The extratropical anomaly patterns are similar to those defined by Nitta (1987) as atmospheric Rossby waves associated with tropical convection. The anomalies are also similar to results of model analyses of extratropical responses to anomalous tropical heating (Murphree 1991).

The inactive composite anomaly pattern is similar to the height anomalies of August 1988, when tropical cyclone activity shifted northward. This suggests periods of persistent tropical cyclone activity north of 20°N

or inactivity can provide a mechanism for generation of anomalous tropospheric heating that can influence atmospheric circulation across the North Pacific to North America. By contrast, no coherent extratropical anomalies are found if tropical cyclone activity is confined to south of 20°N.

This analysis has also been performed with 200-mb data, and results were similar. The extratropical anomalies exhibit a barotropic structure.

These results raise additional questions to be addressed in future analyses. These include identification of the response time of the extratropics to the persistent tropical anomalies. Also, previous investigations of tropical/extratropical relationships concentrated on interannual and intraseasonal time scales. However, these results suggest shorter time scales may also be important. Finally, these results apply to the Northern Hemisphere summer season, when it has generally been thought that tropical/extratropical relationships were at a minimum.

Acknowledgment

This research was supported by the Naval Postgraduate School direct-funded research.

References

Harr, PA, and RL Elsberry, 1991. Tropical cyclone track characteristics and large-scale circulation anomalies. *Mon. Wea. Rev.* 119:448-1468.

Livezey, RE, and WY Chen, 1983. Statistical field significance and its determination by Monte Carlo techniques. *Mon. Wea. Rev.* 111:46-59.

Murphree, T, 1991. Global scale forcing of North American climate anomalies. *Preprints, 19th Conference on Hurricanes and Tropical Meteorology.* American Meteorological Society:Boston.

Nitta, T, 1990. Unusual summer weather over Japan in 1988 and its relationship to the tropics. *J. Meteor. Soc. Japan.* 68:575-587.

_____, 1987. Convective activities in the tropical western Pacific and their impact on the Northern Hemisphere summer circulation. *J. Meteor. Soc. Japan.* 65:373-390.

NOAA, 1988. *Climate Diagnostics Bulletin.* Climate Analysis Center. US Department of Commerce:Washington DC.

Ropelewski, CF, 1988. The global climate for June-August 1988: A swing to the positive phase of the Southern Oscillation, drought in the United States, and abundant rain in monsoon areas. *J. Climate.* 1:1153-1174.

Trenberth, KE, GW Branstator, and PA Arkin, 1988. Origins of the 1988 North American drought. *Science.* 242:1640-1645.

Wallace, JM, and DS Gutzler, 1981. Teleconnections in the geopotential height fields during the Northern Hemisphere winter. *Mon. Wea. Rev.* 109:785-812

Snow Depth as an Indicator of Weather and Climate in the Sierra Nevada

Larry G. Riddle, Daniel R. Cayan, and Edward Aguado

Abstract: Snow is an important determinant of the magnitude and timing of streamflow in the mountains of western North America. Two different measures exist over long historical periods (more than 3 decades): snowcourse surveys and cooperative weather records. Snowcourses monitor the snow depth and snow water content at mid to high elevations at a one time per month interval. Daily cooperative precipitation and snow records provide event-scale information of snow depth and liquid equivalent precipitation, with most stations confined to low and mid level elevations. The purpose of this study is to determine: (1) whether the cooperative station snow depth contains useful weather and climate information, (2) how cooperative snow depth variability is related to snowcourse variability, and (3) how it is related to other weather elements.

From an examination of stations in the Sierra Nevada of California, it is clear that cooperative snow records and snowcourse records have consistent spatial and temporal variability. For over 40 years of record, there is a strong correlation between the two methods of measuring snow. Both measures show strong spatial coherence of monthly snow anomalies between the central and southern Sierra Nevada. The cooperative snow depth provides insight into snowstorms. Event-scale snow density is derived by combining snow depth (SD) with liquid equivalent precipitation (Ppt).

We show that high snow ratio (low density snow or high SD/Ppt) events have low temperatures and high amplitude atmospheric circulation patterns over the eastern North Pacific. In contrast, low snow ratio (high density or low SD/Ppt) events have warm temperatures and a zonal flow pattern with a southerly displaced storm track from Hawaii to the West Coast.

Introduction

There is significant variation in annual and seasonal streamflow in the mountains of the western United States. In the Sierra Nevada of California, the magnitude of annual runoff is closely linked to the magnitude of annual precipitation, but the timing of runoff depends more on temperature and the condition of the snowpack than on when precipitation occurs (Kahrl 1979; Aguado *et al* 1991). This linkage is evident in the lag between precipitation (with a January-February maximum) and streamflow (with a March-May maximum, depending on elevation).

The peak in human consumptive water use (April-July) more nearly coincides with the streamflow maximum than with the precipitation maximum (Roos 1989). Because of this, the water supply in the western United States relies heavily on snowpack for water storage. However, about half of the Sierra Nevada snowpack accumulation areas are in basins that are extremely sensitive to temperature (Roos 1989). If climate change were to increase the mean annual temperature, this could cause earlier runoff and decreased spring snowpack (Gleick 1987; Lettenmaier

In K.T. Redmond, Editor, 1992. Proceedings of the Eighth Annual Pacific Climate (PACLIM) Workshop, March 10-13, 1991: California Department of Water Resources, Interagency Ecological Studies Program Technical Report 31.

and Gan 1990). Our long-term goal is to better understand weather and climate influences on snow and the role snow plays in controlling streamflow variation.

This study is an initial look at the variability of snow in the central and southern Sierra Nevada. A companion study (Cayan *et al* this volume) focuses on the variability of snowcourse water content in the West. In so doing, we want to evaluate the cooperative snow data as a meteorological/climatological indicator. Furthermore, we want to begin to exploit the information it provides on interannual variability of winter storms and snow in the Sierra Nevada. To accomplish this, we examine daily and monthly snow accumulation and liquid water equivalents at two cooperative weather stations and two high elevation snowcourses. We then relate these snow parameters to broad-scale atmospheric circulation, temperature, and precipitation. We accomplish this using three steps:

- Correlate the monthly and seasonal snow measurements.
- Examine the spatial coherence of the two snow measures.
- Examine the difference between high ratio (high snow depth to liquid equivalent precipitation or "dry") snow versus low ratio (low snow depth to liquid equivalent or "wet") snowstorm episodes.

A recent examination of streamflow variability (Riddle, Cayan, and Aguado 1990) has demonstrated the importance of temperature in determining whether precipitation produces runoff or is stored in the snowpack. Linear models developed in that study show seasonal mean precipitation and temperature can explain a large portion of seasonal streamflow in low, moderate, and high elevation basins in central and northern California. In general, these models explain over 60% of seasonal streamflow variation in the moderate and high basins. Nearly 80% of the independent period variation was explained in the highest basins during the heavy runoff, late spring period. The importance of snow in the timing of runoff was emphasized by the dependence of predictor relationships on mean elevation of the watersheds.

Climate is one decisive factor in determining the quantity and character of streamflow (Bruce and Clark 1966); another is basin elevation (Cayan and Peterson 1989). Since there is a strong link between both climate and elevation and snowpack formation, an understanding of the variability of snow water content would contribute to our understanding of climate's role. A better understanding of that role would be beneficial in optimizing water management decisions.

The Study Region and Climatic Data

The study area is the Sierra Nevada from the upper San Joaquin River basin in the southern Sierra near Fresno, California, northward to the Yuba River basin near Marysville, California (Figure 1). From this region,

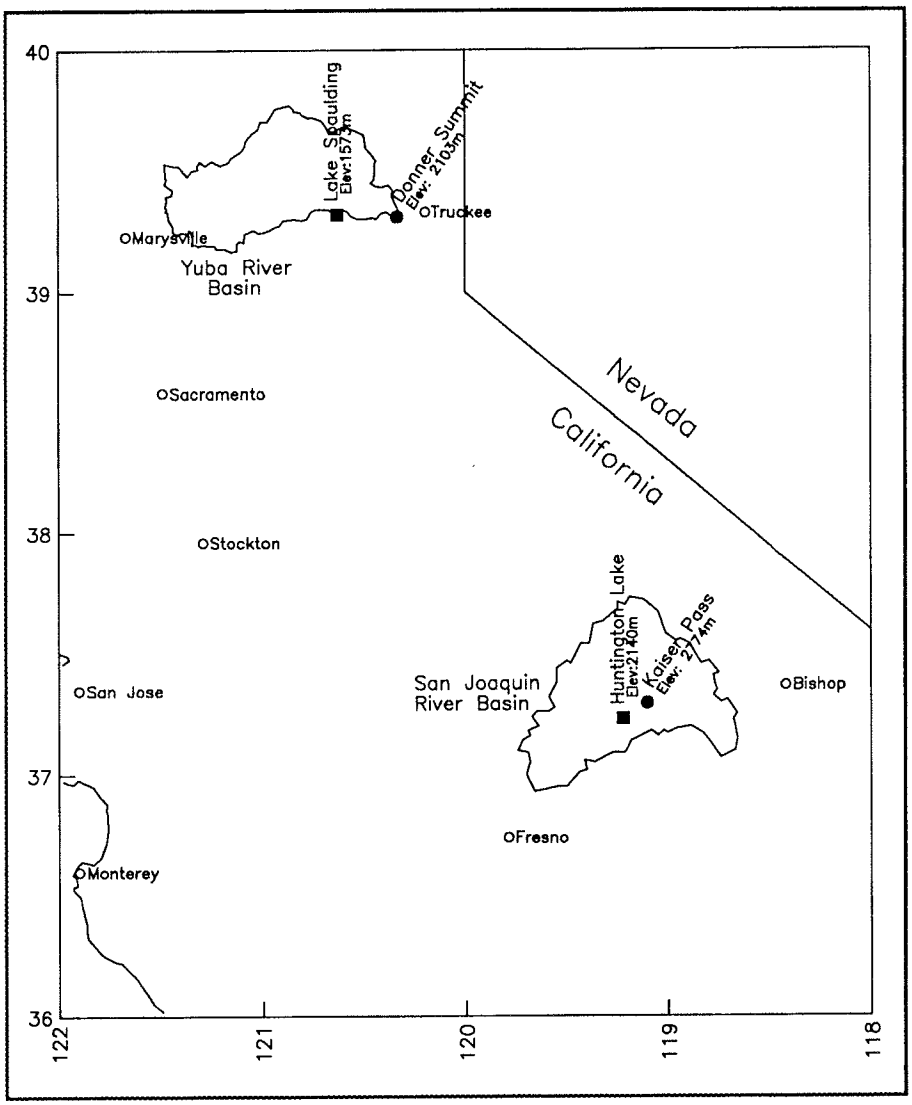

Figure 1. Map showing the cooperative observing stations (closed squares) and snowcourses (closed circles) used in this study. Distance from Donner Summit to Kaiser Pass is about 250 kilometers.

we selected snow observations from two river basins for study. The Yuba River watershed (mean elevation in the 1000- to 2000-meter range) and the upper San Joaquin watershed (mean elevation above 2000 meters), represent moderate and high elevation basins.

There are four primary methods of measuring snow in the Sierra Nevada: snowcourses, aerial markers, snow sensors, and cooperative weather observers. The most familiar method for climate researchers is the snowcourse survey. Snowcourses provide highly accurate measures of snow depth and snow water content at mid to high elevations. Some Sierra Nevada snowcourse records begin as early as 1910, but most of the long-term courses were first surveyed in the 1940s. The primary disadvantages of snowcourse surveys are the coarse temporal resolution and shortage of mid and low elevation data. Snowcourses are usually surveyed, at most, from four to six times each winter. Some are only surveyed once or twice a year. Most snowcourses are above 2000 meters, some are over 3000 meters, but few are below 1500 meters. There were about 400 snowcourses in California, but surveys have been discontinued at over 90 of these (DWR 1991).

Aerial snow depth markers are co-located with over 100 of the snowcourses to provide water managers a quick look at snow conditions between surveys. Most have about 40 years of record. These markers are pipes fitted with metal vanes, allowing depth measurements to be made photographically from aircraft (DWR 1971). These markers are easier and faster but are not as accurate as snowcourses, and they do not measure water content.

There are over 100 snow sensors in California that measure water content at the sensor's location. Most are co-located with snowcourses and most automatically transmit measurements to central locations. Some also measure precipitation and/or temperature. Most are located above 2000 meters, and all are higher than 1500 meters (DWR 1991). Snow sensor measurements are of limited utility. The majority were installed during the 1970-1980s and have short record lengths. They do not provide snow depth data and there may be accuracy problems.

The most numerous and probably the most under-utilized snow measurement records in California are the cooperative weather observer daily snow depth records from the National Climatic Data Center (NCDC). The EarthInfo, Inc. (distributor for NCDC) CD-ROM contains 1,131 cooperative snow station records for California. Of these, 753 station records begin before 1950 and 26 before 1930; 293 stations have 40 or more years of record. Station elevations run from sea level to over 2500 meters. There are 556 stations with at least 20 years of record and less than 20% missing data: 405 of those were still active in 1989. More than 200 stations are in the temperature-sensitive elevation range:

500-999 meters	114
1000-1499 meters	66
1500-1999 meters	28
2000 meters and higher	10

The cooperative snow depth stations are mapped in Figure 2 according to these four elevation categories.

All of the cooperative stations that report snow depth also report daily liquid equivalent precipitation, and most report maximum and minimum temperatures. Beyond the data contained on the CD are many post-World War II records and most of the earliest records, which have not yet been converted to computer-readable form.

Data used in this study are cooperative station weather reports, snowcourse measurements, and upper air heights and temperatures. We do not use snow marker data, because it does not provide any information not available in the snowcourse records, nor snow sensor data, due to the shortness of the records. The cooperative data include daily, monthly, and seasonal precipitation, temperature, and snow accumulation from two weather stations in the Sierra Nevada. The snowcourse water content measurements are from two nearby snowcourses. The upper air data are

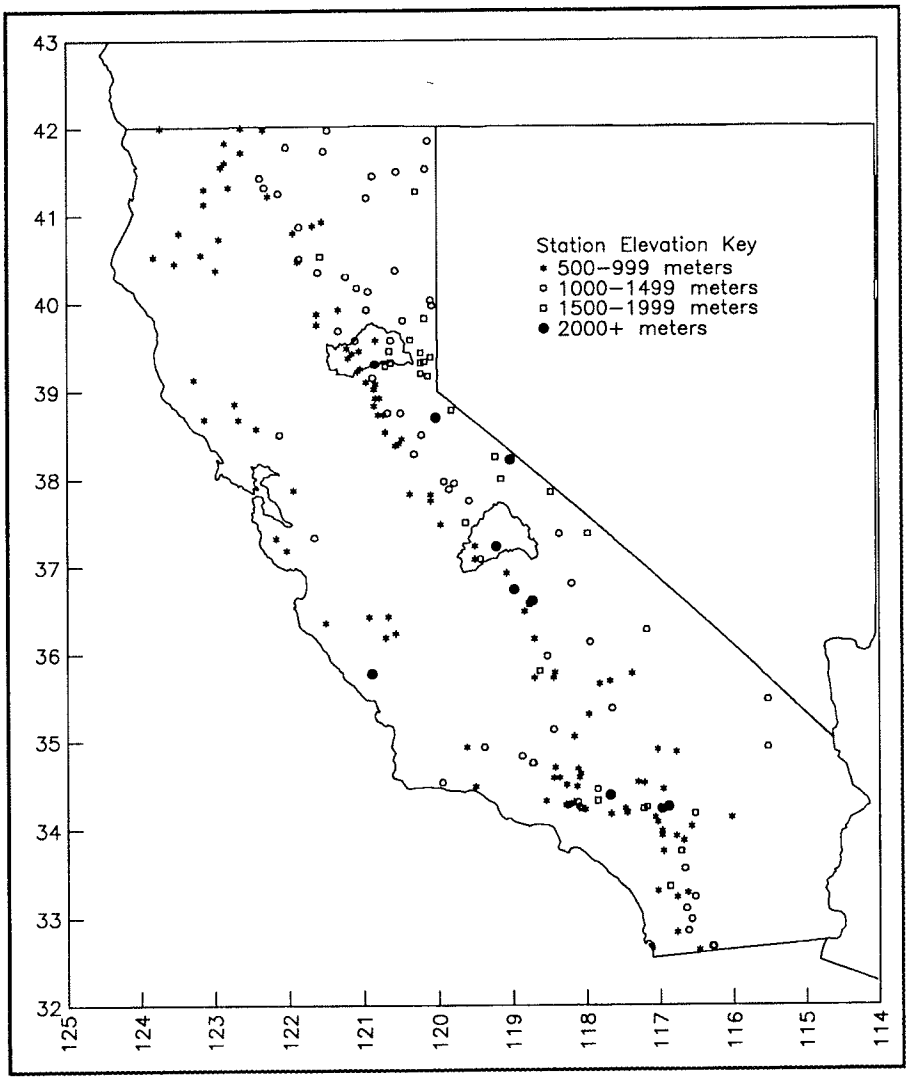

Figure 2. Map showing the 218 long record cooperative observing stations in California.

the twice daily 700-mb gridded heights. Temperature anomalies were derived for the sea surface to 700-mb layer from the 700-mb height and sea level pressure (SLP) for the eastern North Pacific and western United States. The 700-mb height, height anomaly, and temperature anomaly data are from the National Meteorological Center (NMC) gridded data set for the Northern Hemisphere, supplied by the NOAA Climate Analysis Center.

Daily precipitation and snow data are from the National Climatic Data Center (NCDC), NOAA via EarthInfo, Inc. *CLIMATEDATA CD-ROM Volume 2.01*, and EarthInfo software. The two cooperative stations are Lake Spaulding (1573 meters) for the Yuba River and Huntington Lake (2140 meters) for the San Joaquin River (Figure 1 and Table 1). In this study we will examine the utility of the cooperative snow depth data for climate research.

The snowcourse data are from California Department of Water Resources Bulletins 129-70 (*Snow Survey Measurements through 1970*) and 120-71 through 120-89 (*Water Conditions in California*). The snowcourses chosen are Donner Summit (Yuba River) and Kaiser Pass (San Joaquin River) (Figure 1 and Table 1). The Donner Summit snowcourse, at 2103 meters, is about 250 km north of and 670 m lower than the Kaiser Pass snowcourse. Donner Summit is about 25 km east of and 530 m higher than Lake Spaulding. Both Donner Summit and Lake Spaulding are on the divide between the American and Yuba River basins, just on the Yuba River side. Kaiser Pass is roughly 13 km northeast of and 630 m higher than Huntington Lake. Both are in the San Joaquin basin.

Table 1
Cooperative Weather Station and Snowcourse Location and Elevation Data
(The cooperative station mean annual liquid equivalent precipitation, snow accumulation, snow ratio [long-term mean snow / long-term mean precipitation], and mean annual average temperature are also given.
The long-term mean April 1st snow water content is listed for both snowcourses.

Station Name	Location			Station Means			
Weather Station	Lat	Lon	Elev	Ppt	Snow	Ratio	μAT
Lake Spaulding	39.32N	120.63W	1573	1806	6624	3.668	8.5
Huntington Lake	37.23N	119.22W	2140	1004	5410	5.388	8.0
Snow Course	Lat	Lon	Elev	April 1st WC			
Donner Summit	39.31N	120.34N	2103	1013			
Kaiser Pass	37.30N	119.10W	2774	970			

Ppt = Mean Annual Precipitation (mm)
Snow = Mean Annual Snow Accumulation (mm)
Ratio = Snow / Ppt
μAT = Mean Annual Air Temperature (C)
WC = Mean April 1st Snow Water Content

Snow Measurement

The two snow measurements studied here are totally different in both method and intent. Cooperative snow observations are taken daily for climate and weather recording purposes. They provide relatively high temporal, spatial, and elevational resolution on event-scale processes. Each day starts with no snow and records only new snowfall (*ie*, no memory of prior conditions). Ratios of cooperative snow depth to liquid equivalent precipitation apply only to events at single-day resolution. Most observers are volunteers, and observations can be erratic, so each station must be evaluated individually prior to use.

Snowcourse survey measurements are used to gage the water supply. These observations are taken by trained personnel, most of whom work for water controlling or using agencies. These agencies include the

California Department of Water Resources, the US Forest Service, public utilities, and private land companies or irrigation districts. Surveys are conducted one to six times each wet season (December through May), depending on the needs and resources of the controlling agency. The most common dates are on or near the first of the month in February and April. Since they are usually sampled only once per month, snowcourses have low temporal resolution. Although they lack event-scale information, snowcourses integrate conditions throughout the snowpack accumulation/ablation season and are the primary measure of the water supply contained in the snowpack. Ratios of snowcourse depth to water content provide an index of seasonal-scale conditions (Cayan *et al* this volume).

Snow and Liquid Equivalent Precipitation

We computed daily mean snow measurements for Lake Spaulding for 1949 to 1989. Means, means plus one standard deviation, and maxima are shown in Figure 3. There is considerable variation throughout the wet season, with little more likelihood of large events in the early season (day 62 or December 1) than the late season (day 182 or March 31). Lake Spaulding's mean monthly snow accumulation is compared to that of precipitation in Figure 4. Means, means plus/minus one standard deviation, minima, and maxima are graphed over the water year for both variables. While snow accumulation lags about a month behind precipitation at the beginning of the wet season, it decreases and ends about the same time as precipitation in the latter part of the wet season. In the 1949-1989 wet seasons (November 1 through March 31), Lake Spaulding had 7,401 observations where both precipitation and snow values were present. There were 2,528 days with precipitation and 1,565 days with snow, so about 34% of the days had precipitation and about 62% of those had snow.

In terms of 1949-1989 mean monthly precipitation divided by number of days per month, Lake Spaulding received a symmetric 8 mm of liquid equivalent per day during both November and March and 10 mm per day during December, January, and February. Snow is much more complicated. Lake Spaulding received less snow in November (20 mm per day) than it did in April (25 mm per day), a month with less than 60% of November's precipitation. The accumulated snow depth had a bimodal peak, with maxima in January (44 mm per day) and March (42 mm). February shows a distinct decline (39 mm). January and March are the only months that never had zero snow accumulation. The January snow peak coincides with the wet season precipitation peak. The March peak is probably a function of mean storm temperature, with late season storms being colder than those earlier in the season (Lee 1987; Minnich 1986).

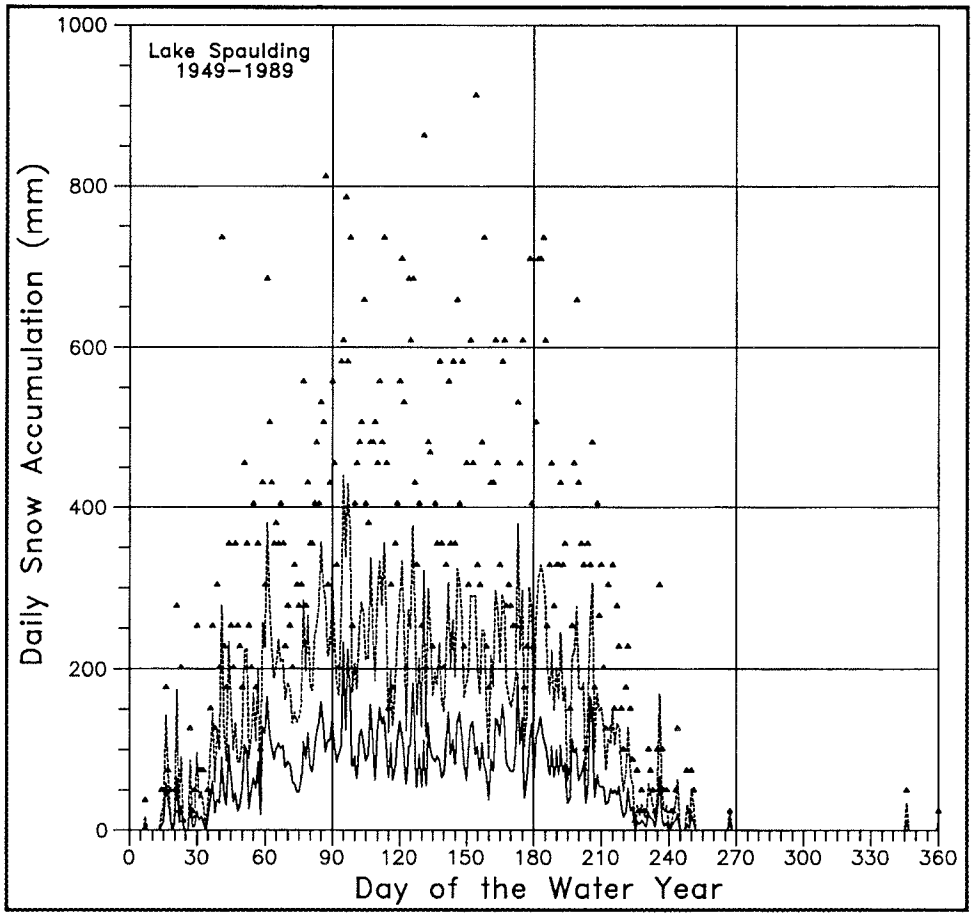

Figure 3. Daily means (solid line), means plus one standard deviation (dashed line), and maxima (closed triangles) snow accumulation at the Lake Spaulding cooperative station.

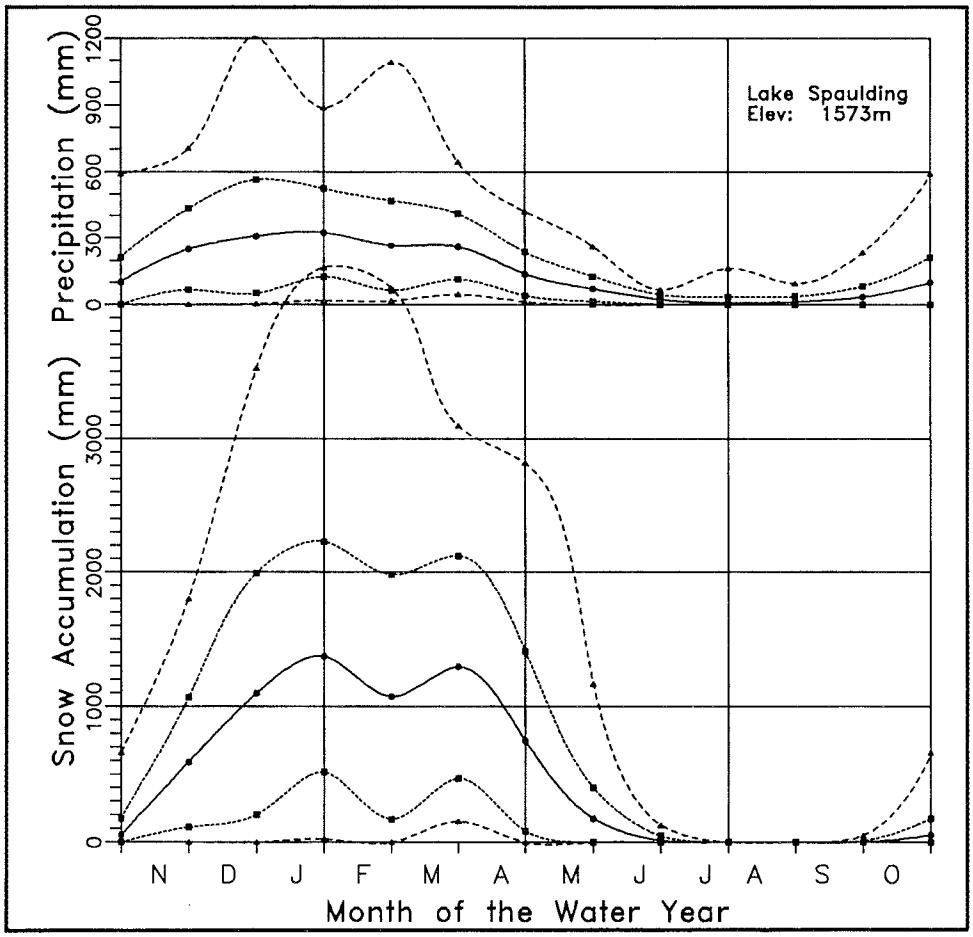

Figure 4. Monthly climatological statistics for the Lake Spaulding cooperative station for precipitation and snow accumulation based on 1949-1989 data. The center solid curved lines are long-term means. The dotted lines to either side of the means are means +/– one standard deviation. The outer dashed lines are maxima and minima. The curves are cubic splines of monthly data.

A comparison of time series of Lake Spaulding's water year snow and precipitation is presented in Figure 5. The 9-year Gaussian-filtered values (closed circles) show a high degree of similarity, but individual yearly values can diverge significantly. The snow peaks at 1952, 1967, 1969, and 1982 (the four highest snow years in this record) coincide with precipitation peaks, but the snow peak in 1979 is a precipitation low while the snow low in 1970 corresponds to a precipitation value that is above normal. These differences illustrate that snow and liquid equivalent precipitation can capture significantly different aspects of climate variability, even though they are generally closely related.

We originally intended to use the Bowman Dam cooperative record for the Yuba River. A close examination of the record at Bowman Dam exhibited a strong correlation with surrounding stations at monthly and annual time scales, but a distinct lack of correlation at a daily scale. We believe this may be due to observational practices that are inconsistent with neighboring stations. This underscores the need to examine each cooperative station before use.

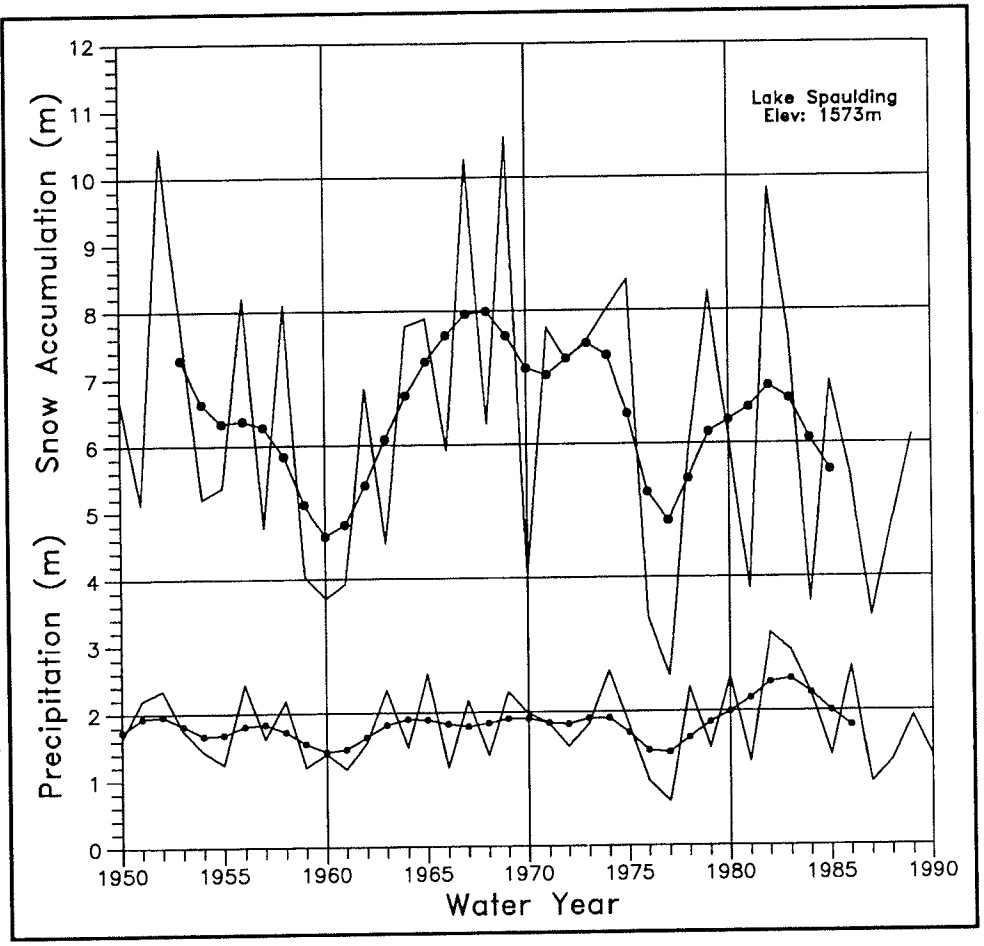

Figure 5. The water year (October 1 through September 30) snow accumulation and precipitation at Lake Spaulding. The correlation coefficient for liquid equivalent precipitation vs. snow accumulation is 0.56. The line connecting the closed circles is the Gaussian 9-year low pass filtered values.

Snow Depth vs. Snow Water Content

A comparison of the time series of the January/February snow accumulation at the cooperative snow stations (Figure 6) and the April 1 readings at the nearby snowcourses (Figure 7) exhibit strong similarities between the monthly and longer scale variability occurring for the two snow parameters.

In-basin correlations between cooperative station and snowcourse values are reasonably high considering the differences mentioned above ("Monthly" in Table 2). When the cooperative values are correlated with month-to-month changes in the snowcourses (the "change in WC" entries in Table 2), the coefficients improve significantly. The highest coefficients overall are exhibited between the cooperative station seasonal accumulations and the snowcourse readings ("Accumulations" in Table 2). This is achieved by comparing the January snowcourse readings with the December cooperative snow accumulation, the February snowcourse with the December plus January cooperative snow, March snowcourse with December through February cooperative snow, and so on.

Table 2
Correlation Coefficients for Each Snowcourse and Associated Cooperative Station

Donner Summit	Jan	Feb	Mar	Apr	May
Lake Spaulding					
Monthly	.51	.48	.51	.32	.59
δWC	.38	.68	.54	.81	--
Accumulation	.66	.76	.75	.73	.74
Kaiser Pass	**Jan**	**Feb**	**Mar**	**Apr**	**May**
Huntington Lake					
Monthly	.47	.53	.57	.37	.40
δWC	.60	.75	.59	.60	--
Accumulation	.54	.72	.80	.75	.91

Monthly = Snow course 1st day of the month water content reading vs. the previous month cooperative snow depth accumulation.
δWC = Snow course monthly change in water content vs. monthly cooperative snow depth accumulation.
Accumulation = Snow course 1st day of the month water content reading vs. the sum of the cooperative snow depth previous months snow accumulation.

There is also significant correspondence between snow variability in the two Sierra basins. The San Joaquin normally receives slightly less snow than the Yuba, although it is at higher elevation. Previous research has demonstrated that the snowcourse anomalies exhibit a high degree of coherency throughout the Sierra Nevada (*eg*, Aguado 1990). Correlation coefficients for the monthly values at each station (Table 3) also show a strong relationship across the 250 kilometers separating the basins. Correlation coefficients for monthly snowcourse measures never fall below 0.8 for the months from January through May. We next examine the validity of using the cooperative snow records to examine event-scale phenomena that may be muted at monthly and seasonal time scales. One such parameter is the snow ratio, the ratio of daily snow accumulation to daily liquid equivalent.

Table 3
Correlation Coefficients for Monthly Snowcourse Water Content Values for Donner Summit vs. Kaiser Pass and Cooperative Snow Depth for Lake Spaulding vs. Huntington Lake

Station Type	Jan	Feb	Mar	Apr	May
Snow Course WC	.82	.85	.87	.83	.81
Coop Snow Depth	.64	.76	.68	.76	.49

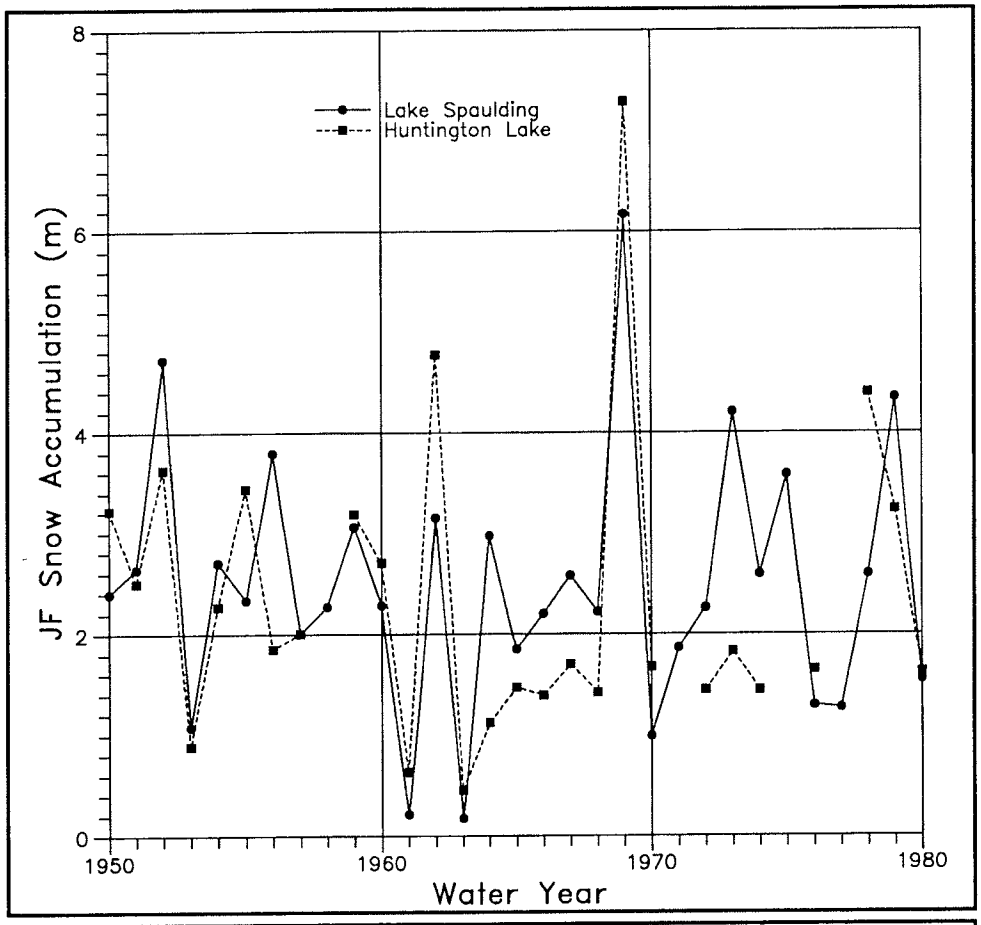

Figure 6. The January/February snow accumulation at Lake Spaulding and Huntington Lake cooperative stations. The correlation coefficient for Lake Spaulding vs. Huntington Lake is 0.70. The graph is limited to January and February to minimize problems with missing data at Huntington Lake, which is particularly spotty in the 1970s and 1980s.

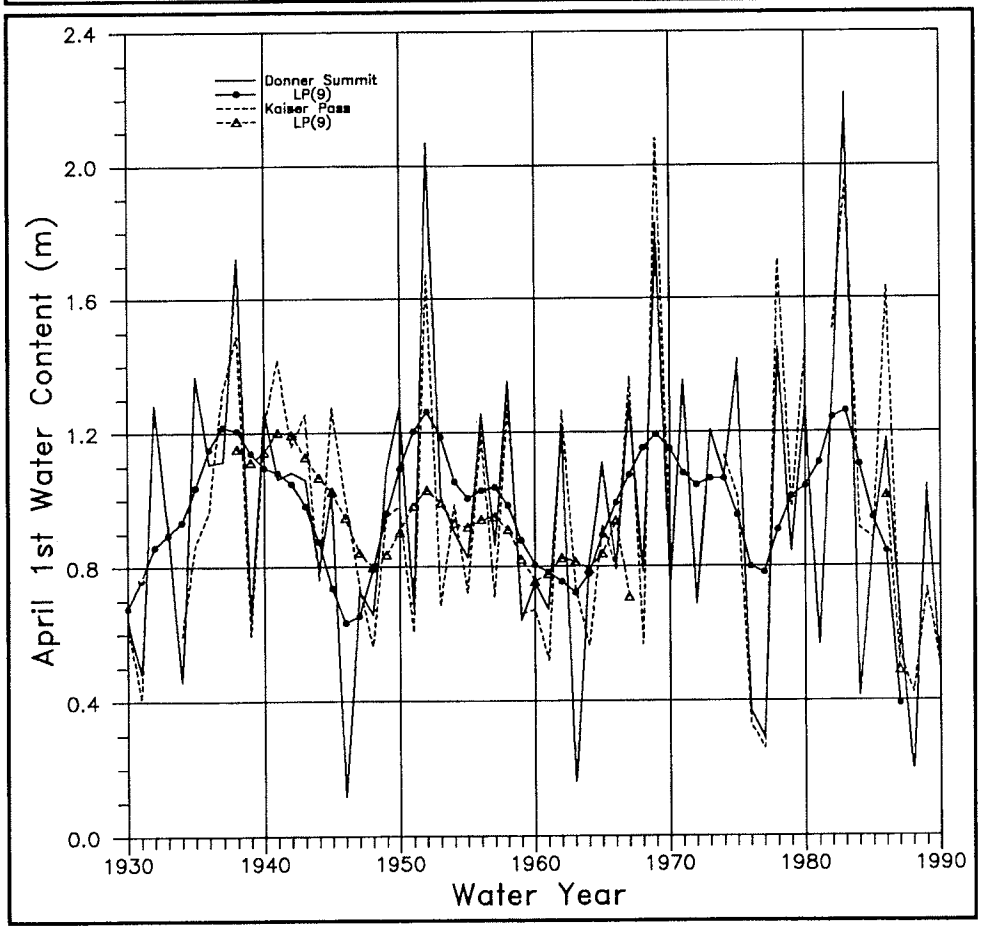

Figure 7. The April 1 snow water content measurements at Donner Summit and Kaiser Pass snowcourses. The correlation coefficient is 0.83. The triangles indicate the Gaussian 9-year low pass filtered values. Kaiser Pass has missing data in the 1970s and 1980s.

The Snow Ratio: Dry Snow vs. Wet Snow

The snow ratio is a measure of the dryness of snow. It is computed by dividing snow accumulation by liquid equivalent precipitation. It is more robust than computing density of snow (liquid equivalent over snow). It is possible to have precipitation without snow but impossible to have snow without precipitation. The former results in a snow density that is undefined, but a snow ratio of zero.

Since we were interested in behavior associated with snow conditions, we selected all days at Lake Spaulding with snow accumulations greater than zero. We divided all those days into four liquid equivalent precipitation categories: light (1 to 4 mm), moderate (5 to 25 mm), heavy (26 to 50 mm), and intense (greater than 50 mm). We then selected the 25 highest and 25 lowest snow ratio days for each category and composited the 700-mb heights, surface to 700-mb layer temperature anomalies, and height anomalies. The light and intense category composites are presented in Figures 8 and 9. It is interesting to note that light precipitation, whether high or low ratio, is associated with low heights near 120W and high heights near 150W and with westerly to northwesterly flow over Lake Spaulding. The main differences are that high snow ratio/light precipitation (HL) days had ridging at 140W, higher highs and lower lows than the low ratio/light precipitation (LL) days, and a significant layer temperature anomaly field in the eastern North Pacific. The moderate and heavy precipitation composites (not shown) exhibit a smooth transition to the intense precipitation composites. The similarities in high and low ratio intense precipitation are southwesterly flow over Lake Spaulding and a deep height anomaly offshore. The high ratio/intense (HI) positive height anomaly is similar in location and intensity to HL, but the low is deeper and farther west. The associated temperature anomaly has also moved west. The low ratio/intense (LI) composite negative height anomaly has also moved offshore and deepened but is still not as intense as HI. The positive height anomaly has moved north into Alaska. The layer temperature anomaly field, while better organized, is still fairly flat. The dominant feature exhibited by the composites is the meridional flow (and associated height and temperature anomalies) found with high ratio snow. Low ratio snow is found during periods of zonal flow.

A comparison of Lake Spaulding liquid equivalent precipitation and temperature recorded during the composited days described above is given in Table 4. We computed means for precipitation and temperature for the eight categories mentioned above. High ratio (dry) snow is associated with cooler temperatures and lighter precipitation. Differences in mean temperature range from 1.4 to 5.2°C between the low and high ratios of the four precipitation classes. However, the temperature behavior is more complicated when minimum and maximum temperatures are examined. In both snow ratio groups, temperature minima vary similarly: as precipitation intensity increases, minimum temperatures increase. Maxima vary inversely: as precipitation intensity increases, high ratio

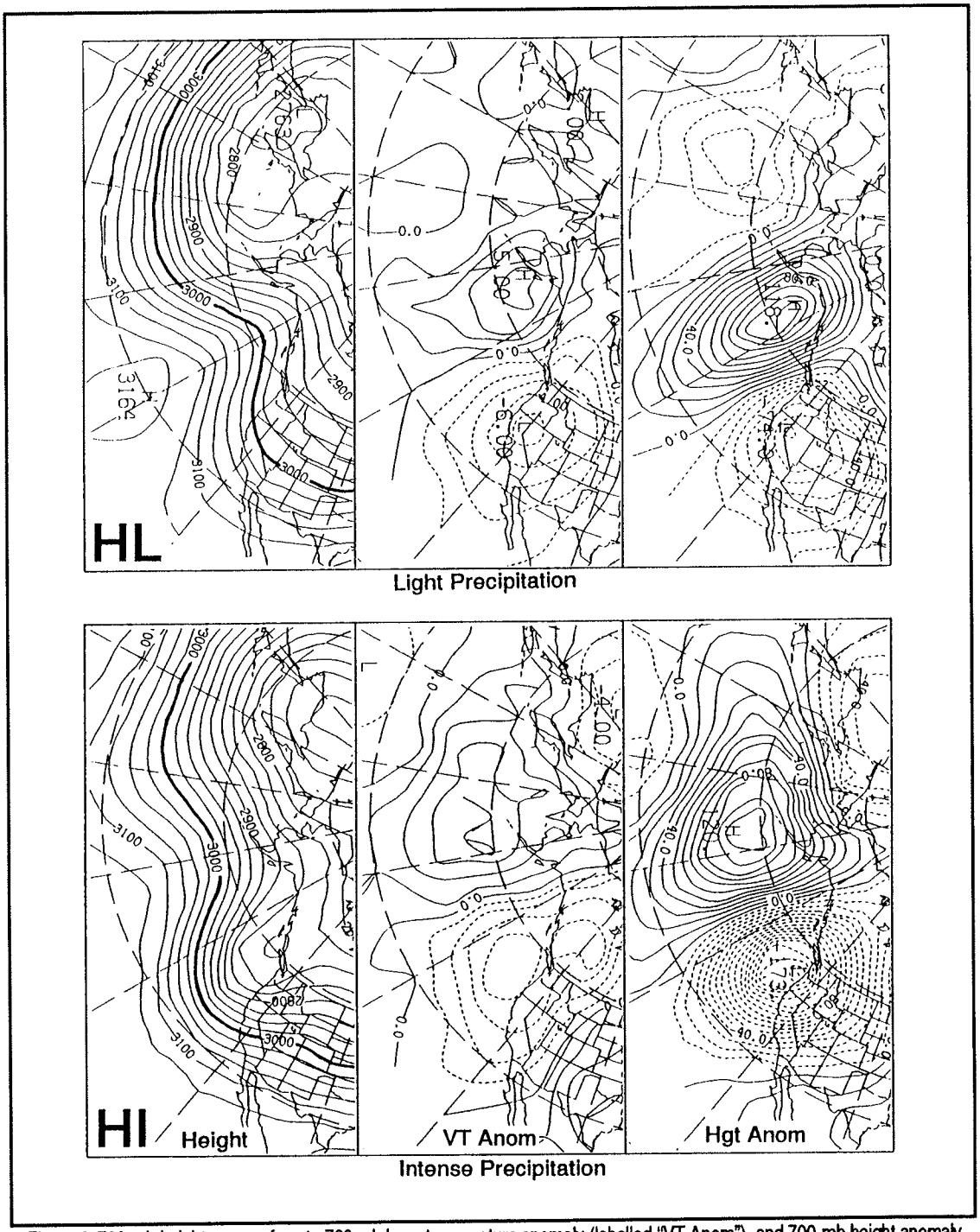

Figure 8. 700-mb height, sea surface to 700-mb layer temperature anomaly (labelled "VT Anom"), and 700-mb height anomaly composites of the low snow ratio light and intense precipitation days.

temperature maxima decrease and low ratio temperature maxima increase. The similar temperature minima patterns are probably related to increasing cloud cover and decreased outgoing longwave radiation. The dissimilar temperature maxima patterns are probably related to the source regions of the air masses ("warm" vs. "cool" storms). The lowest snow ratios occurred with the heaviest precipitation. Also, the precipitation in each low ratio group is consistently higher than that of the corresponding high ratio group.

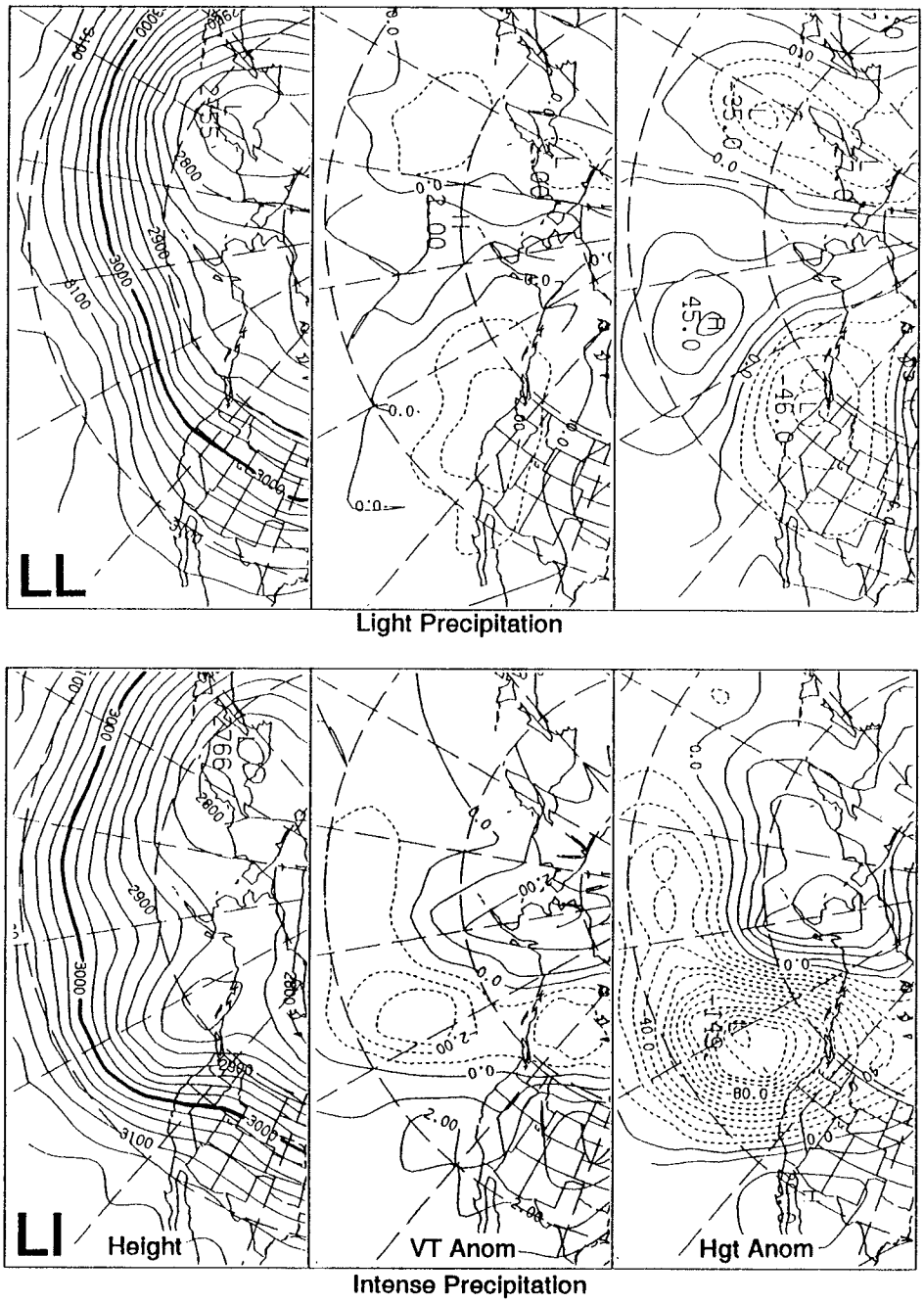

Figure 9. 700-mb height, sea surface to 700-mb layer temperature anomaly (labelled "VT Anom"), and 700-mb height anomaly composites of the high snow ratio light and intense precipitation days.

Table 4
Mean Precipitation and Temperature Values for Lake Spaulding for the 25 Days in Each of the Eight Precipitation/Snow Ratio Categories (4 Precipitation Categories by 2 Snow Ratio Categories) Used in the Study

Category	Precipitation (mm) Ppt	Snow	Ratio	Temperature (C) Max	Mean	Min
High Ratio						
01 - 04mm	1.7	47.6	28.2	5.2	-1.1	-7.4
05 - 25mm	10.0	177.4	18.1	2.0	-2.6	-7.1
26 - 50mm	35.2	463.4	13.1	0.6	-1.7	-4.1
> 50mm	64.2	642.1	10.0	0.0	-2.1	-4.2
Low Ratio						
01 - 04mm	3.8	19.9	5.2	4.8	0.3	-4.3
05 - 25mm	20.1	17.1	0.8	5.6	1.8	-2.0
26 - 50mm	39.5	21.2	0.5	5.4	2.4	-0.5
> 50mm	99.4	21.8	0.2	6.2	3.1	0.0

Ppt = Mean Category Daily Precipitation
Snow = Mean Category Daily Snow Accumulation
Ratio = Mean Category Daily Snow Ratio (Snow/Ppt)

Summary and Conclusions

We examined two measures of snow, cooperative daily snow accumulations and snowcourses, at two widely separated locations in the Sierra Nevada of California. There is considerable spatial coherence in the monthly anomalies of both snow measures.

Cooperative station records must be used with caution, since observation practices vary from station to station and year to year. However, since with over 400 active cooperative stations in California at elevations above 500 meters, it is not difficult to locate a usable station below 1500 meters. The choice of stations above 1500 m is limited.

Cooperative snow depth measurements provide details of winter precipitation during storm events. When combined with station liquid equivalent precipitation, they produce the snow ratios (snow depth to liquid water equivalent) whose data yield information on cool vs. warm storms (or dry vs. wet snow events). The cooperative stations also provide data for the temperature sensitive mid-elevation basin zones that are poorly sampled by snowcourses.

Climatological information extracted from cooperative snow depth records shows seasonal accumulation of snow depth at cooperative stations is related to water content at nearby snowcourses (correlation coefficients are mostly above 0.7). Wet season snow frequency is closely correlated with precipitation frequency; 61% of all wet season precipitation days at Lake Spaulding also recorded snow.

Two snowcourses, Donner Summit (Yuba River basin) and Kaiser Pass (San Joaquin River basin), exhibit similar variability even though they are

250 kilometers apart in space and over 600 meters in elevation. We also showed a strong correlation between the individual snowcourse records and nearby cooperative snow depth records.

An interesting portrait of snowstorm patterns is provided by extreme cases of snow ratio and precipitation intensities. This portrait demonstrates a remarkable contrast in atmospheric circulation pattern and regional temperature for high vs. low snow ratio events. This is provided by composites of 700-mb height and temperature values. High snow ratios are produced by strong ridging near 150W, inducing strong meridional flow just offshore. Low snow ratios are related to pronounced zonal flow that extends from the eastern North Pacific near 30N-35N. These patterns intensify as total precipitation increases in these high or low snow ratio events.

Combined with precipitation and nearby snowcourse water content records, cooperative snow records appear to be a useful resource for both synoptic and climatic studies. Many cooperative snow records are available in computer readable form as far back as 1948. Longer records are available on paper copies, and will likely be digitized as their utility is recognized.

Acknowledgments

LGR and DRC acknowledge support by the University of California, Water Resources Center, Project UCAL-WRC-W-768, and by the NOAA Experimental Climate Forecast Center. Funding for DRC was also provided by the US Geological Survey via an Intergovernmental Personnel Act agreement with the University of California.

References

Aguado, E, 1990. Elevational and Latitudinal Patterns of Snow Accumulation Departures from Normal in the Sierra Nevada. *Theoretical and Applied Climatology.* 42:177-185.

Aguado, E, D Cayan, L Riddle, and M Roos, 1991. Climatic Fluctuations and the Timing of West Coast Streamflow. Submitted to *Journal of Climate.*

Bruce, J, and R Clark, 1966. *Introduction to Hydrometeorology.* Pergamon Press:UK Oxford. 319 pp.

DWR (California Department of Water Resources), 1971. *Bulletin 129-70, Snow Survey Measurements through 1970.* Sacramento. 504 pp.

_____, 1991. *1991 California Snow Survey Measurement Schedule.* Sacramento. 53 pp.

Cayan, D, and D Peterson, 1989. The Influence of North Pacific Atmospheric Circulation on Streamflow in the West. In DH Peterson (ed.) *Aspects of Climate Variability in the Pacific and the Western Americas.* American Geophysical Union Geophysical Monograph 55.

Gleick, P, 1987. The Development and Testing of a Water-Balance Model for Climate Impact Assessment: Modelling the Sacramento Basin. *Water Resources Research.* 23:1049-1061.

Kahrl, W (Editor), 1978. *California Water Atlas.* State of California:Sacramento. 117 pp.

Lee, T, 1987. Seasonal and Interannual Trends of Sierra Nevada Clouds and Precipitation. *Journal of Climate and Applied Meteorology*. 26:1270-1276.

Lettenmaier, D, and T Gan, 1990. Hydrologic Sensitivities of the Sacramento-San Joaquin River Basin, California, to Global Warming. *Water Resources Research*. 26:69-86.

Minnich, R, 1986. Snow Levels and Amounts in the Mountains of Southern California. *Journal of Hydrology*. 89:37-58.

Riddle, L, D Cayan, and E Aguado, 1990. The Influence of Seasonal Precipitation and Temperature on Runoff in California and Southwest Oregon. Presented at the *Seventh Annual PACLIM Workshop*. March 1990.

Roos, M, 1989. Possible Climate Change and its Impact on Water Supply in California. Presented at the *Oceans '89 Conference*. Seattle, Washington. September 1989.

Winter Climate Variability and Snowpack in the West

Daniel R. Cayan, Laurence G. Riddle,
David C. Garen, and Edward Aguado

Introduction

Snowpack is an important source of water supply in the western United States. This study examines the seasonal variability of an extensive history of snow observations over the western United States and Canada. It links variations in snowpack to variations in atmospheric circulation, surface temperature, and precipitation.

The purpose of this study is to determine how snow variations are related to atmospheric circulation, temperature and precipitation, and snowpack over the West. To accomplish this, we derive four categories of snow and precipitation anomalies at a particular snowcourse and examine whether these are accompanied by distinct anomaly patterns in the other variables. Specifically, this investigation seeks to establish:

- Whether the seasonal fluctuations of snowcourse variability are related to atmospheric circulation and, if so, what are the flow patterns associated with different seasonal snow characteristics.
- Whether temperature variability represented by the divisional temperature set is associated with differences in snow.
- Whether these fluctuations have regional-scale spatial coherence.

Data

For several decades, the USDA Soil Conservation Service (SCS) has archived snow observations at several hundred mountain snowcourses in the western United States. This study employs a set of about 400 snow water-content (WC) records for 1950-1989. Many snowcourses have observations taken at the beginning and sometimes the middle of each of the substantial snow-covered months, from January through May. For this study, we use only those taken on or about February 1 and April 1. The SCS snowcourse dataset does not include several snowcourse records on the west side of the Sierra Nevada in California, which are archived by the California Department of Water Resources. These records are on hand, but have not yet been merged with the SCS set and are not included in the analyses shown here. To limit the material presented in this article, we focus on variations associated with variations of snowpack

In K.T. Redmond, Editor, 1992. Proceedings of the Eighth Annual Pacific Climate (PACLIM) Workshop, March 10-13, 1991: California Department of Water Resources, Interagency Ecological Studies Program Technical Report 31.

at Carson Pass at 2621 meters, near the crest of the central Sierra Nevada. Atmospheric circulation is represented by monthly average northern hemisphere 700-mb height.* Monthly "divisional" temperature and precipitation from the National Climatic Data Center are used to represent variability over the coterminous United States and Alaska, augmented by a collection of well-sampled stations from western Canada. The 700-mb height, temperature, and precipitation all cover the 1950-1989 period.

Water Content Variability

The climatology of WC at Carson Pass and precipitation at a nearby station, Twin Lakes, is indicated by means, standard deviations, and extremes of monthly WC and monthly total precipitation in Figure 1. WC statistics are limited to the five months from January through May. In comparison to the winter (about January 1) maximum in precipitation, the WC maximum appears at the beginning of April. This lag, of course, occurs because WC is a cumulative measure of the precipitation. WC variability is relatively uniform throughout the five months, although the maximum WC has occurred in March, followed closely by April and May. The history of seasonal WC at Carson Pass since 1930 is plotted in Figure 2. This record exhibits extremely low WC in the springs of 1931, 1939, 1951, 1976, 1977, 1988, and 1990, in contrast to very high WC in 1952, 1958, 1967, 1969, 1982, and 1983. For the April 1 subset, WC fluctuations vary from about 23% to 188% of the long-term average.

Snow/Precipitation Categories

The WC at Carson Pass and precipitation in the closest climate division (Sacramento drainage) are used to partition the 40-year record into four equal parts depending on whether the November-January precipitation was wet or dry and whether the ratio of February 1 snow to November, December, and January precipitation (denoted WC/PPT) was high or low. The order of this sorting operation was first to divide the years into wet and dry halves, and then to divide each of these into high and low WC/PPT classes of 10 members each. Thus a given year was classified as dry high (DH), dry low (DL), wet high (WH), or wet low (WL).

Snow Water Content *vs.* Large-Scale Climate Variables

To study climate variability associated with these categories at Carson Pass, we constructed composites of four variables by averaging the 10 years entering each. These variables, all expressed as anomalies, included the November-January mean 700-mb height, the November-January mean surface temperature and accumulated precipitation over

* The height of the 700-mb pressure surface is typically about 3 kilometers aloft and provides a good representation of the mid-tropospheric circulation.

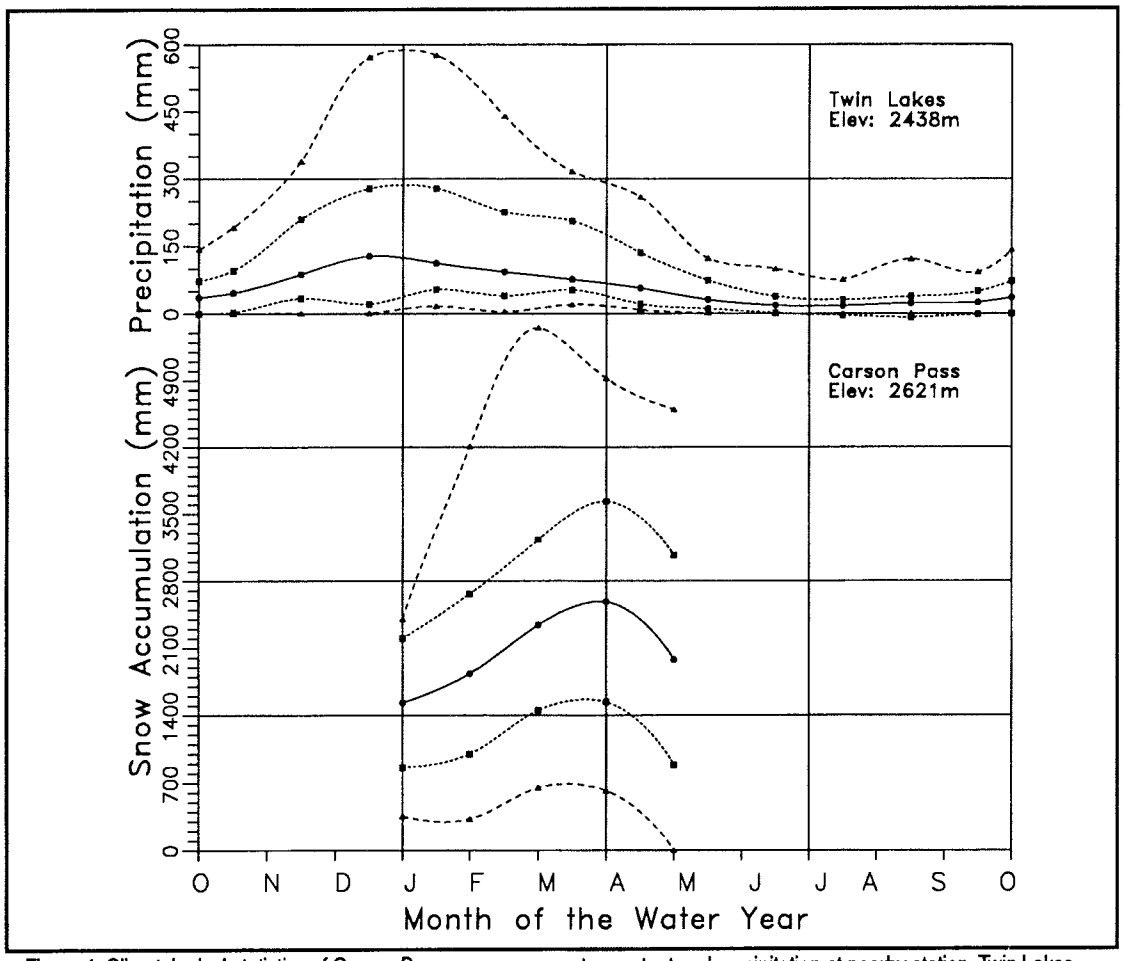

Figure 1. Climatological statistics of Carson Pass snowcourse water content and precipitation at nearby station, Twin Lakes, based on 1950-1988 data. Solid center curve is long-term mean. Upper/lower solid curves are long-term mean +/- one standard deviation. Upper/lower dashed curves are maximum and minimum values within record. Curves are smoothed fits to one value per month (January 1, February 1 ... May 1 for water content; monthly long-term mean for precipitation).

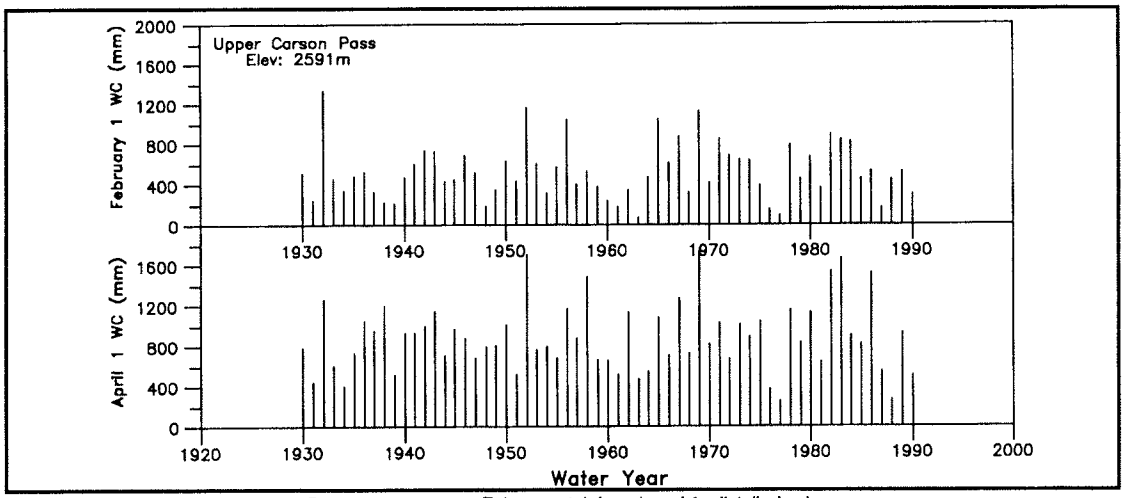

Figure 2. Time history of Carson Pass water content, February 1 (above) and April 1 (below).

the United States and Canada, and the snow water content at snow-courses over the West.

To determine whether the WC records contain a climate signal, we first examine the relationship between the four WC/PPT classes and atmospheric circulation. Composite maps of the 700-mb height anomalies for DH, DL, WH, and WL are shown in Figure 3. The 700-mb patterns have relatively large magnitudes and are distinctly different for the four classes. These patterns are organized with large regional scales over a major portion of the Pacific and North American sector. Furthermore, the physical interpretation of these patterns is consistent with the WC/PPT classes. As expected, positive anomalies over the West Coast dominate the two dry maps (DH and DL), while negative anomalies just offshore characterize the two wet maps. However, there are significant differences between the DH and DL maps. The positive anomaly center is offshore in DH, which permits a northerly flow of cold continental air in California. The positive anomaly in DL is centered directly over the West Coast, preventing the incursion of cold air into the region and keeping the weather dry. Also, the DL positive center extends northward across the North Pole, implying anomalous warmth far to the north. Considering the WH and WL maps, there are important differences in orientation of the negative anomaly features. Those in WH have a more northwesterly axis, implying a cool Gulf of Alaska origin of the winter storms. On the other hand, those in WL have a west-to-east configuration, with high pressure positive anomalies to the north, over the Bering Sea. This implies a lower latitude, warmer storm pattern in WL than in WH.

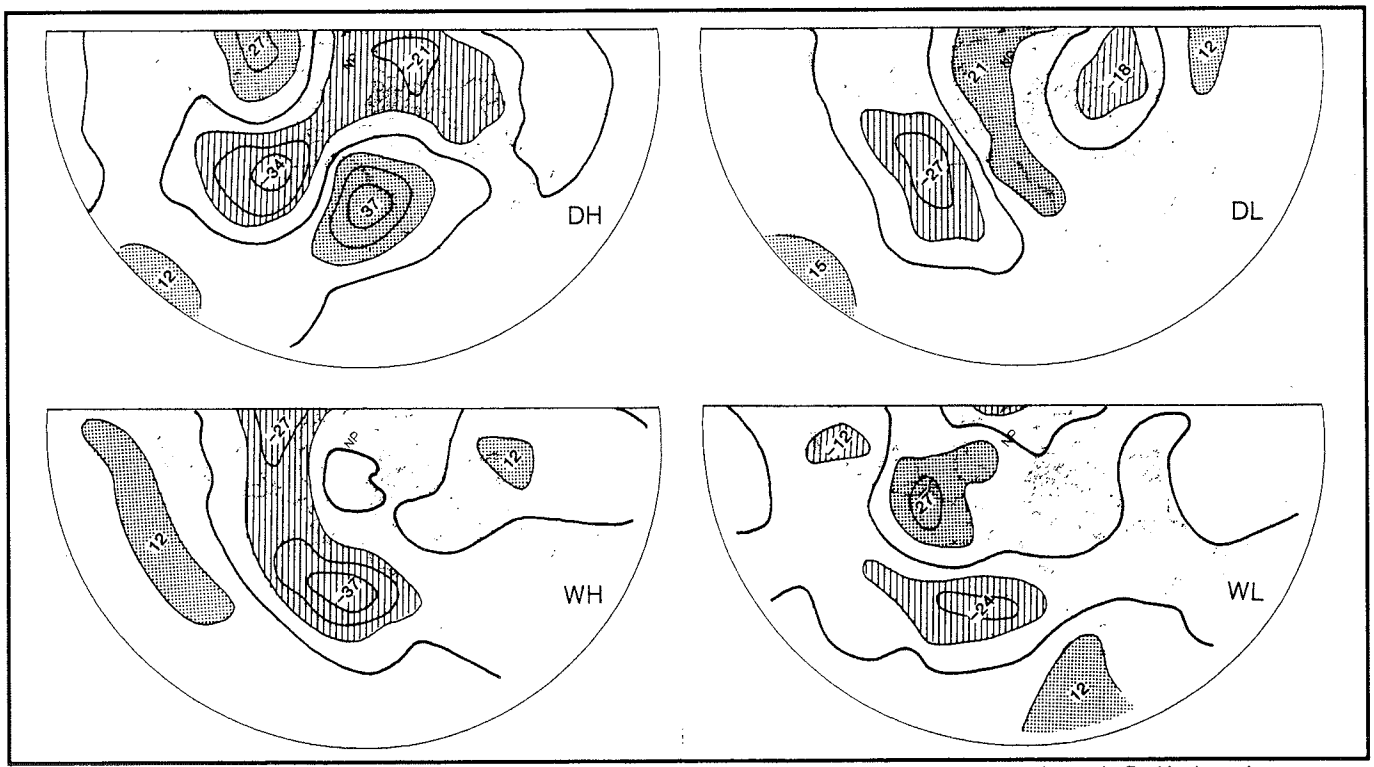

Figure 3. Composite 700-mb height anomalies (m) for Carson Pass DH, DL, WH, and WL cases. Contours at 10-meter intervals. Positive/negative anomalies denoted by stippling/hatching.

The air mass/temperature implications of the four circulation patterns are borne out by the surface temperature anomaly maps in Figure 4. Both of the high ratio classes have negative temperature anomalies in California, although the composite anomaly is not large in the WH case. Both DH and WH have larger negative anomalies elsewhere in the West, and both have positive anomalies downstream. Both of the low ratio classes have positive temperature anomalies in California, although the composite anomaly is not large in the DL case. However, consistent with the strong western high pressure ridge exhibited by the DH 700 mb height, it has an extensive positive anomaly covering virtually the entire West, with strongest magnitudes over western Canada and southern Alaska.

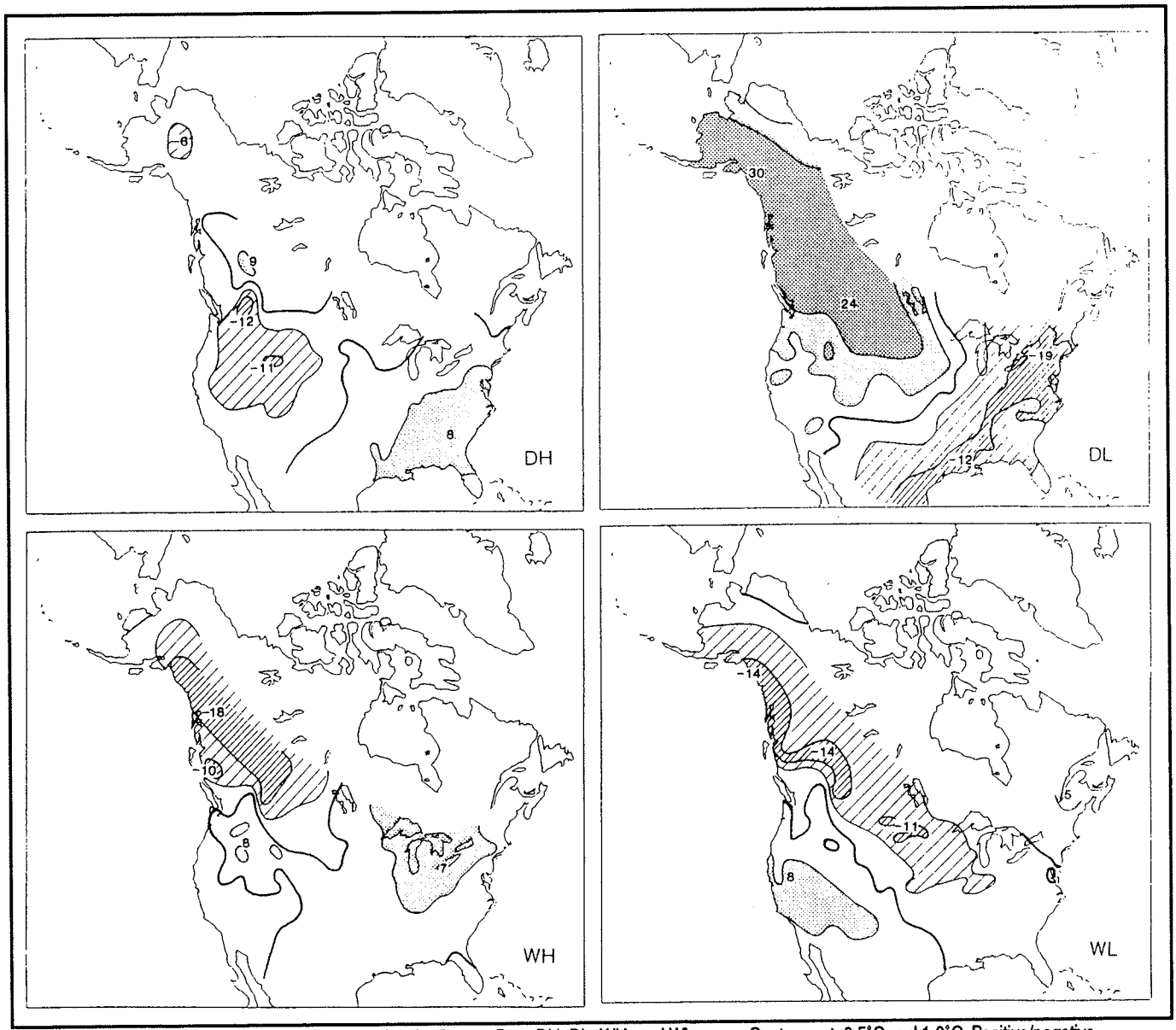

Figure 4. Composite temperature anomalies (0.1°C) for Carson Pass DH, DL, WH, and WL cases. Contours at 0.5°C and 1.0°C. Positive/negative anomalies denoted by stippling/hatching.

The composite precipitation maps, shown in Figure 5, illustrate the distribution of precipitation over the United States that characterizes the four classes. Of course, both DH and DL have negative precipitation anomalies in California, while WH and WL have positive anomalies. Consistent with the circulation and temperature composites, the differences among the two dry and the two wet cases are very marked, however. The driest case over the continent is DL, where both the West Coast and the eastern half of the United States have negative anomalies. Clearly, the North Pacific storm track has been diverted north in this case, as British Columbia and coastal Alaska have positive precipitation anomalies.

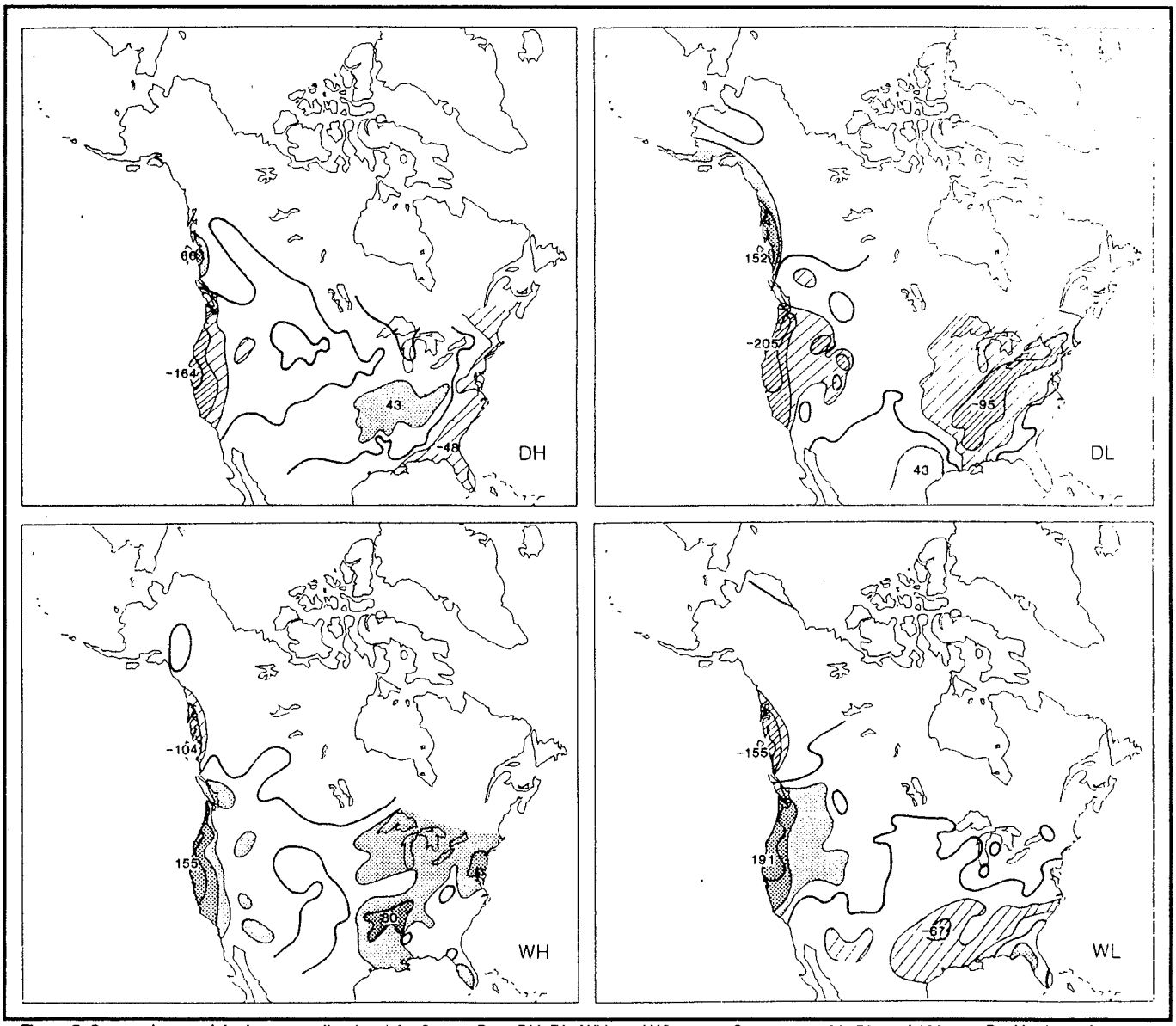

Figure 5. Composite precipitation anomalies (mm) for Carson Pass DH, DL, WH, and WL cases. Contours at 20, 50, and 100 mm. Positive/negative anomalies denoted by stippling/hatching.

Since the composites were based on the WC/PPT ratio and not the WC itself, it is important to note that the two wet classes exhibited positive WC regional anomalies while the two dry classes exhibited negative WC regional anomalies (Figure 6). Even though the classes were based on local WC/PPT behavior, large-scale patterns emerge. In fact, the four composites of snowcourse WC exhibit spatial coherence on a scale of several hundred kilometers that span major portions of the western states. (Part of the reason the WC maps look "spotty" is that the low-lying areas of the west do not generally have snowcourses and the amount of WC [mean and variance] is affected by the elevation of the snowcourse.) This spatial coherence is particularly evident in the WH, and especially

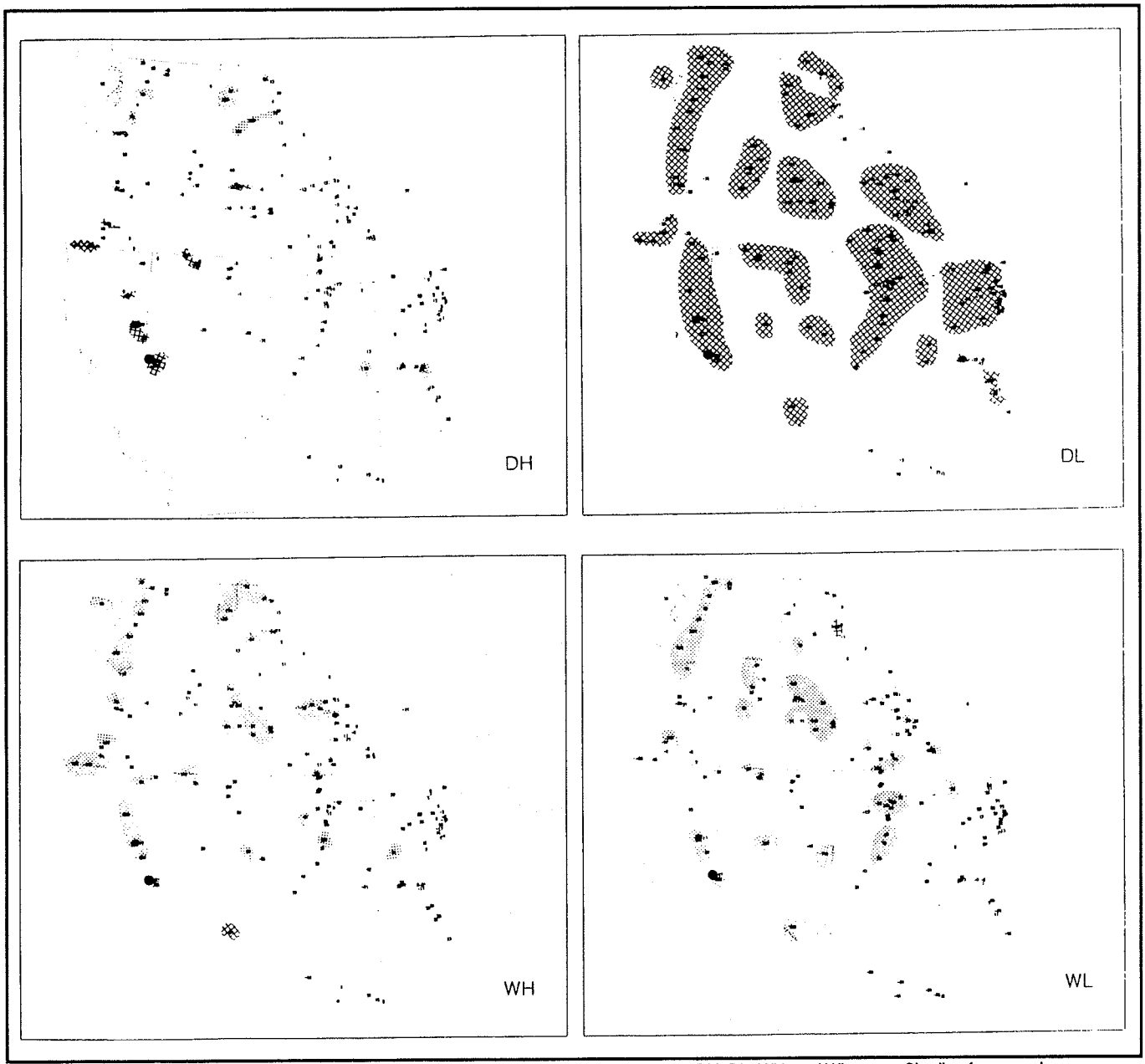

Figure 6. Composite February 1 snowcourse water content anomalies (mm) for Carson Pass DH, DL, WH, and WL cases. Shading for anomaly magnitudes equal or greater than 50 mm. Positive/negative anomalies denoted by stippling/hatching.

the DL patterns where the positive and negative WC anomalies cover virtually the entire western states. On the other hand, the DH pattern exhibited a tendency for a teleconnection — negative WC anomalies in the Sierra, parts of Nevada, and southern Oregon are accompanied by positive WC anomalies through the northwest. The scale of these features is consistent with the large-scale anomalies exhibited by atmospheric circulation (Figure 3) and by the associated regional-scale anomaly patterns in temperature and precipitation (Figures 4 and 5). The major WC anomalies in Figure 6 exceed 50 mm and often exceed 100 mm; tests of statistical significance using a two-tailed *t*-test (not shown) indicate many of these composite anomalies are significantly different from zero at the 95% confidence level.

Table 1
Autocorrelation of Snowcourse Water Content at Upper Carson Pass

	Jan	Feb	Mar	Apr	May
Jan	(19) 1.00	(19) 0.89	(19) 0.64	(19) 0.68	(19) 0.69
Feb		(59) 1.00	(59) 0.83	(59) 0.70	(59) 0.68
Mar			(59) 1.00	(59) 0.87	(59) 0.76
Apr				(59) 1.00	(59) 0.90

Numbers in parentheses are number of pairs of data entering correlation.

The overall persistence of WC at Carson Pass is indicated by the lagged correlations linking the January-May records in Table 1. One-month lag correlations are high, exceeding 0.8. Even at 4 months, the lag correlation from January to May is still 0.68.* The strongest persistence of regional scale WC anomalies is exhibited by the WH, and especially the DL cases, as indicated by the April 1 composites in Figure 7. Recall that the April 1 composites were based on winter PPT and February 1 WC; that is, they are a view of the WC behavior shown in Figure 6 as it progressed into spring two months later. The DL case, which is warm and dry over most of the West, has serious implications as it persists strongly into spring with a water supply deficit, as shown by the negative WC anomalies.

Conclusions

Several decades of seasonal snowcourse measurements in the western United States exhibit realistic climate variability. The snowcourse WC fluctuations are well related to interannual variations in atmospheric circulation, surface temperature, and precipitation. Variations of WC are not locally confined, but exhibit substantial coherence with snowcourses

* Note that although there are relatively few data pairs (19) entering the January-May correlation, the February-May correlation is nearly the same and consists of many more data pairs (59).

elsewhere in the West, in accord with the regional-scale (or larger) variability of the atmospheric circulation, temperature, and precipitation. While this study focused on only one such snowcourse, Carson Pass in the California Sierra Nevada, these conclusions are anchored by similar behavior of WC at other selected snowcourses from other western states.

Concerning the water supply, there is significant persistence of WC from February 1 to April 1. This emphasizes the importance of winter climate variability in determining the water supply.

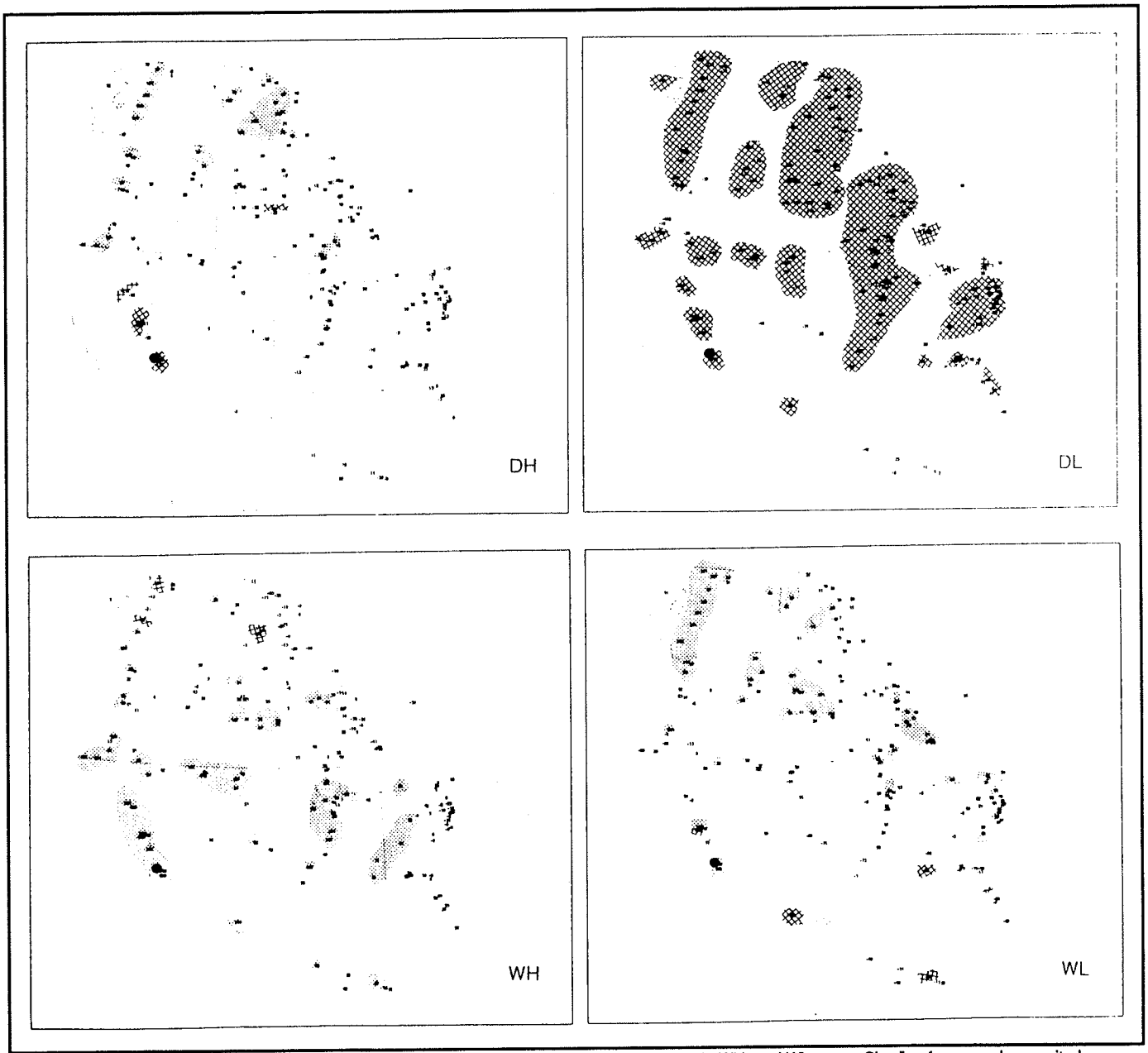

Figure 7. Composite April 1 snowcourse water content anomalies (mm) for Carson Pass DH, DL, WH, and WL cases. Shading for anomaly magnitudes equal or greater than 50 mm. Positive/negative anomalies denoted by stippling/hatching.

Acknowledgments

DRC and LGR acknowledge support by the University of California, Water Resources Center, Project UCAL-WRC-W-768, and by the NOAA Experimental Climate Forecast Center. Funding for DRC was also provided by the U.S. Geological Survey via an Intergovernmental Personnel Act agreement with the University of California.

Real-Time Climate Monitoring Using an AVHRR-Based Vegetation Index

Chet F. Ropelewski and Michael S. Halpert

Abstract: A normalized difference vegetation index (NDVI) has been produced and archived on a 1° latitude by 1° longitude grid between 55°S and 75°N. The many sources of data errors in the NDVI include cloud contamination, scan angle biases, changes in solar zenith angle, and sensor degradation. Week-to-week variability, primarily caused by cloud contamination and scan angle biases, can be minimized by temporally filtering the data. Orbital drift and sensor degradation introduces interannual variability into the dataset. These trends make the usefulness of a long-term climatology uncertain and limit the usefulness of the NDVI. Elimination of these problems should produce an index that can be used for climate monitoring.

Parts of this paper have been published in the proceedings of the Fifteenth Annual Climate Diagnostics Workshop and the proceedings for the OPSAT'90 conference.

Introduction

A normalized difference vegetation index (NDVI), based on weekly digital data provided by the Advanced Very High Resolution Radiometer (AVHRR) on the NOAA operational polar orbiting satellites, has been produced from 1985 through 1990. The digital data are Global Area Coverage at a resolution of 4 km, which is then sampled to 16 km. These data are combined into a 1° latitude by 1° longitude grid. The dataset produced at the Climate Analysis Center consists of the mean, median, standard deviation, number of observations, and a 7-class histogram for each 1° by 1° grid square. Data are archived between 55°S and 75°N.

Computational Problems

The NDVI is the ratio of the difference to the sum of the values from the near infrared channel and the visible channel. Although this calculation is simple, several problems are associated with it. Since the calibration coefficients are determined from linear regressions, low solar zenith angles or illumination can cause channel radiances to appear negative. Therefore, the individual channel data were examined and negative values were removed. Pixels with negative vegetation index values were also eliminated, because a negative NDVI indicates greater reflectance in the visible than in the near IR (which is not what is expected from surface vegetation).

The NDVI has other sources of data contamination. Data errors are known to be caused by cloud contamination, scan angle biases, changes in solar zenith angle, and sensor degradation. Cloud contamination and

In K.T. Redmond, Editor, 1992. Proceedings of the Eighth Annual Pacific Climate (PACLIM) Workshop, March 10-13, 1991: California Department of Water Resources, Interagency Ecological Studies Program Technical Report 31.

noise due to changes in viewing geometry introduce week-to-week variability into the dataset, and sensor degradation and changes in illumination due to orbital drift result in interannual variability. For the vegetation index to have utility for climate monitoring, these problems must be minimized.

Short-Term Variability

Week-to-week scatter of the NDVI is primarily due to cloud contamination, even though the digital data are cloud screened by retaining the largest NDVI value for a given week. The AVHRR infrared window channel is used to further screen for clouds by eliminating pixels whose temperature values are less than a specified value. The current procedure uses a temperature of 10°C during the warm season and a value of -5°C during the cold season. Data inconsistencies also arise from the viewing geometry associated with different scan angles. The AVHRR has scan angles ranging from 55.4° to -55.4° relative to nadir. The NDVI calculated from the back-scatter direction is often lower than values obtained from either nadir or the forward direction. This can be seen in Figure 1, which shows the distribution of vegetation index values stratified by scan angle for an area in the midwestern United States during two adjacent weeks in the summer of 1988. The majority of pixels during early July (Figure 1a) have scan angles from the large back-scatter direction. During the following week (Figure 1b) only four pixels were obtained from these angles, although these four pixels did have low NDVI values. This shift in distribution of pixels results in large week-to-week variability, which in this case is manifested as the spike in the time series shown in Figure 2a.

Due to scan angle biases and cloud contamination, temporal filtering is used to smooth the data. Figure 2a presents an unfiltered time series for 1988 over a 5° latitude by 5° longitude area of the midwestern United States; the data in Figure 2b are filtered with a 3-week median filter. Both are compared to the 4-year mean NDVI. The unfiltered time series shows the large week-to-week variations; the median filtered time series is much smoother and is consistent with the drought during summer 1988.

Interannual Variability

In addition to the week-to-week variations due to cloud contamination and scan angle biases, trends exist in the dataset. These trends are introduced as a result of orbital drift and sensor degradation. Higher vegetation indices occur with larger solar zenith angles relative to nadir over desert areas. Figure 3 shows a weekly time series of the NDVI over a 10° latitude by 10° longitude area of the Sahara Desert. The apparent annual cycle in vegetation over this region is a result of changing solar zenith angles throughout the year, with lower NDVI values occurring with lower angles. Due to orbital drift, the equator crossing time becomes later throughout the life of the satellite. As this occurs, the solar zenith angle

for any given week becomes greater, as does the NDVI for each year. The trend is especially obvious during the winter months, where each peak is higher than the maximum value reached during the previous year. There is an abrupt decrease in NDVI toward the end of 1988 that is associated with the change of satellite from NOAA 9 to NOAA 11. The equator crossing time of NOAA 11 was much earlier than NOAA 9, which resulted in much smaller solar zenith angles. Research is underway to determine if the effects of changing sun angle are as pronounced over vegetated surfaces as over deserts.

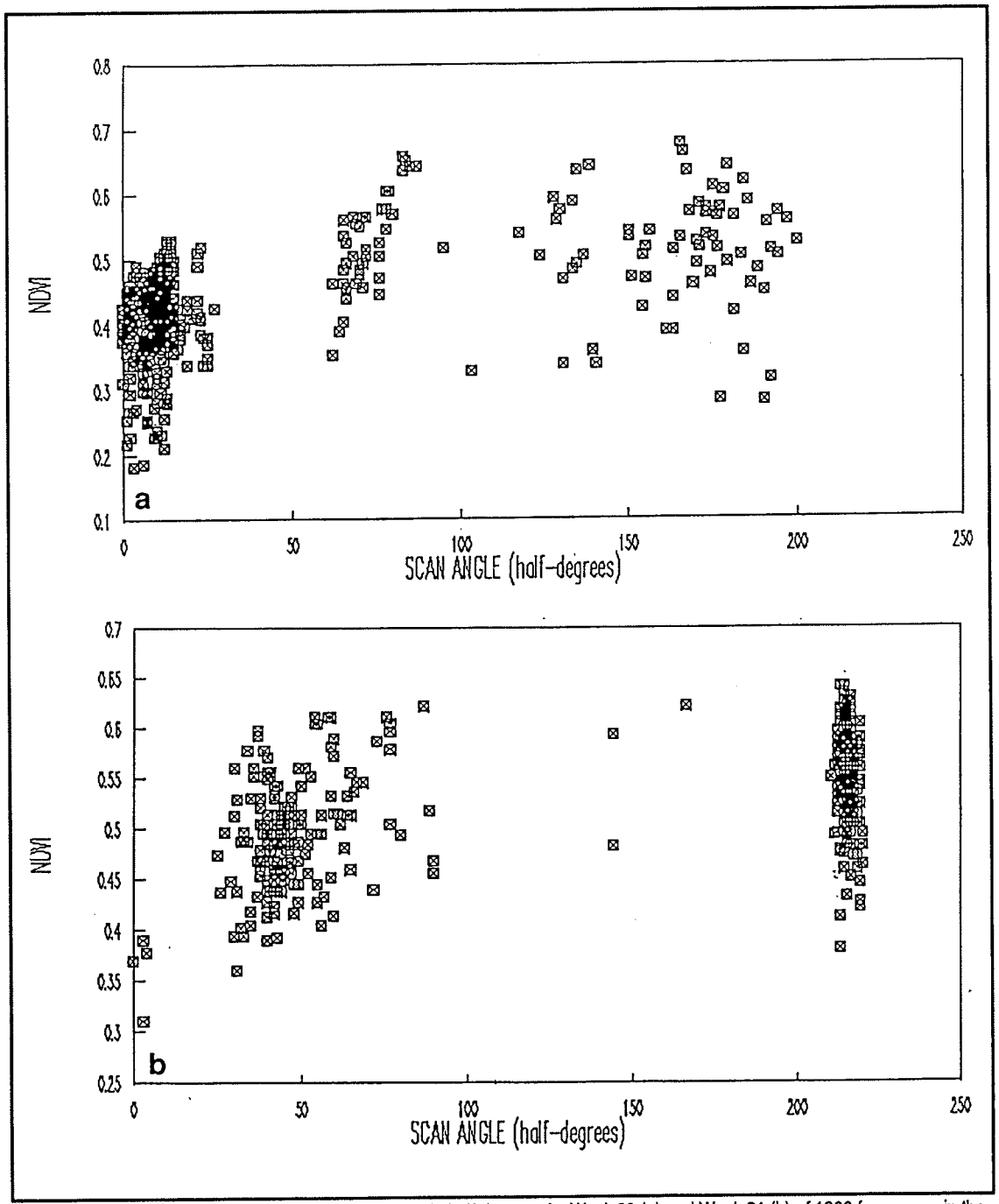

Figure 1. Scatter plots of the NDVI versus scan angle in half degrees for Week 30 (a) and Week 31 (b) of 1988 for an area in the midwestern United States. Scan angles between 0 and 110 represent the back-scatter direction; angles between 110 and 220 are from the forward-scatter direction.

Another indication of the increasing NDVI values over desert areas and the relationship to solar zenith angle is the decrease in total land surface that has NDVI values less than 0.1 (Figure 4). Land area with low NDVI values ranges from more than 50% during the Northern Hemisphere winter to less than 25% during the summer. The summer percentages are derived mainly from indices over the deserts, although low sun illumination in southern South America probably accounts for some of the total land area. During the summer months, the amount decreases from about

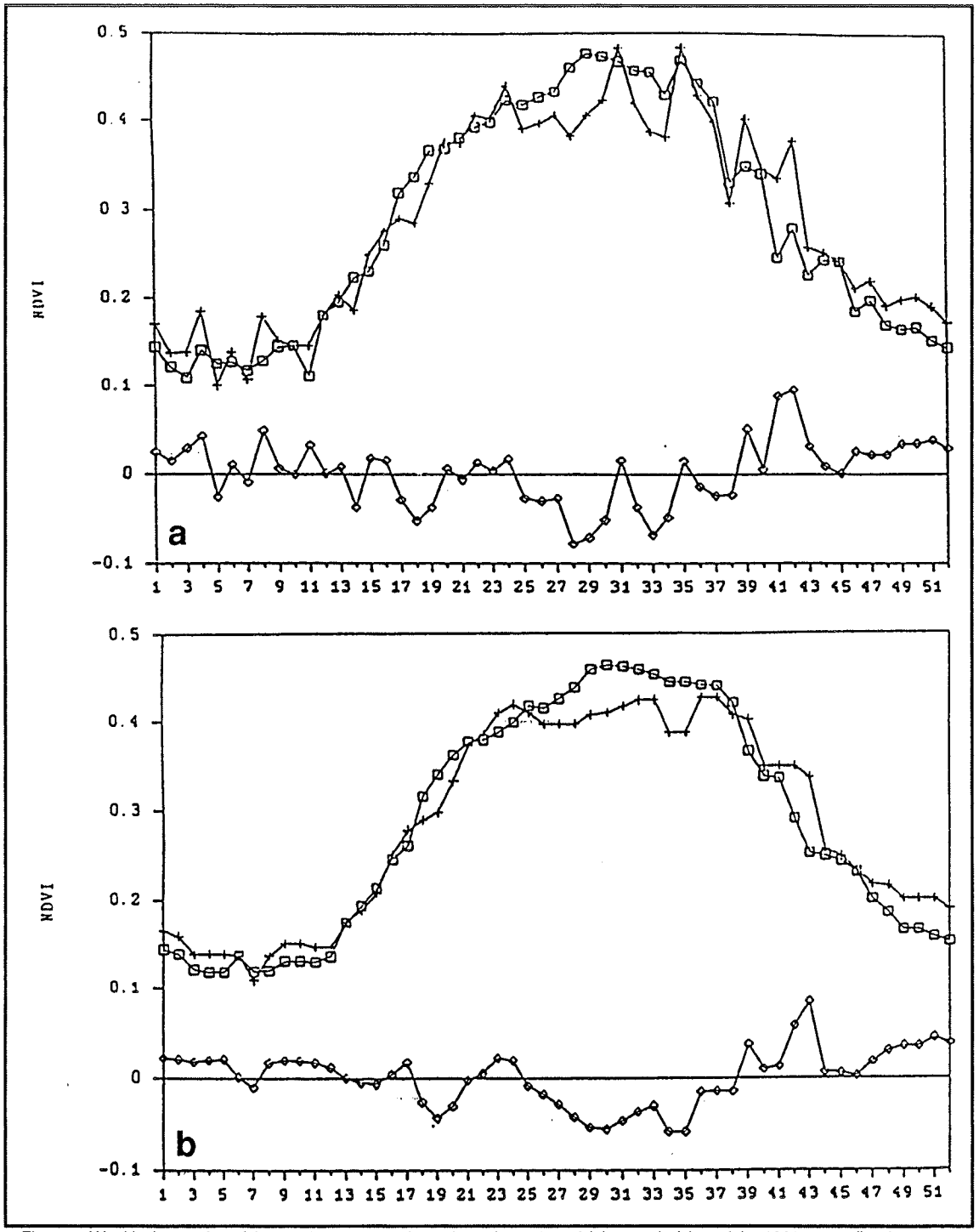

Figure 2. Weekly time series of the 1985-1988 mean (open boxes), 1988 total (plus symbols), and the 1988 anomalies (open diamonds) of the NDVI unfiltered (a) and 3-week median filtered (b). Data are averaged over an area from 38°N-43°N and from 90°W-95°W.

25% in 1985 to less than 20% by 1988. The 1988 curve continues to indicate less land with NDVI values below 0.1 (compared to previous years) until November, when the percentage jumps to about the same percentage found during 1985. This jump is coincident with the change in satellites, which greatly changed the viewing time and, hence, the solar zenith angle.

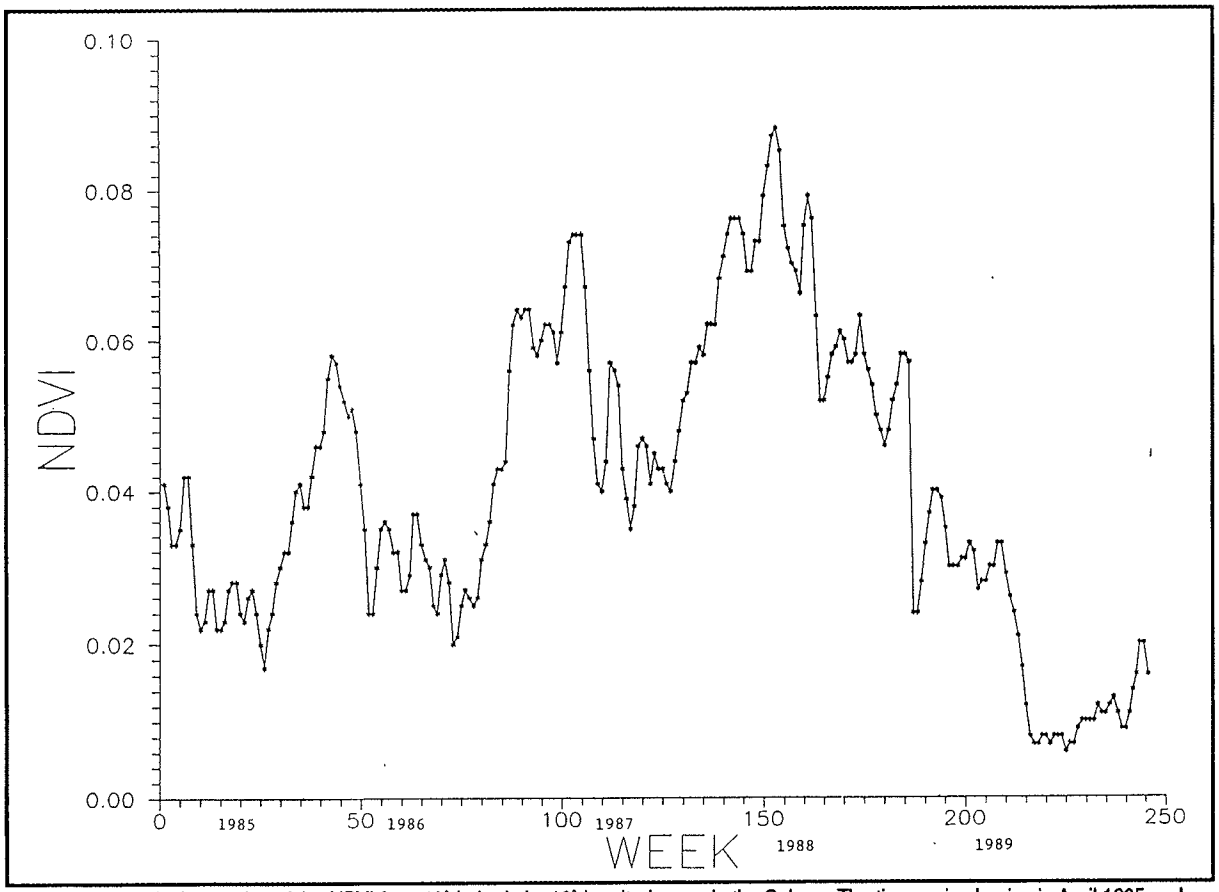

Figure 3. Weekly time series of the NDVI for a 10° latitude by 10° longitude area in the Sahara. The time series begins in April 1985 and runs through December 1989.

Conclusion

Biases introduced into the NDVI as a result of orbital drift and sensor degradation make the usefulness of a long-term climatology uncertain. For this reason, we have not computed anomalies from a prescribed base period for climate monitoring but, instead, make year-to-year comparisons of the vegetation index. Comparisons of July 1987 with the severe drought of July 1988 for the United States indicate mean NDVI values during 1988 were 20 to 30% smaller than in 1987 throughout the Midwest.

NDVI values for September 1990 and 1989 were also compared over the African Sahel. Vegetation index values were greater during 1989, indicating better growing conditions, which is in agreement with precipitation data for this area. However, NDVI values over the Sahel were greater during 1987 than during 1989 even though precipitation amounts indi-

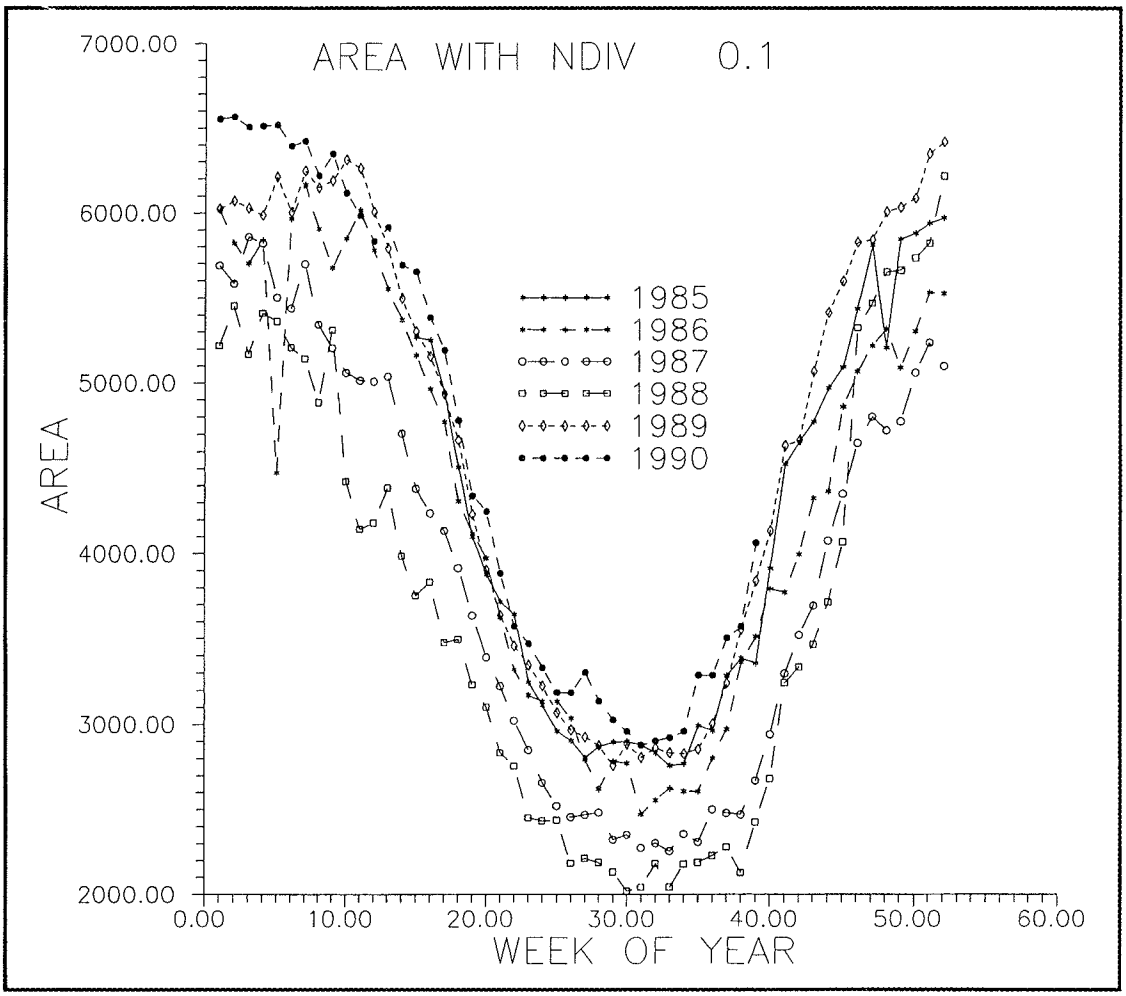

Figure 4. Weekly time series of the percent total land area with NDVI less than 0.1 for 1985-1990.

cate the reverse should have been true. This discrepancy arises from the change in satellite during 1988 and limits the flexibility and usefulness of these yearly comparisons because any year-to-year comparisons must be made between neighboring years, and the data must come from the same satellite.

A weekly vegetation index dataset from 1985 through the present has been produced on a 1° latitude by 1° longitude grid. Despite continuing uncertainties with cloud contamination and scan angle differences, large-scale climate parameters have been identified. The index is not yet stable enough to produce a climatology because of interannual variability associated with sensor degradation and orbital drift. Elimination of these problems should produce an index that can be used for global climate monitoring as well as the diagnostic study of climate variations.

Effects of Observation Time on Interpretation of Climatic Time Series — A Need for Consistency

Kelly T. Redmond

Introduction

Much of what we know about the climate of the United States is derived from data gathered under the auspices of the cooperative climate network. Particular aspects of the way observations are taken can have significant influences on the values of climate statistics derived from the data. These influences are briefly reviewed. The purpose of this paper is to examine their effects on climatic time series. Two other items discussed are: (1) a comparison of true (24-hour) means with means derived from maximums and minimums only, and (2) preliminary work on the times of day at which maximums and minimums are set.

Observing Practices and Conventions

Temperature observations are currently made at about 5200 sites in the cooperative network. The federal government supplies the instruments, calibration, paper forms, and other logistical support; the observer supplies the labor. Because the network has been mostly voluntary throughout its history, the observers choose to observe at a time acceptable to their daily schedule and agreeable to the network managers. Typically these times are morning (7-9 am), evening (4-7 pm), or near midnight. The archive system assumes thereafter that the observer is continuing to reset the instruments at this time. The observer records the maximum and minimum temperature for the 24 hours ending at the observation time (the "observation day"), along with the temperature at observation time. By long-established convention, the observation is ascribed for archive purposes to the day on which the thermometers were reset. Although it is commonly (and erroneously) expected that maximums and minimums are set at their "usual" times of afternoon and early morning, without additional corroborating information there is no way of knowing whether this is true of any particular observation.

The maximum and minimum temperature for an observation day can occur at any time during the 24-hour period. The relationship between the weather of one day and the next leads to two common circumstances. For afternoon readers, the 24-hour maximum was often set the previous afternoon, and for morning readers, the 24-hour minimum was often set the previous morning. A warm day followed by a cool day (for a late

In K.T. Redmond, Editor, 1992. Proceedings of the Eighth Annual Pacific Climate (PACLIM) Workshop, March 10-13, 1991: California Department of Water Resources, Interagency Ecological Studies Program Technical Report 31.

afternoon observer), or a cool morning followed by a warm morning (for a morning reader), leads to a "carryover" of the previous day's extreme temperature. However, in neither case can an opposite sequence of days produce a compensating bias of the opposite sense; cool afternoons cannot carry over into warm afternoons and warm mornings cannot carry over into cool mornings.

The daily mean temperature is taken as the arithmetic mean of the maximum and the minimum. (The validity of this assumption is discussed below.) Carryover effects systematically increase the reported maximum temperature (for afternoon observers) and decrease the minimum temperature (for morning observers). The net effect is that, for exactly the same temperature history, an afternoon observer will report a warmer climate than will a morning observer. The difference with respect to a midnight-to-midnight observer is known as "time-of-observation bias". The existence of such a bias has been known for over three decades (Mitchell 1958) and has been examined by subsequent authors (Baker 1975; Schaal and Dale 1977). Karl *et al* (1986) undertook an extensive analysis of the problem to develop correction factors for the production of homogeneous time series for climate change studies.

Effect of Time-of-Observation Bias on Time series

The principal purpose of this study was to answer the following question: If extreme thermometers are always reset at the same time, are the resulting time series suitable for climate change studies?

Hourly temperature data were obtained from the National Climatic Data Center for Great Falls (1948-1989), Salt Lake City (1948-1989), and Reno (1949-1989). Data have been digitized in hourly increments, except 1965-1976 at Great Falls and 1965-1981 (July) at Reno. Observation day maximums and minimums were found, using the conventions described above, and used to compute time series of monthly mean maximum, monthly mean minimum, and monthly mean temperatures. Extremes were determined from the highest and lowest of the 25 hourly values for each observation day and are, thus, not true extremes for the observation period. This was repeated for observation times at each of the 24 hours. Time series based on the arithmetic mean of the 25 observations for each calendar day were also formed ("24-hour mean"). Means based on the true calendar day extremes (instead of just 25 hourly values) were available for Great Falls and Reno. All times in this study are Local Standard Time. Values are in their original units (degrees F). Comparisons discussed in the tables below used only those days with no missing hourly values.

Table 1 shows a comparison between means calculated from maximum/minimum temperatures for observation days other than midnight-to-midnight and means calculated from midnight-to-midnight maximum/minimum. As earlier studies have shown, stations that record

Table 1

Mean Temperature Derived from Hourly Extremes for each Observation Day Ending at Indicated Time Minus Mean Temperature Derived from Midnight-to-Midnight Hourly Extremes

Value of lowest correlation with the midnight-to-midnight series is shown below, with associated observation time(s). "Range" is the greatest difference in bias.

Units: Degrees F.

Hour (LST)	Annual			January			July		
	GTF	SLC	RNO	GTF	SLC	RNO	GTF	SLC	RNO
00	0.00	0.00	0.00	0.00	0.00	0.00	0.00	0.00	0.00
01	-0.12	-0.11	-0.12	-0.11	-0.07	-0.11	-0.10	-0.10	-0.09
02	-0.25	-0.22	-0.27	-0.29	-0.12	-0.24	-0.25	-0.23	-0.25
03	-0.38	-0.33	-0.42	-0.34	-0.19	-0.38	-0.43	-0.39	-0.40
04	-0.50	-0.44	-0.58	-0.43	-0.23	-0.49	-0.61	-0.55	-0.60
05	-0.57	-0.52	-0.71	-0.48	-0.28	-0.62	-0.69	-0.68	-0.70
06	-0.48	-0.45	-0.52	-0.52	-0.29	-0.69	-0.23	-0.37	-0.02
07	-0.28	-0.15	-0.22	-0.54	-0.29	-0.71	0.16	0.27	0.18
08	-0.05	0.10	0.08	-0.50	-0.25	-0.42	0.26	0.37	0.20
09	0.22	0.28	0.29	-0.19	0.03	0.17	0.31	0.38	0.20
10	0.53	0.40	0.39	0.33	0.36	0.52	0.37	0.40	0.20
11	0.84	0.55	0.51	0.80	0.60	0.82	0.50	0.45	0.22
12	1.20	0.78	0.69	1.28	0.83	1.04	0.74	0.59	0.30
13	1.50	1.01	0.94	1.54	1.01	1.27	1.01	0.76	0.46
14	1.71	1.22	1.16	1.67	1.17	1.49	1.29	0.99	0.68
15	1.78	1.30	1.22	1.69	1.22	1.57	1.46	1.15	0.76
16	1.65	1.22	1.04	1.42	1.05	1.36	1.48	1.14	0.64
17	1.40	1.01	0.71	1.11	0.80	0.96	1.38	1.00	0.43
18	1.03	0.74	0.52	0.73	0.59	0.81	1.06	0.77	0.32
19	0.73	0.53	0.41	0.54	0.47	0.68	0.80	0.55	0.29
20	0.50	0.38	0.34	0.38	0.37	0.57	0.58	0.40	0.28
21	0.35	0.29	0.27	0.27	0.29	0.47	0.47	0.34	0.28
22	0.22	0.19	0.20	0.17	0.21	0.33	0.39	0.31	0.27
23	0.12	0.10	0.11	0.11	0.15	0.20	0.32	0.24	0.23
Lowest Correlation	0.997	0.996	0.996	0.997	0.996	0.996	0.998	0.984	0.993
Hour(s)	7-14	13 16-17	13-14	9-11	15-16	12-13	16	16	6
Range	2.35	1.82	1.93	2.23	1.51	2.28	2.17	1.83	1.46

temperatures in the morning are cooler than stations that record at midnight, and stations that record in the afternoon are warmer. The morning bias remains negative until about local sunrise time. It is interesting that changes in observation time of just one hour can change mean temperatures by 0.3 to 0.5 degree F, and 2-hour changes can raise or lower mean temperature by as much as a degree. For the few cases shown in Table 1, the range of temperatures possible is over 2 degrees, comparable to annual climate changes that might be expected from global warming.

Shown at the bottom of Table 1 is the lowest correlation of the time series of values based on 0000 LST hourly maximum/minimum temperature with time series based on all other reset times, along with the hours having the lowest correlations. "Range" is the difference in temperature between the hours giving the coolest and warmest means.

Time series of annual mean temperature and of July and January temperature, for different observation times, are highly correlated with

those from midnight-to-midnight stations. The lowest correlations from among this set are all higher than r=0.98, and most are higher than r=0.99. The lowest correlations with midnight-to-midnight stations are for those stations with observation times in the afternoon. Correlations have been calculated between time series derived from all possible combinations of observation times. Table 2 shows the lowest values found. The lowest correlations are generally between time series from observation times near sunrise with those from observation times in mid-afternoon. Lowest correlations are only slightly lower than those shown in Table 1.

Table 2
Lowest Correlations Among Any Observation Time Combinations
Time series are based on highest and lowest hourly temperatures.

	GTF	SLC	RNO
January	0.997	0.996	0.994
April	0.993	0.989	0.990
July	0.987	0.979	0.991
October	0.983	0.988	0.993
Annual	0.996	0.992	0.993

Examples of time series are shown in Figures 1 through 5. The close similarity in temporal fluctuations is quite apparent, as might be expected from the extremely high correlations. Slight departures from the long-term relationships can be seen in some years. Karl *et al* (1986) present graphs illustrating that time-of-observation bias varies from year to year.

A station that changes its time of observation during its history is, in essence, moving from one line to another in this family of curves. If the history of observation times is not known, some portion of the "observed" year-to-year temperature variability, and a larger portion of decadal- or longer-scale variability, may be merely an artifact of the observational circumstances.

The main point to be derived from this analysis, however, is that temporal variations in climate behavior can be quite well represented, as long as the observer resets the instruments at a consistent observing time. Even an observation time considered unsuitable for many applications, such as mid-afternoon, will yield a very good record for climate change studies.

Max/Min versus True 24-Hour Means

Table 3 shows the difference between daily means based on maximum/minimum temperatures and daily means based on all 24 (actually 25) hourly values. The approximation that uses the sum of the maximums and minimums divided by two leads to a slight underestimate of the true 24-hour mean. Figure 5 shows two time series for Great Falls computed each way. The two curves lie very close to each other.

Table 3

Mean of 24-Hourly Values Minus Mean Based on Hourly Maximum/Minimum Temperatures

"Hour" is the hour at which the observer resets the thermometer.

"True" refers to means based on true maximums and minimums determined for a calendar day from extreme thermometers.

Hour	GTF	SLC	RNO	Hour	GTF	SLC	RNO
00 (True)	-0.09°F	NA	0.01				
00	-0.06	-0.32	-0.19	15	-1.84	-1.62	-1.41
01	0.06	-0.21	-0.07	16	-1.71	-1.54	-1.23
02	0.19	-0.10	0.08	17	-1.46	-1.33	-0.90
03	0.32	0.01	0.23	18	-1.09	-1.07	-0.71
04	0.44	0.12	0.39	19	-0.79	-0.85	-0.60
05	0.51	0.20	0.52	20	-0.56	-0.71	-0.53
06	0.42	0.13	0.33	21	-0.41	-0.61	-0.46
07	0.22	-0.17	0.03	22	-0.28	-0.52	-0.40
08	-0.01	-0.42	-0.27	23	-0.18	-0.43	-0.30
09	-0.28	-0.60	-0.48				
10	-0.59	-0.73	-0.58	True at	0030	0254	0128
11	-0.90	-0.88	-0.70		0758	0626	0706
12	-1.26	-1.10	-0.88				
13	-1.56	-1.34	-1.13	Years	1948-89	1948-89	1949-89
14	-1.77	-1.54	-1.35	(Not Used)	(1965-76)	—	(1965-81)

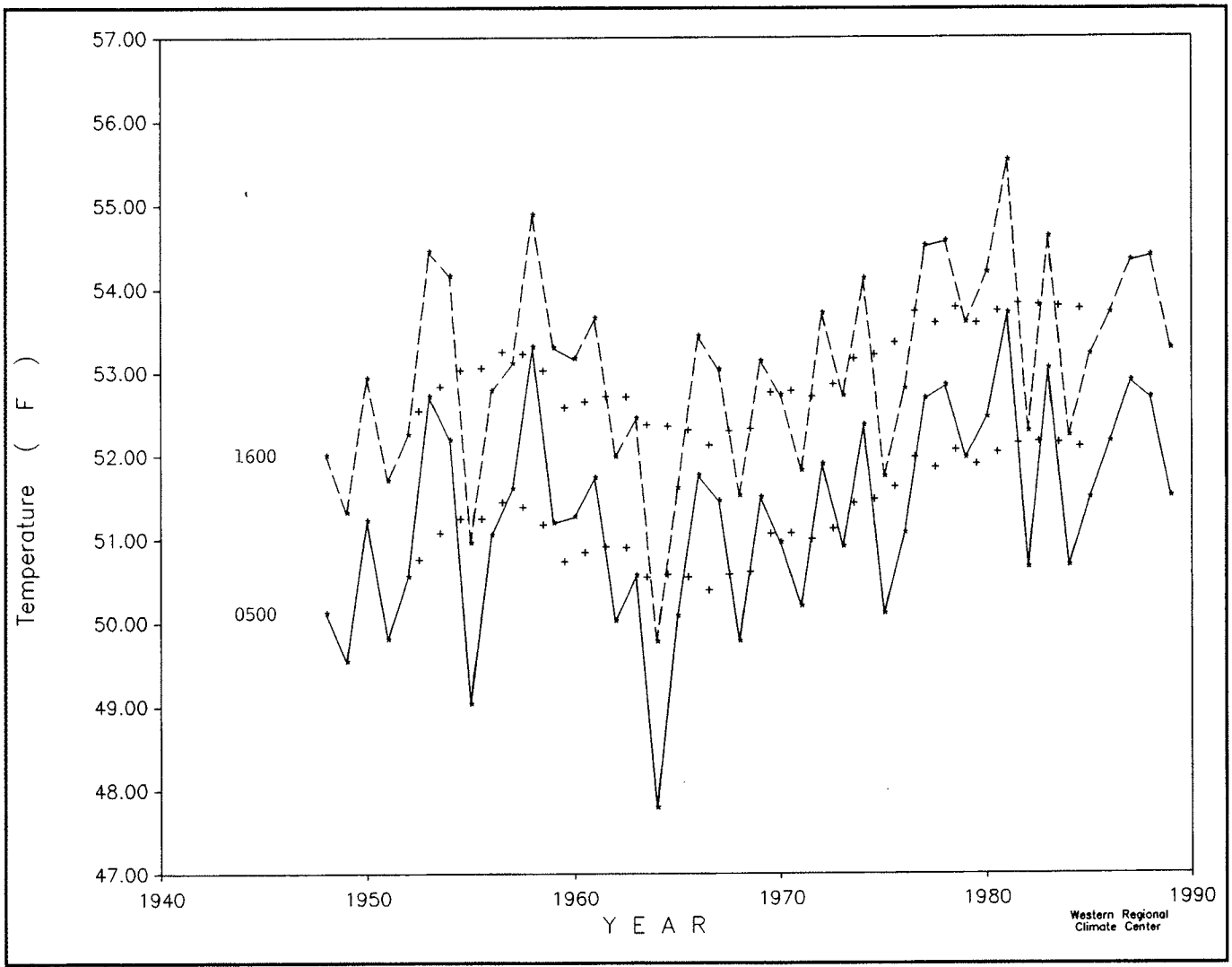

Figure 1. Mean annual temperature at Salt Lake City for observation times at 5 am (solid) and 4 pm (dashed) LST. Crosses are 10-year running means plotted at mid-point.

Time of Maximum/Minimum Temperature

Preliminary studies were undertaken of the times at which maximums and minimums are set. It is commonly expected that maximums will be set in the afternoon and minimums will be set just before sunrise. The greater the extent to which the solar radiation supply governs local temperatures (a "solar" climate), the more this expectation proves to be true. Also, the more one day is like succeeding days, the more this expectation will be true. Of the three sample sites, Reno has the most "solar" climate and Great Falls has the most "advective" climate. For each site, summer climates are more "solar" than winter climates.

This discussion refers to midnight-to-midnight observers only. At all three sites, summer maximums are very likely (about 95 percent of the days) to be set from 1 to 6 pm LST (Table 4). Minimum temperatures are less likely to be set within a span of the same duration. At other times of year, extremes are more likely to be set during other portions of the day. Maximums are more apt to have been set at midnight yesterday than at

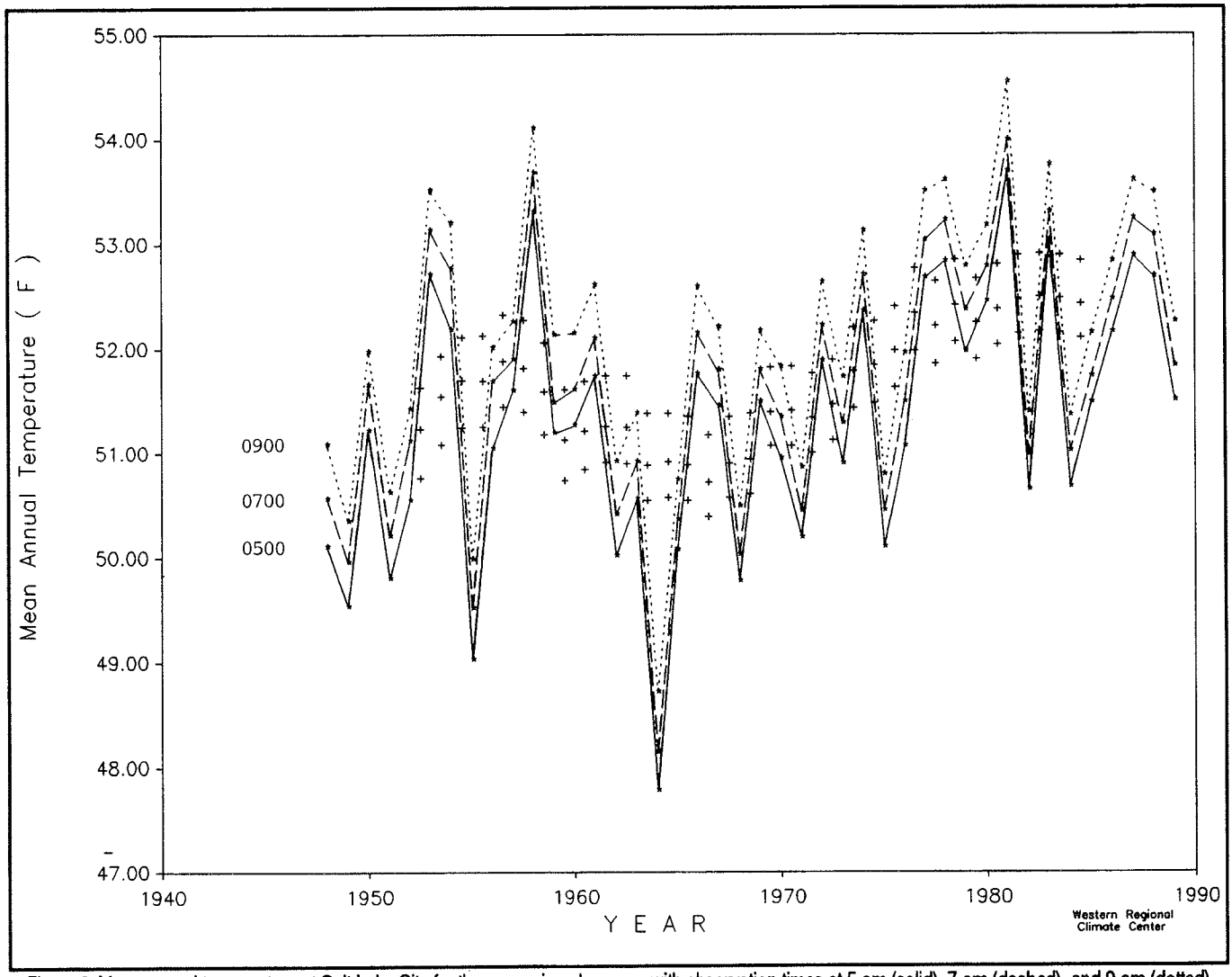

Figure 2. Mean annual temperature at Salt Lake City for three morning observers with observation times at 5 am (solid), 7 am (dashed), and 9 am (dotted) LST. Crosses denote 10-year running means plotted at mid-point.

midnight today. Minimums, on the other hand, are more apt to be set at observation time (midnight today) than at midnight yesterday.

At Great Falls, where winds and thus air mass changes frequently control the temperature, 10.1 percent of the January maximums and 18.9 percent of the January minimums are set at either the start or end of the day. In January, 16.8 percent of the maximums have been set by 8 am, and another 16 percent are not set until 8 pm or later. Nearly a quarter (24.4 percent) of the minimums are set between 7 and 11 pm.

The three examples shown are in continental interiors with dry climates, conducive to large diurnal temperature ranges. Other stations with smaller diurnal ranges, or closer to coastlines, will show greater departures from the pattern of afternoon maximum/morning minimum.

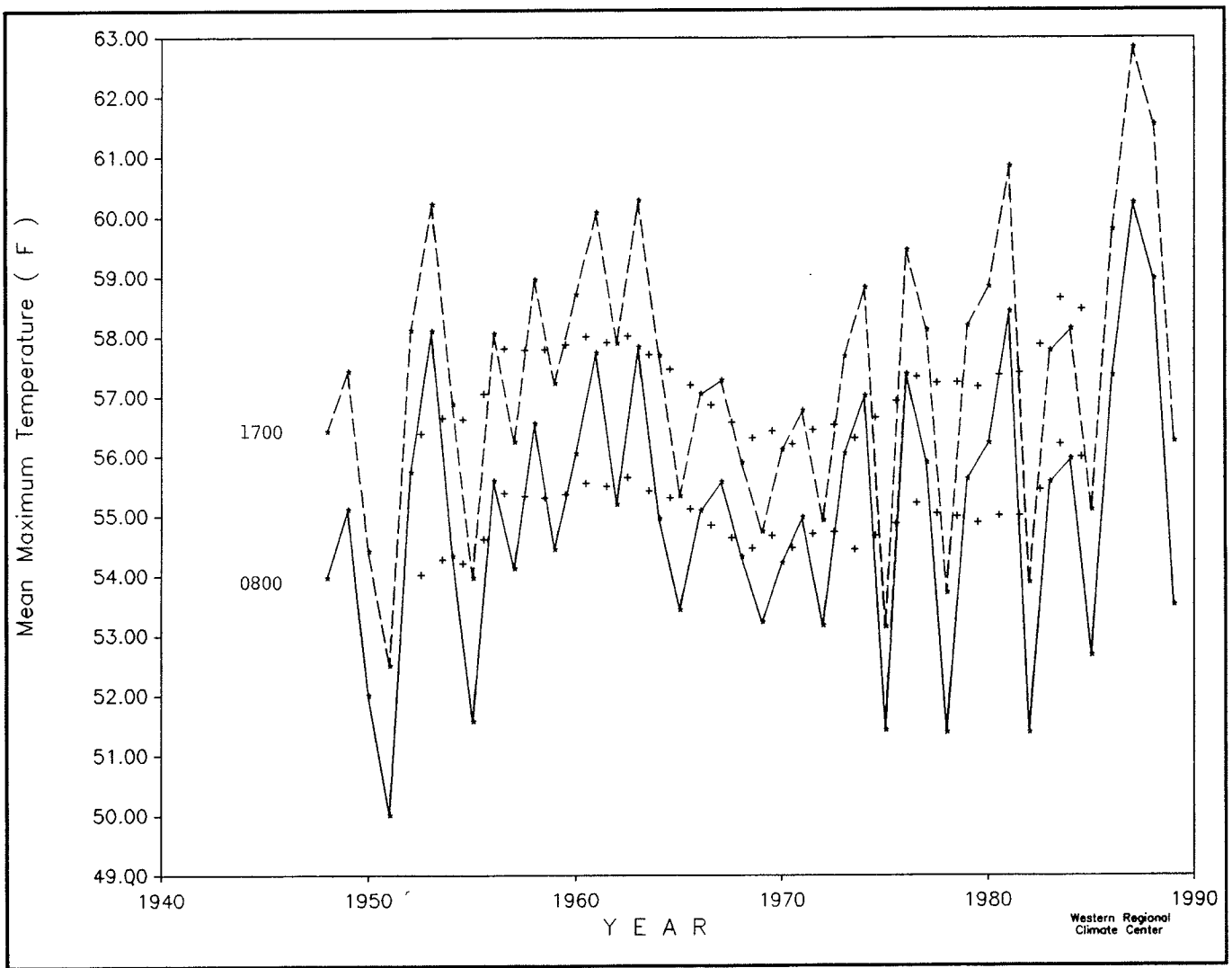

Figure 3. Mean annual maximum temperature at Great Falls for observation times of 8 am (solid) and 5 pm (dashed). Crosses are 10-year running means plotted at mid-point. Means from 1965 to 1976 are from eight values per day at every third hour.

Summary

Use of daily temperature extremes can give quite accurate approximations to the true mean temperature if enough cases are averaged together. Observer choice of a convenient observation time leads to a bias in computed mean temperature. This bias can be as much as a couple degrees Fahrenheit, or of the same magnitude as typical decadal-scale climate changes, or those expected from trace gas increases. However, as long as the observer resets the extreme thermometers at a consistent time of day, the climatic trends and fluctuations about the long-term mean will be preserved very well, no matter what observation time is used.

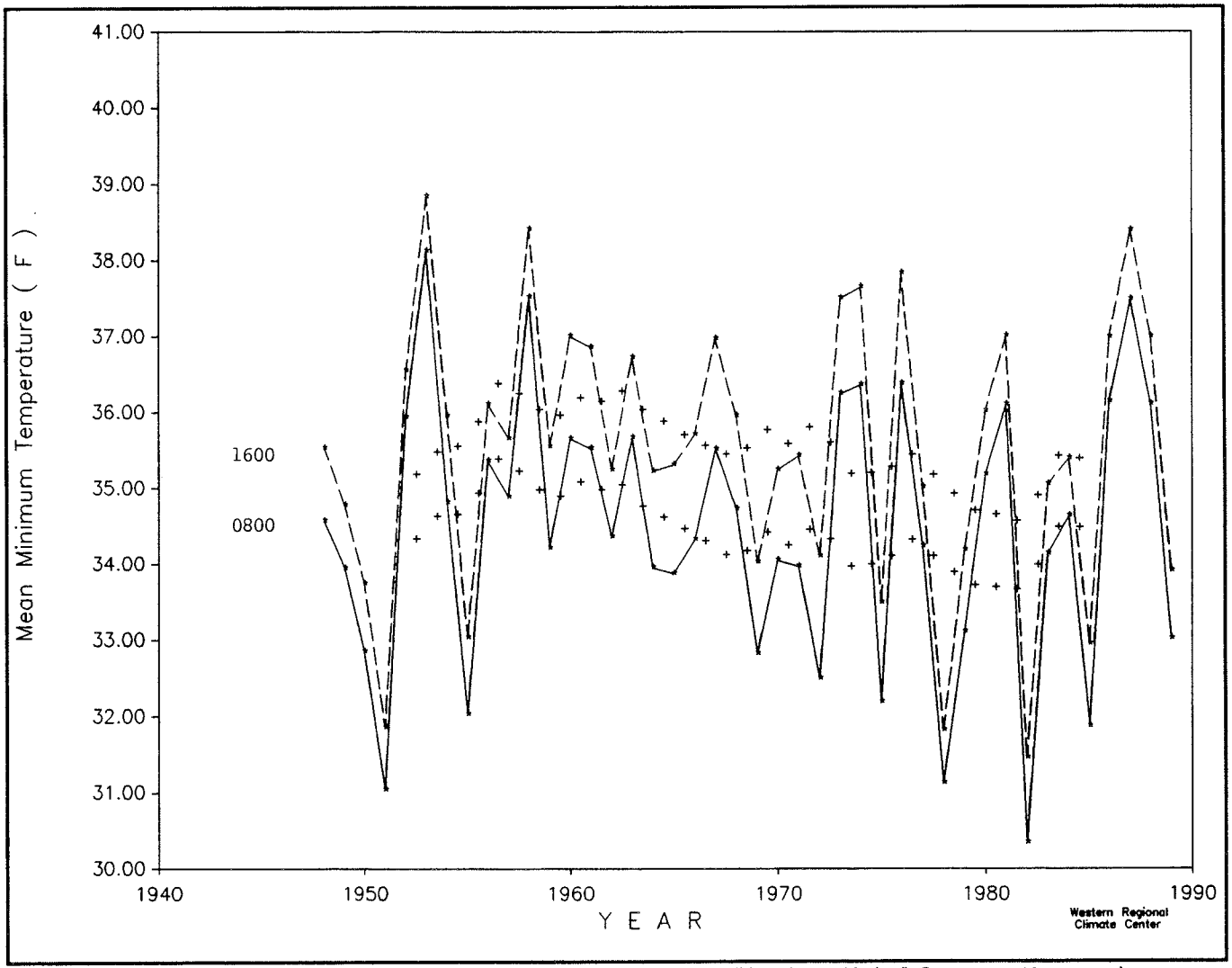

Figure 4. Mean annual minimum temperature at Great Falls for observation times of 8 am (solid) and 4 pm (dashed). Crosses are 10-year running means plotted at mid-point. Means from 1965 to 1976 are from eight values per day at every third hour.

References

Baker, DG, 1975. Effect of observation time on mean temperature estimation. *J. Appl. Meteor.* 14:471-476.

Karl, TR, CN Williams Jr, PJ Young, and WM Wendland, 1986. A model to estimate the time of observation bias associated with monthly mean maximum, minimum and mean temperatures for the United States. *J. Climate Appl. Meteor.* 25:145-160.

Mitchell, JM Jr, 1958. Effects of changing observation time on mean temperature. *Bull. Amer. Meteor. Soc.* 39:83-89.

Schaal, LA, and RF Dale, 1977. Time of observation temperature bias and "climatic change". *J. Appl. Meteor.* 16:215-222.

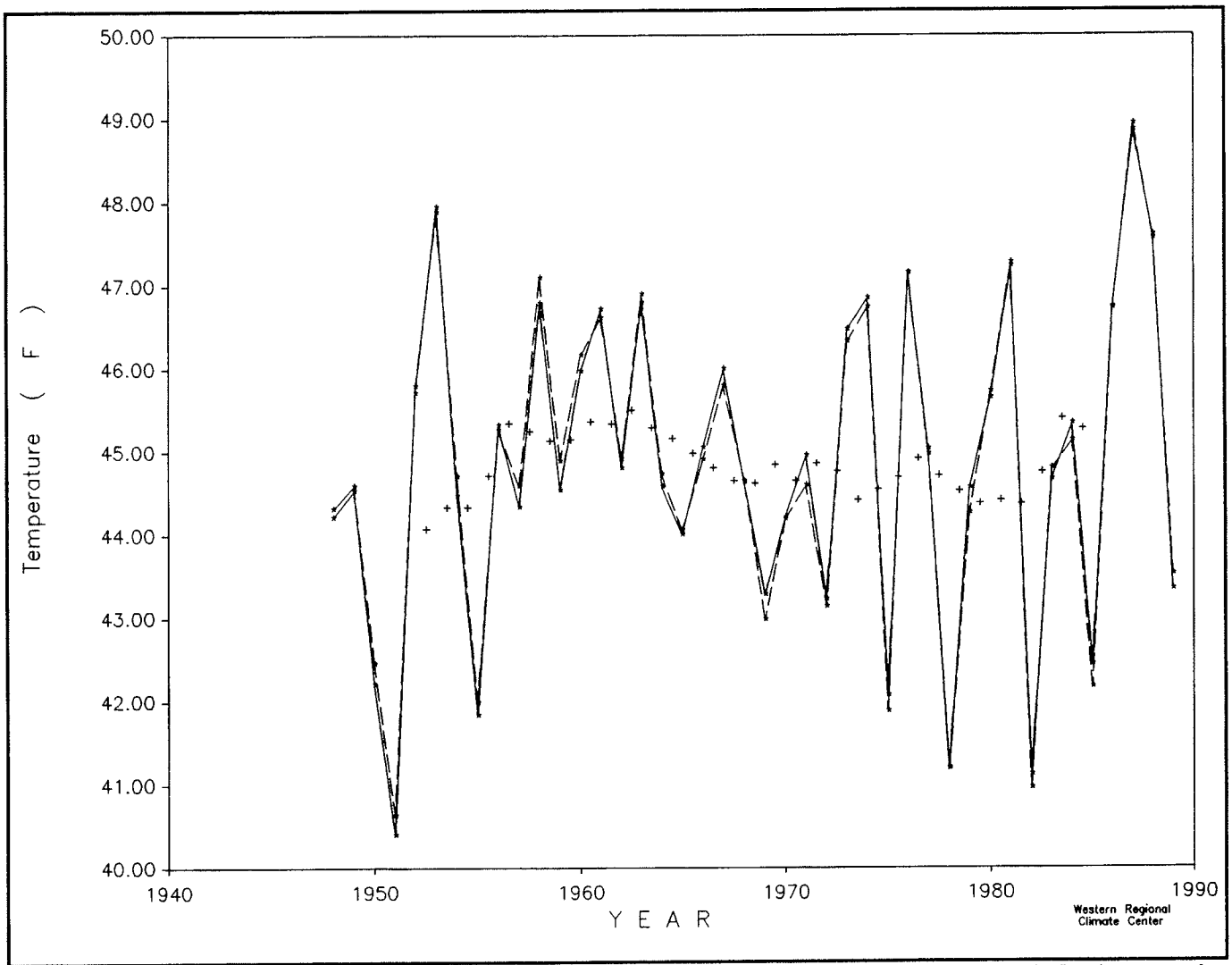

Figure 5. Mean annual temperature at Great Falls based on hourly maximum/minimum temperatures from midnight-to-midnight (dashed) and on means of 24 hourly values (solid). Crosses are 10-year running means of 24-hourly values plotted at mid-point. Means from 1965-1976 are from eight values per day at every third hour.

Table 4

Percentage of the Maximums and/or Minimums at Great Falls, Salt Lake City, and Reno that are Set at the Indicated Times or within the Indicated Hours, for Midnight-to-Midnight Observers

Mid-y is midnight yesterday (start of observation day). Mid-t is midnight today (end of observation day).

Values are in percent (possible range 0-100).

Example: For a midnight observer, 16.8 percent of the maximums at Great Falls in January are set between midnight last night and 8 am.

		GTF				SLC				RNO			
		Jan	Apr	Jul	Oct	Jan	Apr	Jul	Oct	Jan	Apr	Jul	Oct
Max set	Mid-y	5.6	2.7	0.7	3.2	2.8	2.4	0.2	1.2	1.6	0.6	0.1	1.0
Min set	Mid-y	7.3	2.7	1.0	4.7	6.9	3.4	1.7	2.4	3.2	0.8	0.1	0.6
Max set	Mid-t	4.5	0.1	0.0	0.5	2.3	0.0	0.0	0.1	0.4	0.0	0.0	0.0
Min set	Mid-t	11.6	10.2	7.0	11.8	10.9	12.4	10.3	13.8	8.2	7.8	3.2	6.6
Max set	Mid-y-0800	16.8	6.5	1.2	9.3	9.1	5.0	0.3	3.8	5.8	2.0	0.1	2.1
Max set	2000-Mid-t	16.0	0.9	0.1	2.0	8.2	0.2	0.0	0.6	2.2	0.0	0.0	0.4
Min set	1900-2300	24.4	12.7	6.2	18.5	16.9	9.8	5.3	10.0	12.9	9.8	1.6	6.6
Max set	1300-1800	58.2	85.1	94.5	80.0	74.9	86.8	95.4	89.5	84.1	89.1	95.7	91.1
Min set	0400-0900	36.2	53.7	68.4	44.0	45.0	55.4	66.5	55.2	62.4	72.0	87.4	79.3

Elements of the U.S. Carbon Budget: Progress and Preliminary Results

Hermann Gucinski, Charles Peterson, Jeff Kern,
David Turner, Derek Pross, and George King

Background

Anthropogenic releases of carbon dioxide (CO_2) from the burning of fossil fuels are not matched by an equivalent rise in atmospheric CO_2 (Keeling *et al* 1989). To fully understand what happens to the portion of emissions not contributing to the atmospheric increase, one needs knowledge of Earth's carbon pools and the processes that control the exchange between "compartments." The amounts in major reservoirs of carbon are known. In order of decreasing content, they are (Esser 1989, Emanuel *et al* 1984, Box 1988, Post *et al* 1990):

- Oceans contain 37,000 Gigatons (Gt) inorganic carbon plus 1000 Gt organic carbon (where 1 Gt = 1 billion metric tons);
- Below-ground fossil reserves range from 4000 to 10,000 Gt;
- Terrestrial soil and litter combine for 1,200 to 3,000 Gt;
- The atmosphere contains 750 Gt in 1988; and
- Terrestrial vegetation accounts for 420 to 830 Gt.

The concentration of atmospheric carbon is known to within a percent; fossil fuel emissions are known within 5 percent; and other pool estimates have much greater uncertainty. Similarly, the accuracy of flux estimates between compartments is not known with certainty. For example, in some analyses the net flux from terrestrial biota has either been assumed to be zero or has been arrived at by a difference, or deconvolution, with its values assigned equal the amount needed to achieve a global balance (Tans *et al* 1990).

The magnitude of gross annual biogenic flux between the atmosphere and the terrestrial biosphere is about 100 Gt/y (Gigatons per year) from uptake through photosynthesis and a comparable release through respiration and decay of residues. This rate is roughly comparable to the ocean/atmosphere exchange, also estimated at 100 Gt/y. The ocean is believed to be a net sink of 1.6 to 2.4 Gt/y (Post *et al* 1990). Small differences between large numbers are notoriously unreliable, yet the net changes obtained by difference are on the same order of magnitude as the fossil fuel release, about 5.3 Gt/y (Boden *et al* 1990), and land use

In K.T. Redmond, Editor, 1992. Proceedings of the Eighth Annual Pacific Climate (PACLIM) Workshop, March 10-13, 1991: California Department of Water Resources, Interagency Ecological Studies Program Technical Report 31.

related releases, estimated to range from 0.6 to 6 Gt/y (Houghton *et al* 1983). Thus, small alterations in the function of one or more of these system components that regulate carbon pools, whether caused by climate change, human influence, or events external to Earth, could have important consequences for the atmospheric balance.

Terrestrial carbon flux has been difficult to measure and model, because it requires detailed description of vegetation types and soils, the associated biomass, and "performance" over the seasonal cycle. Disturbances, such as conversion of land to agricultural use, biomass burning, and responses to short-term climatic fluctuations, add to the complexity. If the atmospheric burden of CO_2 is assumed constant, then on an annual basis, heterotrophic respiration and net primary production (NPP), or the amount of carbon actually assimilated into biomass by autotrophs, must balance. But the estimated global NPP of 62 Gt/y (Post *et al* 1990) is an aggregate of many subsystems operating at a wide range of spatial and temporal scales. Historically, it has been simpler to assume a steady-state or no net gain in terrestrial carbon storage. The human land use impact can then be added, and the terrestrial balance can thus be "reconstructed," allowing a dynamic picture to emerge. Houghton *et al* (1983) have estimated the net flux from terrestrial systems due to land use changes at 90 to 120 Gt over the period from 1800 to 1980. However, these estimates do not fully account for the observed atmospheric rise in CO_2, and they also diverge from estimates arrived at by the difference technique, also called the deconvolution method (Post *et al* 1990). The latter approach uses the atmospheric record of past concentrations, obtained from ice-core bubbles, and, more recently, ratios of carbon isotopes and models of ocean uptake. Estimates from deconvolution and reconstruction approaches appear to be in reasonable agreement from 1860 to about 1920. However, trends for decades since 1920 have diverged and have opposite signs for the direction of the net terrestrial flux with the divergence approaching 2 Gt/y (Post *et al* 1990).

It may not yet be possible to construct a detailed and precise carbon budget for terrestrial systems on a global scale. However, attempts at such budgets on continental or country scales in data-rich areas* may point the way to improving flux estimates for otherwise data-poor terrestrial ecosystems and help to resolve the apparent contradictions. Carbon budgets will also be relevant in terms of evaluating possible strategies, including management practices, such as large-scale forestation for mitigating the rise in atmospheric CO_2 (Dixon *et al* 1991, Moulton and Richards 1990, Schroeder and Ladd 1991, Sedjo 1989, Trexler 1990) and in determining the sign and magnitude of potential biospheric feedbacks to climate change. These feedbacks could significantly dampen or amplify the rate of climate change (Houghton 1990, Lashoff 1989, Prentice and Fung 1990).

* In addition to remote sensing data, the United States has databases from comprehensive national sampling efforts.

Objective

This report outlines the approaches for estimating the carbon budget for the United States, a data rich subcontinental area, and presents an overview of problems encountered and preliminary results obtained.

Approach

A carbon budget will be assembled to account for the flux of carbon into and out of a selected area, from all possible sources, for a specified point in time or an within an appropriate interval. The budget will allow:

- Estimating a net flux.
- Summarizing any geographical subgroup of flux sources or sinks.
- Evaluating changes due to human activities such as management of the vegetation, changes in man-made emissions, and changes in land-use practices.
- Predicting potential changes in carbon flux as the result of environmental variables, such as climate.

Where the flux of carbon is not limited by available pool size, it is unnecessary to provide a full accounting of such pools. This is the case with anthropogenic emissions from fossil fuels. At present, these are controlled by socio-political, economic, and technological constraints rather than fossil fuel resources. Hence, man-made emissions have been quantified, trends identified, and fossil fuel pool sizes omitted. In the case of carbon flux from terrestrial ecosystems, pool sizes may reflect the magnitude of potential flux directly, and they may be required to arrive at estimates of carbon flux. Carbon pool size determination is an integral part of the analysis.

Anthropogenic Emissions

In addition to CO_2, emission sources include carbon monoxide (CO), methane (CH_4), and volatile organic carbon (VOC), all of which are ultimately oxidized to CO_2. Emissions are separated by economic sector and by fuel type. Emissions are based on the emission factor database developed by Piccot and Saeger (1990) for the year 1985 and supplemented by the analyses of Boden *et al* (1990). Data for the present analyses are geo-referenced at the state level. The gases are not treated in terms of their radiative importance. That is, only their carbon content is reported for the budget.

Biogenic Carbon Pools

Forest ecosystems. Forests rank first among vegetation types in above-ground biomass, and hence in above-ground stored carbon per unit area.

Forest land area is derived from the latest inventory of the US Forest Service (Waddell *et al* 1989). Whereas total tree biomass for timberland (growth >1.4 m^3/ha/y) is readily available (Cost *et al* 1990), total tree biomass for woodlands (growth <1.4 m^3/ha/y), represented by large areas in the western United States, including Alaska, is being compiled by the authors from USFS state inventories and resource reports. Initial efforts will compile information for the contiguous states, using softwood and hardwood categories for above-ground biomass converted to carbon. Conversion factors are taken from Koch (1989). Carbon estimates are currently summarized for timberlands at the state level and supplemented with woodland or other forest carbon estimates for regional aggregations. These estimates will also incorporate data on carbon stored in living roots (Koch 1989). Moreover, our goal is to build an above-ground carbon pool for all forests lands across all ownerships that is geo-referenced by forest cover type. Geo-referencing will allow aggregating the data of productive unreserved timberland by forest type instead of using political boundaries.

Non-forest ecosystems. These ecosystems have considerably less biomass per unit area than forests. Their principal mechanism of carbon sequestration is the allocation of carbon to roots and the ultimate storage of carbon in soils. Examples include savanna, prairie, desert shrublands, tundra, and wetlands, much of which is currently used as rangelands or pastureland. Areal estimates of land cover types were obtained from the National Resource Inventory (NRI) database (Soil Conservation Service 1987) that represent surveys done in 1982 and 1987 and are distributed over Major Lands Resource Areas (MLRA). The NRI data are derived from a statistically based survey that is limited to privately owned lands. The margin of error increases significantly when areas smaller than MLRAs are analyzed. Land use is best summarized for each MLRA, which is a regional physiographic province. Because NRI land cover types are broadly defined, the Küchler Potential Vegetation Map (Küchler 1964) is used to refine cover types that have a natural vegetation component. Carbon pool estimates are taken from the ecological and land management literature.

Agro-ecosystems. Here the dominant characteristic is the annual cycle of the capture of carbon during the growing season and its relatively rapid release back to the atmosphere after harvest. In general, the harvested biomass is a small fraction of the seasonal growth, and it too is released fairly rapidly. For the purpose of the carbon budget, above-ground biomass in agricultural systems is assumed to be zero over one annual cycle.

Soil carbon exclusive of below-ground biomass. The geographic base for the soil carbon estimates is the Food and Agriculture Organization (FAO) and United Nations Educational, Scientific, and Cultural Organization (UNESCO) Soil Map of the World. The Soil Map of the World is the most comprehensive global-scale soil map available (Sombroek 1989). Fifty

example pedons with laboratory data accompany the printed FAO SMW map sheets of North America (FAO 1975) and were used to make volume-basis soil organic carbon calculations grouped by soil unit. The pedons were assumed to be free of coarse fragments and extend to 1 meter depth unless they were Lithosols or known to be very shallow. Soil units with missing carbon were assigned carbon from similar soil units. The area weighted average soil carbon composition for each map unit was calculated based on the soil composition and indications of rock fragments and shallow depth to bedrock.

Biogenic Carbon Flux

Ecosystem carbon flux is primarily composed of the uptake of atmospheric CO_2 through photosynthesis and the release of carbon from autotrophic and heterotrophic respiration. The net flux, or the difference between these two processes over an annual cycle, is the Net Ecosystem Productivity (NEP). NEP for a non-forested ecosystem is typically quite low. The NEP of a forest ecosystem varies by successional stage, with carbon accumulating in the mid-successional stage. Carbon is lost to the atmosphere in early stages due to the combination of enhanced soil respiration and reduced NPP. Carbon is also lost in the late-successional stage due to a high rate of autotrophic and heterotrophic respiration (Sprugel 1985). Disturbance, such as forest harvesting and catastrophic fire may release large quantities of carbon at the end of the successional cycle. Figure 1 shows total respiration, uptake, and resulting NEP, as a function of time, specific for a developing forest. Rather than modeling the process explicitly, the approach here will be to consider only NEP and to base the NEP estimates for different forest types and successional stages on empirical studies. Figure 2 schematizes the relationship of biogenic pools and flux.

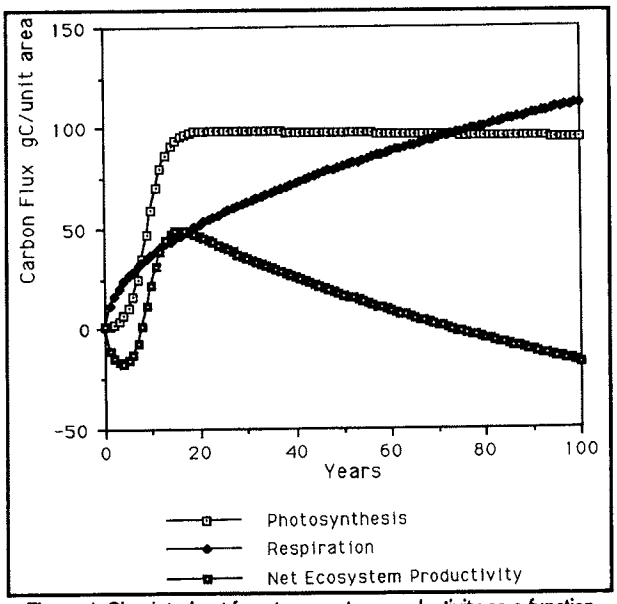

Figure 1. Simulated net forest ecosystem productivity as a function of stand development.

For most forest ecosystems, and for forests of the US in particular, deforestation, harvest, and replanting have modified age distribution of forests. This suggests that forests currently are likely to be a net sink, considering only biogenic flux. Thus, evaluation of the biogenic carbon requires an estimate of the age class distribution within each forest type and region.

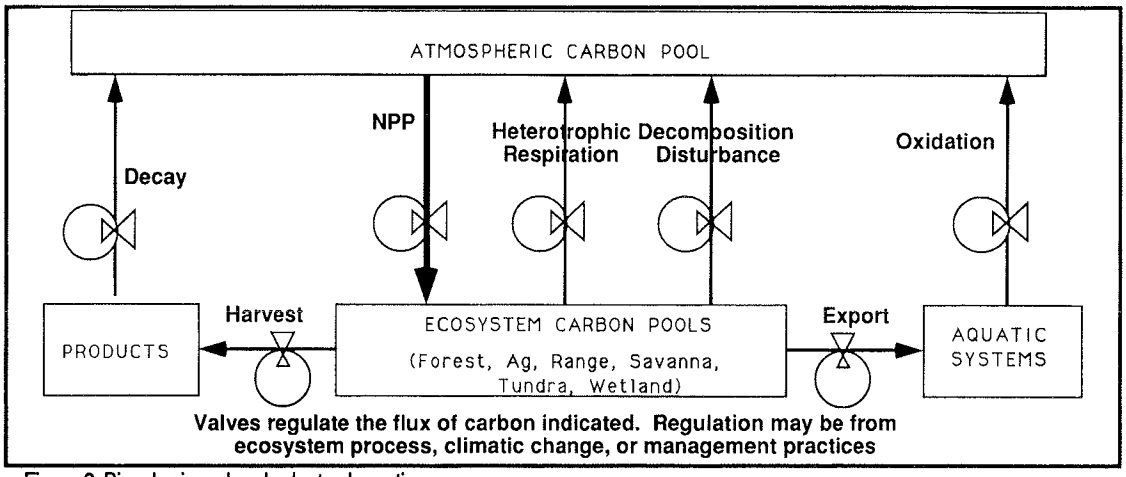

Figure 2. Biospheric carbon budget schematic.

Because harvesting itself may result in large carbon flux (*eg*, burning of slash) and much of the harvested carbon may be used in ways that return it to the atmosphere rather quickly, a complete accounting of forest carbon budget might reveal a different story from one that considers only biogenic flux (*eg*, see Harmon *et al* 1990). Data on the rate of harvesting and the fate of the harvested carbon will be compiled, in addition to the accounting of biogenic flux.

Forest age distribution data (Waddell 1991) will be combined with representative rates of carbon gains or losses (Figure 1), estimated for 30 forest types, using data from Birdsey (1991). These age-specific rates of change in total carbon storage (*ie*, above- and below-ground carbon), are based on empirical studies as well as generic models, (*eg*, soil loss after harvesting). The effects of disturbances such as insect outbreaks are implicit in the database (Birdsey 1991). These carbon flux estimates are primarily based on privately owned timberland. Therefore, it will be difficult to extrapolate these data to public timberlands (the national gorests) and low productivity forest woodlands. For reserved timberland (forest preserves such as designated wilderness or forests in national parks) the assumption of zero NEP may be reasonable, since age class distributions include many older stands that are nearly in carbon flux equilibrium. Uncontrolled fires could also maintain a net carbon accumulation of zero over a broad spatial scale.

The feasibility of obtaining data on age class distributions from National Forest inventory is currently being assessed. As an alternative, remote sensing will also be used to classify areas as pre-canopy closure, closed canopy, or old-growth or maturity. Forests that never achieve canopy closure, such as the Southwest's pinion-juniper forests, are classified as woodlands. They are unlikely to have NEP significantly different from zero, but literature values will be used to assign NEP by vegetation type. The USFS and the Wilderness Society have recently completed analyses of old-growth areas in the Pacific Northwest using high spatial resolution (<100 m) satellite imagery. Incorporation of these data, and use of imagery for other age classes from the Advanced Very High Resolution

Radiometer (AVHRR) sensor on the NOAA polar orbiter satellites, may permit reasonable modeling of the conifer forests of the Pacific Northwest.

Status of Present Analysis

Total anthropogenic emissions of carbon from all sources in the United States reached 1.44 Gt in 1985, or roughly 20 percent of global emissions from fossil fuels. Because forest data are presented by regions, the same regional breakdown for the man-made emissions is used for comparison (Figure 3). In general, the emissions reflect both population density and industrial capacity.

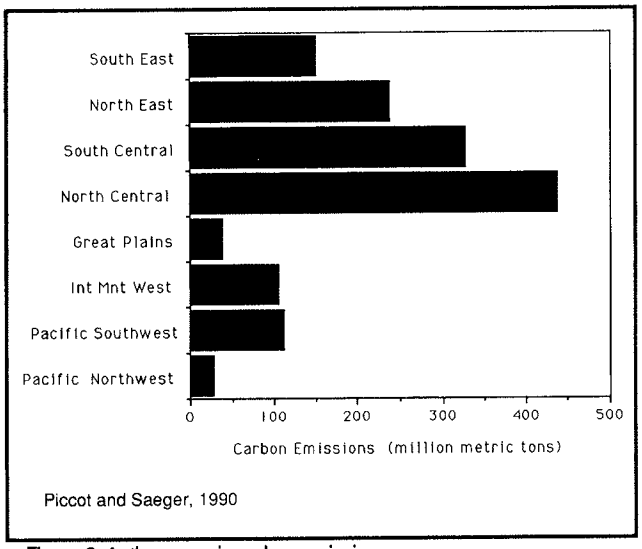

Figure 3. Anthropogenic carbon emissions.

National forests of the contiguous 48 states occupy a total of 243 Mha (million hectares), or roughly 31 percent of the total land area (Waddell *et al* 1989). Of this amount, 201 Mha is considered timberland (including reserved) and the remaining 32 Mha includes "less productive" forests with relatively low NPP (which we refer to as woodlands), such as the Southwest's pinion-juniper forests. Carbon storage on timberland is estimated to be 10 Gt. Above-ground carbon storage for timberland bears no simple relationship to available forest area in the same region, as is shown in Table 1. Non-timberland forests comprise a very large fraction of the total Rocky Mountain and Pacific regions, even more so if Alaska is included (Figure 4). A paucity of above-ground biomass data, and hence carbon data, for woodlands does not at present allow good estimates of pools. For this paper, we have assumed carbon pools (tons/ha) for these "other" forests to be similar to pools for timberlands. Even with this very optimistic assumption, the maximum forest carbon storage in woodlands of the contiguous states is unlikely to exceed 1.9 Gt of carbon. However, based on the lower productivity of these forests, the woodland contribution to the total forest carbon

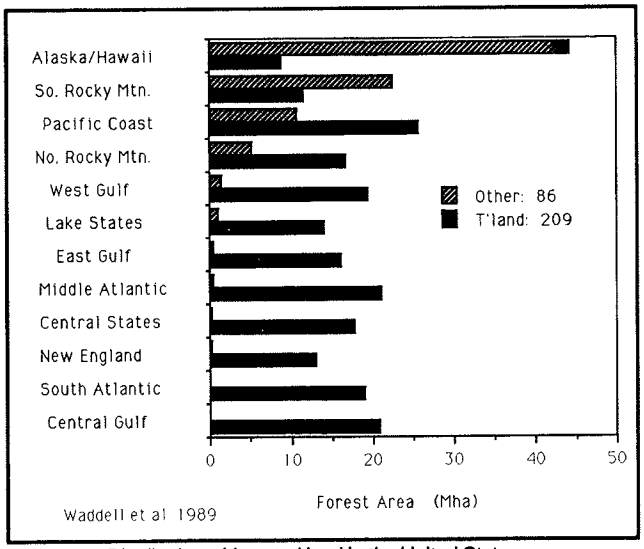

Figure 4. Distribution of forested land in the United States.

Table 1
Area and Aboveground Carbon for Forests in the Contiguous United States

Region/1	Waddell Area					Olson Area		SAF Area	
	Timberlnd/2 w/Reserved Area *Mha*	Other/2 Forest Area *Mha*	Total/2 Forest Area *Mha*	Timberlnd/1 w/Reserved Carbon *Gigatons*	Total/3 Forests Carbon *Gigatons*	Total/4 Forests Area *Mha*	Total/5 Forests Carbon *Gigatons*	Total/6 Forests Area *Mha*	Total/7 Forests Carbon *Gigatons*
Central Gulf	20.90	0.01	20.91	1.07	1.08	32.83	1.83	35.32	1.97
Central States	17.68	0.30	17.98	0.70	0.71	35.03	1.50	57.13	2.45
East Gulf	16.02	0.42	16.44	0.70	0.71	23.66	1.11	27.23	1.28
Lake States	20.04	1.10	21.34	0.82	0.87	31.96	2.02	40.64	2.57
Middle Atlantic	21.02	0.32	21.34	1.01	1.02	25.75	1.34	31.89	1.66
New England	12.93	0.23	13.16	0.65	0.66	14.08	0.77	15.85	0.86
N. Rocky Mountain	16.59	5.14	21.73	0.80	1.05	27.15	1.42	29.42	1.54
Pacific Coast	25.55	10.59	36.14	1.82	2.58	45.83	3.55	41.71	3.23
S. Rocky Mountain	11.56	22.60	34.16	0.37	1.10	42.09	1.47	51.23	1.79
South Atlantic	19.03	0.04	19.07	1.08	1.08	27.17	1.67	30.65	1.88
West Gulf	19.41	1.56	20.97	0.96	1.03	50.81	2.71	46.62	2.49
Total	200.72	42.32	243.24	9.97	11.89	356.36	19.39	407.69	21.72

1 Grouped according to Cost et al (1990).
2 Waddell et al (1989); see text for explanation of forest classification.
3 Using expansion, assuming other forest land equals carbon/ha of timberland.
4 As estimated from Olson et al (1985).
5 Regional carbon estimates based on the Cost et al (1990), applied to Using Olson forest area.
6 Estimate from digitized forest cover types; Eyre (1980).
7 Using SAF (Eyre 1980) forest area, we applied the regional carbon estimates based on the Cost et al(1990).

pool is more likely to approach 1 Gt. The best estimate for the total above-ground carbon in forests of the contiguous states is, thus, about 11 Gt and not likely to exceed 12 Gt.

Using forest area from Waddell (1989), this carbon pool represents a significantly lower estimate for US forests compared to estimates based on previously available forest area. Using forest area of the SAF map (Eyre 1980), we estimated about 408 Mha of forested land in the United States (Table 1). Similarly, estimating forest area from the Olson database (Olson *et al* 1985) yielded about 356 Mha. However, a more accurate estimate of forested land area in the contiguous states is about 237 Mha, based on a recent statistically-based survey (Waddell *et al* 1989). Using survey-based biomass (Cost *et al* 1990) and forest area (Waddell *et al* 1989) to estimate carbon per unit area, the potential above-ground carbon is 22 Gt across SAF forest types and 23 Gt across Olson types (Table 1). In contrast, the survey-based timberland data from Cost (1990) plus our own compilation of woodland biomass (Table 1) would suggest the above-ground carbon for forested land area in the contiguous United States is closer to 12-13 Gt.

The large difference in estimated areal extent of forest lands from both the Olson and SAF databases compared to the inventory area is indicative of two problems with pre-existing maps. One is the difficulty in accounting for land-use changes such as conversion of cropland to forest; the other

relates to resolution. For example, the 30-km resolution of the Olson database introduces error by simplifying boundaries and ignoring heterogeneity within cells, where forest types may include areas of cropland or pasture. The importance of inventories based on ground surveys cannot be ignored in this respect, and the spatial coverage and inclusion of necessary detail can be greatly enhanced by use of remote sensing. The final US carbon budget will include analysis of estimation errors and the effects of error propagation on the final carbon flux surfaces.

Our preliminary soil carbon pool estimate for the surface layer to a depth of 1 meter over the contiguous United States is 97 Gt. This value is bounded by the 85 Gt from Post *et al* (1982) and 112 Gt from Schlesinger (1984). Figure 5 is a soil carbon map that represents the estimates in a geo-referenced format suitable for integration with other map surfaces produced in this effort.

Detailed information on age-class distributions within forest types is currently being compiled for obtaining flux estimates. As indicated by the analysis described above, close attention will be given to the spatial and temporal distribution of these data, and the data in the inventory reports will be augmented by reference to remote sensing information.

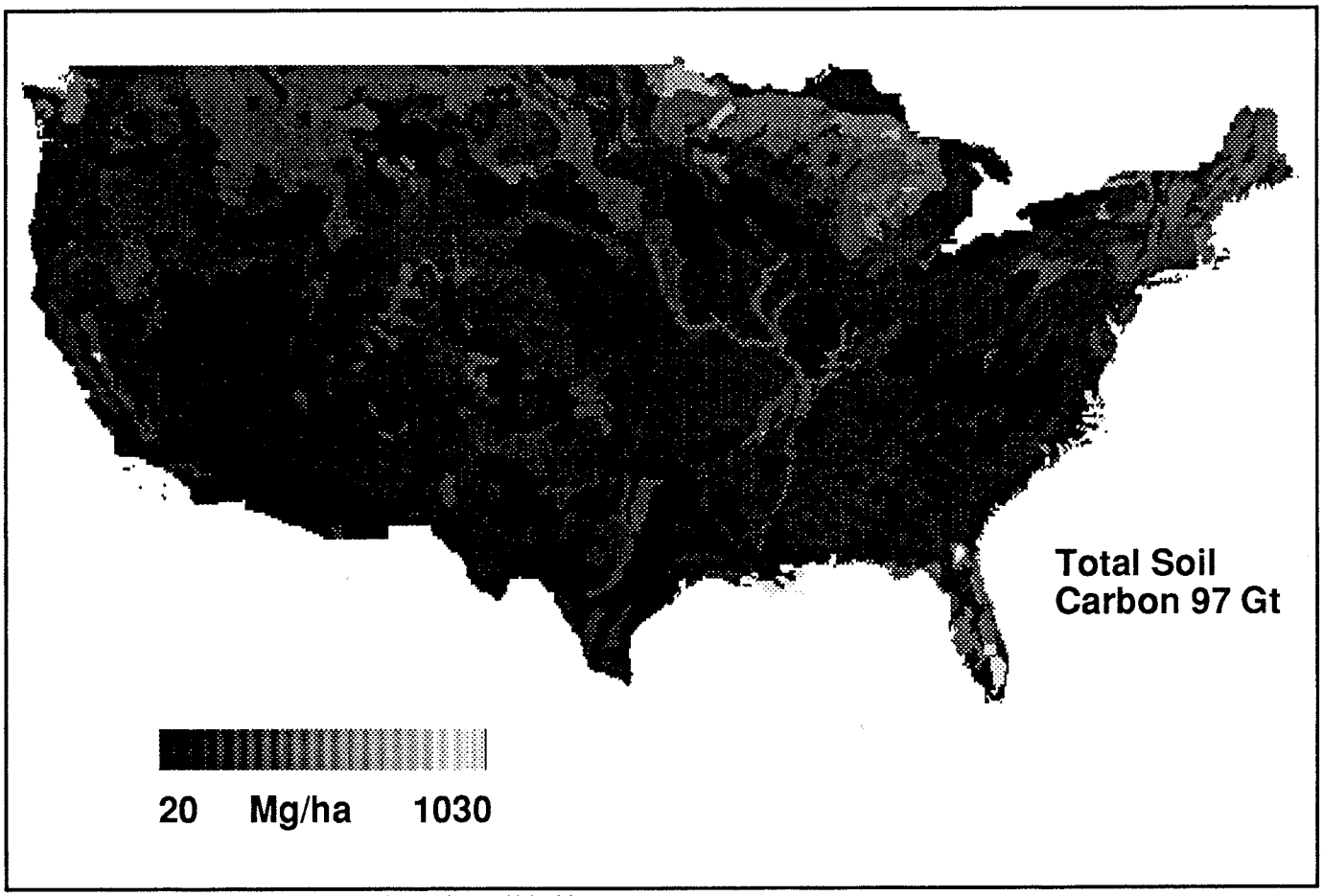

Figure 5. Soil carbon content to 1 meter for the contiguous United States.

Management Scenarios

The effect of management practices in all areas that impact sources and sinks of carbon can be thought of as having two characteristics. One is to change intensity of an activity, which affects flux per unit land area. Examples are changes in tillage, crop rotation, afforestation practices (*eg*, fertilization), emission controls, gains from energy efficiency, *etc.* Another effect is a change in spatial extent of an activity, such as deforestation for harvest, conversion of land uses, and building of landfills.

The GIS (Geographic Information System) analysis used in this approach has a spatial assignment for the carbon pool associated with any source/sink class (vegetation, soil, landfill, stack). We are developing algorithms that associate the source/sink type with a flux per unit area. A change in management practice, or the net effects of the simultaneous change in practices is computed by assigning new values to the corresponding flux intensity terms and recomputing the net budget. For the base year budget, such a change will reflect an annual increment but will not reflect the compounding effect of the changes of, say, forest carbon sequestration over time. Sequestration remains to be incorporated into a dynamic budget, although simple scenarios and sensitivity tests can readily be created to test this compounding effect.

Changes in spatial distribution of lands, vegetation classes, or man-made sources such as landfills can be analyzed with GIS input routines that reclassify map layers as a result of a management initiative. The reclassification will reassign the relevant map segment to another, usually the pre-existing, category and compute the new budget.

Conclusion

The development of a carbon budget for the United States is important in terms of:

- Comparing the relative magnitudes of biogenic and anthropogenic flux.
- Contributing to the construction of a global carbon budget.
- Evaluating possible carbon sequestration and conservation strategies.
- Exploring the magnitude and direction of possible feedbacks to climate change mediated by the terrestrial biosphere.

Efforts at classification of vegetation type and condition bases on existing maps may have large errors. This study, with the use of statistically based inventories, suggests the importance of moving away from pre-existing maps to the creation of new databases from ground inventories and remote sensing. Ultimately, advances in the areas of GIS, ecosystem modeling, and remote sensing will result in better maps and capabilities to extend country-wide estimates of carbon to regions of more limited baseline data.

Acknowledgments

The work is a component of the US EPA Global Climate Research Program, Global Mitigation and Adaptation Team, R.A. Dixon, Team Leader, at the EPA Environmental Research Lab in Corvallis, Oregon. We thank D. Coffey, T. Droessler, A. Hairston, G. Reams, D. Sandberg, and D. Spittlehouse for their helpful comments and criticism.

References

Birdsey, RA, 1991. *Prospective changes in forest carbon storage from increasing forest area and timber growth.* USDA Forest Service:Washington DC. In press.

Boden, TA, P Kanciruk, MP Farrell, 1990. *Trends '90: a compendium of data on global change.* Carbon Dioxide Information Analysis Center, ORNL/CDIAC-36, Oak Ridge National Laboratory:Oak Ridge, TE. 257 pp.

Box, EO, 1988. Estimating the seasonal carbon source-sink geography of a natural, steady-state terrestrial biosphere. *J. Appl. Meteorology.* 27:1109-1124.

Cost, ND, JO Howard, B Mead, WH McWilliams, WB Smith, DDVanHooser, and EH Warton, 1990. *The biomass resource of the United States.* USDA Forest Service Gen. Tech. Rep. WO-57.

Dixon, RK, PE Schroeder, JK Winjum, 1991. *Assessment of promising forest management practices and technologies for enhancing the conservation and sequestration of atmospheric carbon and their costs at the site level.* US EPA report to the Office of Policy, Planning, and Evaluation. Submitted.

Emanuel, WR, GG Killough, WM Post, and HH Sugart, 1984. Modeling terrestrial ecosystems in the global carbon cycle with shift in carbon storage capacity by land-use change. *Ecology.* 65(3):970-983

Esser, G, 1989. Zum kohlenstoff-haushalt der terrestrischen biosphäre. *Poster of the Transactions of the Society for Ecology, Vol XVII.*

Eyre, FH (ed.), 1980. *Forest cover types of the United States and Canada.* Society of American Foresters, Washington, D.C. 148 pp.

FAO/UNESCO. 1975. *Soil Map of the World, Volume II North America,* 1:5,000,000 with text. UNESCO:Paris.

Harmon, ME, WK Ferrell, and JF Franklin, 1990. Effects on carbon storage of conversion of old-growth forests to young forests. *Science.* 247:699-702.

Houghton, RA, 1990. The future role of tropical forests in affecting the carbon dioxide concentration of the atmosphere. *Ambio.* 19:204-209.

Houghton, RA, JE Hobbie, JM Melillo, B Moore, BJ Peterson, GR Shaver, and GM Woodwell, 1983. Changes in the carbon content of terrestrial biota and soils between 1860 and 1980: Net releases of CO_2 to the atmosphere. *Ecological Monographs.* 53:235-263.

Keeling, CD, RB Bacastow, AF Carter, SC Piper, TP Whorf, M Heimann, WG Mook, and H Roeloffzen, 1989. A three-dimensional model of atmospheric CO_2 transport based on observed winds: 1. Analysis of observational data. Pgs. 165-236 in DH Peterson (ed.) *Aspects of Climate Variability in the Pacific and the Western Americas.* Geophysical Monograph 55, American Geophysical Union.

Koch, P, 1989. *Estimates by species group and region in the USA of below-ground root weight as a percentage of ovendry complete tree weight and carbon content of tree portions.* Consulting Report to the USDA Forest Service.

Küchler, AW, 1964. *The potential natural vegetation of the conterminous United States.* Am. Geographical Sic. Special Pub. 36.

Lashoff, DA, 1989. The dynamic greenhouse: feedback processes that may influence future concentrations of atmospheric trace gases and climate change. *Climatic Change.* 14:213-242.

Moulton, RJ, and KR Richards, 1990. *Costs of sequestering carbon through tree planting and forest management in the United States.* USDA Forest Service General Technical Report WO-58. 47p.

Olson, JS, JA Watts, and LJ Allsion, 1985. *Major world ecosystem complexes ranked by carbon in live vegetation: a database.* ORNL-5862. Oak Ridge National Laboratory, Oak Ridge, TN. 180 pp.

Piccot, S, and M Saeger, 1990. *National- and state-level emissions estimates of radiatively important trace gases (RITGs) from anthropogenic sources.* Alliance Technologies Corp, EPA Contract 86-D9-0173. EPA-600/8-90-073.

Prentice, KC, and IY Fung, 1990. Bioclimatic simulations test the sensitivity of terrestrial carbon storage in perturbed climates. *Nature.* 346:48-51.

Post, WM, T-H Peng, WR Emanuel, AW King, VH Dale, DL DeAngelis, 1990. The global carbon cycle. *Am. Scientist.* 78:310-326.

Post, WM, WR Emanuel, PJ Zinke, AG Stangenberger, 1982. Soil carbon pools and world life zones. *Nature.* 298:156-159.

Schlesinger, WH, 1984. Soil organic matter: a source of atmospheric CO_2. In GM Woodwell (ed.) *The Role of Terrestrial Vegetation in the Global Carbon Cycle.* Wiley:London.

Schroeder, P, and L Ladd, 1991. Slowing the increase of atmospheric carbon dioxide: a biological approach. *Climatic Change.* In press.

Soil Conservation Service. 1987. *Basic statistics, 1982 National Resources Inventory.* Statistical Bulletin 756, Iowa State University:Ames.

Sedjo, R, 1989. Forests: a tool to moderate global warming? *Environment.* 31:14-20.

Sombroek, WG, 1989. Geographic quantification of soils and changes in their properties, Chapter 9. AF Bouwman (ed.). *Soils and the Greenhouse Effect.* John Wiley and Sons:Chichester, NY.

Sprugel, DG, 1985. Natural disturbances and ecosystem energetics. In STA Pickett and PS White (eds.) *The Ecology of Natural Disturbances and Patch Dynamics.* Academic Press:New York.

Tans, PP, IY Fung, and T Takahashi,. 1990. Observational constraints on the global atmospheric CO_2 budget. *Science.* 247:1431-1438.

Trexler, MC, PE Faeth, and JM Kramer,. 1990. Forestry as a response to global warming: an analysis of the Guatemala agroforestry and carbon sequestration project. In *Tropical Forestry Response Options to Global Climate Change.* Conf. Proc., Sao Paulo, Brazil. January 1990. USEPA/IBAMA/USP.

Waddell, KL, 1991. Personal communication. Area and volume information not previously summarized in Waddell *et al* (1989).

Waddell, KL, DD Oswald, DS Powell, 1989. *Forest statistics of the United States.* USDA Forest Service Res. Bull. PNW-RB-168. 106 pp.

Validation of a Semi-Lagrangian, Canonical Regression Model of Climates in the Southwestern United States

John F. Stamm and Richard G. Craig

Abstract: A local climate model (LCM) has been developed to simulate the modern and 18 ka climate of the southwestern United States. Measures of monthly temperature (TEMP) and precipitation (PREC) are computed using a canonical regression function of predictor variables that represent the primary and interactive effects of terrain, sea surface temperature, CO_2, solar insolation, and windfield. Annual and seasonal TEMP and PREC are computed from solutions of monthly TEMP and PREC for comparison to proxy paleoclimate estimates. LCM solutions indicate summers were about 1°C cooler and winters 11°C cooler at 18 ka. Annual PREC increased 68% at 18 ka, with large increases in spring and fall PREC and diminished summer monsoonal PREC. Validation of LCM solutions of modern climate indicates residuals on the order of 1°C for monthly TEMP and 10 mm for monthly PREC. Validation of simulations of 18 ka climate indicate a general agreement with proxy estimates of climate for that time. However, the LCM estimates of summer temperatures are about 5 to 10°C higher than estimates from proxy reconstructions.

Introduction

Estimates of paleoclimate in the southwestern United States during the last glacial maximum, 18 ka (thousand years ago), have been derived from proxy sources such as:

- Glacial deposits (Dohrenwend 1984; Leonard 1984)
- Lake deposits (Benson and Thompson 1987; Smith and Street-Perrott 1983; Mifflin and Wheat 1979)
- Fossil pollen (Atwater and others 1986; Davis and others 1985; Markgraf and others 1984; Batchelder 1980, 1976; Merrill and Péwé 1977; Wright and others 1973; Adam 1967)
- Plant macrofossils preserved in pack rat (*Neotoma*) middens (Betancourt 1990; Cole 1990, 1983; Thompson 1990; Spaulding 1985).

Paleoclimate estimates derived from different proxy sources vary, possibly due to different microclimates associated with the different sources (*eg*, climate in valley bottoms versus wooded slopes). Paleoclimate estimates are also available from General Circulation Models (GCMs; *eg*, Kutzbach and Wright 1985). However, in areas of complex terrain, GCM solutions are too coarse for realistic comparisons with proxy estimates of local paleoclimate. With this problem of resolution in mind, a Local Climate Model (LCM) has been developed that interpolates GCM results and boundary conditions to a 15-km resolution. At this resolution,

In K.T. Redmond, Editor, 1992. Proceedings of the Eighth Annual Pacific Climate (PACLIM) Workshop, March 10-13, 1991: California Department of Water Resources, Interagency Ecological Studies Program Technical Report 31.

comparisons of LCM solutions of paleoclimate with proxy estimates are possible.

The Local Climate Model

The LCM is a statistical model and is described in detail by Stamm (1991). A earlier version of the LCM is described by Craig and Stamm (1990). The LCM is based on a canonical regression function (Glahn 1968; Stamm 1991) that estimates monthly TEMP and PREC, where TEMP is a measure of maximum temperature and PREC is a measure of total precipitation. Solution of the canonical regression function requires a set of predictor variables that represent the primary and interactive effects of five boundary conditions:

- Terrain
- Sea surface temperatures (SST) in January and July
- CO_2 concentration
- Solar insolation
- Windfield:
  January surface and 500-mb
  July surface and 500-mb

Thus, the LCM uses boundary conditions that can be estimated for paleoclimate scenarios (*eg*, 18 ka).

Most of the predictor variables represent changes in boundary conditions along windfield trajectories that extend 1000 km upwind and 30 km downwind from solution points. In this way, the LCM is considered a semi-Lagrangian model.

The LCM is calibrated with boundary conditions and instrumental records (from 641 stations in AZ, CA, CO, NM, NV, and UT) from 1980 to 1984. The spatial distribution of these stations is sufficient to allow solutions of the LCM over a large area of the southwestern United States, shown in Figure 1 and herein called the "solution domain". Solutions are made at a 15-km spacing over the solution domain, which extends 225 km north, 330 km south, 810 km east, and 360 km west of 37° north latitude and 116° west longitude (near Yucca Mountain, Nevada).

Solutions of Modern and 18 ka Climate

Solutions of modern climate are made by setting boundary conditions to those representing 1980-1984. Given these boundary conditions, predictor variables are computed at all grid points in the solution domain and applied to the canonical regression function. Annual and seasonal TEMP

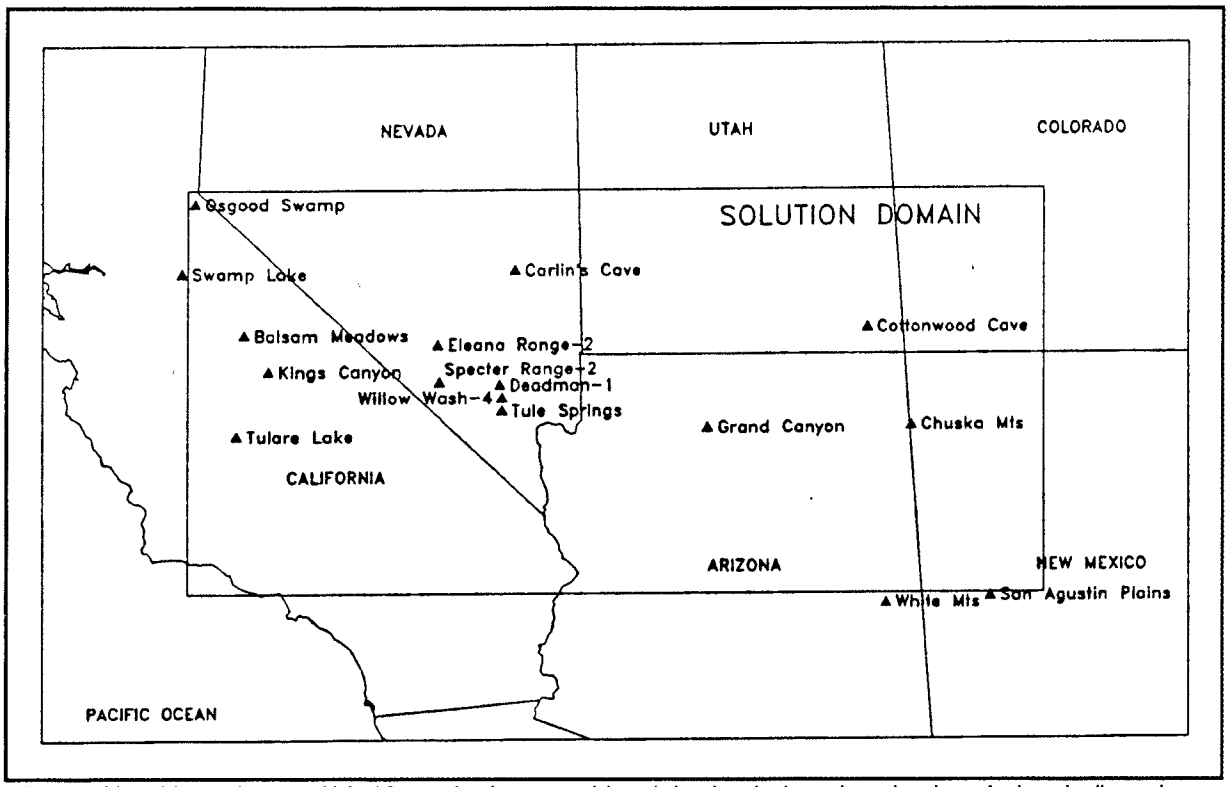

Figure 1. Map of the southwestern United States showing extent of the solution domain. Approximate locations of selected pollen and packrat midden sites are also shown.

and PREC are computed from monthly TEMP and PREC for comparison to LCM solutions of paleoclimate.

Solutions of paleoclimate are made by setting boundary conditions to those for 18 ka. Boundary conditions for 18 ka are described as:

- Terrain elevations adjusted to a 121-meter drop in sea level (Fairbanks 1989).
- Windfields obtained from GCM solutions (Kutzbach and Wright 1985).
- SST obtained from CLIMAP (1981).
- CO_2 concentrations as found in the Vostok ice core (Barnola *et al* 1987).
- Solar insolation as computed by Berger (1978).

These boundary conditions are described in detail by Stamm (1991). We note that windfields have an important influence on LCM solutions. In general, GCM windfields for 18 ka (Kutzbach and Wright 1985) are similar to the modern windfield. However, the January surface windfield in the southwestern United States for 18 ka differs from the modern windfield. The modern windfield is dominantly westerly, allowing a substantial influence by the Sierra Nevada. The 18 ka windfield had a significant south-southwesterly component, allowing moisture to be transported into the Great Basin through the Sonoran Route with less influence from the Sierra Nevada.

Given the boundary conditions for 18 ka, the predictor variables are computed for all grid points in the solution domain and applied to the canonical regression functions. Solutions of monthly TEMP and PREC are then used to compute annual and seasonal TEMP and PREC. Departures (18 ka minus modern LCM solutions) are computed for comparison to proxy estimates of paleoclimate.

Figures 2 and 3 show the averages of monthly TEMP and PREC for the modern and 18 ka in the solution domain. The salient features of the LCM solutions are summarized below:

Annual TEMP decreased 5°C at 18 ka:
- A 11°C decrease in winter TEMP
- A 1°C decrease in summer TEMP

Annual PREC increased 68% (168 mm) at 18 ka with:
- Diminished summer monsoonal PREC
- A 100% (90 mm) increase in spring PREC
- A 200% (100 mm) increase in fall PREC

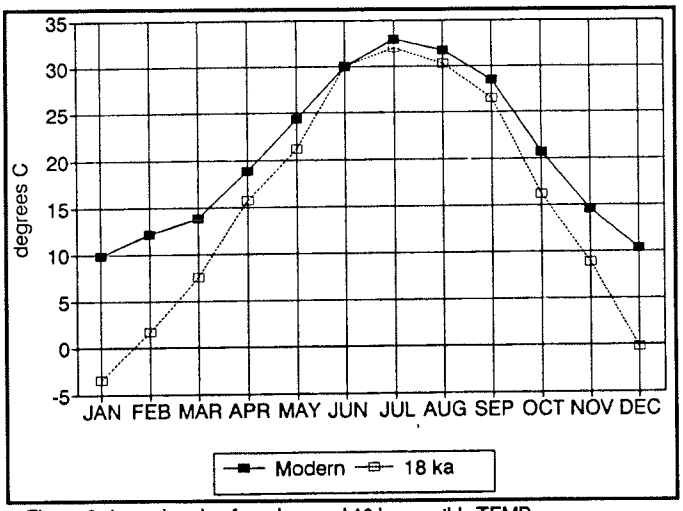

Figure 2. Annual cycle of modern and 18 ka monthly TEMP in the solution domain.

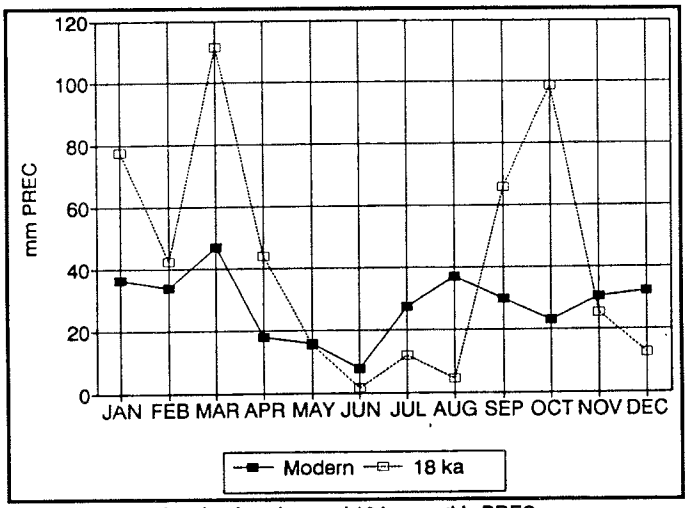

Figure 3. Annual cycle of modern and 18 ka monthly PREC in the solution domain.

Validation of LCM Solutions of Modern and 18 ka Climate

LCM solutions of modern climate have been validated against modern climate observations. Paired t-tests (Walpole and Meyers 1972) of LCM solutions against climate data from 1980 to 1984 (from 98 stations in AZ, CA, CO, NM, NV and UT) indicate no significant error in LCM solutions. Paired t-tests, using a Monte Carlo approach and a sample size of five, of LCM solutions and climate data for 1975 to 1979 (from 725 stations in AZ, CA, CO, NM, NV and UT) indicates residuals on the order of 1°C for monthly TEMP and 10 mm for monthly PREC.

LCM solutions of 18 ka climate are validated by comparison with proxy estimates of paleoclimate. Table 1 summarizes these comparisons. Dohrenwend (1984) studied glacial landforms and cirque altitudes in the

western Great Basin to estimate mean annual temperature and accumulation-season precipitation (ASP) during the full glacial. He computed a 5.5°C drop in mean annual temperature and a 370 mm increase in ASP, based on lapse rates of 7.6°C per 1000 m and 500 mm of ASP per 1000 m. Dohrenwend prefers a reconstruction for the full glacial with slight changes in ASP and mean annual temperatures 7°C lower. LCM solutions at the locations of alpine cirques and glaciated valley bottoms used by Dohrenwend (1984, Table 2) indicate a 4.2°C drop in TEMP and a 25 mm increase in ASP at 18 ka.

Table 1
Comparison of LCM Solutions of Climate Change at 18 ka with Other Estimates of Late Wisconsinan Climate Change

Temperature is given as change in °C. Precipitation is given as percent or millimeters of change. Winter=December, January, February. Summer=June, July, August.

	Temperature			Precipitation		
Source	Annual	Winter	Summer	Annual	Winter	Summer
Cirque Elevations* (Dohrenwend 1984)	−5.5 to −7.0				+370mm to 0mm	
LCM (at Cirque Locations)	−4.2	−9.7	−0.1	+62mm	+25mm	−36mm
Pluvial Lake Model by Mifflin and Wheat (1979)**	−3			+68%; +165mm		
LCM (Walker Lake)**	−6	−11	−2	+70%; +181mm	+5%; +6mm	−39%; −12mm
Pollen Sites in White Mountains (Merrill and Péwé 1977)	−5 to −6			+25% to +30%		
LCM (White Mts, NV)	−4	−11	+1	+17%	+26%	−83%
Packrat Sites in Mojave Desert*** (Spaulding 1985)	−6 to −7	<−6	−7 to −8	+30% to +40%	+60% to +70%	−40% to −50%
LCM (Spaulding's Packrat Sites)	−7	−14	−2	+106%	+50%	−74%
Packrat Site at Cottonwood Cave (Betancourt 1990)			−6			10% of Annual
LCM (Cottonwood Cave, NM)	−2	−8	+3	+21%	+44%	6% of Annual
Packrat Sites in Grand Canyon (Cole 1990)	−6.7			+24% to +41% +87mm		
LCM (Grand Canyon)	−5.8	−11.9	−0.8	+22%; +54mm	+4%	−81%

* Winter PREC is reported as December, January, February, March.
**PREC is reported as precipitation on the lake.
***Spaulding (1985) does not specifically define winter and summer months.

The Great Basin and Mojave deserts contain nearly 100 basins that filled with large pluvial lakes in the Late Wisconsin (Benson and Thompson 1987; Mifflin and Wheat 1979). Smith and Street-Perrott (1983) indicate that pluvial lakes could be maintained if the higher elevations received at least 400 mm of precipitation. However, they recognize that this estimate does not consider contributions of runoff from lower elevations. The LCM solution of mean annual PREC for the solution domain at 18 ka is 510 mm, apparently sufficient for pluvial lake growth.

Mifflin and Wheat (1979) developed a hydrologic balance model to estimate the change in mean annual precipitation and annual lake precipitation (precipitation directly on the lake surface) at the pluvial maximum, 15 to 12.5 ka. They suggest a 3°C decrease in mean annual temperature and a 52 to 80% increase in lake precipitation, with an average of about 68%. For comparison, LCM solutions have been computed for the surface of Walker Lake, Nevada, a subbasin of Lake Lahontan. Lake Lahontan experienced a high lake stand, though not to its maximum stand, at 18 ka (Benson and Thompson 1987). LCM solutions for Walker Lake indicate a 5.6° decrease in annual TEMP and a 70% increase in annual PREC at 18 ka. This closely matches Mifflin and Wheat's estimates and suggests LCM solutions are sufficient to support pluvial lake growth at 18 ka.

Proxy paleoclimate estimates from fossil pollen and plant macrofossils preserved in pack rat middens are available for several sites in the southwestern United States. These sites (Figure 1) include:

Balsam Meadows . . . . . Davis and others (1985)
Carlin's Cave . . . . . Thompson (1990)
Chuska Mountains . . . . . Wright and others (1973)
Cottonwood Cave . . . . . Betancourt (1990)
Deadman-1 . . . . . Spaulding (1985)
Eleana Range-2 . . . . . Spaulding (1985)
Grand Canyon . . . . . Cole (1990)
Kings Canyon . . . . . Cole (1983)
Osgood Swamp . . . . . Adam (1967)
San Agustin Plains . . . . . Markgraf and others (1984)
Specter Range . . . . . Spaulding (1985)
Swamp Lake . . . . . Batchelder (1980)
Tulare Lake . . . . . Atwater and others (1986)
Tule Springs . . . . . Spaulding (1985)
White Mountains . . . . . Batchelder (1976); Merrill and Péwé (1977)
Willow Wash-4 . . . . . Spaulding (1985)

Comparisons of LCM solutions with proxy estimates from these sites are discussed in detail by Stamm (1991). In summary, LCM solutions of PREC for 18 ka compare favorably with estimates derived from pollen and pack rat records, except for those sites in the western Sierra Nevada (Balsam Meadows, Kings Canyon, Osgood Swamp, Swamp Lake, Tulare Lake). LCM solutions of 18 ka climate for the western Sierra Nevada indicate a 210 mm increase in spring PREC, a 250 mm increase in fall PREC, and slight decreases in winter and summer PREC. Pollen and pack rat records for this area indicate a drier climate during the late-glacial. However, solutions of seasonal increases in PREC may not be unreasonable. For example, Adam and West (1983) suggested a 2,250 mm increase in annual precipitation at 18 ka for Clear Lake, in the northern California Coast Ranges.

The LCM solutions of TEMP are in partial agreement with estimates of temperature from pollen and pack rat records for the southwestern United States. The LCM does not indicate more equable temperatures, as suggested by VanDevender and others (1987). Rather, amplified seasonality is indicated. The LCM agrees with suggestions of cooler winter temperatures during 18 ka at pack rat sites in the Great Basin and Colorado Plateau (Carlin's Cave, Cottonwood Cave, Deadman-1, Eleana Range-2, Specter Range-2, Willow Wash-4) but does not indicate decreased summer temperatures at these sites, as suggested by Spaulding (1985), Betancourt (1990), and Thompson (1990). The disagreement of LCM solutions of summer TEMP and proxy reconstructions of summer temperature is on the order of 5°C to 10°C (Table 1). However, the LCM provides measures of maximum temperature, which may be less sensitive to change in summer months than mean or minimum temperature. Disagreement may also be due to the 15-km resolution of the LCM in comparison to the collection range of pack rats, which is about 30 meters (Finley 1990).

Conclusions

The general agreement of LCM solutions for 18 ka with various proxy estimates of Late Wisconsin climate suggests that LCM solutions are reasonable and that differences among proxy estimates may be largely due to variations in their spatial and temporal domains. The LCM may, therefore, provide a means to compare proxy estimates from different sources. Additionally, the general agreement of the LCM with proxy paleoclimate estimates suggests GCM solutions of 18 ka climate and associated boundary conditions for the southwestern United States are reasonable.

Acknowledgments

The research was performed under appointment to the Nuclear Engineering, Health Physics, and Radioactive Waste Management Fellowship Program administered by Oak Ridge Associated Universities for the US Department of Energy.

References

Adam, DP, 1967. Late-Pleistocene and Recent palynology in the central Sierra Nevada. Pgs. 275-301 in EJ Cushing and HE Wright Jr, eds. *Quaternary paleoecology.* INQUA, Volume 1. Yale University Press:New Haven.

Adam, DP, and GJ West, 1983. Temperature and precipitation estimates through the last glacial cycle from Clear Lake, California, pollen data. *Science.* 219:168-170.

Atwater, BF, DP Adam, JP Bradbury, RM Forester, RK Mark, WR Lettis, GR Fisher, KW Gobalet, and SW Robinson, 1986. A fan dam for Tulare Lake, California, and implications for the Wisconsin glacial history of the Sierra Nevada. *Geological Society of America Bulletin.* 97:97-109.

Barnola, JM, D Raynaud, YS Korotkevich, and C Lorius, 1987. Vostok ice core provides 160,000-year record of atmospheric CO_2. *Nature.* 329:408-414.

Batchelder, GL, 1980. A late Wisconsinan and early Holocene lacustrine stratigraphy and pollen record from the west slope of the Sierra Nevada, California. *Sixth American Quaternary Association Meeting: Abstracts with Programs.* p.125.

_____, 1976. Late Quaternary environmental interpretations from palynological data, White Mountains, Arizona. *Fourth American Quaternary Association Meeting: Abstracts with Programs.* p.125.

Benson, LV, and RS Thompson, 1987. The physical record of lakes in the Great Basin. Pgs. 241-260 in WF Ruddiman and HE Wright Jr, eds. *The geology of North America, Volume K-3: North America and adjacent oceans during the last deglaciation.* Boulder, Colorado.

Berger, AL, 1978. Long-term variations of daily insolation and Quaternary climate changes. *Journal of Atmospheric Science.* 35:2362-2367.

Betancourt, JL, 1990. Late Quaternary biogeography of the Colorado Plateau. Pgs. 259-292 in JL Betancourt, TR VanDevender, and PS Martin, eds., *Packrat middens: the last 40,000 years of biotic change.* The University of Arizona Press:Tucson.

CLIMAP Project Members, 1981. *Seasonal reconstructions of the earth's surface at the last glacial maximum.* Geological Society of America Map Chart Series MC-36.

Cole, KL, 1990. Late Quaternary vegetation gradients through the Grand Canyon. Pgs. 240-258 in JL Betancourt, TR VanDevender, and PS Martin, eds. *Packrat middens: the last 40,000 years of biotic change.*

_____, 1983. Late Pleistocene vegetation of Kings Canyon, Sierra Nevada, California. *Quaternary Research.* 19:117-129.

Craig, RG, and JF Stamm, 1990. A statistical model of climates in the Southwest U.S. Pgs. 26-29 in JL Betancourt, ed. *Proceedings of the Sixth Annual Pacific Climate (PACLIM) Workshop.* California Department of Resources:Sacramento.

Davis, OK, RS Anderson, PK Fall, MK O'Rourke, and RS Thompson, 1985. Palynological evidence for early Holocene aridity in the southern Sierra Nevada, California. *Quaternary Research.* 24:322-332.

Dohrenwend, JC, 1984. Nivation Landforms in the western Great Basin and their paleoclimatic significance. *Quaternary Research.* 22:275-288.

Fairbanks, RG, 1989. A 17,000-year glacio-eustatic sea level record; influence of glacial melting rates on the Younger Dryas event and deep-ocean circulation. *Nature.* 342:637-642.

Finley, RB Jr, 1990. Woodrat ecology and behavior and the interpretation of paleomiddens. Pgs. 28-42 in JL Betancourt, TR VanDevender, and PS Martin, eds. *Packrat middens: the last 40,000 years of biotic change.* The University of Arizona Press:Tucson.

Glahn, HR, 1968. Canonical correlation and its relationship to discriminant analysis and multiple regression. *Journal of Atmospheric Sciences.* 25:23-31.

Kutzbach, JE, and HE Wright Jr, 1985. Simulation of the climate of 18,000 years BP: Results for the North American/North Atlantic/European sector and comparison with the geologic record of North America. *Quaternary Science Reviews.* 8:147-187.

Leonard, EM, 1984. Late Pleistocene equilibrium-line altitudes and modern snow accumulation patterns, San Juan Mountains, Colorado, USA. *Arctic and Alpine Research.* 16:65-76.

Markgraf, V, JP Bradbury, RM Forester, G Singh, and RS Sternberg, 1984. San Agustin Plains, New Mexico: age and paleoenvironmental potential reassessed. *Quaternary Research.* 22:336-343

Merrill, RK, and TL Péwé, 1977. *Late Cenozoic geology of the White Mountains, Arizona.* State of Arizona Bureau of Geology and Mineral Technology Special Paper No.1. Temple, Arizona. 65 p.

Mifflin, MD, and MM Wheat, 1979. *Pluvial lakes and estimated pluvial climates of Nevada.* Nevada Bureau of Mines and Geology:Reno. Bulletin 94, 57 p.

Smith, GI, and FA Street-Perrott, 1983. Pluvial lakes of the western United States. Pgs. 190-214 in HE Wright Jr, ed. *Late Quaternary environments of the United States, Volume 1, The Late Pleistocene.* University of Minnesota Press:Minneapolis.

Stamm, JF, 1991. *Modeling local paleoclimates and validation in the Southwest United States.* PhD Dissertation. Kent State University:Kent, OH. 231 p.

Spaulding, WG, 1985. *Vegetation and climates of the last 45,000 years in the vicinity of the Nevada Test Site, south-central Nevada.* US Geological Survey Professional Paper 1329. 83 p.

Thompson, RS, 1990. Late Quaternary climate and vegetation in the Great Basin. Pgs. 200-239 in JL Betancourt, TR VanDevender, and PS Martin, eds. *Packrat middens: the last 40,000 years of biotic change.* The University of Arizona Press:Tuscon.

VanDevender, TR, RS Thompson, and JL Betancourt, 1987. Vegetational history of the deserts of southwest North America: The nature and timing of the Late Wisconsin-Holocene transition. Pgs. 323-352 in WF Ruddiman and HE Wright Jr, eds. *The geology of North America, Volume K-3: North America and adjacent oceans during the last deglaciation.* Geological Society of America:Boulder, Colorado.

Walpole, RE, and RH Meyers, 1972. *Probability and statistics for engineers and scientists.* Macmillan:New York. 506 p.

Wright, HE Jr, AM Bent, BS Hansen, and LJ Maher Jr, 1973. Present and past vegetation of the Chuska Mountains, northwestern New Mexico. *Geological Society of America Bulletin.* 84:1155-1180.

A Numerical Simulation of Cool/Wet and Warm/Wet Episodes in the Western United States

Shyh-Chin Chen, Dan R. Cayan, John O. Roads, and Mike Dettinger

Wintertime precipitation in the mountains of the western United States during a warm or cool period has a pronounced influence on streamflow (Cayan 1990). During a warm year, streamflow at intermediate elevations responds more immediately to precipitation events; during a cold year, much of the discharge is delayed until the snow melts in spring and summer. Previous efforts at studying these extremes have been hampered by a limited number and length of observational analyses. In this study, we augment this limited observational record by analyzing a simplified general circulation model (Chen and Roads 1988, 1989; Chen *et al* 1991). We first analyze the ability of the model to reproduce major characteristics of warm and cool storms. Then a longer model run is investigated to understand inter-annual and inter-decadal variability of winter mean precipitation and temperature along the west coast of the United States. In addition to having a self-consistent hydrologic budget, this model is able to generate substantial numbers of low frequency events that are quite realistic. The model also has stationary statistics (*eg*, no problems due to station moves or missing data).

Compared to other general circulation models in the community, this model can be integrated efficiently due to many simplifications in the physical parameterizations and the resolution in the model (Chen *et al* 1991). However, it still takes several months to integrate the model for 544 consecutive perpetual winters. Here we define 90 model simulation days as a winter in the model. From this fairly long record of model data, time-series of precipitation and temperature are examined for three adjoining model gridpoints that represent the far West: 123.75W/40.99N, 123.75W/37.42N, and (118.125W/37.42N. All three of these points are in upslope regions of the model smooth orography. Averaged over these three points, the model climatological temperature is 2.5°C and precipitation is 0.212 cm day^{-1}. In a typical model time-series (Figure 1, center graph), slowly varying daily temperature anomalies are embedded in highly fluctuating short-term temperature variations; precipitation occurs in even shorter bursts. These characteristics are similar to those observed winter time-series (Figure 1, bottom graph) obtained from compiling station data near central Sierra in the American River basin for winters of 1981-82, 1982-83 and 1987-88 (see also Cayan 1990).

In K.T. Redmond, Editor, 1992. Proceedings of the Eighth Annual Pacific Climate (PACLIM) Workshop, March 10-13, 1991: California Department of Water Resources, Interagency Ecological Studies Program Technical Report 31.

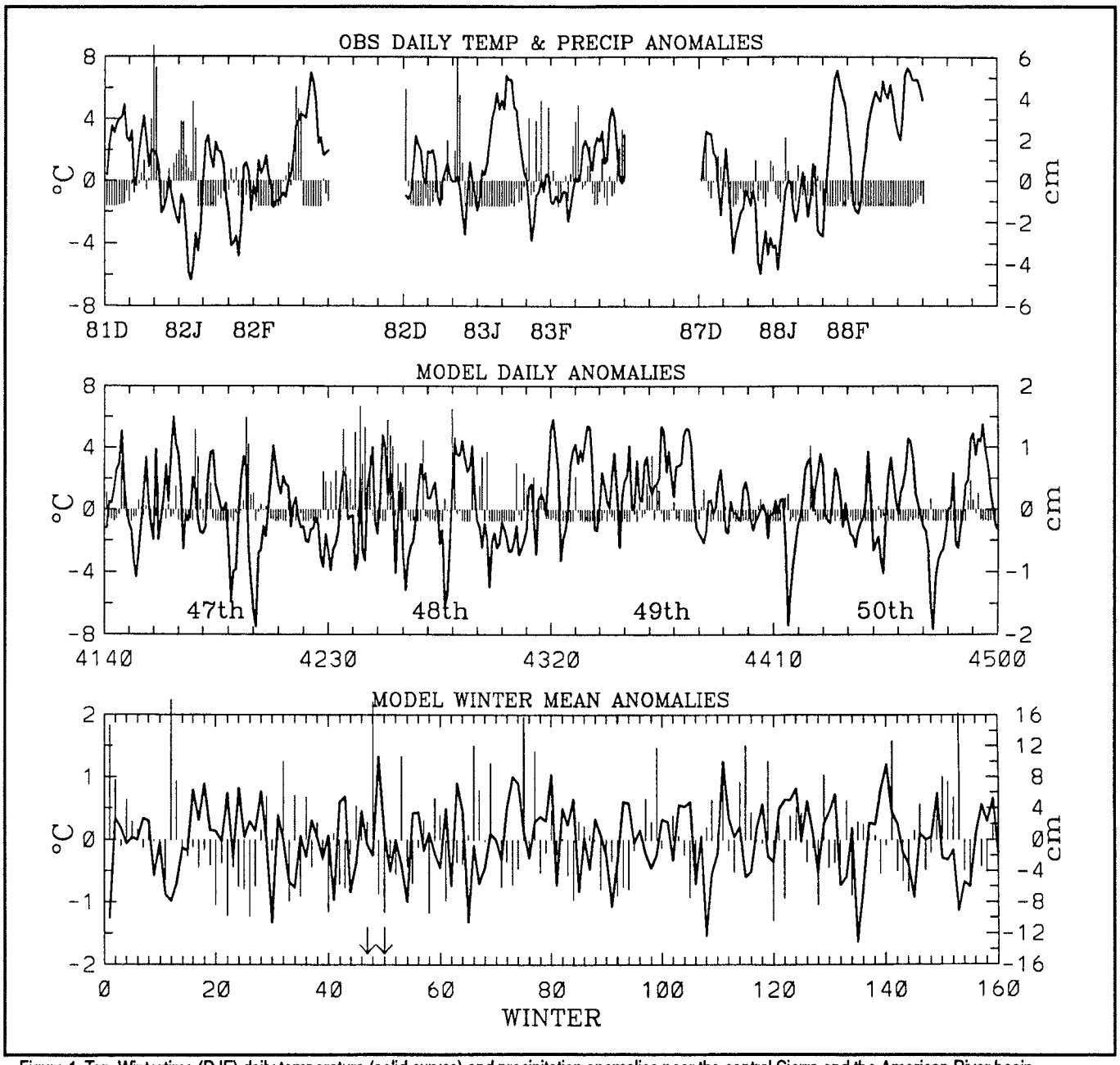

Figure 1. Top. Wintertime (DJF) daily temperature (solid curves) and precipitation anomalies near the central Sierra and the American River basin. Temperature anomalies are in degrees Celsius, and daily accumulated precipitation anomalies are in centimeters.
Center. Same as Top except for model day 4140 through 4500.
Bottom. Same as Center except model winter mean anomalies for the first 160 winters are shown. Precipitation anomalies, in centimeters, refer to the 90 days accumulated rainfall anomalies. Two downward arrows mark the model's 47th through 50th winters; daily sequences for these winters are shown in the center graph.

To discriminate warm from cool/wet events, a warm/wet event is defined if the temperature and precipitation anomalies of a storm are higher than one standard deviation. Similarly, a cool/wet event is defined when the temperature and precipitation anomalies are lower than one standard deviation. Using this criterion, the warm/wet and cool/wet daily episodes can be easily identified in a scatter diagram of the daily temperature and precipitation anomalies as shown in Figure 2 (left graph). As may be seen, the daily events have temperatures clustered mostly around climatology with fewer numbers reaching large positive and negative anomalies (*ie*,

roughly a Gaussian-type distribution). Precipitation events are quite different, however. During the storm days there are large anomalies; on most other days there is very little rainfall or none at all. Nevertheless, several warm/wet and cool/wet storm extremes can be found. The composite 500-mb anomaly circulation patterns during the warm/wet and cool/wet daily episodes are similar to those from observations based on northern California temperature and precipitation (Chen *et al* 1990). Generally, cool storms have intense positive anomalies over the northern-central Pacific and transport cold Arctic air to the West Coast. In contrast, warm storm circulations are characterized by anomalous southwesterlies and presumably more rainfall than snowfall occurs in the warm/wet event. In essence, circulation differences between cool and warm storms in the model are similar to observed differences, although the model warm/wet negative anomaly to the west of California is not as zonally extensive as it is in nature.

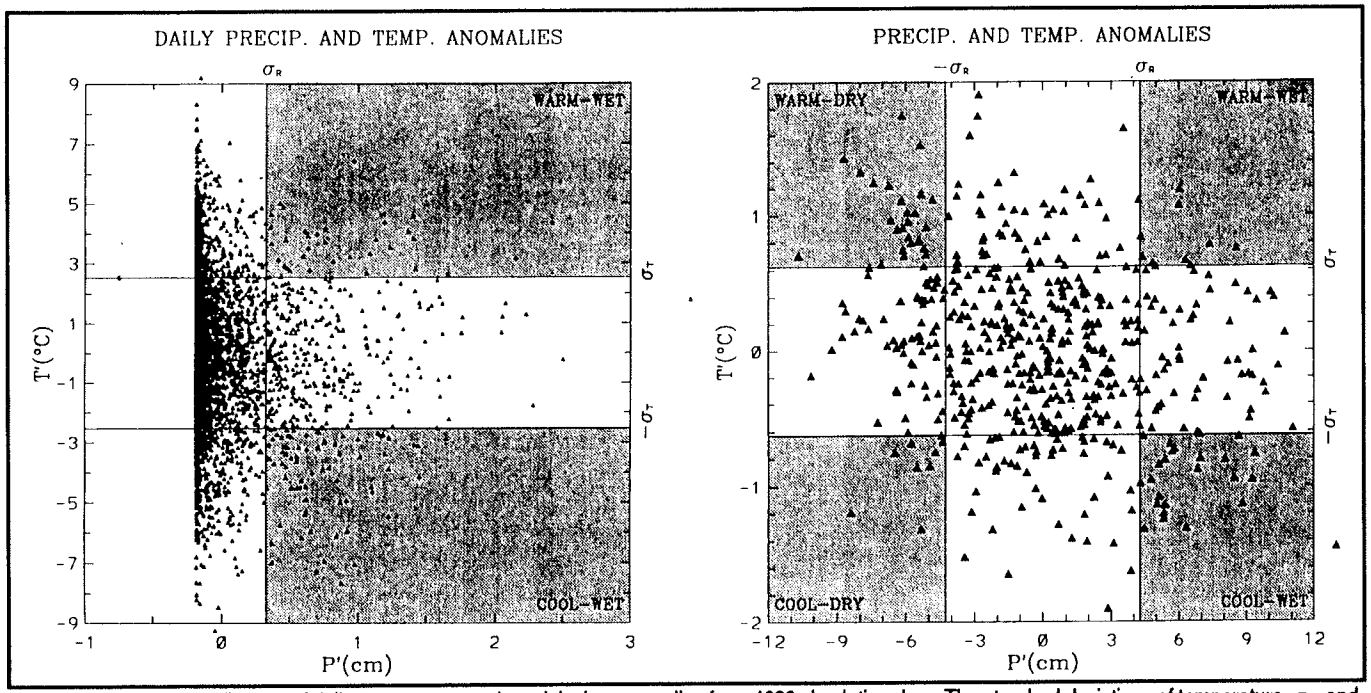

Figure 2. Left. Scatter diagram of daily temperature and precipitation anomalies from 4829 simulation days. The standard deviations of temperature, σ_T, and precipitation, σ_R, divide the parameter space into two extremes, warm-wet and cool-wet, which are shaded.
Right. Safe as left except winter-mean anomalies for 544 simulated winters are shown. The parameter space is divided into four extremes (warm-wet, warm-dry, cool-wet, and cool-dry winters) by $\pm\sigma_T$ and $\pm\sigma_R$.

Let us now examine the low frequency behavior of the model. Figure 1 (center graph) shows the winter-mean anomalies time-series for the first 160 simulated winters. Pronounced low frequency ("interannual" and "interdecadal") variations over the West Coast are evident, even though the model is integrated under a controlled environment in which the sea surface temperature, a frequently discussed external forcing parameter postulated to be responsible for the short-term climate variation over the United States (*eg*, Trenberth *et al* 1990; Namias 1991), is unchanging. Many other external forcing parameters are also unchanged, such as feedback in cloud radiation, soil moisture, albedo, greenhouse gases, *etc.*

The precipitation variability is quite large; in many cases deviations from the climatology are as large as the climatology itself. Extended wet and dry periods occur. For example a dry spell starts near the 15th winter and persists for about 10 winters; a wet period also occurs near the end of the series. Many similar extended dry and wet periods over the West Coast (not shown) are also found throughout the entire time-series.

The scatter diagram of this seasonal time-series is given in Figure 2 (right graph). Unlike the daily distributions shown in Figure 1 (center), the drought can be clearly identified by those periods with precipitation anomalies less than one standard deviation. Except for extremes at the four corners of the parameter space, the majority of the cases are clustered around the climatologies. However, the model has a slight tendency to become dry during warm spells or wet during cool spells (the correlation of the anomalies is -0.23). This relationship may be due to the time-invariant sea surface temperature; the cooler atmosphere will extract more moisture from the ocean surface through evaporation than the warmer atmosphere does. However, several warm/wet and cool/dry extremes have a robust circulation that offsets the evaporation effect.

From the winter extremes we compile composite circulations. Figure 3 shows composite 500-mb heights over the northern hemisphere of these wintertime extremes. Since these composite patterns are constructed from a local index, the circulation over the western United States region is consistent with the index. For example, in the cool/wet case, the anomalous circulation indicates a weakening of the wintertime Alaskan ridge over the West Coast and a southward displacement of the jet stream. These anomalous climatic conditions would favor more frequent intrusions of cool storms from the northern Pacific. In contrast, the warm/dry circulations displace the wintertime storm track farther northward into Canada as a result of the enhanced Alaskan ridge over the western United States.

Interestingly, anomalous circulation patterns associated with the local extremes have clearly identifiable global features (Figure 3). Moreover, the pattern associated with the warm/dry (warm/wet) extreme appears to be a mirror image of the cool/wet (cool/dry) extreme. This indicates there may be two oscillating circulation patterns associated with the atmospheric hydrological and temperature extremes over the west coast of the United States. In other words, the short-term climatic extremes over the western United States are governed by the variation of large-scale circulation patterns in this model. Since this simulation is performed under fixed external forcing conditions, it is fair to say the variations we found here are due to the intrinsic nonlinear dynamic nature of the atmosphere. We need more thorough analyses to understand the spatial and temporal behavior of these dominant patterns. In particular, we intend to determine how these spatial patterns are associated with the evolving low frequency patterns in the model.

In reality, many external forcings (*eg*, sea surface temperature variations) will interfere with the evolution of these anomalous circulations. However, studies of a simplified atmosphere should prove helpful in better understanding and ultimately predicting hydrological extremes in California and elsewhere.

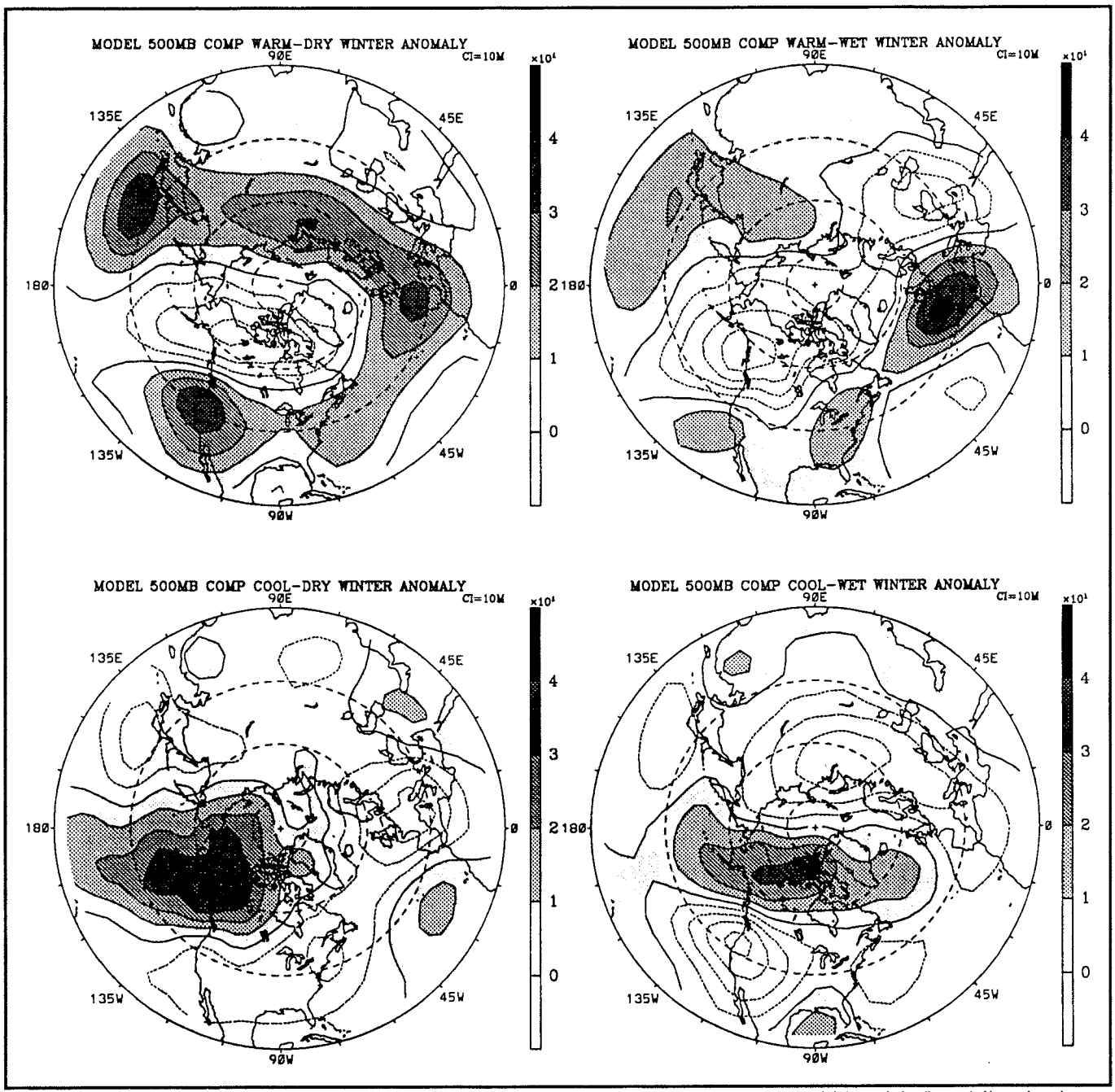

Figure 3. Composite 500-mb height anomalies for winter-mean extremes, warm-dry (upper left), warm-wet (upper right), cool-dry (lower left), and cool-wet (lower right). The contour interval is 10 meters, and positive values are shaded.

References

Cayan, DR, 1990. Cool vs. warm winter precipitation and its effect on streamflow in California. J. Betancourt (ed.), *Proceedings of the 7th Annual PACLIM Workshop.*

Chen, S-C, and JO Roads, 1989. Winter simulation in a simplified NMC spectral model with empirically-determined forcings. *Proceedings of the 14th Annual Climate Diagnostics Workshop.* La Jolla, CA, Oct. 16-20, 1989.

_____, 1988, Development of a simplified NMC spectral model with empirically-determined forcings, *Proceedings of the 13th Annual Climate Diagnostics Workshop.* Boston, MA, Nov. 1-4, 1988.

Chen, S-C, JO Roads, and J Alpert, 1991. Variability and predictability in an empirically-forced global model. Sumitted to *J. of Atmos. Sci.*

_____, 1990, Warm/wet and cool/wet western U.S. simulations in a general circulation model. *Proceeding of the 15th Annual Climate Diagnostics Workshop.* Ashville, NC, Oct. 29-Nov. 2.

Namias, J, 1991. Spring and summer 1988 drought over the contiguous United States — causes and prediction. *J. Climate.* 4:54-65.

Trenberth, KE, GW Branstator, and PA Arkin, 1990. Origins of the 1988 North American drought. *Science.* 242:1640-1645.

Anomalies in North American Climate: The South Asian-Tropical West Pacific Connection

Tom Murphree, Jeng-Ming Chen, and Pat Harr

Abstract: How do tropical heating fluctuations create North American climate anomalies? We propose some answers using the results from a simplified global atmospheric model. We find that the South Asian-tropical west Pacific area is especially effective at stimulating North American responses. The relatively strong tropical/extratropical interaction between these two areas is the result of two major processes acting on the Rossby wave signal induced by the tropical heating fluctuations. These factors are:

- Wave guiding by the Asian-north Pacific subtropical jet; and
- Wave amplification within unstable regions on the jet flank.

These factors allow relatively small, remote, and short-term tropical fluctuations to have relatively large impacts on North American climate.

Introduction

The extratropical atmosphere is sensitive, over a range of time scales, to fluctuations in tropical atmospheric heating. The extratropical north Pacific/North American (PNA) area seems to be especially responsive to tropical forcing. Thus PNA climate variations are often linked to tropical heating anomalies. However, the mechanisms behind tropical-extratropical interactions are still poorly understood. The major problem is that the atmospheric environment in which the interactions occur is a complex and active medium. Thus the complicated signal propagation and amplification properties of the ambient atmosphere must be considered.

We present a study of some of the mechanisms involved in tropical-extratropical interactions. We focus on short-term summer PNA variations associated with tropical heating anomalies and, in particular, anomalies in the south Asian-tropical west Pacific area. The interaction mechanisms studied are those that occur in a simplified global atmospheric model. Observational analyses provide qualitative support for the simplified model results (Harr *et al* 1991).

The Model

The simplified model used is based on the nonlinear shallow water equations on a global spherical domain. The equations are spectrally formulated with rhomboidal-25 truncation, giving a resolution of 2.8° latitude, 4.7° longitude. The equivalent depth is 2000 meters, which means the model waves have a relatively deep internal mode structure. The ambient atmospheric conditions are taken from the European Centre

In K.T. Redmond, Editor, 1992. Proceedings of the Eighth Annual Pacific Climate (PACLIM) Workshop, March 10-13, 1991: California Department of Water Resources, Interagency Ecological Studies Program Technical Report 31.

for Medium-range Weather Forecasting (ECMWF) monthly mean analyses for 1979-1987 at 200 mb, with full horizontal variation retained. A steady forcing is applied that maintains the wavy initial state of the model atmosphere in the absence of any anomaly forcing. Dissipation is applied in the form of:

- Relaxation back toward the climatological initial conditions on a 15-day time scale; and
- Biharmonic diffusion.

To produce anomaly solutions, a steady anomaly forcing is applied to the geopotential equation. This forcing is localized in the tropics and simulates one or more heating disturbance in the tropical troposphere. Peak forcing is at the center of the forcing and is equivalent to 3.5 K/day heating. The model with perturbation forcing is integrated to a steady state, which is reached within 20-60 model days. The model response to the tropical forcing is defined as the anomaly solution minus the solution without such forcing.

Simulations of the June 1988 Drought

In June 1988 the observed tropospheric geopotential height anomaly field (Figure 1a) showed a marked positive PNA pattern. A positive PNA pattern has height anomalies that are approximately: low over the northeast Pacific, high over North America, and low over the western north Atlantic. A negative PNA pattern would be the same, except for reversed signs (*cf.* Wallace and Gutzler 1981). The positive height anomaly over North America was a dynamical representation of drought conditions observed in June 1988. In addition to the PNA pattern, the June 1988 height anomalies showed a distinct pattern of anomalies of about zonal wave number five stretching across the north Pacific and around the globe at about 45N-60N.

The tropical heating anomalies that may have been influential in developing these height anomalies are implied by the tropical outgoing longwave radiation anomalies (OLRA) for June 1988 (Figure 1b). These show a complex pattern of both anomalous heating and cooling throughout the tropics. The largest and most intense OLRA during June 1988 was a negative one in the west Pacific, corresponding to unusually high tropical cyclone activity. Another prominent negative OLRA is in the east Pacific. This OLRA corresponds to the east Pacific heating anomaly focused on in some other studies of the June 1988 North American drought (*eg*, Trenberth *et al* 1988). (Note: *Negative* OLRAs imply *positive* tropospheric heating anomalies.)

As a case study, we have used the simplified model with a climatological June ambient state to examine the role of these tropical anomalies in forcing the PNA height anomalies. Figure 2 shows model responses to approximations of these two OLRAs in a June ambient flow. Both the

Figure 1. Observed June 1988 anomalies from *Climate Diagnostics Bulletin*, June 1988.

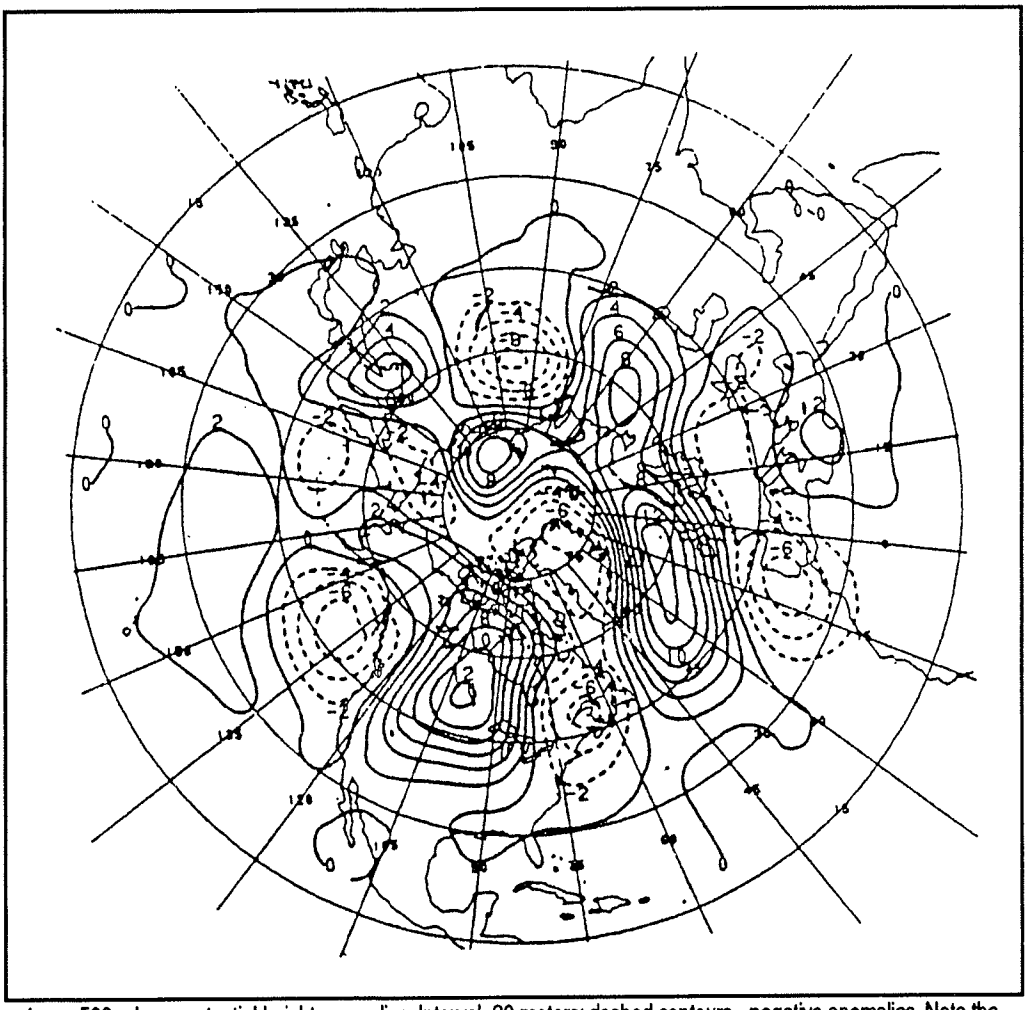

1a — 500-mb geopotential height anomalies. Interval=20 meters; dashed contours= negative anomalies. Note the PNA pattern and zonal wave number five pattern.

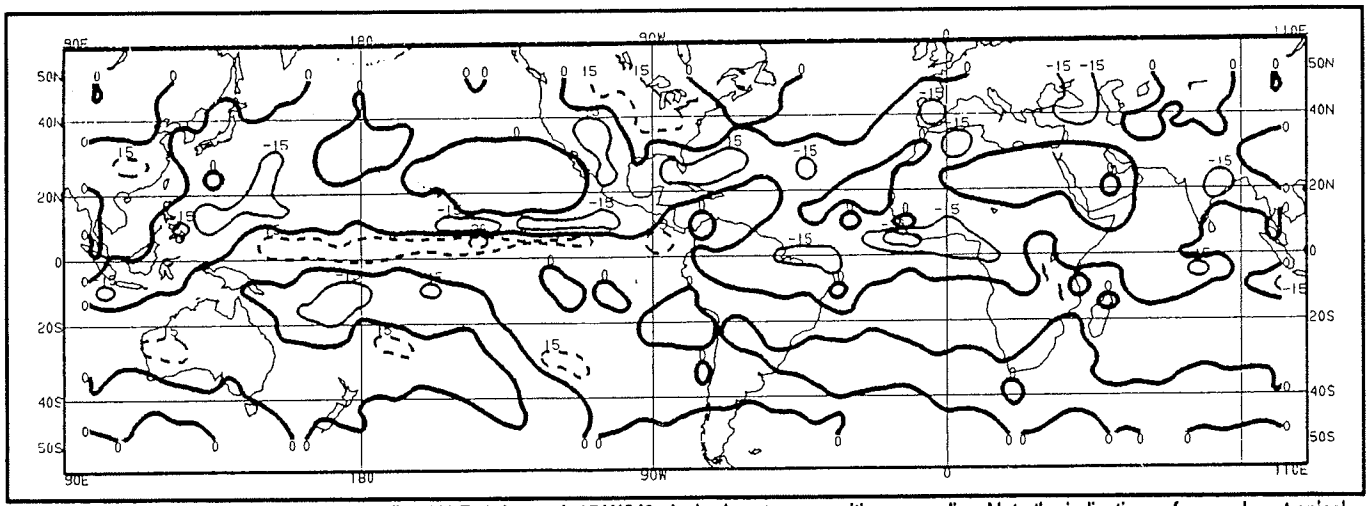

1b — Outgoing longwave radiation anomalies (OLRA). Interval=15 W/M2; dashed contours=positive anomalies. Note the indications of anomalous tropical heating where the OLR anomalies are negative (solid contours); for example, in the tropical west Pacific.

west and east Pacific forcings produce reasonable simulations of the observed anomalies over much of the north Pacific, North America, and north Atlantic (Figure 2a,b). The simulation is improved when both of these forcings are included (Figure 2c). In particular, the phase of the low-high-low pattern across North America is improved by including both forcings. The responses to other forcings representative of the June 1988 tropical OLRAs show that most give either a positive or a negative PNA pattern, depending primarily on their sign and longitude.

A useful diagnostic tool for interpreting the energetics of these response patterns is the quasi-geostrophic wave activity flux vector developed by Plumb (1985). The vector length shows the intensity of the wave activity; the vector direction shows the wave energy propagation direction; and the vector divergence (or convergence) shows wave activity sources (or sinks). Because these vectors are calculated from a quasi-geostrophic approximation of a wave field, they do not necessarily give a realistic impression of the wave flux *within* the tropics (10S-10N, say). However, *beyond* the tropics, the vectors can give a useful picture of any Rossby wave activity that has arisen due to ageostrophic processes.

The horizontal components of the wave activity flux vectors corresponding to the responses of Figure 2 are shown in Figure 3. The vectors for the west Pacific forcing (Figure 3a) show some northward and eastward propagation out of the forcing area, with zonal propagation along and south of the jet into North America. Near the jet exit, the vector divergence indicates an amplification of wave energy. However, the largest energy source is in the subtropical eastern Pacific, where the vectors are strongly divergent. This part of the Pacific is also the downstream end of a region of potential barotropic instability (in the Rayleigh-Kuo sense). Thus the response to the west Pacific forcing seems to depend on the extraction of energy from the unstable ambient jet (*cf.* Peng and Williams 1986; Crum and Stevens 1990). From this east Pacific area, energy propagates southeastward into the tropics, as well as eastward and northeastward into North America.

The flux vectors for the east Pacific forcing (Figure 3b) show a large propagation of energy from both the forcing area and the unstable subtropical east Pacific area. The flux from the jet exit is much weaker than for the west Pacific forcing case. The northward component of the energy flux into North America is more pronounced for this case than for the west Pacific forcing case. Farther downstream, off the east coast of the United States, there is a marked equatorward component of propagation.

These model results show remote and relatively localized and short-term variations in tropical heating may affect PNA height variations. In particular, the results show heating anomalies in the south Asian and tropical west Pacific areas may have an especially large impact. Such heating anomalies might include intraseasonal variations of the Asian

Figure 2. Model geopotential height responses to idealizations of the tropical west and east Pacific tropical forcings observed in June 1988 for a climatological June ambient state.
Interval = 4m, zero contour omitted. Forcing centers indicated by plus signs.

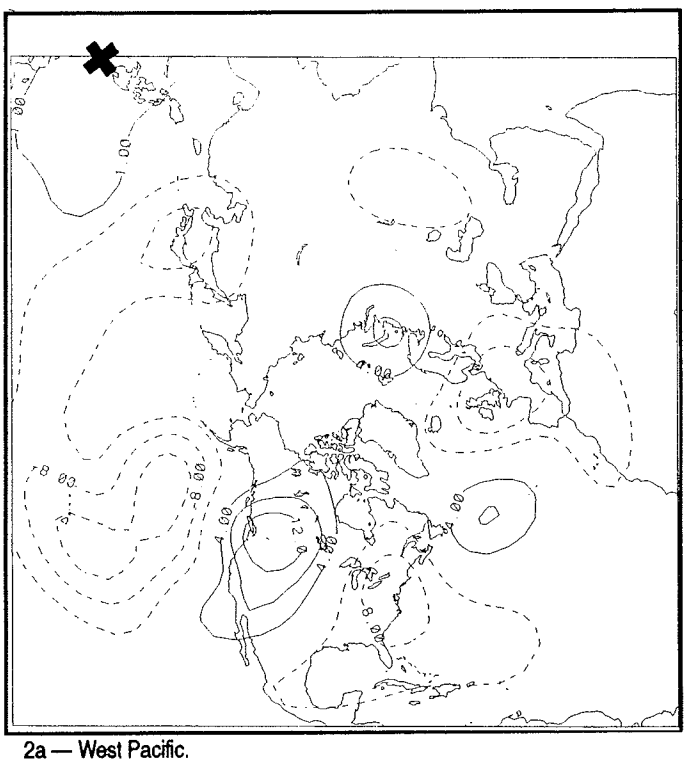

2a — West Pacific.

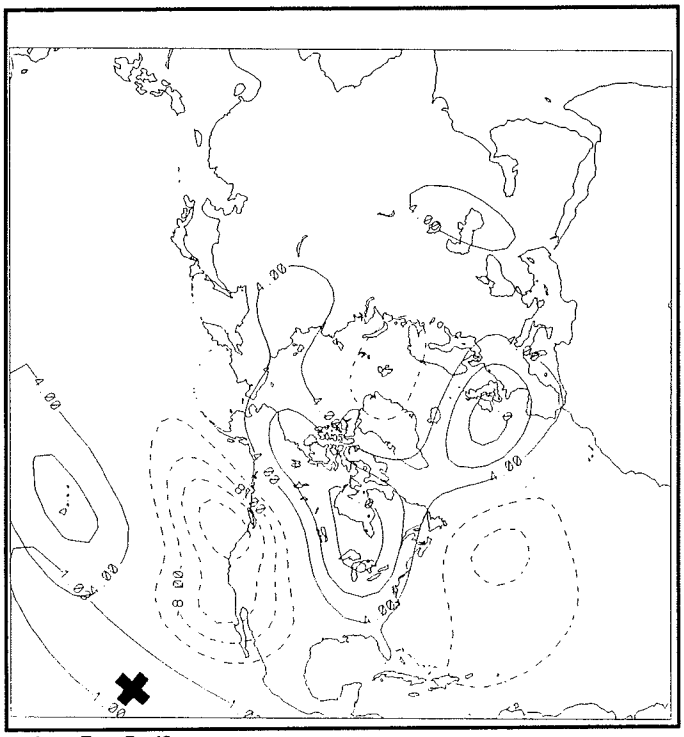

2b — East Pacific.

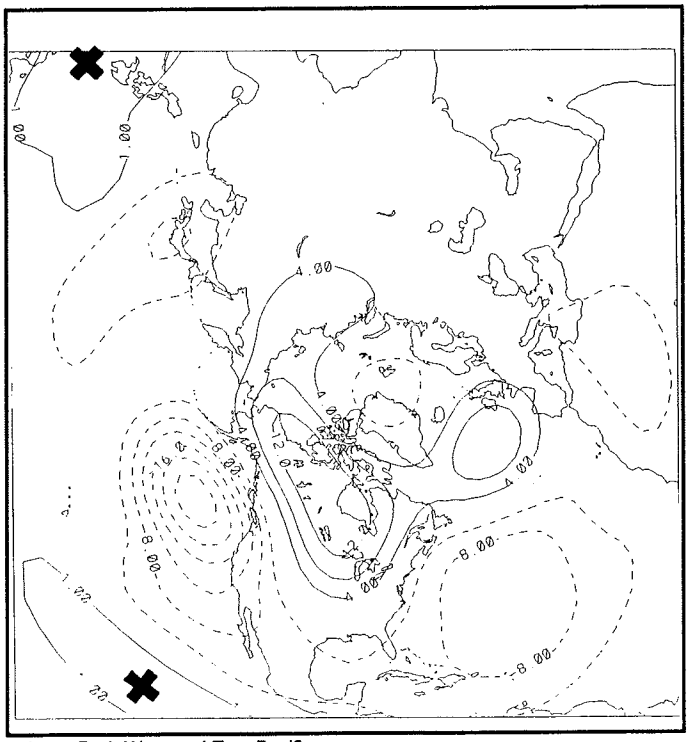

2c — Both West and East Pacific.

Figure 3. Wave activity flux vectors (Plumb fluxes) for responses shown in Figure 1(a,b).
Heavy curve shows jet axis (>30 m/s). Closed curves show subtropical areas of potential barotropic instability. Note the waveguiding by the jet and the large energy sources at the jet exit and at the downstream end of the Asian/north Pacific unstable area.

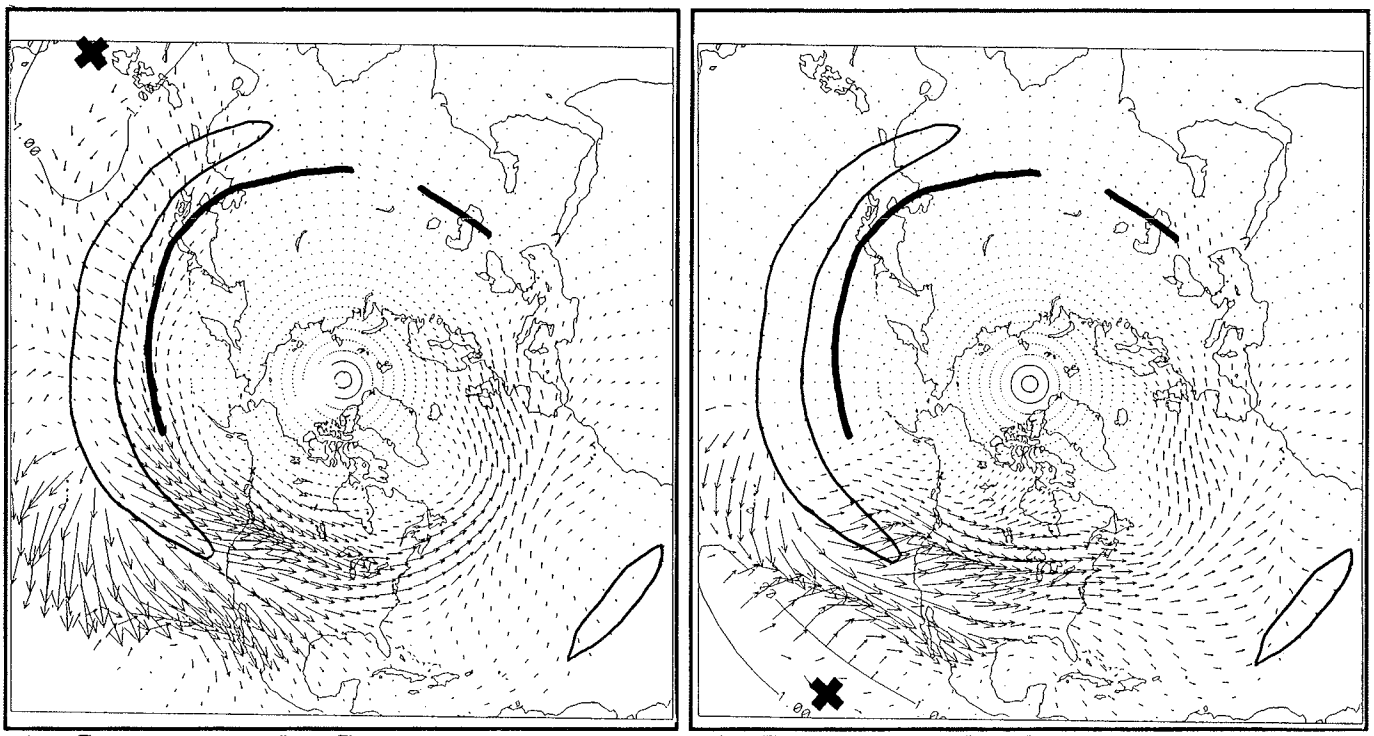

3a — Flux vectors corresponding to Figure 2a.

3b — Flux vectors corresponding to Figure 2b.

monsoon or of west Pacific tropical storm activity. Our observational analyses of tropical-extratropical interactions associated with variations in west Pacific typhoon activity support the basic conclusions of the simplified model (Harr *et al* 1991). This typhoon variability is itself related to tropical intraseasonal oscillations.

These basic conclusions also apply, in large part, to our studies of interactions during the northern winter. One example of a winter result from the simplified model is shown in Figure 4. In this case, a positive tropical forcing is placed just east of Sri Lanka, leading to a strong PNA pattern. The flux vectors show a clear propagation of energy along the jet, with poleward and equatorward propagation near the jet exit. The strongest energy sources are in the subtropics and well to the east of the tropical forcing.

Figure 4. Model height (a) and the corresponding Plumb fluxes (b) for a climatological January ambient state and a forcing centered just east of Sri Lanka (at 7N, 37E, just outside of plot frame).

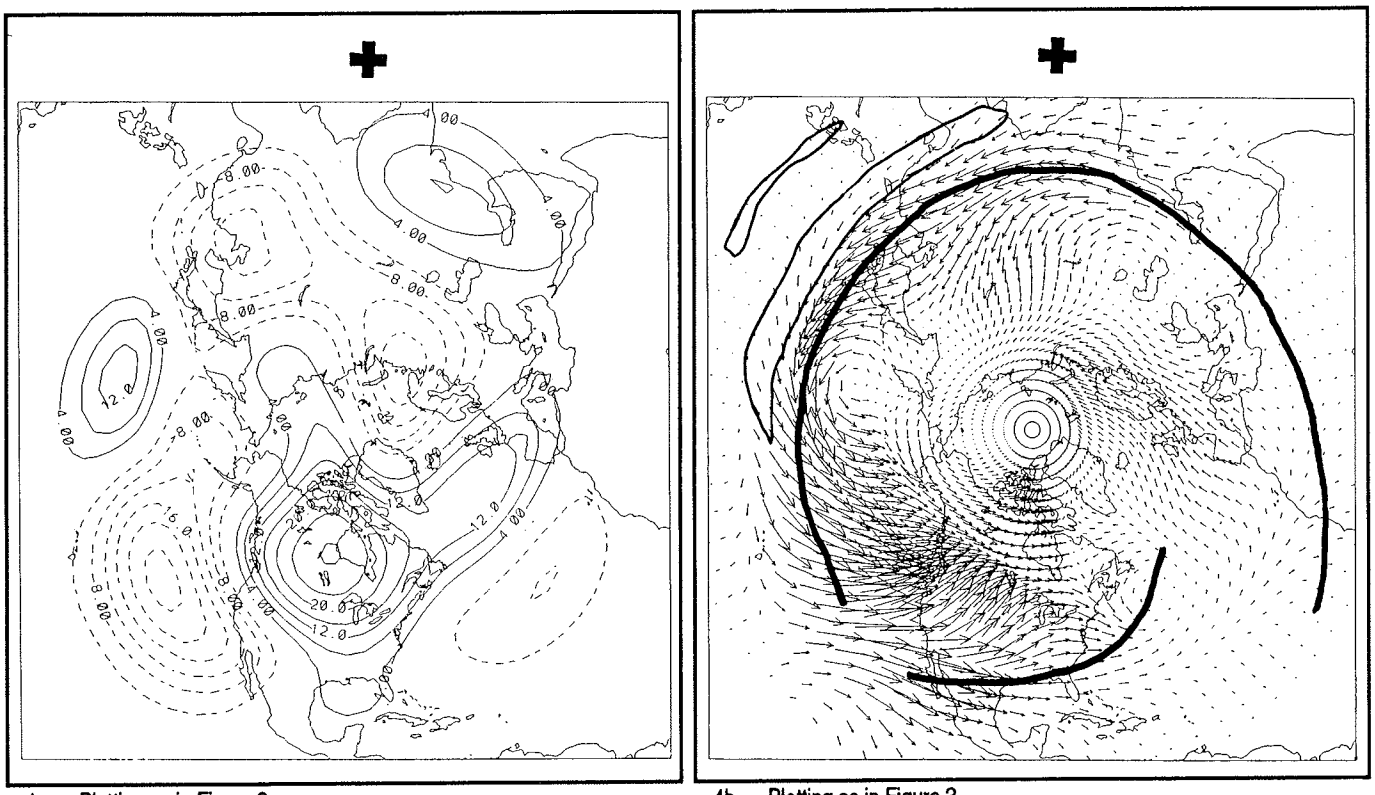

4a — Plotting as in Figure 2.

4b — Plotting as in Figure 3.

Summary

These results show that widely separated forcings can produce similar PNA responses. Thus PNA patterns are, in general, complex interference patterns arising from both nearby and remote forcings. The results also show that the mechanisms by which a tropical forcing influences conditions in the PNA area depend on the location of the forcing within the ambient flow. The wave-guiding and amplification features of the ambient flow, in particular the Asian-north Pacific jet, tend to organize the responses to widely separated forcings over the PNA area. The high sensitivity of the PNA area comes from its location downstream (in a wave propagation sense) of the subtropical north Pacific wave-guide and amplification regions for Rossby waves. The PNA area is especially responsive to south Asian-tropical west Pacific heating anomalies because these anomalies occur at the upstream end of the wave-guide and amplification areas.

A schematic picture of how remote forcings may exert a large influence in the PNA area is shown in Figure 5. Note that both wave-guiding and amplification on the unstable jet flank are important in producing a PNA response to remote forcing. Figure 5 also shows a southward propagation of energy out of the jet exit and into the Southern Hemisphere. Other model results (not shown) indicate model responses in the eastern tropical Pacific and the southeast Pacific-South American area may be

related to energy propagating from the north Pacific jet exit. This may explain the high perturbation kinetic energy observed in the eastern tropical Pacific (Murakami and Unninayer 1977) and some Southern Hemisphere teleconnection patterns (*cf*, Park and Schubert 1991).

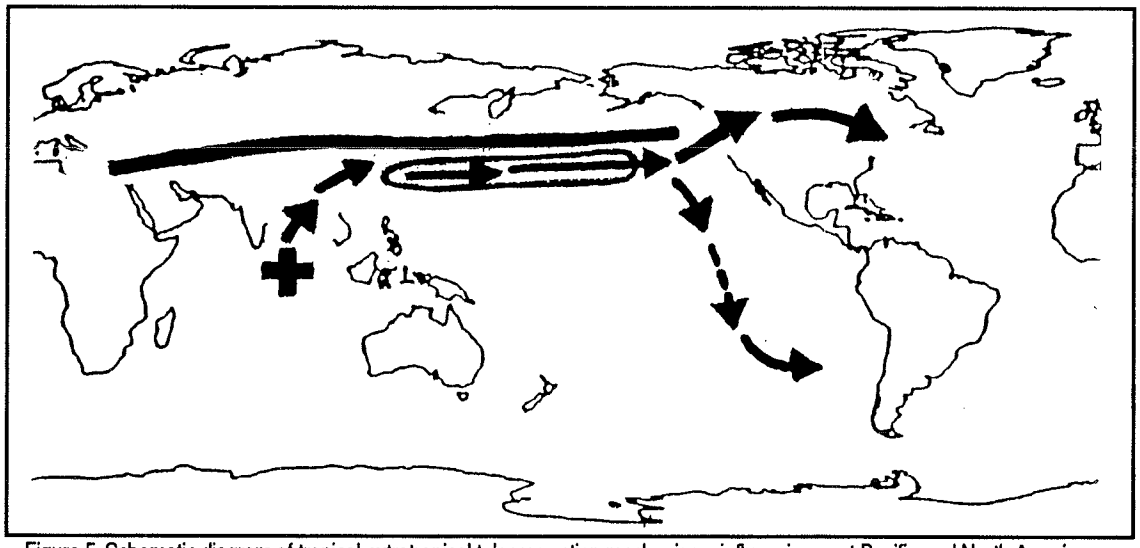

Figure 5. Schematic diagram of tropical-extratropical teleconnection mechanisms influencing east Pacific and North American areas. Plus symbols = tropical heating anomaly; Arrows = Rossby wave energy propagation; Heavy line = jet axis; Closed curve = subtropical area of barotropic instability. The overall chain of events is: (1) poleward propagation out of heating anomaly; (2) waveguiding of energy along jet and through subtropical unstable area; (3) amplification of wave response all the way through the unstable area; and (4) poleward and equatorward propagation at jet exit and at downstream end of unstable area.

References

Crum, FX, and DE Stevens, 1990. Barotropic instability with downstream and asymmetric cross-stream variations: idealized calculations. *Journal of the Atmospheric Sciences*. 47:5-23.

Murakami, T, and S Unninayer, 1977. Atmospheric circulation during December 1970 through February 1971. *Monthly Weather Review*. 105:1024-1038.

Harr, P, J-M Chen, and T Murphree, 1991. The relationship of western Pacific monsoon and tropical cyclone activity to North Pacific and North American climate anomalies. *Proceedings of the Eighth Annual Pacific Climate (PACLIM) Workshop*. March 10-13, 1991.

Park, C-K, and SD Schubert, 1991. Low-frequency intraseasonal oscillations and the Pacific/Atlantic teleconnection. Pages 143-148 in *Proceedings of the Fifteenth Annual Climate Diagnostics Workshop*. October 29-November 2 1990.

Peng, MS, and RT Williams, 1986. Spatial instability of the barotropic jet with slow streamwise variation. *Journal of the Atmospheric Sciences*. 43:2430-2442.

Plumb, RA, 1985. On the three dimensional propagation of stationary waves. *Journal of the Atmospheric Sciences*. 42:217-229.

Trenberth, KE, GW Branstator, and PA Arkin, 1988. Origins of the 1988 North American drought. *Science*. 242:1640-1645.

Wallace, JM, and DS Gutzler, 1981. Teleconnections in the geopotential height field during the northern hemisphere winter. *Monthly Weather Review*. 109:785-812.

The Los Alamos General Circulation Model Hydrologic Cycle

John O. Roads, Shyh-Chin Chen, Chih-Yue Kao,
David Langley, and Gary A. Glatzmaier

Introduction

As the global population has increased, so have human influences on the global environment. From various modeling studies, we know the almost inevitable global rise in CO_2 and other trace gases will cause an increase in global temperature (see, *eg*, Kellogg 1991). Along with this temperature increase, modeling studies have also suggested the global hydrological cycle will intensify and result in increased precipitation and evaporation. This postulated overall intensification of precipitation may not be entirely beneficial. Surface moisture necessary to sustain productive agriculture may still decrease. Dry surface regions may expand to cover larger land areas and, while wet regions may become wetter, they may shrink to smaller areas over the ocean.

A few general circulation model (GCM) sensitivity experiments (*eg*, Manabe and Wetherald 1987) suggest evaporation will intensify over North America and Europe relative to precipitation (even if precipitation increases), resulting in drier mid-latitude continents. However, other GCM sensitivity studies have found the opposite behavior. Meehl and Washington (1988) showed a moister North American continent could result from the intensified hydrological cycle. The difference in sensitivity apparently depends on soil moisture storage, ground water runoff, and spring rainfall and snowmelt, as well as the other components of the heavily parameterized hydrologic cycle.

Observations are consistent with the idea that precipitation and perhaps other components of the global hydrologic cycle are increasing. Roads and Maisel (1991) and Vinnikov *et al* (1990) suggested precipitation over the United States may have increased during at least the past few decades. Bradley *et al* (1987) and Diaz *et al* (1989) further indicated that precipitation appears to have increased in almost all mid-latitude temperate land zones. At the same time, precipitation appears to have decreased over tropical land regions. Over the oceans, the changes are unknown. Observations are also consistent with the idea that soil moisture may, in fact, be increasing. Vinnikov and Yeserkepova (1991) showed there was an increasing trend of soil moisture over most of the Soviet Union and attributed this increasing trend to the increasing trend of precipitation over the region.

In K.T. Redmond, Editor, 1992. Proceedings of the Eighth Annual Pacific Climate (PACLIM) Workshop, March 10-13, 1991: California Department of Water Resources, Interagency Ecological Studies Program Technical Report 31.

Although it is tempting to ascribe recent continental desiccations to greenhouse radiative forcings, droughts have occurred in the past and will occur in the future as the global hydrologic cycle undergoes its natural variations. For example, Trenberth *et al* (1990) and Namias (1991) suggested the 1988 summer drought over the Midwest region of the United States was due to forcings by oceanic and land surface variations rather than to greenhouse radiative forcings. Chen *et al* (1991) suggested even surface forcings may be irrelevant to large interannual variations in the US West Coast hydrologic cycle; the recent California drought was simulated with an atmospheric GCM overlying a fixed ocean and land surface.

How can we better understand and predict these natural and potential anthropogenic variations? One way is to develop a model that can accurately describe all the components of the hydrologic cycle, rather than just the end result variables such as precipitation and soil moisture. If we can predict and simulate variations in evaporation and moisture convergence, as well as precipitation, then we will have greater confidence in our ability to at least model precipitation variations.

Therefore, we describe here just how well we can model relevant aspects of the global hydrologic cycle. In particular, we determine how well we can model the annual and seasonal mean global precipitation, evaporation, and atmospheric water vapor transport. Seasonal variations are about the largest short-term climate variation we can easily observe. If we can globally model these large amplitude variations correctly, we will have greater confidence in our ability to globally model and predict the more subtle variations associated with forced and natural interannual variability.

A prototypical model of the global hydrologic cycle is the Los Alamos GCM (see Kao *et al* 1990), which is a derivative of the original National Center for Atmospheric Research (NCAR) GCM. We compare aspects of the hydrologic cycle in a 10-year simulation with this GCM to global observations. Global observations of the water vapor, water-vapor flux, and water-vapor flux divergence are derived from the National Meteorological Center's final analysis for 1986 to 1990. The new precipitation dataset of Legates and Willmott (1990) is used for global precipitation observations. Global evaporation is derived as a residual of the precipitation and water-vapor flux divergence.

All of the observations can have non-negligible errors. Therefore, the GCM output reciprocally aids in our understanding of the observed hydrologic cycle.

Results

Overall, comparisons between the LANL GCM and observations are quite good. Most of the large-scale features, as described by the moisture flux stream function, moisture flux potential, precipitation potential, and evaporation potential, are quite close. Seasonal cycle variations are quite reasonable. Even smaller scale features, such as the moisture flux convergence, precipitation, and evaporation, are well simulated. We are, in fact, quite pleased with most of the simulation. Certain aspects of the simulation may, therefore, be studied further to determine characteristics of the global interannual variability; interannual variations are much more difficult to examine with the presently incomplete observations.

The most noticeable discrepancy between the GCM and observations is in the moisture field itself, which is too small because of a cold bias. This cold bias is smallest in the lower troposphere. However, the dry bias is spread more evenly throughout the troposphere, because of the exponential variation of moisture with temperature. Moreover, the dry bias is really only noticeable in the rotational fluxes. The divergent moisture fluxes are only slightly larger for the slightly more intense GCM hydrologic cycle. Thus, we are almost certain that the GCM dry bias does not have a large impact on the perceived global atmospheric hydrology. Still, we are concerned about a misplaced South Pacific convergence zone over Australia; also nearby is the Indonesian archipelago that has some of the largest values for precipitable water and precipitation in the world. If values in this region are incorrect, these errors may have had wide ramifications elsewhere and may be related to the misplaced South Pacific convergence zone in the GCM. Therefore, it is possible that correction of this GCM dry bias will result in substantial improvements in the GCM's hydrologic cycle here and elsewhere. We are also concerned about the misplaced summertime moist convergence and precipitation over the United States. In essence, both large- and small-scale errors probably need to be corrected so we can have utmost confidence in the ability of this GCM to globally simulate interannual variability.

In any event, there was relative summertime continental dryness in the mid-latitude regions of this model, which is consistent with previous GCM studies. However, the dryness was less, presumably because a 2-bucket model was used here, which may be more realistic. There was also summertime soil moisture saturation in the tropical regions of the model; the opposing soil moisture tendencies are related to monsoon precipitation regimes and global moisture convergence. It is plausible that part of the currently observed mid-latitude precipitation and soil moisture trend is due to a change in moist convergence; that is, more moisture may currently be transported into middle latitudes from tropical latitudes, resulting in increased precipitation in middle latitudes and decreased precipitation in lower latitudes. However, this global variation could be part of the natural variability of the large-scale global hydrologic

cycle that is masking a potentially more ominous trend. It is incumbent upon us to learn more about these and other variations in the hydrologic cycle from both observations and models. We will investigate such questions, once we have fixed some of the more serious discrepancies in this GCM's hydrologic cycle.

Further details of this study can be found in Roads *et al* (1991).

References

Bradley, RS, HF Diaz, JK Eischeid, PS Jones, and PM Kelly, 1987. Precipitation fluctuations over Northern Hemisphere land areas since the mid-19th century. *Science.* 237:171-175.

Chen, S-C, DR Cayan, and JO Roads, 1991. Simulation of the California drought. *Science.* To be submitted.

Diaz, HF, RS Bradley, and JK Eischied, 1989. Precipitation fluctuations over global land areas since the late 1800s. *J. Geophys. Res.* 94:1195-1210.

Kao, C-Y, GA Glatzmaier, and RC Malone, 1990. Global three-dimensional simulations of ozone depletion under postwar conditions. *J. Geophys. Res.* 91:1039-1053.

Kellogg, WW, 1991. Response to skeptics of global warming. *Bull. Amer. Meteor. Soc.* 72:499-511.

Legates, DR, and CJ Willmott, 1990. Mean seasonal and spatial variability in gauge-corrected global precipitation. *International Journal of Climatology.* Vol. 10, pp. 111-127.

Manabe, S, and RT Wetherald, 1987. Large-scale changes of soil wetness induced by an increase in atmospheric carbon dioxide. *J. Atmos. Sci.* 44:1211-1235.

Meehl, GA, and WM Washington, 1988. A comparison of soil-moisture sensitivity in two global climate models. *J. Atmos. Sci.* 45:1476-1492.

Namias, J, 1991. Spring and Summer 1988 Drought over the Contiguous United States — Causes and Prediction. *J. Climate.* 4:54-65.

Roads, JO, S-C Chen, J Kao, D Langley, and G Glatzmaier, 1991. Global aspects of the Los Alamos general circulation model hydrologic cycle. *J. Geophys. Res.* Submitted.

Roads, JO, and TN Maisel, 1991. Evaluation of the National Meteorological Center's medium range forecast model precipitation forecasts. *Wea. & Forecasting.* 6:123-132.

Trenberth, K, GW Branstator, and PA Arkin, 1990. Origins of the 1988 North American drought. *Science.* 242:1640-1645.

Vinnikov, KY, PY Groisman, and KM Lugina, 1990. Empirical data on contemporary global climate changes (temperature and precipitation). *J. Climate.* 3:662-677.

Vinnikov, KY, and IB Yeserkepova, 1991. Soil moisture: Empirical data and model results. *J. Climate.* 4:66-79.

High-Resolution Computation of Isotopic Processes in Northern California Using a Local Climate Model

Richard G. Craig, Neil L. Ingraham, and John F. Stamm

Abstract: We describe a coupled local climate/isotope model that can calculate Rayleigh-type processes of distillation and fractionation of hydrogen isotopes along individual air mass flowlines in the western United States. The climate model is an extension of that detailed earlier by Craig and Stamm (1990). The isotope calculations are a more spatially detailed application of the stepwise Rayleigh-process equation of Rozanski *et al* (1982). Volumetric effects of evapotranspiration (ET) are included. The model allows sensitivity studies of the influence of ET recycling.

This model is applied to evaluate the applicability of a hypothesis, formulated by Yonge *et al* (1989) for British Columbia, that observed δD can be explained by a simple single-stage Rayleigh process without the need to incorporate the effects of ET. We find that no values of vapor flux provide a plausible representation of the data when ET rate is zero, and no ET rate provides a plausible fit to the data when that rate is held constant throughout the traverse studied. Our results support the hypothesis of Ingraham and Taylor (1991) that several distinct ET regimes exist and that, beyond about 50 km inland, ET recycling is an important element of the isotopic budget. The combination of a spatially detailed climatic model with observational data on δD can help to constrain important hydrologic parameters.

Introduction

Evapotranspiration (ET) is perhaps the least understood component of the hydrologic cycle (Brutsaert 1982); nevertheless, its effect can dominate the hydrology of western North America. Stable isotopes of water have proven to be effective tools for understanding and characterizing other components of hydrologic systems. Thus, for example, the nature and degree of depletion by rain-out — the "Continental Effect" of Friedman *et al* (1964) — is interpreted in terms of increasing depletion of the heavier isotope (*eg* deuterium, D) as larger fractions of precipitation are extracted from the atmosphere. The effect of evapotranspirational recycling on the stable isotopic ratios of inland meteoric water represents one potential source of information that can help to quantify that component in western North America; however, these effects have not been conclusively quantified. Such quantification would require computing the geographic variations of δD along an atmospheric flow path (Rozanski *et al* 1982). The erratic variations of climate due to orographic effects have precluded such efforts to date.

Several researchers have used the geographic variation in stable isotopic ratios in meteoric water along transport paths as a tool to determine the amount of terrestrial recycling. Rozanski *et al* (1982) computed stable

In K.T. Redmond, Editor, 1992. Proceedings of the Eighth Annual Pacific Climate (PACLIM) Workshop, March 10-13, 1991: California Department of Water Resources, Interagency Ecological Studies Program Technical Report 31.

isotopic evolution of air masses crossing central Europe assuming westerly transport across a coarse grid (5°x10°) with a stepwise Rayleigh distillation:

$$R(p)_i = \alpha_i R(v)_{i-1} f_i^{\alpha\,(i)-1} \qquad (1)$$

where:

$R(p)_i$ =isotopic ratio of precipitation in cell i,
$R(v)_{i-1}$ =isotopic ratio of water vapor in upwind cell,
α_i =fractionation factor in cell i,
f_i =fraction of vapor remaining within cell *i*,

including the effects of winter precipitation and summer ET.

Rozanski *et al* (1982) found evaporative recycling to be volumetrically important in defining isotope ratios. They concluded that variations in local precipitation were primarily controlled by upwind regional-scale precipitation/ET events modified only slightly by local temperature fluctuations.

Rindsberger *et al* (1983) (see also Leguy *et al* 1983) demonstrated empirically that distinct trajectories (terrestrial versus oceanic) produce detectable differences in the isotopic composition of precipitation in Israel. Salati *et al* (1979) attributed a depletion in $\delta^{18}O$ of 0.075 per mil/100 km in precipitation of the Amazon Basin to a large contribution of moisture recycled by ET. Gat and Matsui (1989) have recently analyzed the ratio of evaporation to transpiration in the Amazon Basin using a steady-flux model incorporating deuterium excess values (defined as $d=\delta D - 8\ \delta^{18}O$). The lack of geographic variation in the stable isotope ratios of ground water has been explained as representing a closed hydrologic system (Ingraham and Taylor 1986, 1991). However, Salati *et al* (1979) found a lack of geographic variation in an open system where extreme ET recycling nourishes downwind precipitation.

Not all researchers have observed the influence of ET on the stable isotopic ratios of inland meteoric waters. Smith *et al* (1979) compared isotopic composition of precipitation in California and western Nevada to isotopic fractionation in a pseudo-adiabatically rising air mass. However, their analysis neglected possible precipitation over the ocean prior to reaching the coast and did not assess upwind ET recycling of water. Yonge *et al* (1989) modeled the stable isotopic ratios of surface waters across western Canada to the Great Divide (over 500 km distance inland) in terms of a single-stage Rayleigh distillation curve and concluded that precipitation west of the Divide did not appear to be greatly affected by ET.

When δD values reported by Ingraham and Taylor (1986, 1991) for the surface and shallow ground water are plotted *vs.* distance from the Pacific Ocean, distinct segments of isotopic depletion are discernible. The isotopic depletion within each segment appears regular on a large scale,

and each segment is continuous with the next. Coastal segments display linear depletion trends of various slopes, while those representing the Great Basin, a vast area of interior drainage, show little further decrease in δD with distance from the coast.

The differing isotopic characteristics of the "trends" were interpreted (Ingraham and Taylor 1986, 1991) as indicating distinct hydrologic regimes that correlate with relative differences in the vertical fluxes of meteoric water estimated from measured ET and precipitation. The two continental segments appear to require terrestrial recycling of meteoric water to explain the geographic variation in δD of inland meteoric water. This hypothesis motivates the current study, wherein we provide quantitative measures of the impact of terrestrial recycling on δD. An important question, which we address here, is whether single-stage Rayleigh processes can explain the observed variation of δD as suggested by Yonge *et al* (1989). Because of the difficulty of computing ET directly, we choose an alternative strategy and specify ET as a fixed fraction of precipitation. This provides a first order estimate of the effects of evaporative recycling on the isotope signature.

Method

We use a coupled climate/isotope model to predict the stable isotopic composition of meteoric water along a transect across northern California. The climate model (Craig and Stamm 1990) considers wind flowlines, temperature, and amount of precipitation when determining the climate at a specific location. By extending the climate model to compute the effect of Rayleigh processes (Rozanski *et al* 1982) on stable isotopic ratios in meteoric waters, we can study their variations along the atmospheric flowline at a level of detail (10 km) where the isotopic variation within a grid cell is negligible. In this way we can estimate the impact of terrestrial recycling on the stable isotopic ratios of inland meteoric water.

We compute total precipitation and maximum temperature in a mountainous region with important orographic effects by use of a statistical semi-Lagrangian computation of climatic variables calibrated from a canonical analysis of the instrumental record (Craig and Stamm 1990). The model is formulated to represent the physical influence of orographic processes through surrogate measures (*eg*, height the air mass rises over orographic barriers upwind). The grid spacing is sufficiently fine to represent orographic variations within the area and so that variation of Rayleigh processes within a grid cell is negligible. This model also provides temporal detail on the climate variables at a monthly scale.

Our method of isotopic analysis follows closely that of Rozanski *et al* (1982). We differ in using a grid spacing almost two orders of magnitude more fine. Also, whereas Rozanski *et al* could use 10-year averages of observational data to define the climate of their large grid boxes, such data are not available at the scale needed to represent orographic

influences in western North America. Thus, we use estimates of mean monthly temperature and precipitation derived from the climate model calibrated with 5-year averages of instrumental data. As did Rozanski *et al*, we assume isotopic enrichment during ET is negligible. Although this may be a poor approximation on an annual basis in our study area, we feel this assumption is allowed in an initial investigation such as this when attention is confined to the wet season and for the application we report. Rozanski *et al* (1982) also assumed atmospheric transport was zonal throughout the year. We restrict our assumption to the wet season and suggest that observational data support this assumption as a first order approximation (Figure 1).

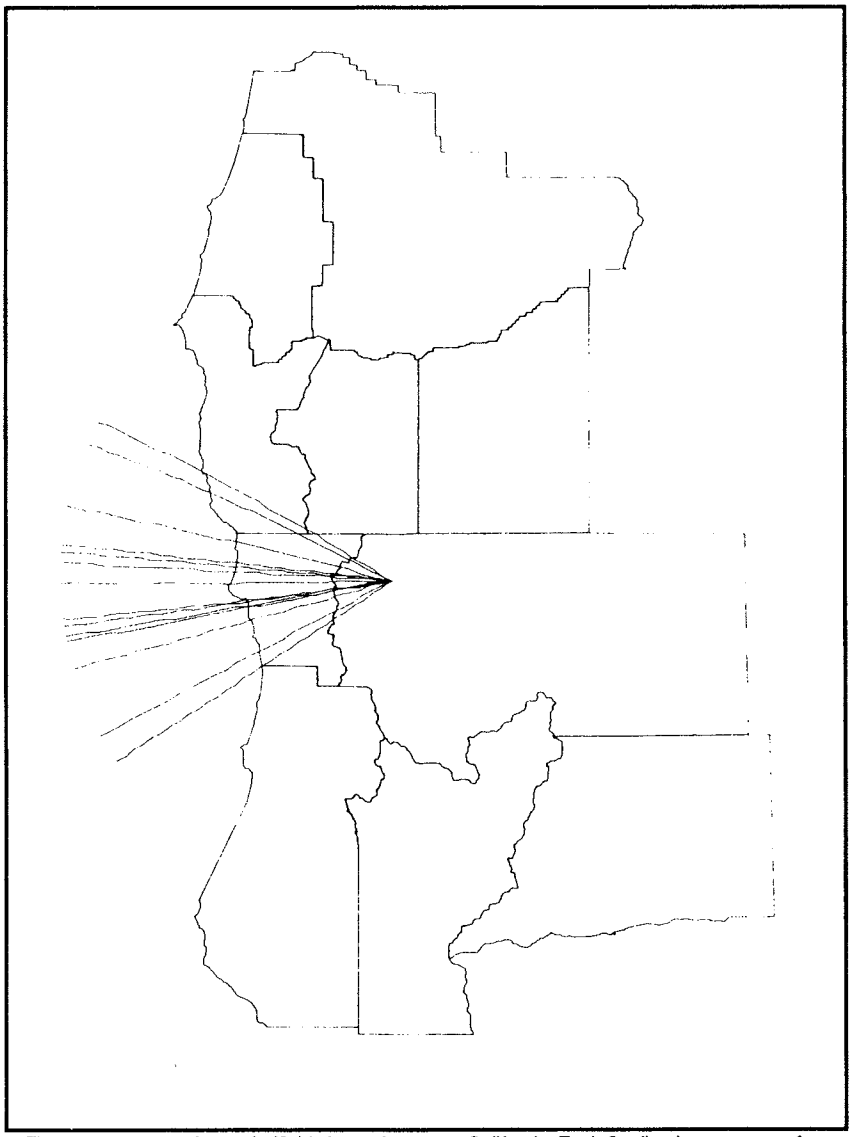

Figure 1. Average winter windfields in northwestern California. Each flowline is an average for December to March from 700-mb observational data of the National Meteorological Center from 1975 to 1988. Point of convergence is Happy Camp, Siskiyou County, California. County outlines provide orientation.

The climate in this region is essentially bimodal, with a cool wet season and a hot dry season (Court 1982). We have chosen to model the isotopic processes for only the wet season. We define the wet season as November through March. Both observational data (for example, Court 1982) and model results (Figure 2) show about 75% of precipitation falls during this period. We assume isotopic processes here are dominated by the continental effect during the wet season, and we focus on deriving estimates of degree of depletion of precipitation that are consistent with the observed depletion of surface water samples. Thus, we acknowledge that isotopically important processes can operate during the dry season, but we assume their effect will be to enrich the surface water.

To illustrate these calculations, we select a traverse at the same latitude (~41°30'N) as Traverse I of Ingraham and Taylor (1991)

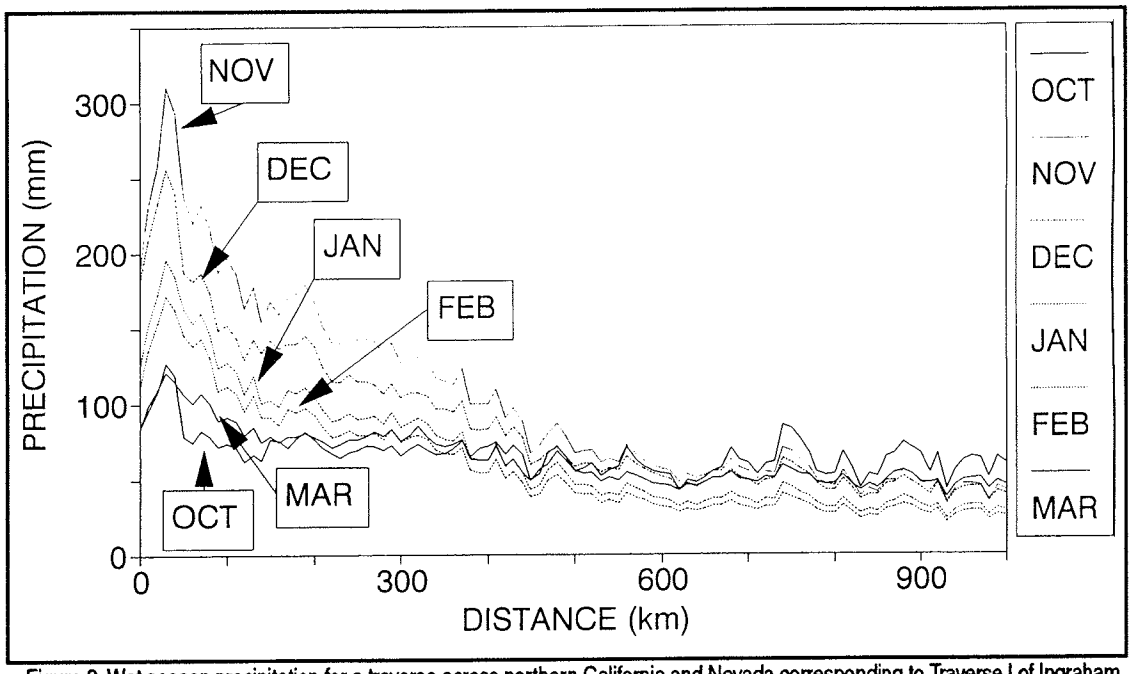

Figure 2. Wet season precipitation for a traverse across northern California and Nevada corresponding to Traverse I of Ingraham and Taylor (1991). These curves represent model solutions of monthly total precipitation.

and extending 400 km from the coast. This traverse corresponds closely to the average atmospheric flowlines of upper level air masses during the wet season in this area (Figure 1). We use the local climate model of Craig and Stamm (1990) to compute monthly temperature and precipitation at each (10x10 km) grid cell along this transect. We fix the initial δD of precipitation at the coast (δD_0) as the mean of the values of δD of precipitation observed by Ingraham and Taylor (1991) at that location. Since the climate model is calibrated to estimate the mean monthly value of maximum daily temperatures, we reduce that figure by 5°C to estimate mean monthly average daily temperature (for example, Barry 1981 p. 22).

Rayleigh processes (fractionation and distillation) during formation of precipitation are computed using the equation of Rozanski *et al* (1982). We use the formula of Majoube (1971) to estimate the fractionation factor, α, as a function of temperature during formation of precipitation. All fractionation is assumed to result from vapor-to-liquid phase transitions. We use surface temperature extrapolated to about the 800-mb altitude at the dry adiabatic lapse rate for this computation. ET is computed as a fraction, Φ, of the amount of precipitation at the grid cell during the wet season. That fraction is fixed throughout the traverse but can be varied from one experiment to another. Evaporated water advects downwind to mix in the next grid cell at a velocity, Ω, that can be varied for each experiment but is also constant throughout the transect. Volumetric mixing of isotopic compositions of evaporating and atmospheric vapor is computed at each step. Thus, we assume complete mixing occurs throughout the vertical column (to 325-mb level) within 10 km.

Twenty-one surface and shallow ground water samples from Traverse I of Ingraham and Taylor (1991) were compared to model solutions. The

traverse was aligned parallel to the atmospheric flow path so as to determine maximum changes in isotopic composition in meteoric water as it passes from west to east. The traverse included several physiographic and hydrologic provinces, among them the Great Basin. Shallow ground waters were considered to be the type of sample that best represented average precipitation, being the least sensitive to extreme yearly, seasonal, and intra-storm isotopic variability, yet reflecting the current climate and hydrologic regime.

Iterative Procedure

We first fix the amount of precipitable water, Σ, in the air mass (integrated from sea level to the 320-mb level) at the coast as 10.6 mm water equivalent based on wet season values reported by Court (1982). Σ can be changed, but we kept it at that value for all computations reported here.

ET is expressed as the fraction, Φ, of wet season precipitation that evaporates or transpires during the wet season. We fix Φ as a constant along the entire transect. From this and the previously computed precipitation, P_i, we estimate the amount of surface water evaporated and/or transpired at each cell, i, of the traverse.

$$ET_i = \Phi \times P_i$$

We also fix an initial value for advection velocity, Ω. From Ω and Σ we compute the flux of vapor to the first cell in the traverse. For example, with Ω=3.7 m/sec, the flux is 39 kg m^{-1} sec^{-1}. Using P_i and ET_i, we compute the residual atmospheric vapor volume and isotope ratio in each cell after mixing, and F_v.

Having solved all the hydrologic parameters needed, we next compute the isotopic implications of these fluxes using the equations of Friedman *et al* (1964) and Rozanski *et al* (1982). The resulting predicted isotopic ratios of precipitation are plotted (*eg*, the solid line in Figure 3) and compared to observation (squares and triangles in Figure 3).

Based on this comparison, free parameters (Φ and Ω) may be modified and a new calculation can be completed. These iterations proceed until an acceptable fit is achieved. We assume that at any chosen location, precipitation will be more depleted in D than the ground water, since ground water is subjected to evaporation and isotopic enrichment. This should be true if there is no significant shallow inter-basin flow between the (10x10 km) grid cells, if the system is volumetrically equilibrated, and if all significant isotopic processes are confined to the wet season. Thus, we can use the isotope data in conjunction with the model to search for estimates of Φ and Ω that are consistent with the observations. We next describe a series of experiments leading to our conclusions about such values.

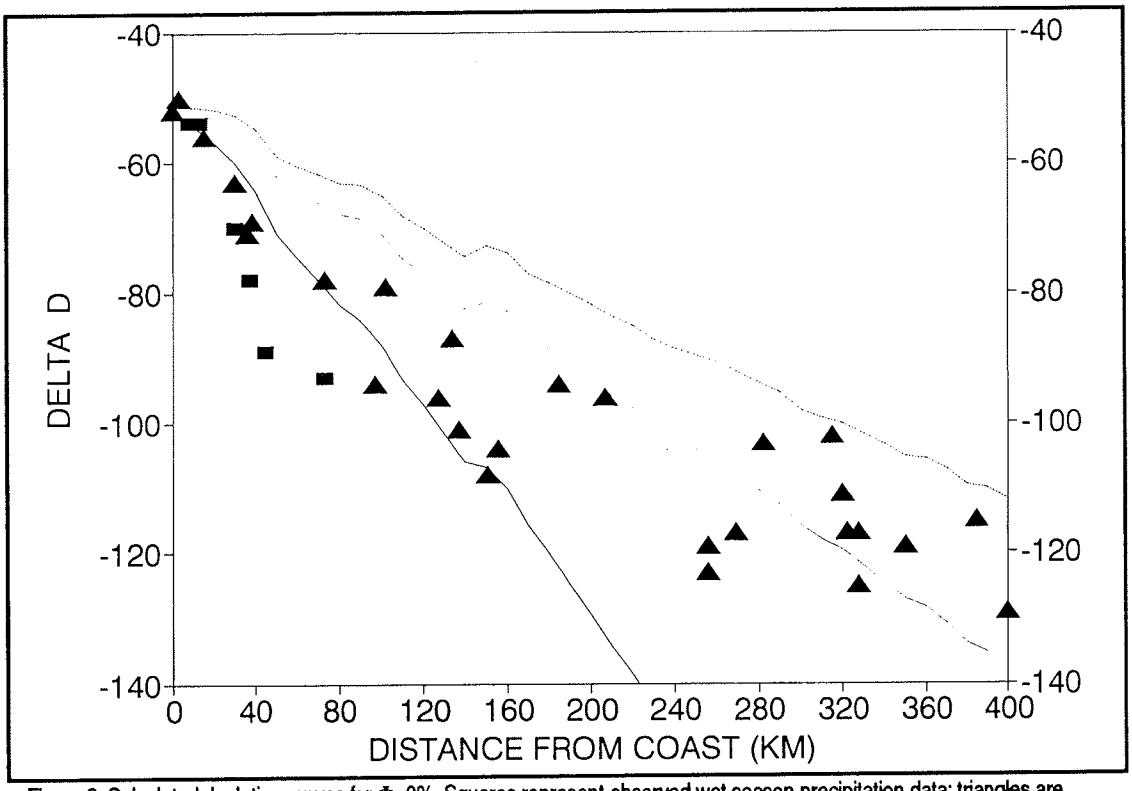

Figure 3. Calculated depletion curves for Φ=0%. Squares represent observed wet season precipitation data; triangles are ground water data of Ingraham and Taylor (1991). (A) Ω=3.7 (top line); (B) Ω=2.0 (bottom line); (C) Ω=3.0 (center line).

Results

Figure 3 shows results for a control experiment (A) in which Ω=3.7 m/sec, about the average 700-mb zonal velocity in this area (Schutz and Gates 1971), and Φ=0.0. Virtually no depletion of the precipitation occurs, and this can only be ascribed to selection of an Ω that is too high to be realistic. We conclude that a lower Ω is more appropriate. After some experimentation, we found that Ωs of the order 2 m/sec provide the closest fit.

Figure 3 shows two additional experiments that bracket what appears to be the most likely range of advection velocities if ET recycling is not considered (*ie*, Φ=0.0). For example, experiment B, with Ω=2.0 yields a curve too depleted relative to the observational data. Experiment C (Ω=3.0 m/sec) illustrates a close fit to the data. The predicted values of precipitation in experiment C are less depleted than observed in the western portion of the traverse and more depleted than observed in the eastern portion.

We note that none of these experiments yields what we consider to be "good" fits to the data. In particular, they all imply continuing depletion of precipitation with increasing distance inland; something that is not seen in the data. We hypothesize that the observed "leveling off" of the isotope record is due, at least in part, to the volumetric effect of evaporative recycling. As moisture is returned to the atmosphere, the rate of

decrease of the volume of water vapor is lessened. The term F_V in Equation (1) does not decrease as fast and, therefore, depletion of precipitated water is less. To test this hypothesis, we perform three experiments (D, E, and F) with Φ set at 20% (Figure 4). In these experiments we consider the effect of varying Ω over a small range when some evaporative recycling is included.

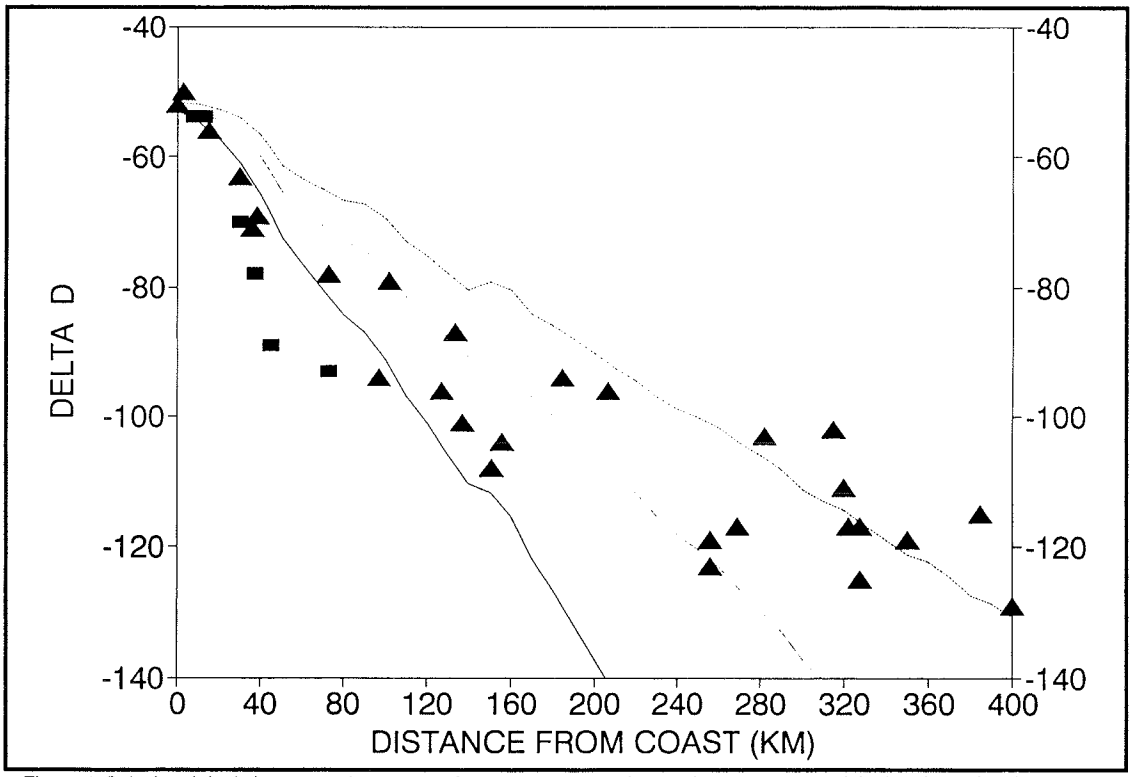

Figure 4. Calculated depletion curves for Φ=20%. Squares represent observed wet season precipitation data; triangles are ground water data of Ingraham and Taylor (1991). (A) Ω=1.5 (bottom line); (B) Ω=2.0 (center line); (C) Ω=2.5 (top line).

Again, none of the curves provides what we believe is a good fit to the data. The effect of recycling is to lower the advection velocity needed to produce curves similar to those of Figure 3. In general there is a trade-off between these two parameters; higher values of the one can be balanced by lower values of the other. Thus, our results do not require recycling to be important in this area, but changes in slope can be explained by recycling. Also, if Ω is held constant, changes in slope of the depletion curve may be parsimoniously explained by known variations in Φ.

Figures 3 and 4 illustrate the general forms of depletion trends that can be obtained with a constant value of Φ or if a simple single-stage Rayleigh process is at work. At higher values of Φ (we experimented with 40%, 60% and 80%), the model curves show variations in slope but display that same general form. Modest variations of Ω are required to achieve the same fit. All curves show a relatively steep curvilinear decline within the first 55 km inland, and we attribute this to "rainout" due to the high precipitation amounts near the coast. Precipitation is so high in that segment (Figure 2) that effects of changes in Ω and Φ are of second order.

None of the results captures the magnitude of depletion actually observed. This is because we have constrained our solutions to remain stable throughout the length of the traverse with constant Ω and Φ. Any solution that captures the early depletion deviates wildly from the data before it extends 100 km from the coast.

To illustrate this point, we show a solution (Figure 5) with Φ=0%, Ω=1.0, and an initial δD=–45 per mil. In this case we see an almost perfect fit of model to observed data over the first 55 km. This leads us to ask whether Ω=1.0 could be a reasonable value to use throughout the traverse. We find that the form of curve in Figure 5 is extremely sensitive to the value of Φ; Φ=5% gives a poorer fit to the precipitation data. It is interesting to determine what Φ would give a low enough slope to agree with the ground water data beyond 55 km. Interestingly, we find that no Φ can give such a slope when Ω=1.0; a change of Ω must be involved. In Figure 5 we also show results with Ω=2.7 and Φ=20% and δD_0=–90 per mil. We suggest that the slope and location of this solution corresponds roughly to the depletion actually implied by the data beyond 55 km and that changes in Ω and Φ along the traverse can explain the observed variation of δD. The interaction between Φ and Ω do not allow us to specify a unique combination at this time, and we leave that as a future exercise.

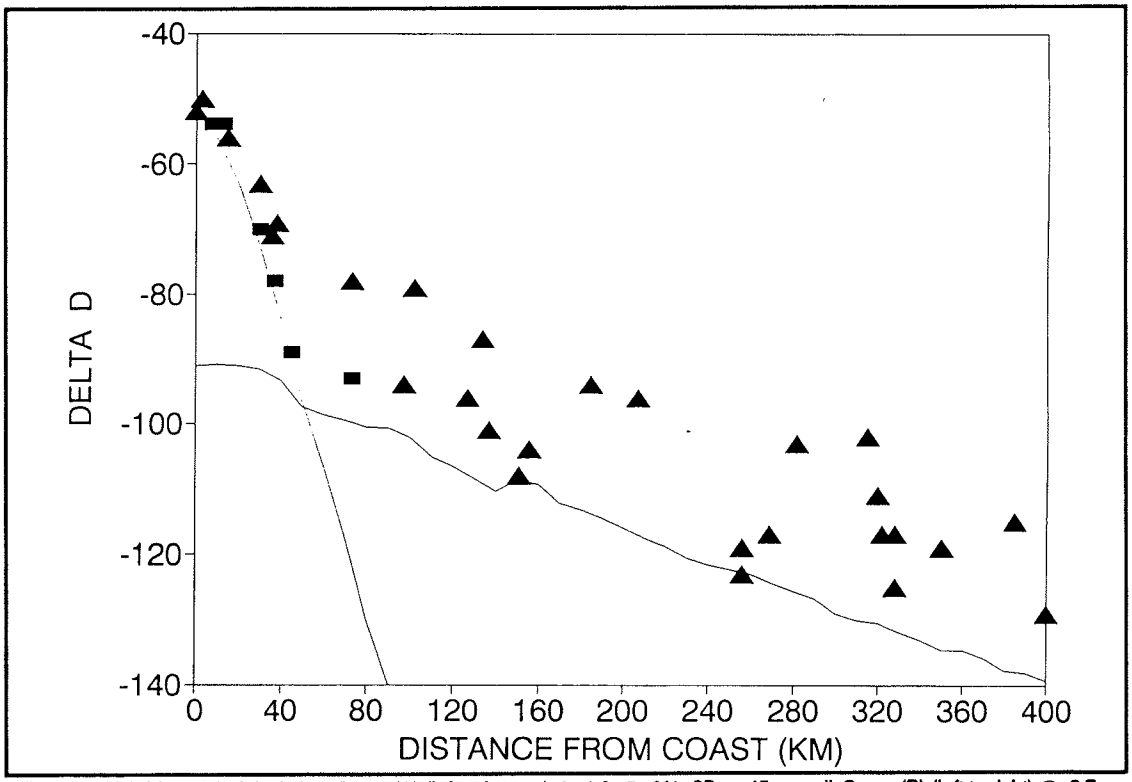

Figure 5. Hybrid model of depletion. Curve (A) (left to bottom) Ω=1.0, Φ=0%, δD_0=–45 per mil. Curve (B) (left to right) Ω=2.7, Φ=40%, δD_0=–90 per mil.

Discussion

Fractionation, rain-out, and recycling along an air mass streamline were computed at 10-km steps using model-derived averages of temperature and precipitation. The results provide a useful representation of geographic variations of the stable isotope compositions of inland meteoric waters under the assumption of a simple single-stage Rayleigh process or with constant evapotranspirational recycling. The modeled isotopic compositions become too depleted if predicted by simple Rayleigh distillation of eastward moving air masses and if no recycling occurs. For a constant advection velocity, recycling tends to progressively enrich inland waters in D relative to single-stage Rayleigh distillation and significantly influences both the degree and rate of depletion. Thus δD of inland meteoric waters can be better understood by including the effects of upwind evapotranspirational recycling.

It appears a large fraction of the observed geographic variation of the δD of ground water can be explained by winter precipitation when the effects of ET are included. The effect of ET in the recycling of previously precipitated and relatively enriched waters from upwind areas is important in the traverse studied. We find several values of Φ can provide approximate fits to the data using appropriate values of Ω. Thus we can envision relatively parsimonious models in which Ω decreases slowly across the traverse while Φ steadily increases with distance from the coast. It appears such a pattern could explain the observed variation of δD and is reasonable given the observed velocities (Schutz and Gates 1971) and known increasing aridity along the traverse (Court 1982). We are modifying our model to study this hypothesis.

We have found that only low advection velocities (on the order of 1-3 m/sec) can provide δD values in the –50 to –130 per mil range observed. Furthermore, the solutions are quite sensitive to the exact value selected. Such advection velocities are low compared to observed average wind velocities (Schutz and Gates 1971). Possible explanations are:

- Advection of water drops and droplets takes place at a lower velocity than movement of the air mass.
- Advection velocity is the same as air mass velocity; however, the average velocity is much different than instantaneous velocity during a storm.
- Turbulence reduces net transport (advection velocity) below average velocity.
- Vertical profiles of isotope fractions (for example, Ehhalt, 1974) differ sufficiently from the vertical profiles of velocities that the vertically integrated flux cannot be described using the average velocity.
- Most advection occurs low in the atmosphere, below the 800-mb level, where frictional effects reduce transport speeds.

We suggest that this last explanation is a simple interpretation that can easily be studied. If this is correct, it suggests that models of isotope dynamics will require a high degree of resolution in the lower levels of the atmosphere. For example, the version of the GISS model most frequently used for isotope studies (GISS II) has nine vertical layers (Hanson *et al* 1983).

With simple single-stage Rayleigh distillation — and if precipitation is constant — a plot of isotopic composition versus F_V is a convex upward curve, the "Rayleigh curve". Figures 3-5 show that, when the abscissa is distance and realistic variations in precipitation are considered, the plot can be quite complex.

Qualifications

We have assumed Φ is constant along the entire traverse. We also assume that seasonal averages are representative of the average behavior over a season when analyzed at a finer temporal resolution. A storage term was not included in the model. In addition, the model does not include the effects of kinetic fractionation. ET is not accompanied by fractionation, thus all recycled water isotopically is equivalent to transpiration that effectively occurs without fractionation. We are now modifying the model to relax some of these assumptions.

Conclusions

Computation of fractionation, rain out, and recycling along an air mass flowline at 10-km spacing using monthly averages of temperature and precipitation provides a useful representation of spatial variations of isotope ratios in an area dominated by orographic precipitation. These computations are not possible without spatially detailed estimates of average temperature and total precipitation for the entire wet season. The combination of a spatially detailed climatic model with observational data on δD can help to constrain important hydrologic parameters.

No acceptable fit to the entire suite of observational data was obtained when the isotopic effects of terrestrially evapotranspired and recycled water were ignored. When ET is added to the model, and if distinct ET regimes are allowed, acceptable fits may be available. We see a need to consider the effects of more realistic estimates of variations in Φ, especially as occur in the transition to the Great Basin. Advection velocities capable of explaining the variation of isotope signatures in ground water in this area appear to be lower than average 800-mb zonal velocities. Thus, isotopically important advection may be most important below the 800-mb level.

It is important to recognize that curvature in a plot of isotopic composition versus distance inland need not be diagnostic of single-stage

Rayleigh distillation. A plot of isotope compositions versus F_V in a single-stage Rayleigh distillation is a curve if precipitation is spatially constant. It may appear as a straight line if precipitation decreases linearly with distance. However, if the abscissa is distance and with more realistic measurements or predictions (as allowed by this climate model) of the variations in precipitation, the Rayleigh curve may appear quite complex.

Acknowledgments

This work was funded by the Nevada Agency for Nuclear Projects/Nuclear Waste Projects Office under U.S. Department of Energy grant number DE-FG08-85NV10461. The opinions expressed in this paper do not necessarily represent those of the State of Nevada or the U.S. Department of Energy. We thank Dr. Barry Roberts for assistance with calculating windfields and calibrating the climate model for this area.

References

Barry, R, 1981. *Mountain weather and climate.* Methuen. 313p.

Brutsaert, W, 1982. *Evaporation into the atmosphere.* D. Reidel Pub. 299p.

Craig, RG, and JF Stamm, 1990. A statistical model of climates in the southwestern U.S. Pgs. 27-31 in JL Betancourt and AM MacKay (eds.), *Proceedings of the Sixth Annual Pacific Climate (PACLIM) Workshop.* Calif. Dept. Water Resources, Inter. Ecol. Stud. Prog. Tech. Rept. 23.

Court, A, 1974. The Climate of the conterminous United States. Pgs. 193-343 in RA Bryson and FK Hare (eds.), *Climates of North America, Vol. 11, World Survey of Climatology.* Elsevier:Holland.

Ehhalt, DH, 1974. *Vertical profiles of HTO, HDO, and H_2O in the troposphere.* NCAR Tech. Note, NCAR-TN/STR100.

Friedman, I, AC Redfield, B Shoem, and J Harris, 1964. The variations of the deuterium content of natural waters in the hydrologic cycle. *Reviews of Geophysics.* 2:177-224.

Gat, JR, and E Matsui, 1989. The buildup of oxygen-18 and deuterium in atmospheric moisture as a measure of the relative importance of the evaporation and transpiration fluxes from the Brazilian Amazon. *Eos Transactions.* 70:296-297.

Hansen, J, G Russell, D Rind, P Stone, A Lacis, S Lebedeff, R Ruedy and L Travis, 1983. Efficient three-dimensional global models for climate studies: models I and II. *Monthly Weather Review.* 111:609-662.

Ingraham, NL, and BE Taylor, 1991. Light stable isotope systematics of large-scale hydrologic regimes in California and Nevada. *Water Resources Research.* 27:77-90.

_____, 1986. Hydrogen isotope study of large-scale meteoric water transport in Northern California and Nevada. *Journal of Hydrology.* 85:183-197.

Leguy, C, M Rindsberger, A Zangwil, A Issar, and JR Gat, 1983. The relation between the ^{18}O and deuterium contents of rain water in the Negev Desert and air-mass trajectories. *Isot. Geosci.* 1:205-218.

Majoube, M, 1971. Fractionnment en oxygene 18 et en deuterium entre l'eau et sa vapeur. *J. Chim. Phys.* 10:1423-1436.

Rindsberger, M, M Margaritz, I Carmi, and D Gilad, 1983. The relation between air mass trajectories and the water isotope composition of rain in the Mediterranean Sea area. *Geophysical Research Letters*. 10:43-46.

Rozanski, K, C Sonntag, and KO Münnich, 1982. Factors controlling the stable isotope composition of European precipitation. *Tellus*. 34:142-150.

Salati, E, A Dall'Olio, E Matsui, and JR Gat, 1979. Recyling of water in the Amazon Basin: an isotopic study. *Water Resources Research*. 15:1250-1258.

Schutz, C, and WL Gates, 1971. *Global climate data for surface, 800 mb, and 400 mb: January*. Advance Research Projects Agency, R-915-ARPA, ARPA Order No. 189-1, Rand Corporation, Santa Monica, CA.

Smith, GI, I Friedman, H Klieforth, and K Hardcastle, 1979. Areal distribution of deuterium in eastern California precipitation, 1968-1969. *Journal of Applied Meteorology*. 18:172-188.

Yonge, CJ, L Goldenberg, and HR Krouse, 1989. An isotope study of water bodies along a traverse of southwestern Canada. *Journal of Hydrology*. 106:245-255.